Environmental and Economic Implications of Thermal Energy Storage for Concentrated Solar Power Plants

Submitted in partial fulfillment of the requirements for

the degree of

Doctor of Philosophy

in

Engineering and Public Policy

Sharon J. Wagner

B.S., Environmental Science, University of Massachusetts Amherst

Carnegie Mellon University

Pittsburgh, PA

August, 2011

Acknowledgements

This research was made possible through support from the National Science Foundation Graduate Research Fellowship Program, the Steinbrenner Institute of Carnegie Mellon University, and the Climate Decision Making Center (CDMC) at Carnegie Mellon University's Department of Engineering and Public Policy, which is sponsored through a cooperative agreement between the National Science Foundation (SES-0345798) and Carnegie Mellon University. I express my sincerest gratitude to these funding sources for enabling this research.

I am very grateful to my research advisor and thesis committee chair, Professor Edward S. Rubin for all of the support and guidance he has given me in this endeavor. His patience, calm and rational approach to quality research, and his wealth of knowledge have been invaluable to the completion of this thesis. I also express my sincere appreciation to the other members of my thesis committee - Professor Jay Apt, Professor H. Scott Matthews, and Dr. Aimee Curtright – for their patience, guidance, and wisdom throughout this process.

I am very grateful to the Department of Engineering and Public Policy faculty, staff, and students for providing the opportunity to learn and grow in a challenging, caring, and unique academic environment. I especially want to thank the following people who have provided technical advice and/or research-related support: Cara Libby from the Electric Power Research Institute; Harvey Stephens from Nextera Energy; Michael Berkenpas, Haibo Zhai, Karen Kietzke, Sean McCoy, Inês Azevedo, Deanna Matthews, and Professors Granger Morgan, Lester Lave, Mitchell Small, and Shawn Litster from Carnegie Mellon University

I express my greatest gratitude to my husband and son, Larry and Jacob Klein, for their incredible patience and invaluable moral support during some challenging times. I am so grateful to my mother Mary Wagner, sisters Andrea and Carrie Wagner, and in-laws Lynn and Robert Klein for helping in so many ways to enable me to complete this dissertation. Finally, I would like to dedicate this thesis to my late father, Edwin Cecil Wagner, who always believed in me and supported me in anything I set out to do. Dad, I hope you don't mind that you are no longer the most educated in the family ☺

Abstract

In response to renewable energy policies and incentives, the parabolic trough (PT) concentrated solar power (CSP) industry has recently experienced much national and global growth. Although thermal energy storage (TES) is a commercial technology that can extend PT power plant operational hours beyond sunny periods, currently no United States PT plants use this technology. This study examines the question of whether renewable energy policies should include provisions to encourage TES for CSP. This question is examined through an analysis of the economic and environmental tradeoffs associated with the choice of a backup system for a PT plant.

An engineering-economic model has been created to quantify the levelized cost of electricity (LCOE) and expected annual profit of a parabolic trough plant with three different backup configurations: 1) no storage/ no natural gas backup (except for heat transfer fluid freeze protection); 2) 1-12 hours of two-tank indirect molten salt TES; and 3) natural gas backup (in the form of a heat transfer fluid heater) to match each TES capacity. An overview of the key inputs and outputs related to this model is presented in Figure 1, which displays an iterative process used to select the solar field area that minimizes the LCOE for each plant configuration modeled. The results of this model show that TES can increase the unsubsidized, pre-tax LCOE of a PT power plant by 4-26% compared to no storage/backup. TES and NG backup also have similar LCOE values across most storage/backup capacities. Under current federal incentives and with fixed electricity pricing, TES can increase the expected annual profit compared to no storage/backup and compared to NG backup.

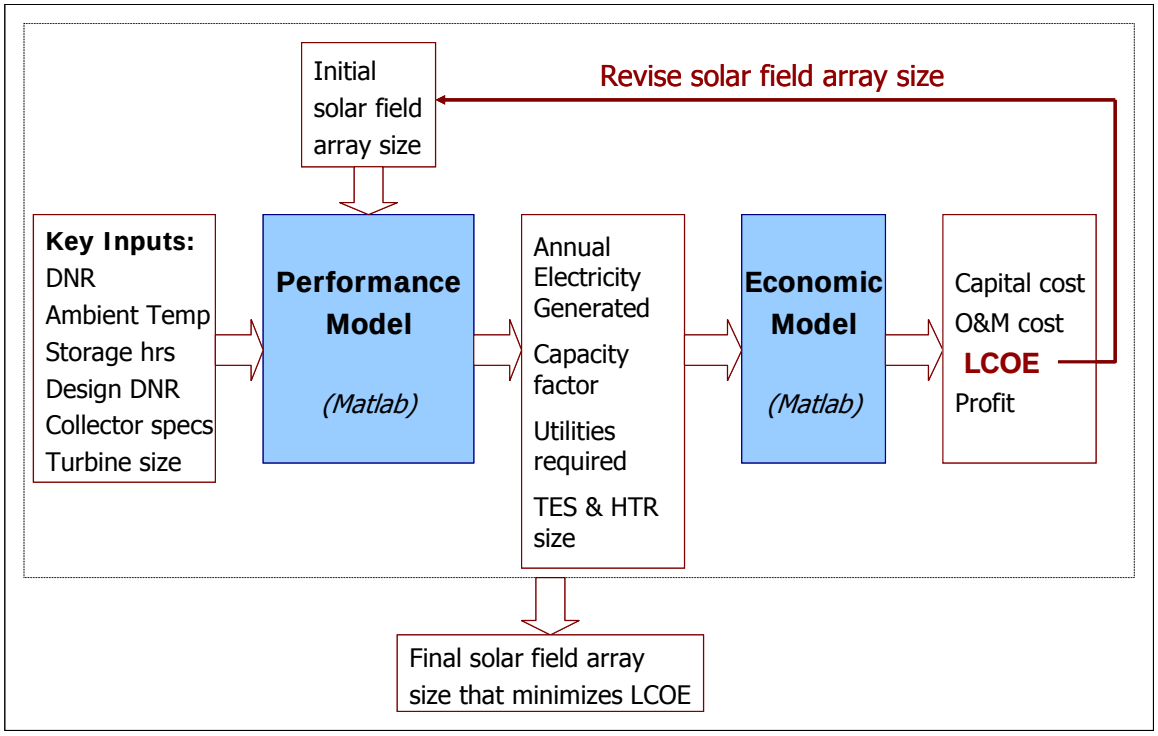

Figure 1 - Engineering-Economic Model Overview[1]

In addition, a life cycle assessment was conducted to compare the cumulative energy demand, greenhouse gas (GHG) emissions, water and land use associated with different storage/backup configurations. The results of this analysis show that TES can reduce life cycle GHG emissions up to 7% compared to no storage/backup and up to 210% compared to NG backup. Life cycle water use decreases with increasing storage capacity/NG backup. In each case, TES and NG have similar life cycle water use values. On-site water use increases slightly with TES/NG backup. Life cycle land use is similar for the three plant configurations overall.

[1] DNR = direct normal radiation; TES = thermal energy storage; HTR = natural gas-fired heater; O&M = operation and maintenance; LCOE = levelized cost of electricity

A sensitivity analysis was conducted to understand how key model inputs affect economic and environmental results. This analysis revealed opportunities for a multi-variable optimization that incorporates variations in heat transfer fluid mass flow rates along with changing storage capacities and solar field areas. When these changes are incorporated, TES can lower the LCOE of a parabolic trough plant compared to the no-storage alternative and NG backup alternative.

A further analysis was conducted to examine the tradeoffs between the economic and environmental implications of TES. The analysis included comparisons between environmental and economic results; a multi-criteria decision analysis that considers a range of preferences for different attributes; and a calculation of the carbon price required for each configuration modeled in the study to be competitive with new coal-fired electricity generation. The results of the decision analysis show that under most preference scenarios examined, no storage/backup is preferred over any of the TES/NG capacities. If some backup system is required, TES is preferred over natural gas backup, except where economic outcomes are strongly preferred. A carbon price of \$150-\$240/tonne CO_{2eq} is required for PT to be competitive with coal-fired generation, depending on the TES configuration. The study concludes with recommendations for research to further refine and extend the current analysis.

Table of Contents

List of Tables

List of Figures

Chapter 1: Background

Climate change concerns have motivated thirty-seven states and Washington D.C. to adopt renewable portfolio standards (RPS) or goals. Seventeen of these states include a specific provision to encourage solar energy development [1]. With the United States electricity industry responsible for approximately 40% of national greenhouse gas emissions [2], these policies, along with federal incentives, have created a recent momentum for the development of large solar energy projects. Parabolic trough (PT) concentrated solar power (CSP) has dominated the utility-scale solar electricity market since the 1980s, with a current U.S. capacity of 419 megawatts (MW) and nearly 6 gigawatts (GW) under development [3]. One key advantage of CSP over other solar technologies is its ability to store energy for later use. As the PT market continues to grow, industry leaders are divided over the question of whether a thermal energy storage (TES) system should be included in new installations. Proponents claim that TES improves power plant economics by extending operational hours into peak demand periods, while opponents argue it represents a significant increase in the already high capital cost of a PT plant, further reducing the likelihood of obtaining project financing. This dissertation explores the TES question from a policy perspective with the overall goal of analyzing the benefits and costs associated with TES from a societal standpoint.

1.1 Overview of Concentrated Solar Power

Concentrated solar power (CSP) uses solar heat energy to heat a fluid to generate electricity, in contrast to photovoltaic (PV), which converts solar radiation directly to electricity. Since CSP

relies on heat energy, it can use only the direct normal portion of the global solar irradiance that enters Earth's atmosphere, in contrast to PV, which can use direct and indirect radiation. In other words, one limitation of CSP compared to PV is that CSP cannot generate electricity during cloudy periods, while PV can. However, since CSP uses heat energy, it is possible for there to be enough thermal inertia in the operating fluid to sustain energy production for cloudy periods that last up to a half hour [4]. CSP also has the capability of storing thermal energy for later use during periods with little or no solar radiation. In addition, utility-scale CSP has historically been seen as less costly than PV, although this perception is changing as international PV cell manufacturing costs continue to decrease rapidly. Anecdotal reports indicate that developers are even going as far as to switch from CSP to PV due to these declining costs, but most sources indicate that the cost of CSP and PV are approximately equivalent. In any case, this study focuses on CSP electricity generation rather than PV because of the unique thermal storage capabilities CSP possesses.

Although several types of CSP exist, there are three technologies that are currently under construction and development in the U.S. [3]: parabolic trough, dish engine, and power tower (also known as central receiver). Table 1 displays the current installed and operating capacity and capacity under construction and development for each of these three technologies. Parabolic trough has historically led the pack with a 97% share of installed capacity, but if all projects under construction and development proceed as planned, this share will drop to 55% with power tower and dish gaining a larger portion of the market.

Table 1 – Status of key CSP technologies in the United States (adapted from [3])

CSP Technology	Current installed capacity (MW)	Approximate capacity under construction/development (MW)
Parabolic Trough	420	5,500
Power Tower	4	3,600
Dish Sterling Engine	4	900
Other	5	0
Total	433	10,000

Figure 2 displays photographs of three prominent CSP technologies in the U.S. Each of these technologies uses a reflective surface to concentrate direct normal solar radiation (DNR) onto some type of receiver. In the case of dish engine, a series of mirrors arranged in a satellite dish formation concentrate DNR onto a *point receiver* – the power conversion unit (PCU) in the center of the dish [5]. The receiver transfers the heat to a fluid, and as the fluid expands against a piston or turbine, it produces mechanical power, which is used to run a generator [6]. Traditionally, the dish engine has been characterized as a small-scale distributed generation resource, but three of the projects currently under development in the U.S. range from 145 MW to 409 MW in capacity [3].

Figure 2 - Prominent CSP Technologies in the U.S.

From left to right: Power Tower [7], Parabolic Trough [8], Dish Engine [9]

The power tower is also called a central receiver or solar tower and consists of a large array of dual-axis tracking mirrors, called heliostats, which concentrate the sun's energy onto a *point receiver* on top of the tower. The heat is transferred to a heat transfer fluid (HTF) in the tower and used to generate electricity through a traditional steam power cycle. Although power towers do not yet make up a significant portion of U.S. CSP capacity, the feasibility of the technology has been demonstrated in field tests around the world over the last 15 years.

The parabolic trough CSP uses a series of long, curved single-axis tracking mirrors to concentrate DNR onto a *line receiver* – a steel absorber tube in the center of the trough. The heat transfer fluid in the absorber tube transfers the thermal energy to a traditional steam power cycle to generate electricity. Many developers have selected power tower over parabolic trough recently because it is expected to be less costly and more efficient over the long run [10]. However, with decades of utility-scale operational experience, parabolic trough is still favored because investors and loan-granting institutions have more confidence in the technology than power tower. With the high capital cost associated with any CSP option, many financiers are more willing to put their money on the less risky option [3]. Therefore, despite the potential benefits of power tower, trough technology still dominates the U.S. CSP industry in the near-term, and for this reason, it is the subject of this study.

1.2 Advantages and Disadvantages of Thermal Energy Storage (TES) for CSP

As mentioned above, a key advantage of CSP over PV is the ability to store energy as heat for later use during periods of low or no DNR. Although the concept of thermal energy storage is not new, its application in the CSP industry is still considered somewhat experimental. The first commercial CSP plant to use TES was Andasol 1 in Spain, which began operation in 2008. This 50 MW parabolic trough power plant stores heat in molten salt, which provides up to 7.5 hours of plant operation during periods of no DNR [11]. Several plants under construction and development globally have plans to implement a TES system, yet the advantages and disadvantages of TES are still a hotly debated topic in the industry.

TES allows a CSP plant to extend operational hours into the evening and can help operators manage variability during extended cloudy periods. Reduced variability enables the CSP plant to become a dispatchable generator. Operating during evening hours, especially during the summer, could enable the CSP plant to earn more revenue by capitalizing on peak demand pricing. In addition, since the thermal energy is stored before being converted to electricity, the round trip efficiency of a TES system for a CSP plant may be close to 100%, which is higher than any other energy storage technology [12]. From an environmental standpoint, TES has another important advantage in that it enables the plant to generate more low-carbon energy and rely less on fossil fuels for backup.

All of these advantages come at a price, however. There may be a performance penalty associated with the TES system if a heat exchanger is required. There is a significant increase in

the capital cost of the plant due to the TES system itself (storage medium, tanks, piping, and heat exchanger if necessary) and possible additional solar collectors to maintain the same power output while storing energy. In the current economic recession, these cost increases are particularly important because it is already difficult for many developers to find financing for plants without storage. TES may increase operation and maintenance costs as well since the TES system itself will require maintenance and additional workers, and any increase in solar collector numbers requires additional mirror washing and potential repairs. Additional collectors also mean an increase in land use, which is especially important in the ecologically sensitive desert regions that are particularly well-suited for CSP technology. In fact, several CSP projects currently under development in the U.S. are now facing lawsuits from environmental groups due to this issue, and some have even had to withdraw applications or significantly alter construction plans due to these environmental concerns [13].

1.3 Research Motivation

Figure 3 shows a map created by the National Renewable Energy Laboratory (NREL), which indicated areas in the United States most suitable for CSP deployment. This map indicates the potential for up to 200 GW of installed CSP capacity in the southwest U.S using existing transmission lines [14]. This translates to between 12-20% of current U.S. electricity generation, assuming: 4,119 terawatt-hours (TWh) of net electricity generation in the U.S. in 2008 [2], and 30% to 50% capacity factor[2]. Given the urgent directive by climate experts to drastically reduce greenhouse gas (GHG) emissions as quickly as possible [15], and the complicated set of limitations associated with low-carbon electricity generation technologies in general, it is

[2] 30% capacity factor is the average capacity factor reported in Price et al, 2002 [15]; 50% was selected to represent a plant with molten salt storage

imperative that the nation explore each technology option that is ready for deployment. CSP is a proven technology, and if the potential outlined by NREL is to be realized, policy-makers must consider how best to steer that deployment. Thermal energy storage (TES) could enable CSP to approach baseload electricity generation, which may be critical in the long-term for replacing fossil fuel generation. There may be reason to include provisions for encouraging the use of TES in future CSP plants through RPS or other policy measures.

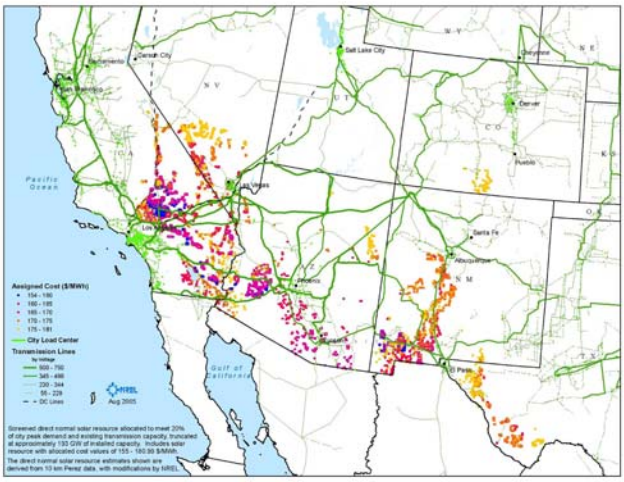

Figure 3 - Concentrating Solar Power Prospects of the Southwest United States [14]

1.4 Framing the Problem

State renewable portfolio standards and goals encourage CSP deployment in southwestern states either by mandating that utilities purchase a certain percentage of their energy from renewables, and sometimes from solar in particular, or by granting financial incentives to develop low-carbon electricity generation capacity. Federal incentives, like the 30% investment tax credit/cash grant option, accelerated depreciation, and the federal loan guarantee [16] help make building CSP projects financially appealing. Clearly these policies are succeeding on some level because, if all

projects currently under construction and development proceed as planned, there will be a 23-fold increase in U.S. CSP capacity within the next decade. However, very few of the new projects being developed will include TES, which prompts the question: should renewable energy policies be doing more to encourage TES?

1.4.1 The Need for Backup Energy in CSP

All CSP plants require a backup system whether at the most basic level to facilitate plant shut-down and start-up or to smooth variable output and extend operational hours. Traditionally, CSP plants have used a combination of natural gas and electricity to provide this backup power. The oldest CSP plants, the Solar Electric Generating Stations (SEGS) in California, have a separate natural gas boiler that can produce additional steam for the power cycle when there is insufficient DNR in the solar field [17]. These plants traditionally have used natural gas to supply up to 25% of the annual thermal input to the steam generator per Federal Energy Regulatory Commission (FERC) regulations [18]. Nevada Solar One, which began operating in 2007, uses a natural gas-fired heater to maintain the heat transfer fluid at a constant temperature during cloudy periods, and this backup system can supply up to 2% of the plant's electricity [19].

If a CSP plant does not incorporate its own backup system, it will need to use electricity from the grid for start-up, shutdown, and other auxiliary loads. Thus, it will likely still be using a fossil fuel backup system indirectly since these plants are being sited in states that get the majority of their electricity from coal or natural gas [20]. Moreover, the grid operator likely will need to ramp up quick-starting natural gas plants during periods of intermittency to compensate for the

drop in energy output from the CSP plant. So, the concept of a "solar only" plant does not exist in the reality of current electricity generation profiles.

1.4.2 Choosing between TES, no TES and Natural Gas at the Plant Level

During the development of a CSP project, there is a choice between three main options: 1) use fossil energy backup at the plant level (i.e., install an additional boiler or use heat transfer fluid heater); 2) use fossil energy backup at the grid level (i.e., use a small amount of electricity from the grid, but don't incorporate any back-up system at the plant level and rely on the grid operator to adjust for variable output); or 3) use a non-fossil energy backup system at the plant level. Since the majority of currently operating CSP plants use natural gas for option 1, and the only commercially operating non-fossil energy backup system at the plant level is molten salt TES, for the purposes of this study, this choice becomes: 1) use natural gas at the plant level; 2) don't use any backup at the plant level; and 3) use molten salt TES at the plant level.

1.4.3 Research Questions

The overarching research question that guides this study is: should renewable energy policies be doing more to encourage TES for CSP? This question requires an analysis of the policy tradeoffs associated with the choice of a backup system for a CSP plant. These policy tradeoffs can be decomposed into economic and environmental concerns from a societal standpoint. Although economic implications tend to concern business-owners primarily, they are also important to society because high costs and low profits at the plant level often translate into higher electricity bills at the consumer level. Environmental concerns are clearly important at

the societal level due to the growing number of environmental policies, standards, and goals in recent decades.

The key economic questions considered in this study are:

- Can TES reduce the levelized cost of electricity from a CSP plant?
- Can TES increase the profitability of a CSP plant?
- How do different electricity pricing structures affect the profitability of TES with CSP?
- If TES is economically preferred over other options, how does increasing storage capacity change the results?
- Do current U.S. renewable energy incentives encourage or discourage TES from an economic standpoint?
- Are there other incentive structures that may encourage TES more effectively?

The key environmental questions considered in this study are:

- How does the TES affect the life cycle greenhouse gas emissions of a CSP plant?
- How does the TES affect the life cycle and operational water use of a CSP plant?
- How does TES affect the land use associated with a CSP plant?
- How does this environmental profile change with varying storage capacities?

These economic and environmental questions lead to a set of policy questions that integrate the two analyses:

- Is there a clear environmental benefit versus economic cost to incorporating TES with CSP (or vice versa)?

- If so, do the benefits outweigh the costs?
- If not, in what circumstances might TES be preferred over other backup options?
- How might renewable energy policy be adapted to better reflect these social tradeoffs?

1.5 Thesis Structure

This document describes the methods and results associated with an analysis of the social tradeoffs associated with TES for CSP. Chapter 2 describes the history and current status of parabolic trough (PT) CSP technology and TES. It also summarizes the literature on engineering-economic modeling and environmental life cycle assessment (LCA) of TES for CSP. Chapter 3 describes an engineering model that was created to simulate the hourly and annual electricity generation associated with a PT plant in order to observe the effect of varying storage capacities on plant performance. This chapter also describes a parallel model that was created to compare a PT plant with natural gas backup instead of TES. Chapter 4 explains the economic model used to calculate the levelized cost of electricity, expected annual profit, and net present value of each plant. Chapter 5 outlines the procedure for the hybrid life cycle assessment that was conducted to calculate the greenhouse gas emissions and water use associated with each plant. This chapter also describes the land use and operational water use calculations that are part of the environmental portion of the analysis. Chapter 6 describes an uncertainty analysis that was conducted to quantify uncertainty associated with key parameters used in the models and the level of sensitivity in model results associated with variations in these parameters. Chapter 7 explores the social tradeoffs associated with the results of the environmental and economic analyses through straightforward comparisons and also through the use of a multi-

attribute utility function. Chapter 8 offers a broad set of conclusions from the results and synthesizes policy recommendations regarding how TES may be included in future renewable energy policy.

Chapter 2: Literature Review

2.1 Parabolic Trough (PT) Technology

The main components of a parabolic trough plant include the solar field, power cycle and power backup system (see Figure 4). The solar field consists of a series of solar collector assemblies (SCAs) that concentrate the sun's energy onto an absorber tube called a *receiver* in the center of the curved reflector surface. A heat transfer fluid (HTF) – usually, a synthetic oil called Therminol VP-1 – is heated in the receiver and pumped to a heat exchanger, where the thermal energy is transferred to water to generate steam in a traditional Rankine steam power cycle. The cooled HTF is then re-circulated through the solar field.

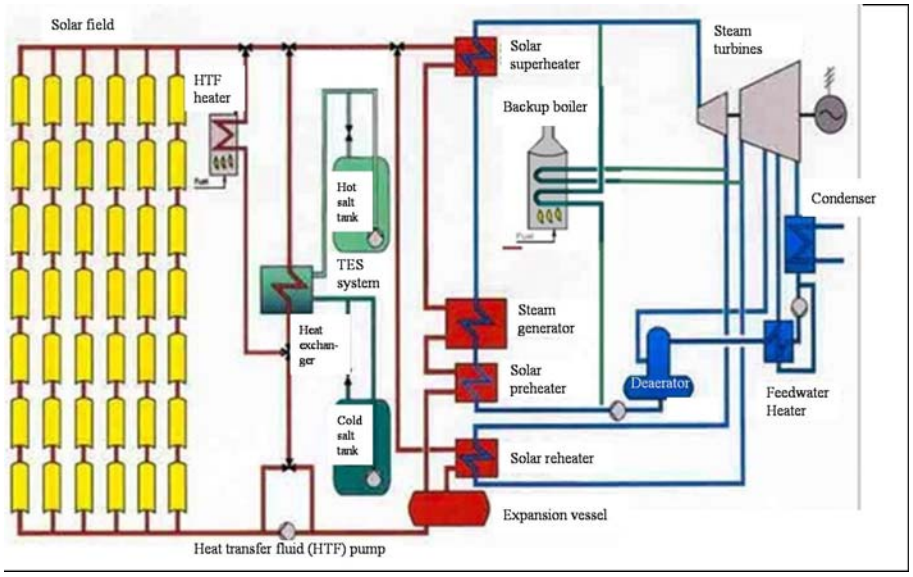

Figure 4: Diagram of a Parabolic Trough Plant

The red lines on the left represent heat transfer fluid flows. The blue lines on the right represent steam flows in the power cycle, and the green lines in the middle represent molten salt flows in the backup thermal energy storage system (TES). Three backup options are shown here: HTF heater, TES system and backup boiler; however, most plants will use one or two of these options. (Adapted from [21])

2.1.1 Solar Collector Assembly: Metal Support Structure

Each SCA is comprised of a set of collectors and a tracking system (see Figure 5) that includes sensors, controls, and a drive. The collectors in a parabolic trough solar field are normally aligned on a north-south horizontal axis and track the sun on a single axis (east to west) to maximize electricity production during the summer [10]. Each collector (see Figure 6) consists of a metal support structure, a set of parabolic reflector panels, and the receiver tube, also called the heat collection element (HCE). Each collector rotates independently from the one next to it by means of a ball joint, and header piping connects each set of SCAs in a row with all other rows and the power block [22],[23].

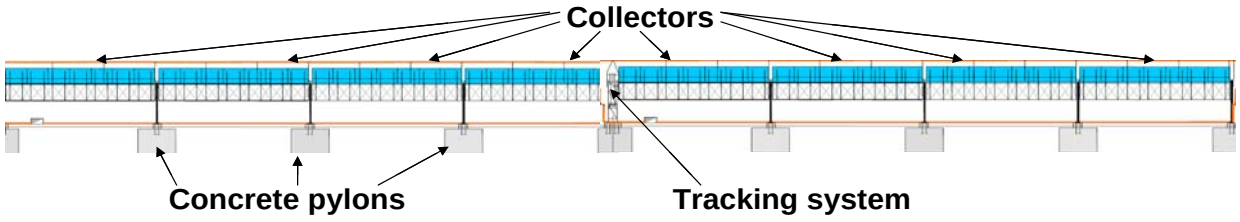

Figure 5: Solar Collector Assembly (SCA) – adapted from [24]

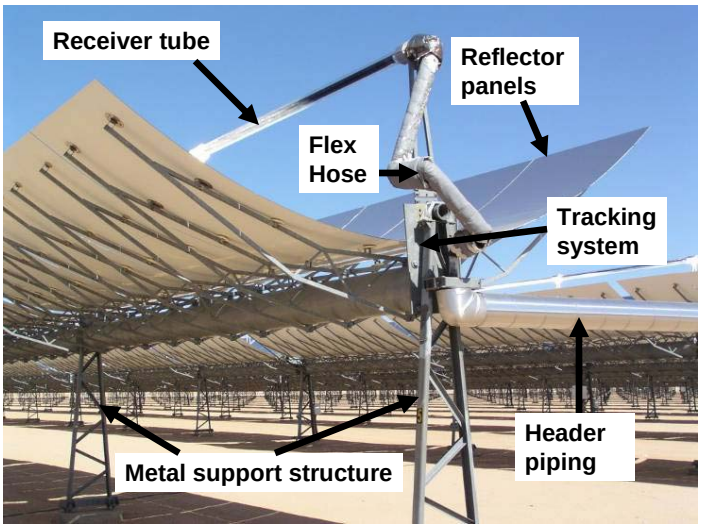

Figure 6: Main Components of a Solar Collector (adapted from [14])

Although the CSP industry still has a relatively small number of manufacturers and suppliers for collectors, receivers, and other key solar components, the industry is growing quickly, and there is a small variety of choice for each component. In terms of the SCA, there are four main designs for the metal support structure (see Figure 7). The LS-2 was designed by Luz International Limited and implemented at the earlier Solar Electric Generating Stations (SEGS I through VI) in California. It has a torque-tube structure that gives torsional stiffness but uses more steel than other designs. Luz designed the LS-3and implemented it at SEGS VII through IX in order to reduce manufacturing costs by using less steel and reducing the precision of the design [23]. The LS-3 is larger and uses a bridge truss structure instead of the torque tube [22]. Unfortunately, the manufacturing costs associated with the LS-3 were not as low as expected, and LS-3 operational experience at SEGS indicated reduced thermal performance and maintainability (alignment) compared with the LS-2 [23].

Figure 7 – SCA Metal Support Structure Designs.
From left to right: LS-2 Torque-Tube [22], LS-3 Bridge Truss [22], Solargenix Space Frame [22], Eurotrough Torque Box [25]

The EuroTrough collector was created by a consortium of European companies and research laboratories (Inabensa, Fichtner Solar, Flabeg Solar, SBP, Iberdrola, Ciemat DLR, Solel, and CRES) [23] and uses a metal support structure that combines the advantages of the two Luz designs by using a torque box with the stiffness of the LS-2 but the lower steel content of the LS-3 [22]. The stiffer design allows the collector length to be extended from 100 to 150 meters, which decreases the number of drives and interconnecting pipes required in the solar field and reduces collector cost and thermal losses. Additional advantages of the EuroTrough design are less glass breakage during high wind conditions, the ability to be mounted on an inclined site (3%), a weight that is 14% less than the LS-3 collector, simplified manufacturing processes, more compact transport from factory to plant, a 10% reduction in cost, and a 3% improvement in performance over the LS-3 [23]. The third generation Eurotrough collector is called the SKAL-ET and is currently in commercial use at Andasol 1 and 2 [25].

The metal support structure used in the Solargenix (formerly Duke Solar) collector is made of aluminum and is patterned after the LS-2 structure but is about half the weight of the LS-2. It uses a unique design that was originally developed for bridges and buildings and is easier to assemble than other designs. It achieves the same performance as the LS-2 but at a lower installed cost [23]. Acciona Solar Power bought 55% of Solargenix in 2006 [25]. A fourth design was created by Industrial Solar Technology (IST) but was historically used in lower

temperature process heat applications. However, the IST collector became the foundation for the Abengoa ASTRO, now in operation at the Solnova plants in Spain [26], [27]. Table 2 displays technical details concerning each of these solar collector options. As the CSP market continues to grow, more and more companies are developing proprietary collector designs. Fernandez-Garcia et al. [25] present more specific information about these designs and describe the variety of pre-commercial collector designs that were tested prior to the first trough plants.

Table 2 - Technological Specifications of Main Solar Collector Types (adapted from [23])

Collector	Structure	Aperture width (m)	Focal Length (m)	Mirror Area per drive (m^2)	Receiver diameter (m)	Module Weight (kg/m^2)	Peak Optical Efficiency (%)	Operational Experience
LS-2	Torque tube	5	1.49	235	0.07	29	76	SEGS I-VII
LS-3	Bridge truss	5.76	1.71	545	0.07	33	80	SEGS VII-IX
EuroTrough SKAL-ET	Torque box	5.76	1.71	817	0.07	29	80	Andasol 1 & 2
Solargenix (now Acciona)	Space frame	5	1.49	235-313	0.07	24	80	Alvarado I, Majadas I, Palma del Río II, Nevada Solar One, Saguaro
IST (now Abengoa ASTRO)	Space frame	2.3	0.76	424	0.04	24	78	Solnova 1, 3, 4

2.1.2 Solar Collector Assembly: Reflector Panels

All currently operating parabolic trough power plants use mirrors to reflect the sunlight onto the absorber tube. Flabeg Solar International manufactures the majority of parabolic mirrors in operation today, but RioGlass Solar, Guardian, and Saint-Gobain also manufacture glass for

trough plants [25], [28]. These mirrors have a reflective silver layer on the backside of the glass, covered with several protective coatings, and are relatively expensive to replace [22]. They are made from a low-iron 4-mm float glass with a solar-weighted transmittance of 98% [23], which refers to the fraction of sunlight that strikes the glass and passes through [29]. New mirrors have a solar-weighted reflectance of 93.5% [23], which refers to the fraction of sunlight that strikes the mirror and is reflected away from it [29]. Price et al. [23] describe a number of alternatives to glass mirrors that have been under development for more than 20 years, but so far, these technologies have not been able to prove the long-term performance of glass, which is required to secure the type of financing required by current trough projects. The potential exists for mirror costs to decline as competition increases in both the manufacture of mirrors and the supply of glass to parabolic mirror manufacturers.

2.1.3 Solar Collector Assembly: Receiver Tubes

The SCA peak optical efficiency displayed in Table 2 is influenced by the maintainability of the metal support structure, the accuracy of the tracking mechanism, the mirror reflectance and transmittance, and the absorptivity of the linear receiver tube. The receiver, which is also called a heat collection element (HCE), consists of a 4-meter-long, 70-mm diameter stainless steel tube at the mirror focal line of the parabola. The tube is coated with a cermet solar-selective absorber surface. An anti-reflective evacuated glass tube, 115-mm in outer diameter, surrounds the HCE to reduce convective and radiative heat losses to the environment [22]. Traditional glass-to-metal seals and metal bellows help to ensure a vacuum-tight enclosure and to allow for the thermal expansion difference between the steel and glass materials. The vacuum is normally

maintained at 0.0001 mm Hg (0.013 Pa). Maintenance issues that must be addressed with this type of receiver include loss of vacuum in the glass envelope, glass breakage, and degradation of the cermet coating. This last problem usually occurs when the vacuum fails or the glass breaks and oxygen interacts with the coating. Receiver tubes at SEGS are typically replaced every 1-5 years due to damage [23]. Figure 8 presents a diagram of a typical receiver.

Luz International Limited used to manufacture the receivers for all of the SEGS plants, but Solel Solar Systems acquired the Luz receiver manufacturing line when Luz went bankrupt. Solel has been manufacturing spare parts for the SEGS plants using their improved design, the "UVAC", which has better solar-selective absorber coating and an internal reflective shield that protects the inside of the glass-to-metal seal when the sun angle is low. The improved cermet coating also eliminates the oxidization failures that used to occur in the Luz receivers when the tubes lost vacuum [23]. The latest version is the Solar Receiver UVAC 2010, now manufactured by Siemens, with an absorbance factor greater than 96% and vacuum maintenance designed for 25 years [30]. Schott Solar is currently the main competitor for Solel/Siemens, providing receiver tubes for Nevada Solar One and Andasol 1 and 2 [31].

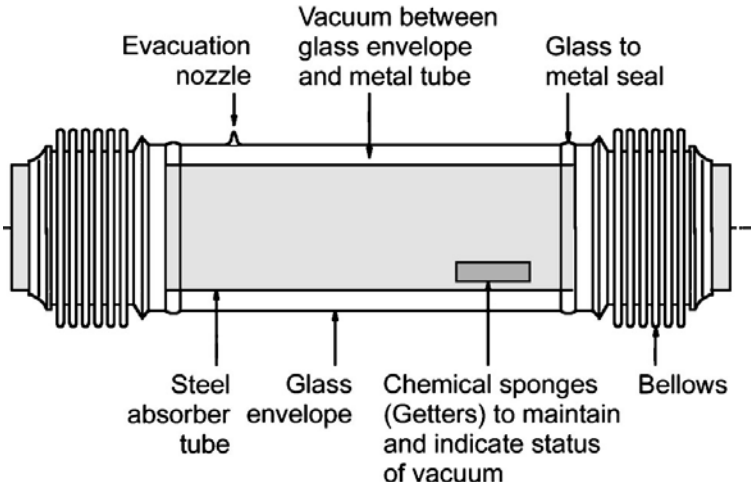

Figure 8 - Typical Heat Collection Element [23]

2.1.4 Heat Transfer Fluid

The type of heat transfer fluid (HTF) used in the solar field ultimately determines the operational temperature of the solar field and what type of thermal storage system can be installed at the plant. The operational temperature of the solar field determines the maximum power cycle efficiency that can be maintained [23]. Table 3 lists the maximum operating temperature possible with several HTFs that have been used or considered for use with parabolic trough. The first CSP plant, SEGS I, used a mineral oil called Caloria, but the use of biphenyl-diphenyloxide (more commonly known as Therminol VP-1) became more common since it increases the operating temperature up to 400^{o}C. Archimede, in Italy, is the only commercially operating trough plant in the world that uses Solar Salt as the HTF [32].

Table 3 - Heat Transfer Fluid Options

Fluid	Chemical Composition	Max temp (^oC)	Min temp (^oC)	Volume specific heat capacity (kWh/m^3)	Cost ($2010/ kg)	Properties [23]
Caloria (mineral oil)	Hydrotreated or solvent dewaxed heavy paraffinic petroleum distillates [33]	300 [23]	-10 [23]	0.56 [34]	$0.60 [34]	Flammable
Therminol VP-1 (synthetic oil)	73.5% diphenyl oxide; 26.5% biphenyl [35]	400 [35]	12 [35]	0.52 [36]	$2.60-$4.70 [37],[36]	Flammable
Silicon oil	Polymethyl-phenylsiloxane [38]	400 [23]	-40 [23]	0.53 [34]	$9.60 [34]	Flammable
Solar Salt	60% $NaNO_3$; 40% KNO_3 [37]	600 [37]	220 [37]	0.79 [37]	$1.00 [39]	High thermal stability, corrosive
Hitec [37]	7% $NaNO_3$; 53% KNO_3; 40% $NaNO_3$	535	142	0.71	$1.10	High thermal stability, corrosive
Hitec XL [37]	7% $NaNO_3$; 45% KNO_3; 48% $Ca(NO_3)_2$	500	120	0.80	$1.40	High thermal stability, corrosive
Ionic liquids	Organic methyl-imidazole salts [23]; omimBF4 used as baseline [36]	416 [23]	-75 [23]	0.97 [40]	$5.50 [40]	Good thermal properties, no mass production

Table 3 lists several other characteristics for each HTF as well: minimum operating temperature, volume specific heat capacity, cost and key properties. The minimum operating temperature determines the temperature at which freeze protection must be provided to the HTF so it does not become a solid and clog the vast array of receiver tubes. Freeze protection is typically provided through a natural gas-fired heater. The volume specific heat capacity was calculated from the data provided in the references cited in Table 3 within the operating temperature of a typical

trough plant (300-400^{o}C), and provides a measure of the relative thermal quality of each HTF. The costs listed in the table were converted to $2010 from the referenced sources using the United States Department of Labor Bureau of Labor Statistics CPI Inflation Calculator [41] . Although synthetic oil is the HTF of choice in most trough plants today, the high cost and flammability associated with oils with higher operating temperatures are not conducive to the dual role an HTF may potentially have as a storage fluid in a TES system. On the other hand, the high minimum operating temperature and corrosivity of the molten salts (solar salt, Hitec, and Hitec XL) present challenges in the operation and maintenance of the solar field. Ionic liquids may serve as future HTFs for parabolic trough if a market can be established and the cost reduced. Information on other HTFs can be found in [42].

2.1.5 Power Cycle Options

Most trough plants operating today generate electricity using a traditional reheat Rankine steam power cycle, which is very similar to that used for many coal, nuclear, and natural gas-fired power plants. Alternatives to the traditional Rankine cycle that are in operation at some of the newer trough plants include Integrated Solar Combined Cycle (ISCC), Direct Steam Generation (DSG), and Organic Rankine Cycle (ORC).

2.1.5.1 Rankine Cycle

In a trough plant with a Rankine cycle, a series of shell-in-tube heat exchangers transfers heat from the HTF to the power cycle to generate high-pressure superheated steam. The main components of the power cycle (steam generator, superheater, preheater, reheater, turbines,

pumps, condenser, feedwater heaters, and deaerator) are displayed in Figure 4. After passing through the steam cycle heat exchangers, the cold HTF returns to the solar field to be reheated. An expansion vessel accommodates the additional volume that ensues when the HTF is heated from the minimum operating temperature to the maximum operating temperature [43].

A cooling system is required to reduce the temperature of the condensate after passing through the turbines, and all commercially operating trough plants use a "wet" cooling system, which consists of cooling towers, circulating pumps and a chemical feed system. The cooling water, which is at ambient wet bulb temperature, is pumped through the condenser and rejects the heat absorbed from the steam cycle condensate through a counter-flow water-to-air cooling tower by latent heat of evaporation [43]. Although the cooling water is re-circulated through a "closed loop", the wet cooling system loses about 1,000 gallons/MWh of water through evaporation, blowdown, and drift [44]. An alternative to this system is a "dry" cooling system, which uses a series of fans to condense the steam from the turbine outlet through forced convection heat transfer at the dry bulb temperature. This type of system requires a larger heat transfer surface area than the wet system because air has a much lower heat transfer coefficient than water (W/m^2K), and it requires more parasitic energy to operate the fans. The dry system also has a higher capital cost than the wet system and results in a performance penalty on the Rankine cycle because the steam is condensed at a higher temperature than with the wet system [45]. These limitations have prevented current trough plants from using dry cooling; however, concerns over water supply in desert areas are driving developers to consider dry cooling for future plants as it reduces overall water consumption by about 90% [44].

2.1.5.2 Integrated Solar Combined Cycle (ISCC)

ISCC uses the solar field to generate steam for a Rankine bottoming cycle in a combined-cycle power plant (see Figure 9). The steam turbine can be oversized so the steam generator uses the steam generated by the solar field, and the waste heat from the gas turbine is used to reheat and superheat the solar steam. However, this results in partial load operation of the steam turbine during non-solar hours, which reduces efficiency compared to using a more consistent heat source in the bottoming cycle [23]. Compared to a conventional parabolic trough plant with a Rankine cycle, ISCC offers three main advantages: 1) the conversion of solar thermal energy to electrical energy is more efficient; 2) the incremental unit cost of the larger steam turbine in the ISCC system is smaller than the unit cost in a conventional trough plant; and 3) an ISCC plant does not suffer from the thermodynamic inefficiencies associated with daily shutdown and start-up [46]. A number of ISCC plants are in various stages of planning and development. One is currently operating in the U.S. (the Martin Next Generation Solar Energy Center in Florida), and one is currently operating in Italy (Archimede in Sicily). Archimede has approached the partial load problem by integrating TES with ISCC [47]. Although ISCC has some key advantages over traditional parabolic trough design or trough with storage/natural gas backup, it is a technology that is primarily based on electricity generated by fossil fuels as the solar portion is usually only a small percentage of the overall plant generation. This study does not consider ISCC as one of the plant configurations to be modeled because this study focuses on technologies that are primarily based on solar energy. It is recommended that future studies examine how ISCC and primarily solar-based technologies compare across economic, environmental and social indicators.

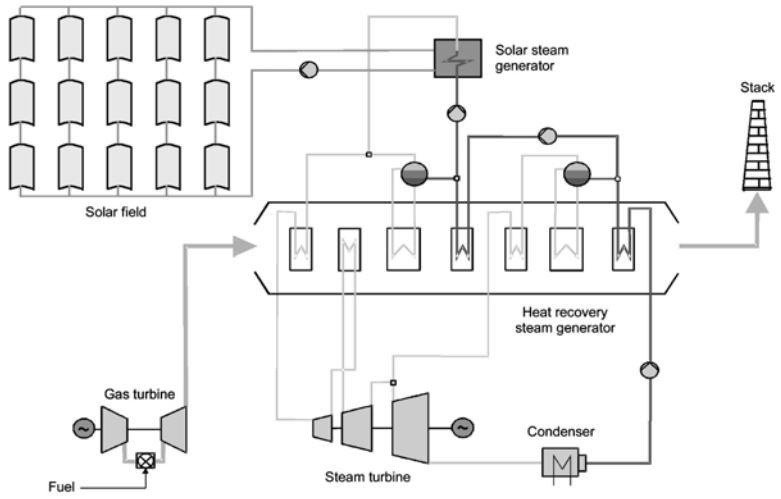

Figure 9 - Schematic of an Integrated Solar Combined Cycle Plant [23]

2.1.5.3 Direct Steam Generation (DSG)

DSG is the process of producing steam directly in the solar field instead of using a HTF to indirectly generate steam through heat exchangers. DSG is projected to reduce overall plant investment costs and increase heat transfer efficiency and power cycle efficiency. The cost of the solar field piping increases with DSG because the solar field fluid working pressure increases above 100 bar, but overall costs may decrease because there is no longer a need for HTF-to-steam heat exchangers, an oil expansion tank, an oil blanketing system, or any other component associated with the HTF circuit. Heat transfer efficiency increases because there is no intermediate heat exchanger, and power cycle efficiency increases because the system can operate at higher temperatures and pressures, and less pumping energy is required [23]. Svoboda, Dagan, and Kenan conducted a study on a trough field attached to an ISCC plant (equivalent to a 10-MW trough plant) and found that DSG could result in a 7% increase in

annual performance, 9% decrease in capital costs associated with the solar field and HTF circuit, and a 10% decrease in the levelized cost of electricity (LCOE) [48].

The Direct Solar Steam (DISS) project at Plataforma Solar de Almería (PSA) in Spain successfully demonstrated the feasibility of DSG with a small array of 11 parabolic trough collectors (aperture area of 3,000 m^2) for 3,000 hours between 1999 and 2001 [49] ,[50]. The results of this experiment indicated that two main issues need to be resolved with DSG before it can be commercially viable: 1) advanced solar field components need to be developed to allow temperatures to reach 550^oC at a pressure of 100 bar (the DISS test reached a maximum temperature of 375 ^oC at 100 bar) in order to achieve the main performance advantage of DSG – increased steam cycle efficiency; and 2) cheaper water/steam separator replacement options need to be developed in order to achieve cost reductions.

The INDITEP project, promulgated by a Spanish-German consortium of engineering companies, power equipment manufacturers, research centers and businesses, advanced the knowledge gained at DISS by using DSG in a 5 MW solar field to power a Rankine cycle. The INDITEP project expanded the solar field to 700 Eurotrough collectors and experimented with some of the key solar field components, including water/steam separators and controls. DISS and INDITEP participants are collaborating on two new DSG projects: 1) the Puertollano GDV pre-commercial plant and 2) the REAL-DISS project. The Puertollano GDV pre-commercial plant will use 400 Eurotrough collectors to generate steam at 411^oC and 70 bar for a 3 MW Rankine power cycle with dry cooling [25]. A consortium of partners, including PERSEO, IDAE, CIEMAT, AGECAM and Navarro Piquer, initiated construction of this plant in October 2010, and

commissioning is scheduled for mid-2012. Iberdrola Renovables coordinates the project, which had a budget of 20.8 million Euros at the end of 2009 [51]. Figure 10 presents a simplified schematic of the Puertollano GDV pre-commercial plant.

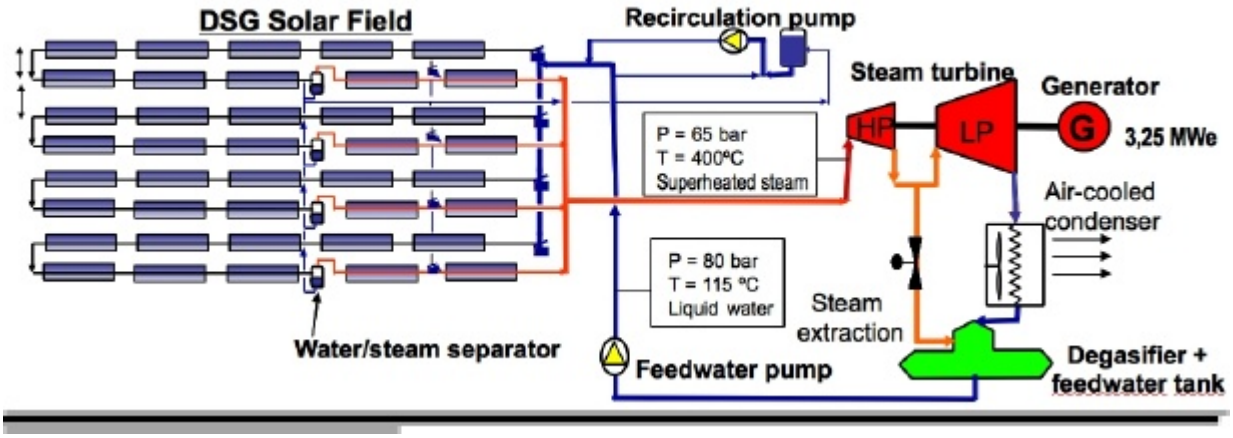

Figure 10 - Simplified Puertollano GDV Plant Schematic [51]

A consortium of German and Spanish partners, including ENDESA, Flagsol GmbH, MAN Ferrostal, Senior-Berghöfer, SCHOTT, Züblin, and Solar Millenium are developing the REAL-DISS project, which intends to demonstrate DSG at 500^{o}C and 100 bar and develop commercial components for future commercial-scale DSG plants. The first stage of this project, which was expected to end in 2009, involves designing components such as receiver tubes, receiver connectors, and an energy storage system, and testing them at the 1.1 GW ENDESA coal power plant in Carboneras, Spain under real operating conditions. Once this phase is complete, the next steps are a 5 MW demonstration plant and, eventually, a 50 MW commercial DSG plant [25].

Five DSG projects in different stages of planning and operation use the Solarlite collector, which is made of composite materials and a thin glass mirror [52]. The first is a co-generation power

plant called Woltow in Germany that operates a 40 kW turbine at 64-215^{o}C and 16.5 bar and provides heat for a fish farm. Two other trough DSG co-generation plants are planned for operation at 330^{o}C and 30 bar: Soneva Fushi (Maldive Islands) and Soneva Kiri (Thailand). These plants will also provide cooling and/or sea water desalination [25]. The Kanchanaburi power plant (KTSE-9100) in Thailand is expected to be the first large-scale DSG trough plant in Asia. A solar field area of 45,000 m^2 will generate steam at 330^{o}C and 30 bar for a 5 MW turbine and incorporate 62 MWh (approximately 3-4 hours) of thermal energy storage [53]. The plant is owned and will be operated by Thai Solar Energy, and it is expected to begin generating electricity for the grid in March or April 2011 [54]. The Suphanburi project, which is very similar to KTSE-9100, will begin operation in Thailand soon after Kanchanaburi is complete [53].

2.1.5.4 Organic Rankine Cycle (ORC)

Organic Rankine Cycle (ORC) uses an organic fluid, such as butane or pentane, instead of water in the power cycle and has been used traditionally with small applications that operate at lower temperature/pressure (i.e., geothermal power plants). Compared with a Rankine cycle, ORC has the following potential advantages for power plants ranging from 100 kW to 10 MW in size: simple design, lower capital cost of components, lower operational pumping parasitics, higher efficiency than more complex steam cycles operating at the same solar field outlet temperature, less need of on-site operations personnel, and reduced water consumption by about 98% compared to conventional CSP plants [23]. Saguaro, a 1 MW plant in Arizona, is the only commercially operating trough plant with ORC in the U.S.

2.1.6 Power Backup System

CSP plants can only operate with direct normal solar radiation and, therefore, require a backup system to respond to extended cloudy periods during the day, whether to enable the power cycle to continue to operate at full capacity or to enable the plant to shut down. Figure 4 shows three different backup systems that are currently being used at commercially operating parabolic trough plants: a natural gas-fired heater, a natural gas-fired boiler, and a thermal energy storage system. All trough plants currently use a heater for HTF freeze protection when ambient conditions threaten to solidify the HTF in the solar field. Some plants use this heater to provide backup capacity during cloudy periods and/or night time, and older plants use a natural gas-fired boiler to generate additional steam for the power cycle during evening peak demand hours. Several recently constructed power plants in Spain use a TES system, and this option is described in more detail in the following section.

A fourth option is ISCC, but this option is excluded from further consideration on the basis that it represents a different type of power plant. The backup systems depicted in Figure 4 can be used with a power plant that is designed to be primarily a solar power plant; whereas, ISCC represents a primarily fossil fuel-fired power plant that is adding solar capacity. Another backup system that is not depicted in Figure 4 is auxiliary electricity, which is required by all plants for equipment such as computers and controls that need to be operated 24 hours per day.

2.2 TES Technology

The term "thermal energy storage" encompasses the storage of hot or cold energy for later use. On the demand-side, "hot" TES is usually coupled with rooftop solar thermal collectors, which capture heat energy during the day to be stored in a hot water tank, and a "cold" TES system runs a chiller at night to generate ice, which is used during the day to produce chilled water for air conditioners. On the supply-side, the term is usually used to describe a system that stores the heat energy from a CSP plant in a solid or liquid medium. Many industry leaders see thermal energy storage (TES) as the "holy grail" of CSP because it smoothes out variation in solar power during the day and allows electricity generation to extend into nighttime peak demand hours (see Figure 11). Others criticize TES because it raises the already high capital cost of a CSP plant, increasing the difficulty in obtaining financing. There is a wide variety of ways TES can be implemented with CSP, and this section describes a selection of technologies that have been studied for decades and are already in operation or have the potential to be coupled with CSP plants in the near future. TES technologies can be categorized in three main ways: 1) by the type of storage material; 2) by the containment system used for the storage material; and 3) by the heat transfer process.

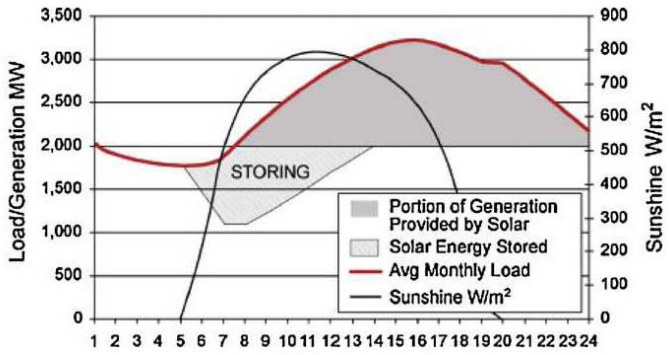

Figure 11 - Using Energy Storage to Meet Demand with CSP [55]

2.2.1 TES Storage Materials

Fernandez et al. categorize the chemical and physical properties of thousands of TES candidate materials that have been investigated in recent decades [56]. For simplicity, this section summarizes a selection of TES candidate materials that have been investigated for use in commercial parabolic trough applications. Currently-operating trough plants with TES use liquid storage materials, but many researchers are investigating solid and phase change materials for future trough plants. Liquid storage materials that are currently in use or have been used in the past with solar thermal applications include water, oil and molten salts. Water is currently suitable only for low-temperature applications due to its relatively low energy density and the need for costly pressurized tanks and insulation at higher temperatures [23].

Researchers have been investigating storage media and HTFs for CSP for decades. Table 4 presents a summary of demonstration projects implemented between 1981 and 1996. All of these projects used power towers to capture solar thermal energy, but were nonetheless influential in shaping future storage media research for trough plants. The first commercially operating parabolic trough plant (SEGS I - 1984) used mineral oil as the storage fluid. This TES system was damaged in a fire in 1999 and not replaced. Subsequently, trough plants switched to synthetic oil as the HTF in order to operate the steam cycle at higher temperatures. Synthetic oils are currently not suitable as storage material because they are too expensive, would require expensive pressurized storage tanks, and represent too great of a fire hazard at the operating temperature [23].

Table 4 - Summary of Early TES Storage Media Power Tower Demonstrations [57]

Project	Country	Power output (MWe)	Heat transfer fluid	Storage medium	Operation began
5SPS	Spain	0.5	Liquid sodium	Sodium	1981
EURELIOS	Italy	1	Steam	Nitrate salt/water	1981
SUNSHINE	Japan	1	Steam	Nitrate salt/water	1981
Solar One	USA	10	Steam	Oil/rock	19S2
CESA-1	Spain	1	Steam	Nitrate salt	1983
MSEE/Cat B	USA	1	Molten nitrate	Nitrate salt	1984
THEMIS	France	2.5	Hitec salt	Hitec salt	19S4
SPP-5	Russia	5	Steam	Water/steam	1986
TSA	Spain	1	Air	Ceramic	1993
Solai Two	USA	10	Molten nitrate salt	Nitrate salt	1996

Molten salts have become the CSP TES industry leader because they are non-toxic, have high operating temperatures and relatively high energy density, have low vapor pressures, and are relatively inexpensive (compared with oils) [58]. The term “molten salts” encompasses a variety of materials; the selection presented in Table 3 represents the salts that have been proven feasible with CSP in a number of studies and applications. Solar salt (otherwise known as nitrate salt) is currently preferred because it is the least expensive of the options, but it also has the highest freezing point, which leads to technical difficulties in maintaining the temperature of the salt above freezing in the pipes and tanks. All currently operating trough plants with TES use Solar Salt [47]. Researchers at Sandia Laboratories are investigating the chemical and physical properties of several varieties of molten salts with the overall goal of identifying a cost-effective composition with a lower melting point than commercially available molten salts [58].

The term “ionic liquids” is a term that generally describes a group of organic and semi-organic salts in order to distinguish them from the more advanced (in terms of time and money spent on

research and development) “molten salts” in TES research. Chemists make the distinction between these groups mainly through the selection of a rather arbitrary melting point limit, which may be subject to change in the future. The term “ionic liquids” generally refers to a group of salts with melting points below 120^{o}C, whereas the term “molten salts” describes a group of salts with melting points above this threshold. The names can be a bit misleading since molten salts are also ionic, and ionic liquids are also molten salts. Furthermore, although molten salts are usually inorganic and ionic liquids are mostly organic, some ionic liquids are inorganic [40].

Table 5 presents the cost and average volumetric heat capacity at 400^{o}C of several solid media that have been the subject of CSP TES research. Concrete has been the subject of most recent solid media CSP TES investigations due to its relatively low cost and acceptable heat capacity [34]. In this system, an array of pipes is built into the solid storage structure and the heat fluid passes through them, transferring the thermal energy to and from the concrete (see Figure 12). Two concrete storage systems were tested at the storage test facility at the Center for Solar Energy and Hydrogen Research ZSW in Stuttgart, Germany between 1991 and 1994. The results of these tests showed that the highest uncertainty with a concrete thermal storage system is the long-term stability of the concrete after thousands of charging cycles [23].

Table 5 - Characteristics of Solid Media for CSP TES [34]

Storage Medium	Average Heat Capacity kWh_t/m^3	Media Cost US$/kWh_t
Reinforced concrete	100	1
NaCl (solid)	100	2
Cast iron	160	32
Cast steel	180	150
Silica fire bricks	60	18
Magnesia fire bricks	120	30

Figure 12 - Concrete Thermal Energy Storage System [59]

Laing et al. [60] designed and tested two different 350 kWh solid media storage systems with a parabolic trough collector loop up to 390°C at Plataforma Solar de Almeria in Spain. One of the systems used castable ceramic as the storage medium, and the other used high temperature concrete. Results showed the concrete to be preferable because it had lower cost, higher material strength, and it was easier to handle. However, the ceramic had the following advantage of higher storage capacity and higher thermal conductivity. The overall results of this project, called WESPE, indicated that a solid media storage system is technically feasible at a total cost of 20 euros/kWh thermal capacity [61].

The German Aerospace Center (Deutches Zentrum fur Luft-und Raumfahrt e.V - DLR) implemented a follow-up project called WANDA, through which they examined the cost associated with the external equipment needed for a concrete TES system, and compared the levelized cost of electricity (LCOE) and environmental profile of a trough plant with molten salt storage to a plant with concrete storage. This analysis indicated that the use of a concrete TES system could reduce LCOE by about 2% and reduce environmental impacts compared to the molten salt system [62]. Currently, there are no large-scale commercially operating trough plants with concrete TES, as the technology is still considered to be experimental.

The solid and liquid storage materials discussed above store sensible heat, or heat generated through a change in temperature. Phase change materials (PCMs), on the other hand, enable the storage of latent heat in the form of heat of fusion (solid-liquid transition), heat of vaporization (liquid-vapor), or heat of solid-solid crystalline phase transformation. PCM TES systems are attractive because they can be smaller in size (lower cost) than sensible heat TES systems since the energy density can be higher; however, unresolved issues include: more complicated heat transfer design, difficulty in selecting appropriate storage materials, and degradation after several phase change cycles [34]. Although PCMs have not yet been demonstrated with conventional trough plants, they have a promising future in DSG research [63],[64].

2.2.2 TES Containment System

The containment for the TES system is determined by the storage media: a solid TES system is contained in the solid media, and there is a wide variety of containment options for PCMs [65]. Liquid TES containment systems generally come in two forms: single-tank and two-tank. The

simplest and most widely used design currently is the two-tank system, which involves one tank (or set of tanks) for the cold fluid and one tank/set for the hot fluid. The single-tank configuration is called the "thermocline" because it stores the hot and cold fluids in a single tank with a thermocline region in between to separate the two temperatures. The advantage of this system is that it most of the storage fluid can be replaced with low-cost filler material. The main challenge is in maintaining the thermal integrity (proper temperature difference between hot and cold storage fluids) of the thermocline zone [59]. Sandia National Laboratory's National Solar Thermal Test Facility demonstrated that a filler material comprised of quartzite and silica sand can replace about two-thirds of the salt required for a two-tank thermal storage system (see Figure 13). The thermocline maintained its integrity for three days while the plant was not in operation during this experiment, and the results of further analysis showed that it has the potential to be up to 35% cheaper than the two-tank storage system [23].

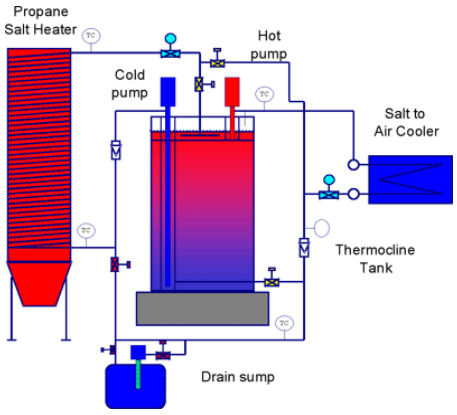

Figure 13 - Thermocline Storage System Demonstrated by Sandia National Laboratory [59]

An oil-based thermocline TES system was demonstrated to work well at Solar One from 1982-1988 [55]; although, this project resulted in fires due to the mineral oil storage fluid, and there were problems integrating the system with the power tower steam cycle [23]. The National

Renewable Energy Laboratory (NREL) has continued the work conducted by Sandia to conduct computational fluid dynamics modeling of thermocline tanks and the heat transfer between solid filler material and molten salt. Due to operational issues that still need to be resolved with thermocline systems, NREL advocates the use of a two-tank system in near-term CSP plants [66].

2.2.3 TES Heat Transfer Process

There are two main options for the heat transfer process in a TES system: indirect and direct. An indirect system uses a heat exchanger to transfer heat from the HTF to the TES system (see Figure 4), and a direct TES system stores the HTF directly without the use of a heat exchanger (see Figure 14). Most current systems are indirect due to the issues associated with molten salts as HTFs and oils as storage fluids (see sections 2.1.4 and 2.2.1, respectively). However, direct systems are expected to improve power plant performance and cost by eliminating the efficiency penalty and capital cost associated with the heat exchanger.

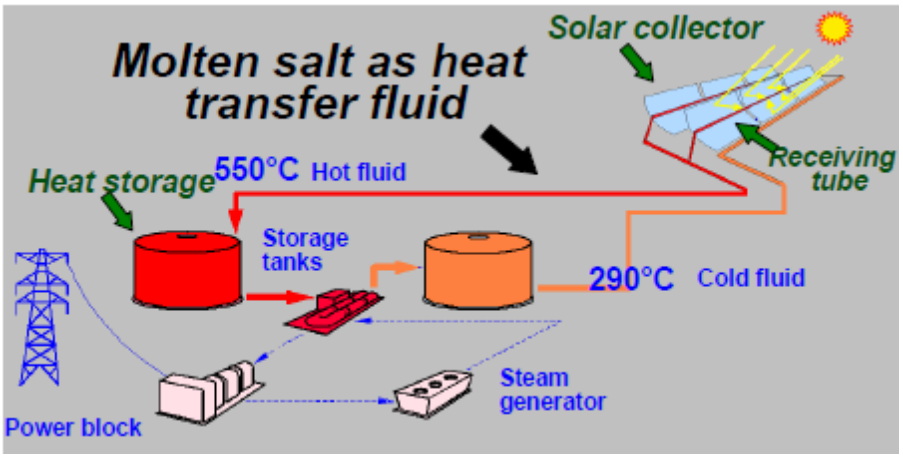

Figure 14 - Diagram of a Direct TES System [32]

2.2.4 Commercially-Operating TES Systems

Despite the variety of TES options that have been researched for decades, only two TES technologies are in use in commercially-operating trough plants: two-tank indirect molten salt and two-tank direct molten salt. The first technology has been operating commercially since 2008, and is employed in five trough plants in Spain with a combined turbine capacity of 250 MW and 37.5 hours of energy storage (see section 2.3). The second technology has been operating since 2010 in Italy at a turbine capacity of 5 MW and 8 hours of storage. Roughly 10% of global trough capacity under construction/development includes plans for TES: nine plants (total capacity - 450 MW) will be located in Spain, and 1 plant (Solana – 280 MW) will be in the United States.

2.3 History and Current Status of Parabolic Trough and TES

Luz International Limited built the first commercial parabolic trough (PT) solar thermal power plant in the Mojave Desert in 1985, and installed eight more solar electric generating stations (SEGS) by 1991. Today, these nine SEGS plants have a combined capacity of 354 MW, and their daily operation over the last two decades has enabled much research and development in parabolic trough technology. Luz attempted to build a tenth plant but ended up filing for bankruptcy because they could not secure construction financing, and the cost of the technology became too high to compete with declining energy costs and reduced federal incentives for renewable power [23]. SEGS I and II are now owned by Cogentrix [67], and SEGS III through

IX are owned by Nextera Energy [68]. From 1985 to 2001, SEGS gross production was approximately 8.3 gigawatt-hours (GWh) [10].

Table 6 summaries key characteristics of the SEGS plants and the other seventeen PT plants now in operation around the world. After Luz went bankrupt, PT development ceased until 2006, when Arizona Public Service installed a 1 MW operation called Saguaro in order to help the utility meet the goals of the Arizona Corporation Commission's Environmental Portfolio Standard [69]. The following year, Nevada Solar One began selling PT-generated electricity to Nevada Power Company and Sierra Pacific Power to help these utilities meet the requirements of the Nevada renewable portfolio standard [70]. In 2007, Spain enacted Royal Decree 661, which granted a fixed tariff of 0.269375 Euro/kWh for CSP plants up to 50MW for 25years [71]. This legislation began a wave of PT installations in Spain beginning with Andasol 1 in 2008, and continuing today with 600 MW of PT capacity currently operating in Spain. Italy and Iran followed suit to contribute to a current global PT operational capacity of approximately 1 GW. In addition to the current operations displayed in Table 6, there are nearly 19 GW of CSP capacity under construction or development worldwide [3].

Table 6 - Current Parabolic Trough Plants[3]

Plant Name	Location	Owner	First Op. Year	Turbine Capacity (MW)	Solar Field Area (acres)	Total Land Area (acres)	Annual Output (GWh)	CF[4]	Backup System[5]	Cap. Cost ($2010/ kWe)[6]
SEGS I-II	Daggett, CA	Cogentrix Energy, LLC	1984-1985	43.8	68	217 [73]	111 [23]	29%	NG boiler (25%) [19]	Un-known
SEGS III-IX	Kramer Junction & Harper Lake, CA	NextEra Energy Resources	1987-1991	310	505	2,000 [68]	970 [23]	36%	NG boiler (25%) [19]	$5,945 [23][7]
Saguaro	Tucson, AZ	Arizona Public Service	2006	1	3	14 [74]	2	23%	Un-known	$6,490 [74]
Nevada Solar One	Boulder City, NV	Acciona Energy	2007	64	88	400	134	23%	NG heater (2%) [19]	$4,108 [70]
Andasol 1 & 2	Granada, Spain	ACS/Cobra Group	2008-2009	100	252	988	316	36%	7.5 hr TES; NG heater (12%)	$8,496 [75]
Alvarado I	Badajoz, Spain	Acciona Energy	2009	50	90[8]	321 [76]	105	24%	Un-known	$6,684 [77]
Ibersol Ciudad Real	Puertollano, Spain	IBERCAM	2009	50	71	371	103	24%	NG heater	$5,308
Shiraz	Iran	Un-known	2009 [78]	0.25 [78]	1 [79]	Un-known	Un-known	Un-known	fossil fuel [79]	Un-known
Archi-mede	Sicily, Italy	ENEL	2010	5	8	20	9	21%	8 hr TES; NG heater; ISCC	$15,250 [80]

[3] Except where indicated, the data in Table 6 were obtained from: [47] (February 18, 2011, March 8, 2011). *NREL: Concentrating Solar Power Projects - Parabolic Trough Projects*. Available: http://www.nrel.gov/csp/solarpaces/parabolic_trough.cfm

[4] CF = Capacity factor; calculation: (Annual Output x 1,000)/(Turbine Capacity x 8,760 hours)

[5] Backup systems: percentages in parentheses indicate the maximum amount of thermal input that can come from natural gas; "NG boiler" refers to a natural gas-fired boiler that is used to add steam to the power cycle; "NG heater" refers to a natural gas-fired heat transfer fluid (HTF) heater that is used to raise the temperature of the HTF; "TES" refers to a thermal energy storage system and "hr" refers the number of hours the thermal energy from the TES system can run the power cycle with no solar input; "ISCC" = Integrated Solar Combined Cycle

[6] Capital cost figures were obtained from the references cited and converted to $2010 using the CPI Inflation Calculator ([41] BLS. (March 10, 2011). *U.S. Bureau of Labor Statistics: CPI Inflation Calculator*. Available: http://www.bls.gov/data/inflation_calculator.htm) and the average $US per Euro exchange rate ([72] (March 10, 2011). *x-rates.com: American Dollars to 1 Euro*. Available: http://www.x-rates.com/d/USD/EUR/hist2009.html) for the year in which the capital cost was cited.

[7] Assumption: SEGS III-VI had the same cost per kWe, and SEGS VIII and IX had the same cost per kWe.

[8] Solar field area calculation: 768 x 470m^2 x 2E-04 acres/m^2; where, 768 = the number of solar collectors (manufactured by Acciona) and 470 = the aperture area of the solar collectors at Nevada Solar One (also manufactured by Acciona)

La Florida	Badajoz, Spain	Renovables SAMCA	2010	50	137	544 [81]	175	40%	7.5 hr TES; NG heater (12%)	Un-known
Majadas I	Majadas de Tiétar, Spain	Acciona Energy	2010	50	100 [82]	334	105	24%	NG heater (15%) [82]	$6,290 [82]
Martin Next Gen. Solar Energy Center	Indiantown, Florida	Florida Power & Light	2010	75	131[9]	500	155	24%	ISCC	$6,351
Palma del Río II	Córdoba, Spain	Acciona Energy	2010	50	100[10]	334	115	26%	Un-known	$6,661 [85]
Solnova 1, 3, 4	Sevilla, Spain	Abengoa Solar	2010 [86], [87]	150	222	853	344 [88]	26%	NG heater (15%) [88]	$7,448[11] [89]
Extresol 1 & 2	Badajoz, Spain	ACS/Cobra Group	2010-2011 [90], [91]	100	252	988	316	36%	7.5 hr TES; NG heater (12%)	$7,961 [91], [90]

As mentioned in Chapter 1, all PT plants require a backup system of one kind or another. Table 6 summarizes the backup systems used in each currently operating PT plant. The SEGS plants use a natural gas-fired boiler to provide up to 25% of the thermal energy input to the power cycle. Twelve of the newer generation PT plants use a natural gas-fired heat transfer fluid (HTF) heater to raise the temperature of the HTF during periods of low or no solar radiation. This type of heater supplies 2-15% of the thermal input to the power cycle depending on the specific plant. Many people refer to PT plants with these two types of backup systems as "solar only", which is a misnomer since natural gas is also used in the energy generation. In reality, PT plants with NG boilers or NG heaters are solar-fossil hybrid operations even if they are on the low end of the

[9] Solar field area calculation: 190,000 x 2.8 m^2; where, 190,000 = approximate number of mirrors [83] FPL. (March 10, 2011). *FPL's Martin Next Generation Solar Energy Center: World's First Hybrid Solar Energy Center*. Available: http://www.fpl.com/environment/solar/pdf/Martin.pdf, and 2.8 m^2 = estimated mirror aperture area [84] FLABEG. (2010, March 10, 2011). *MIRRORS FOR PARABOLIC TROUGH*. Available: http://www.flabeg.com/index.php?id=142&L=1

[10] Assumption: Palma del Rio II has the same solar field area as Majadas I since both have the same number of solar collectors and are owned by the same company

[11] Assumption: cost of Solnova 1 = cost of Solnova 3 = cost of Solnova 4

hybrid spectrum (2% input). On the higher end of the hybrid spectrum are the two Integrated Solar Combined Cycle (ISCC) plants listed in Table 6: Archimede in Italy and Martin Next Generation Solar Energy Center in Florida. These two plants use the steam generated by the solar field in the bottoming cycle of a natural gas combined cycle plant. Archimede is unique in that it is the first commercially-operating plant to use molten salt as the HTF and to combine a TES system with ISCC. Five other plants listed in Table 6 incorporate a TES system, but these plants all use synthetic oil as the HTF in the solar field and molten salt in the TES system.

The technical differences and variety of locations associated with the currently operating fleet of PT plants make it difficult to calculate meaningful average characteristics such as capacity factor or cost. However, most of the newer generation plants can be categorized according to three main backup technologies: 1) NG heater (12-15%); 2) 7.5 hr TES with NG heater (12%); and 3) unknown. Four plants use a NG heater capable of providing up to 12-15% of the thermal input to the power cycle: Majadas I and Solnova 1, 3, and 4. Five plants incorporate a NG heater with up to 12% thermal input and a two-tank molten salt indirect TES system capable of running the power cycle at full-rated capacity for up to 7.5 hours without any solar input: Andasol 1 and 2, La Florida, and Extresol 1 and 2. There was no information in the available literature about the specific backup system for four plants: Alvarado I, Ibersol Ciudad de Real, Palma del Río II, and Saguaro. Although the details of the backup system for these plants are unknown, it is unlikely that they incorporate TES because plants that do incorporate TES tend to advertise it to show they are using cutting edge technology. The plants with an "unknown" backup system, therefore, likely use a natural gas heater, but the percentage of thermal energy input that comes from natural gas is unknown.

Figures 15 and 16 display the average capacity factor and average capital cost, respectively, of the 14 currently operating PT plants that could be classified according to their backup technology. Figure 15 indicates that currently operating PT plants with storage and natural gas backup have capacity factors up to 12% points higher on average than plants with just natural gas backup and no thermal storage. Figure 16 indicates that on average, current plants with TES cost approximately 20% to 30% more than plants without TES. The fact that the capacity factor and cost of the plants with unknown backup systems are so similar to the capacity factor and cost of the plants with NG heaters lends support to the speculation that plants in the "unknown" category probably use a NG heater.

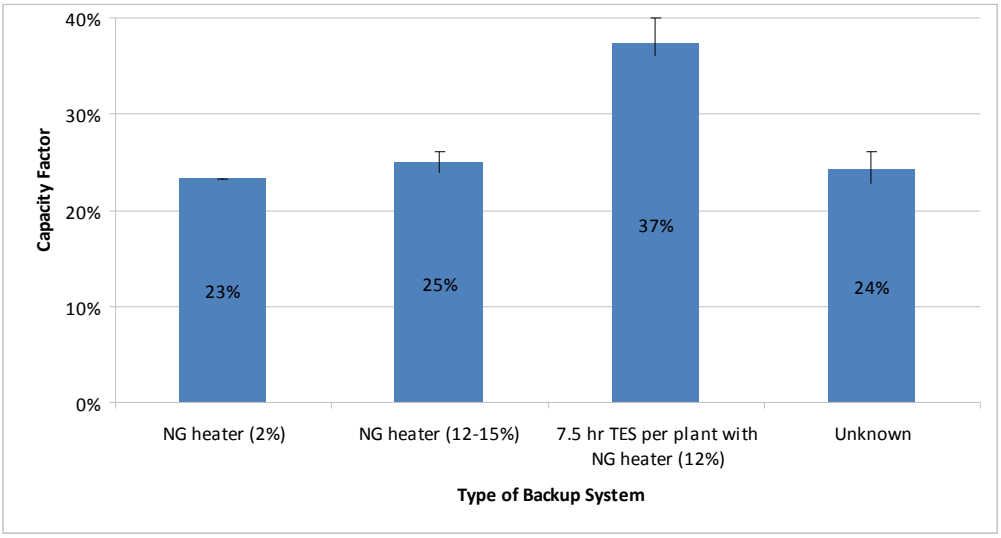

Figure 15 – Average Capacity Factor of Current PT Plants

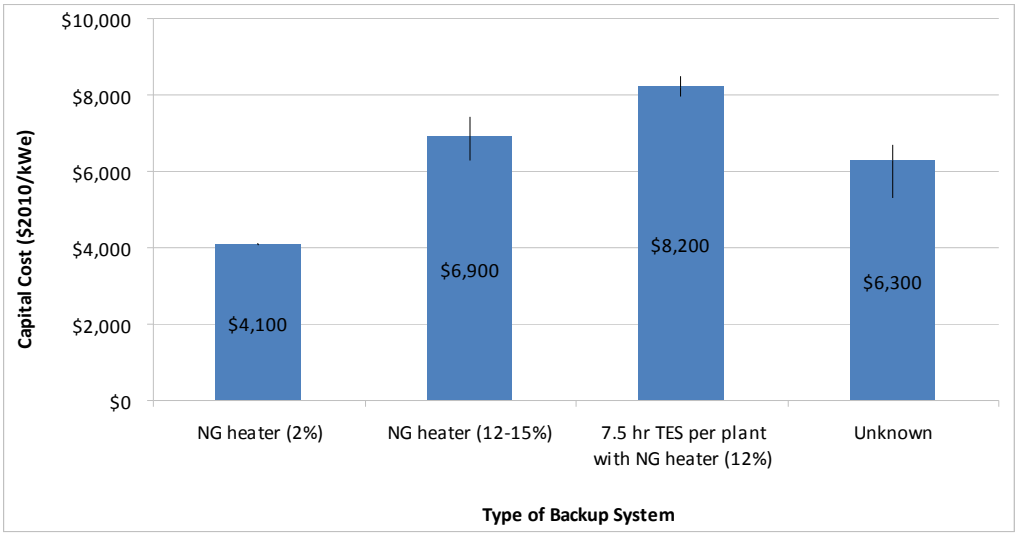

Figure 16 – Average Capital Cost of Current PT Plants

Thermal energy storage has been an integral part of CSP since the first commercial parabolic trough plant, SEGS I, began operating in 1984. SEGS I initially operated with a direct two-tank TES system that stored the HTF (a mineral oil called Caloria) for up to three hours of backup energy [Advances in CSP]. This system was damaged in a fire in 1999 and never replaced [NREL power plant data website]. Newer plants began using a synthetic HTF called Therminol VP-1 in place of Caloria because it could operate at higher temperatures (up to 400°C versus up to 307°C with Caloria). This choice precluded future TES systems similar to SEGS I because Therminol VP-1 is eight times more expensive than Caloria [Survey of Thermal Energy Storage for PT Power Plants]. Herrmann and Kearney [Survey of Thermal Energy Storage…] summarize the state of TES research as it applies to CSP through 2002, and conclude that "the most cost-effective near-term option for thermal storage for parabolic trough power plants is currently a two-tank storage system, with molten salt as storage medium". This conclusion appears to have been accepted and echoed by the CSP industry at large as the only commercially operating CSP plants with storage today use a two-tank molten salt TES system. Greentech

Media maintains an up-to-date list of CSP projects under development and/or construction throughout the United States [92]. Only 1 trough plant under development in the U.S. includes plans to incorporate TES, while nine planned trough operations will use TES in Spain [3]. There has been speculation that this discrepancy is due to the different incentive structures in each country, a topic that will be explored more in later chapters.

2.4 Engineering-Economic Analysis of PT and TES

In the past three decades, several models have been developed to estimate the performance and cost of parabolic trough CSP and TES [93]. However, very few of them are currently available for public use. NREL developed a spreadsheet-based model of trough performance and cost, called Excelergy [94], which was used for several in-house studies between 2002 and 2006. A study conducted by KJC Operating Company and Sandia on the SEGS plants [95] describes some physical and economic parameters specific to the SEGS plants that served as the basis for Excelergy. The objective of this study was to reduce the operation and maintenance (O&M) costs at the SEGS plants. O&M technologies were developed and tested at the Kramer Junction SEGS plants in Boron, CA. Annual O&M costs were reduced by 37% (from about $0.04 to $0.025/kWh) and an optimum solar field O&M plan for future CSP plants was developed based on the lessons learned through the study.

An NREL study prepared by Nexant and Pilkington Solar International GmbH (now Flabeg Solar) [46] examined two potential approaches for improving the economic feasibility of trough plants, using models developed by Pilkington, which were incorporated in the development of Excelergy. The first approach was TES, and the second was ISCC. The study was divided into

five tasks: 1) Survey of TES; 2) TES for Rankine Cycle; 3) Preferred ISCC Configuration; 4) Annual Performance of Integrated ISCC with TES; and 5) Annual Performance of Integrated ISCC without TES. During the first task, they examined several TES concepts in the temperature range of 200-425ºC, and concluded that molten salt and concrete TES systems should have priority for near term deployment based on the cost and state of technology at the time. The study conducted for the second task identified a preferred near-term TES concept for a 55 MW trough plant located in southern California desert with a storage capacity of 440 megawatt-hour thermal (MWht) (3 hours). The results showed that a two-tank direct oil TES system offered the best combination of predictable performance, thermal efficiency, and capital cost, but a two-tank direct salt system offered the best combination of predictable performance and low technical risk.

The third task involved the evaluation of nine ISCC plant concepts with the goal of selecting a potential ISCC design for near term projects. The conceptual designs were developed using GateCycle™, and the preferred design used a 125 bar single reheat steam cycle with variable live steam conditions. Task 4 involved estimating the performance of various ISCC plant configurations based on the design selected in Task 3 at a Barstow, California site. LCOE was calculated for 12 modeled configurations at a range of $127-178/MWh, using a solar field size that minimized the LCOE. Task 5 examined the potential for annual solar contributions as high as 20 percent in ISCC plants by integrating a two-tank molten salt TES system with ISCC at LCOEs in the range of $128-223/MWh. This study proved the technical feasibility of the ISCC-TES system design and analyzed the results with varying TES capacities and solar field sizes. The results showed that the solar share could be increased from 8.2 to nearly 17 percent by

integrating a 16 hour TES system, achieving 24-hour operation at design capacity during summer periods. During the course of completing these specific tasks, Nexant and Pilkington also developed estimates for the solar collector field and associated equipment and analyzed the effects of plant design parameters and fuel types on carbon dioxide emissions from ISCC plants.

Kelly, B. and Kearney, D. [96] describe in detail a spreadsheet piping model they developed for Excelergy, and several other studies describe cost estimations that have been performed using the program. Kearney et al. [37] report on an investigation of the feasibility of using parabolic trough technology with molten salt as the heat transfer and storage fluid. This study showed that the levelized cost of electricity (LCOE) of a trough power plant could be reduced by 14% by using a two-tank direct TES system at an operation temperature of 450^{o}C. This paper indicates that Excelergy was based on earlier programs developed by Flabeg and Luz.

Sargent and Lundy [10] was selected by the U.S. Department of Energy to conduct an independent "due-diligence-like" analysis of the cost and performance of parabolic trough and power tower solar technologies, to be compared with similar results from Sunlab that used Excelergy. Sunlab is a cooperative virtual laboratory created by NREL and Sandia National Laboratories [97]. The Sargent and Lundy study concluded that CSP technology is a proven technology for energy production, there is a potential market for CSP technology, and significant cost reductions are achievable if CSP is deployed at a reasonable rate and incentives are maintained to reach market competitiveness. The study estimated initial trough subsidized electricity costs to be about $130/MWh, and future costs (in 2020) to be $62/MWh (both values are in $2002 and include a 10% investment tax credit and accelerated depreciation). These costs

were similar but slightly larger than the Sunlab/Excelergy estimates, which included the same financial assumptions. Sargent and Lundy reported that these cost reductions could be achieved through aggressive deployment scenarios, plant scale-up, and technological advance.

Price, H. and Kearney, D. [98] review the cost of energy and potential for reducing the cost of energy from trough plants, and concludes that there is significant opportunity for reducing the cost by increasing plant size and incorporating several advanced technologies, including larger collectors, improved receiver selective coatings, and advanced thermal storage technologies. They also note that financial and market incentives and other approaches such as hybridization or ISCC might be necessary to encourage near-term development and set the stage for accelerated trough growth. The results indicate a trough LCOE of $110/MWh (in $2002), which is expected to decrease to $90/MWh with advanced technologies. These cost estimates appear to be derived from Excelergy.

In 2004, NREL subcontracted the Center for Business and Economic Research at the University of Nevada to investigate possible economic impacts from different levels of investment in CSP generation in the state of Nevada. Schwer, R.K. and Riddel, M. [99] use costs presented in the Sargent and Lundy study to examine three deployment scenarios by varying the number of 100-MWe trough plants constructed and operated in the state. They conclude that developing the state's solar resources will have a significant, positive effect on Nevada's economy, and the degree of impact depends on the scenario and the timing of the construction and operations and maintenance (O&M) schedule.

Around the same time as the Nevada study, Black & Veatch Corporation conducted a CSP feasibility study for the state of New Mexico [100]. The study objective, as defined by Governor Richardson's CSP Task Force, was to "identify a viable commercial CSP project of 50 MW or larger that could be in operation by 2007". Black & Veatch assessed the commercial viability of several CSP technologies based on the following factors: development status, risk assessment, equity requirements, water issues, equipment reliability, storage options, O&M costs, siting requirements, industry capability and depth, performance, cost of energy, and transmission considerations. The team used cost and performance data from SunLab and from vendors, and identified a 50 MW trough plant in southwest/central New Mexico as the most favorable option at a LCOE of $89 to $117/MWh (including a 10% federal investment tax credit, accelerated depreciation, $0.02/kWh state production tax credit, a property tax exemption, a GRT exemption, and a state-sponsored partial performance guarantee). However, they conclude that this LCOE is still nearly double the wholesale price of electricity, which means that load serving entities would have to purchase CSP electricity at an above-market rate to induce the commercial development of a CSP plant in New Mexico by 2007. The report states that one 50 MW CSP plant built in New Mexico would increase net state tax revenues by $70 million if New Mexico provided the full set of state incentives.

Kelly [101] conducted an analysis for NREL to determine the effect of Rankine cycle capacities greater than 80 MWe on the LCOE of trough plants. This study used GateCycle™ to develop performance models for three Rankine cycles: 88 MWe, 165 MWe, and 220 MWe. Kelly used the Excelergy optimization function to determine the preferred "solar multiple" for each plant as a solar-only project without thermal storage and as a solar-fossil hybrid project with a natural

gas-fired HTF heater. The solar multiple is a coefficient to The solar field piping model developed by Kelly, B. and Kearney, D. [96] had been integrated into Excelergy by this time, and the LCOE for each case were estimated using the default cost values in the program. This study indicated that LCOE decreased with increasing plant capacity for both plant types (solar-only and hybrid), and the lowest LCOE occurred with a net plant capacity of 220 MW at $140/MWh for the solar-only plant and $147/MWh for the hybrid plant.

Kelly [102] performed a follow-up study, which incorporated an economic analysis of a 80 MW trough plant located near Barstow, CA to determine the preferred design conditions for a dry cooling tower and the anticipated increase in LCOE that could result from using a dry cooling system instead of a wet cooling system. He used GateCycle™ to create 6 different dry cooled models with different initial temperature differences, and calculated the turbine output and cooling fan power demand for each dry cooled configuration and for a reference wet cooled plant. Kelly also estimated the annual plant performance and capital cost of the air cooled condenser and developed Excelergy equations to estimate Rankine cycle performance as a function of dry bulb ambient temperature. The annual net electricity and water consumption for all 7 configurations was estimated at ambient temps from 40-130^{o}F. Capital and O&M costs were developed for the 7 plants and used as inputs to an annual cash flow analysis to calculate LCOE, which ranged from $127/MWh (wet) to $141/MWh (dry). The overall conclusion of this study was that dry heat rejection imposed a nominal 8-9% penalty on LCOE, which could be reduced to 7-8% with further optimization efforts, but the results depend heavily on the cost of water (Kelly assumed $1.4 per 1000 gallons).

In a separate study, Kelly and Kearney [103] used GateCycle™ and Excelergy to compare the effect of different heat exchanger areas and TES capacities on the performance and cost of a 50 MW trough plant operating with a two-tank indirect molten salt TES system. This study concluded that this type of TES system could help reduce the plant's LCOE, but the lowest cost TES design will not necessarily result in the lowest LCOE (calculated in the range of $10-12/MWh). Therefore, it is essential to conduct a detailed analysis of the system design in order to determine the optimum TES configuration and solar field size for a given set of objectives.

Stoddard et al. of Black and Veatch [104] were contracted by NREL to assess the potential economic return, energy supply impact, and environmental benefits of CSP for the State of California. This study used Excelergy data to calculate an LCOE of $148/MWh for near-term CA trough installations (including incentives) and $115/MWh for CSP plants installed in 2015. The representative plant design in this study was a 100 MW trough plant with 6 hours of TES. These costs were found to be competitive with simple cycle natural gas-fired combustion turbines, commonly used as "peakers" in CA, which Black and Veatch calculated to have an LCOE of $168/MWh. Black and Veatch concluded that CSP investment delivers greater economic and employment returns to California than corresponding investment in natural gas equipment. More specifically, each dollar spent on CSP could contribute approximately $1.40 to California's Gross State Product (GSP); whereas, each dollar spent on natural gas plants was estimated to contribute about $0.90 - $1.00 to GSP. The results of this study were based on the following financial assumptions: 30 yr economic life, 5 yr tax life, 42.5% debt percentage, 8% cost of debt, 12.7% cost of equity, 9.3% weighted average cost of capital (WACC – used as discount rate), 40.75% tax rate (state and federal combined), 11.8% levelized fixed charge rate,

30% and 10% ITC, 2.5% inflation rate, real discount rate 6.8%. The study also assumed no natural gas purchase for the CSP plant. The future CSP cost projections were based on "learning curves" that describe the reduction in capital and operating costs observed as more CSP plants are deployed. These learning curve cost reductions relate to technology advances, scale up, effects of mass production resulting from large scale deployment and improvements in construction efficiency.

Cavalcanti and Petti [105] describe a performance model they created to estimate the potential for trough technology to generate electricity in the semiarid area located at the Brazilian northeast region, throughout the São Francisco river basin. They simulated the performance of a 30 MW SEGS-like power plant using experimental solar irradiation and a Microsoft Excel model based on the TRNSYS STEC library, SEGS VI data, and the methodology employed by Excelergy. The results indicate that 94,190 MW installed capacity is feasible for this region.

In 2004, NREL, Sandia, and the U.S. DOE Solar Energy Technologies Program (SETP) began collaborating to develop the Solar Advisor Model (SAM), which is an open source software program that models the performance and cost of CSP and other energy technologies [106]. SAM was originally based on Excelergy and the Transient Systems Simulation program (TRNSYS), developed at the University of Wisconsin to model thermal and electrical energy system components. TRNSYS is a commercially available program that includes a special trough library developed by DLR and Sandia National Laboratory [107]. Since TRNSYS is a performance-only model, it requires the development of a separate cost model that is compatible with the TRNSYS software to calculate LCOE. Excelergy was integrated into SAM for this

purpose, and early versions of SAM calculated the LCOE of trough plants based on empirical data and analysis from the SEGS plants [108].

In 2008, at the outset of this study, I conducted a parametric analysis in SAM version 2.0 to observe how changes in TES inputs affect performance and cost outputs, and this analysis revealed three inconsistencies between the model and literature: 1) changes in the type of storage fluid and type of TES had no effect on the model outputs, 2) the model made no adjustment to solar field size with increased TES capacity, and 3) SAM used a flat cost per kWh for TES ($40). Price et al. [23] report that direct TES may increase plant efficiency and reduce cost, and solar field size must increase to adjust for increasing TES capacity. Kelly, B. and Kearney, D. [103] report a range of TES costs from $26-80/kWh. Between 2008 and 2010, several new versions of SAM were released with each version improving on the accuracy and flexibility of the model and the documentation.

Between 2008 and 2010, several new versions of SAM were released with each version improving on the accuracy and flexibility of the model and the detail of the documentation. In 2010, SAM developers recognized the limitation in the software to predict the performance and cost of new technologies or component configurations since the original software was based on top-level empirical performance curves specific to the SEGS plants. Therefore, a new version of SAM was implemented by NREL to augment the Excelergy-based empirical model by including a new "physical" trough model derived from physical first principles. The physical trough model matches the annual performance of the empirical model, adds flexibility in modeling

different system configurations, and enables more detailed performance calculations in the major system components [108].

SAM has also evolved to incorporate a dry cooling option and updated costs developed by WorleyParsons [43], [45]. Turchi et al. [109] summarize the analyses WorleyParsons conducted on trough cooling technologies and describe how the systems were integrated with and validated by SAM. The results indicate that switching from 100% wet to 100% dry cooling results in LCOE increases of approximately 3% to 8% for 100 MW parabolic trough plants throughout most of the southwestern United States. The LCOE was calculated to be $173-$186/MWh for the wet-cooled case and $177-$195/MWh for the dry-cooled design. The authors concluded that adding TES can reduce the negative impact of dry cooling on LCOE. For example, the paper shows that replacing wet cooling with dry cooling in a trough plant with no storage in Las Vegas increased LCOE by $9-15/MWh, and the increase in LCOE between the same plants with 6 hours of storage at the same location was $8-$12/MWh. In this example, adding storage reduced the increase in LCOE associated with dry cooling by 11-23%. In addition, in all cases modeled in the study, the transition from wet to dry cooling reduced water consumption by over 90%. The study noted that hybrid cooling can reduce the LCOE increase (LCOE = $178-$189/MWh for the hybrid option), but at a higher capital cost and operational complexity.

Wagner and Kutscher [110] describe a hybrid wet/dry cooling model (see Figure 17) created for use with the physical trough model in SAM, but not yet publicly available. They use this model to explore the effect of various hybrid cooling technology specifications on revenue for trough plants in four representative locations of the American Southwest. The paper also introduces a

cost model that was developed to estimate the additional expense associated with a hybrid plant. Key assumptions used in this study include: 6 hours of full-load thermal storage, a solar multiple of 2.0, a solar field area of 910,500 m^2, power block gross output rating of 110 MW, and 35.48% thermodynamic cycle efficiency. The results of this analysis show that the hybrid cooling system reduces water consumption significantly compared to wet cooling while providing a noticeable improvement in bid price compared to dry cooling, where bid price is a combined metric of plant performance with respect to cost, revenue, profitability, and utility rate factors. Hybrid cooling during peak demand periods can reduce the bid price penalty for dry cooling by up to 2% in hot climates.

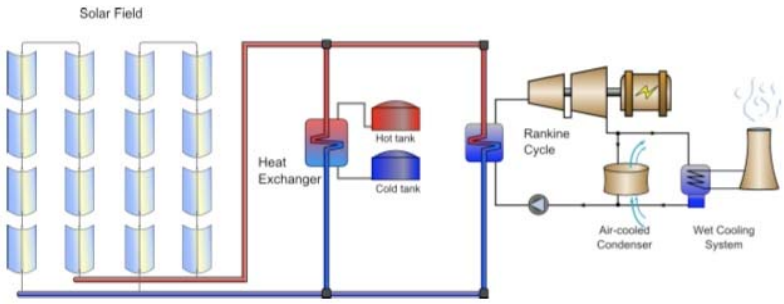

Figure 17 - Diagram of a Trough Plant with a Hybrid Cooling System [110]

Turchi et al. [111] use SAM to estimate the current and future costs for parabolic trough and molten salt power towers in the US market. By assuming that future trough plants (2015-2020) will achieve higher field temperatures by deploying molten-salt heat transfer fluids with low melting-points, they find that the LCOE for both technologies will drop below $110/MWh (assuming a 10% investment tax credit and other financial inputs outlined in the paper). They also conclude that both technologies can be deployed with large amounts of TES, yielding capacity factors as high as 65%, while maintaining an optimum LCOE.

Sioshansi and Denholm [112], use a mixed-integer program (MIP), which is based on SAM Version 2.0, to examine the value of CSP and TES in several regions of the southwestern U.S. The model optimally dispatches CSP with TES into existing electricity markets in Texas, California, Arizona and New Mexico for maximum net revenue from energy sales, in order to examine how the potential operating profits of a 110 MW trough plant vary with plant size. The study describes the sensitivity of the results to the optimization process selected, the plant cooling technology, and the possibility of selling ancillary services. Profit is defined as revenue from energy sales less variable costs of $.70/MWh generated (not LCOE). The study also compares the total capital cost of the plant (including incentives) to the first year annual revenue, and calculates the year-1 break-even cost and return on investment, assuming 11% CCR. The authors conclude that TES has the potential to increase CSP value by allowing generation to be shifted to higher-priced hours and by increasing the use of thermal energy from the solar field.

All of the above studies were either conducted by NREL, conducted by consulting firms contracted by NREL or DOE, or used methodologies in connection with NREL's Excelergy/SAM programs. No academic studies, independent of these NREL-based investigations, could be found that evaluate the performance and cost of PT/TES for U.S. installations. Lazard [113], a U.S.-based financial advisory and asset management firm, conducted an in-house investigation of the LCOE of various competing electricity technologies, including trough CSP. They estimate the capital cost of a 200 MW trough plant with no TES to be $4,500/kW with wet cooling and $5,800/kW with dry cooling, including capitalized interest costs during construction, and the annual O&M cost to be $66/kW. These costs translate to a LCOE in $2008 of $108/MWh (wet cooling) and $145/MWh (dry cooling) based on the

following assumptions: capacity factor of 29% (wet) and 26% (dry), 2-yr construction time, 20-yr facility life, 30% investment tax credit, accelerated asset depreciation, 60% debt at 7% interest rate, 40% equity at 12% cost, 20-year economic life, 40% tax rate, and 5-20 year tax life. The dry cooling LCOE reaches $349/MWh in the absence of U.S. federal tax incentives under the same financial assumptions. Lazard collaborated with "a leading consulting and engineering firm to the power & energy industry" to determine the LCOE that would provide an after-tax IRR to equity holders equal to an assumed cost of equity capital.

Several international researchers have conducted performance-cost analyses of parabolic trough for non-U.S. locations. Quaschning [114] examined 61 sites in Europe and North Africa with global annual irradiation ranging from 923 to 2,438 kWh/m^2 and calculated the usable irradiation, annual system output, and LCOE for PV and trough CSP systems. This study used Greenius, a model developed by DLR, to provide key economic inputs and to calculate the system output, efficiencies and other technical parameters. The results include near term trough LCOE of 12 euros/MWh, and 9 euros/MWh in 10 years, both with highest irradiance values modeled. Quaschning concludes that a minimum solar irradiance value of 1,300 kWh/m^2 is required for trough to be more economical than PV. However, the source of cost data in this study is unclear, and it is unclear whether the reported costs include incentives.

Montes et al. [115] describe a parametric optimization of the LCOE for a 50 MW solar-only PT plant in Spain (no TES or fossil fuel backup) with five different solar field sizes. The lowest unsubsidized LCOE obtained was 133 euros/MWh at a solar multiple of 1.16. Poullikkas [116] conducted a feasibility study to investigate whether the installation of trough CSP is

economically feasible for the island of Cyprus. He performed a parametric cost-benefit analysis, which involved 1,470 simulations that varied plant capacity (25-100 MW), capital investment (2,000-8,000 euros per kW), operating hours (5-24 hrs per day), required land leasing (0-3 euros per m^2), and CO_2 price (0-30 euros per ton). Andreas used the independent power producer technology selection (IPP) algorithm version 2.1 software tool to calculate the LCOE, net present value (NPV), internal rate of return (IRR), and payback period were calculated for each case based on the following assumptions: annual solar potential of 2,000 kWh/m^2 to the solar field, 14% solar to electric efficiency, 20 year power purchase agreement (PPA) and 0.26 euro/kWh feed-in tariff (current market regulations). The results of the study indicate that for every 1 euro/m^2yr increase in land leasing price, the LCOE increases by 1.43 euro/kWh, and the largest plant size resulted in the most attractive investment. Andreas concludes that trough installation in Cyprus can be profitable and economically feasible under certain conditions that depend on the size of the plant, degree of storage, initial cost and cost of land.

Izquierdo et al. [117] examine the effect of the solar multiple, capacity factor and storage capacity on the cost of electricity from CSP plants in Spain in order to define the optimal operational range in terms of solar electricity produced and its generation cost. They find the optimal solar multiple values to be between 1.5 and 2.5 for no storage, and storage capacity varies the optimal SM (see Figure 18). Key assumptions used in this study include 75% collector optical efficiency, 380^{o}C absorber temperature and costs from the European Concentrated Solar Thermal Roadmap (ECOSTAR) study that was developed in part by DLR. Pitz-Paal et al. [118] describe the ECOSTAR study in more detail and demonstrate how parabolic trough with DSG has the potential to reach a LCOE of 162-187 euros/MWh by scaling

up plant size and adopting technological innovations.

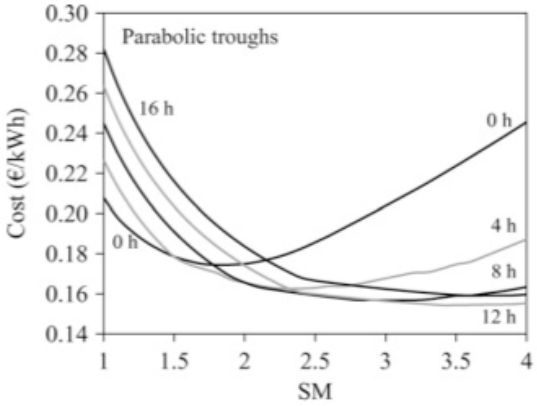

Figure 18 - Effect of Solar Multiple and Storage Capacity on LCOE [119]

Purohit and Purohit [120] describe a preliminary attempt to assess the technical and economic feasibility of CSP technologies in India. They use Andasol 1 as a reference case for the evaluation of trough potential at 50 Indian locations, and calculate the LCOE of these systems to be 9.34-28.42 Rs/kWh. They conclude that in the Rajasthan and Gujarat states this LCOE is lower than the feed-in tariff, and they recommend that CSP be installed at locations with direct solar radiation of 1,800 kWh/m^2 or more.

2.5 Environmental Life Cycle Assessment of PT and TES

Few studies examine the area of environmental life cycle assessment (LCA) for CSP plants. Norton et al. [121] appears to be the first study to address this topic. The paper describes a LCA of the CO_2, NO_x, and SO_2 emissions for electricity generation from biomass, hydro, PV, CSP, and wind. The article lacks detail in terms of specific assumptions and calculations, but they estimate trough CSP life cycle CO_2 emissions at 30 g/kWh, with an expected reduction to 20 g/kWh in the future. The next academic study to discuss the environmental effects of CSP is

Tsoutsos et al. [122], which provides a qualitative assessment of potential effects including noise, visual intrusion, greenhouse gas emissions, water and soil pollution, impacts on sensitive ecosystems.

Recently, more studies have attempted to quantify the environmental effects of CSP and document assumptions more clearly. Koroneos et al. [123] describe a LCA of the environmental impacts associated with 1 MWh of electricity from a power tower CSP plant. Viebahn et al. [124] describe a scenario analysis conducted to examine the potential of solar thermal technologies for the future. A life cycle assessment of the greenhouse gas (GHG) emissions associated with each technology used in the scenario analysis is presented. Viebahn et al. report life cycle GHG emissions of 161 g/MWh and land use of 14 mm^2a/MWh (where mm^2a refers to annual mm^2) for a parabolic trough plant similar to Andasol 1 (46 MW turbine capacity, 15% natural gas backup, 7.5 hours of molten salt indirect storage, oil HTF).

Lechón et al. [125] also conducted a LCA of GHG emissions for an Andasol-type plant (50 MW turbine capacity, 7.5 hours of indirect molten salt TES, 15% natural gas backup, oil HTF). They also estimated the life cycle cumulative energy demand (CED) of the plant and the GHG emissions and CED of 17 MW power tower plant. Assumptions and date are relatively well-documented in this study. The system boundary for the LCA is presented in Figure 19, and the results are displayed in Table 7. Figure 20 displays the contribution of different parts of the operation phase of the trough plant to the GHG emissions. The study also summarizes literature values for trough life cycle GHG emissions for comparison; these values range from 17 to 234 g CO_2 eq/kWh.

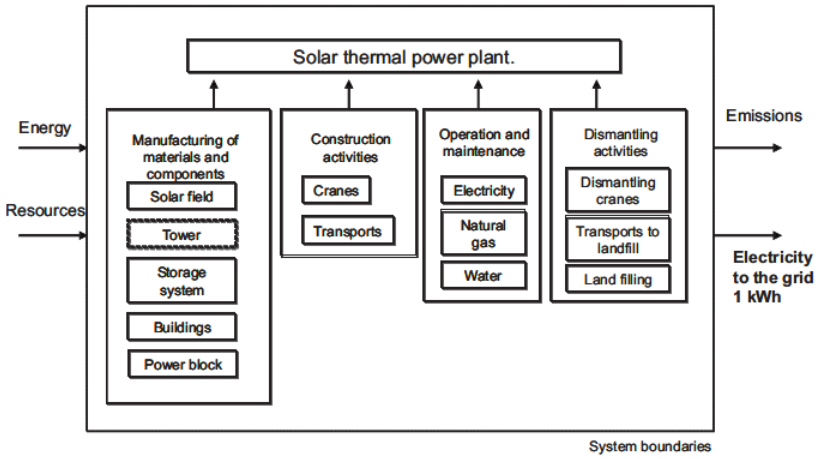

Figure 19 - LCA System Boundary [125]

Table 7 - Life Cycle Greenhouse Gas Emissions for CSP Plants in Spain [125]

g CO_2 equiv./kW h	Central tower	Parabolic trough
Solar field	5.61	7.88
Power block	0.64	0.50
Storage system	9.49	14.60
Tower	0.04	
Buildings	1.03	0.46
Construction	0.18	0.34
Decommissioning	$4.31E-04$	$1.98E-02$
Subtotal	17	24
Operation	186	161
Total	203	185

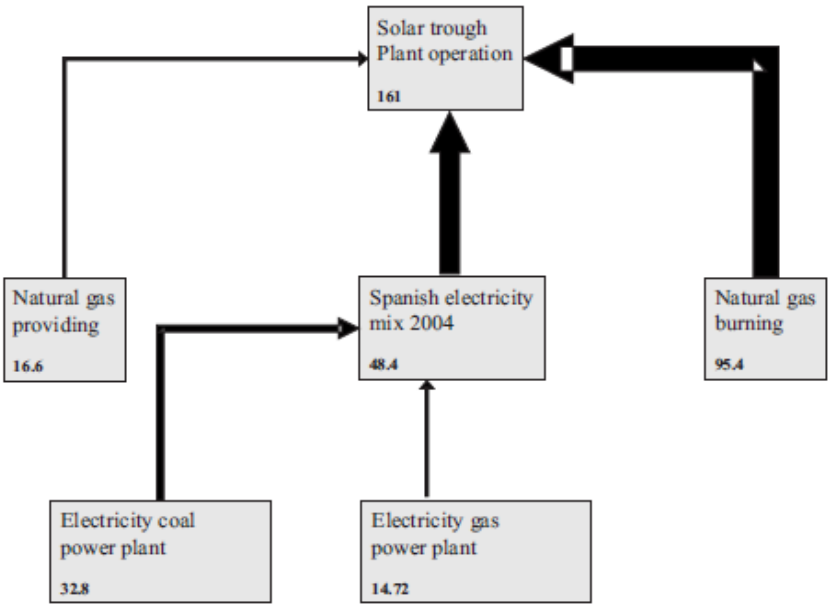

Figure 20 - GHG emissions (g CO2eq/kWh) during the Operation of a CSP Plant [125]

Lechón et al. used the software tool Simapro to conduct the life cycle inventory (LCI) with data from firms investing in CSP plants in Spain and from the LCI database ECOINVENT 1.2. The CED, GHG emissions, and several other impact categories were calculated as defined in the LCIA, the impact assessment method developed by the Leiden University Institute of Environmental Sciences (CML). A recycling scenario representative of Spain in 2004 was selected to estimate disposal impacts. The "energy payback time", defined as the time it takes for the power plant to save the same amount of primary energy that is consumed for its production, operation, and dismantling, was calculated to be about one year for each technology. The authors conclude that both technologies have an environmental profile much better than the current Spanish electricity mix.

More recently, Piemonte et al. [126] used SimaPro7 to conduct a LCA of the CED, greenhouse gas emissions, land use, abiotic depletion, eutrophication, acidification, and human toxicity associated with an Archimede-type trough plant (molten salt as storage fluid and HTF). Data for the construction phase of the LCI were obtained from the Italian research center, ENEA. It was assumed that the case study plant generates 2,880 MWh/year, and a biomass furnace provides 1.58 megawatt-hours thermal (MW_{th}) back-up energy to balance protracted cloudy periods. The results show the life cycle GHG emissions to be 141,788.4 kg CO_{2eq} per year (about 49 kg CO_{2eq}/MWh), which, the authors conclude, is much lower than a conventional fossil-fired plant.

Burkhardt et al. [127] of NREL published the first U.S.-based LCA of trough CSP GHG emissions, CED, and water consumption. Their hybrid LCA examines the manufacturing, construction, O&M, dismantling, and disposal stages associated with a wet-cooled 103 MW trough CSP plant with 6.3 hours of two-tank indirect molten salt TES located in Daggett, CA (a hypothetical WorleyParsons plant design). They compare this reference plant with four other plant designs: 1) the reference plant with dry-cooling instead of wet cooling, 2) the reference plant with a thermocline TES system instead of a two-tank system; 3) the reference plant with a synthetic salt instead of salt that is mined; and 4) the reference plant with a thermocline synthetic salt TES system. The results of the analysis are summarized in Table 8.

Table 8 - Summary of NREL LCA Results for a Parabolic Trough CSP Plant [127]

Plant design	Cooling system	6.3-hr TES system	GHG (g CO_{2eq}/kWh)	CED (MJ_{eq}/kWh)	Water (L/kWh)
1	wet	2-tank, mined salt	26	0.40	4.7
2	dry	2-tank, mined salt	28	0.43	1.1
3	wet	thermocline, mined salt	24	0.37	4.6
4	wet	2-tank, synthetic salt	39	0.50	4.9
5	wet	thermocline, synthetic salt	28	0.40	4.7

The authors used SimaPro v7.1 and the ECOINVENT LCI database to provide GHG emissions, energy flows and embodied water when primary data were unavailable, and they used the U.S. 2002 Industry Benchmark EIO-LCA model to estimate these burdens for select components and systems, including pumps, compressors, turbine generator set, and miscellaneous controls and electronic equipment, based on costs extracted from primary data sources. Manufacturers of key trough components provided detailed information on embodied materials, transportation methods, energy flows, and direct GHG emissions from manufacturing processes. Where necessary, the authors estimated the quantity of raw materials to manufacture system components. Water data were obtained from a glass manufacturer for the mirrors and from the Ecoinvent database for all other components. Design parameters for the TES systems were obtained from previous NREL studies mentioned above, and the authors estimated the impacts from the manufacture of synthetic salt for the thermal energy storage system with reaction equations obtained from industrial chemical literature and LCI data from Ecoinvent. The inherent assumptions in this process are that synthetic potassium nitrate is produced by reacting potassium chloride with nitric acid, and synthetic sodium nitrate is produced by neutralizing nitric acid with sodium hydroxide.

Much fewer water and land use LCAs have been published recently than GHG emissions assessments. Fthenakis and Chul Kim [128] present a review of land use data for electricity generation technologies, including wind, PV, hydro, geothermal, biomass, coal, nuclear, and natural gas and synthesize these data into life cycle land use estimates. Although they do not

conduct their own assessment of CSP land use, they report that previous studies estimate trough to use 366 m^2/GWh over a 30-year plant lifetime. Fthenakis and Chul Kim [129] also present a review of studies concerning water use in electricity generation and use "full life-cycle accounting" to evaluate water demand factors for coal, nuclear, natural gas, PV, and wind power plants. In addition, they report operational water use values for biomass, geothermal, hydro, concentrated PV, CSP, oil, natural gas combined cycle (with and without carbon capture and sequestration (CCS)), integrated gasification combined cycle (with and without CCS), and coal with CCS. For trough CSP, they report literature values for operational water use of 300 L/MWh with dry cooling and 2,100-3,800 L/MWh for wet cooling.

Two other recent studies assess water use in the operational stage of a trough CSP plant. Florida Power and Light (FPL) [130] contracted WorleyParsons Group to provide a conceptual design for the Beacon Solar Energy Project, a 250 MW trough facility that is expected to go online in California in 2012 [3]. As part of this directive, WorleyParsons compared the capital costs, thermal performance, and operational water consumption of the base plant design (wet cooling) to alternative designs with dry cooling and hybrid cooling systems. Three options reflecting different pricing, sizing, performance and water use were considered for each design in order to get a feel for the sensitivity of different options to key parameters. WorleyParsons calculated the capital costs (with a range +/-30% range of accuracy) of each design using budgetary quotes obtained from vendors and in-house estimates, and they used GateCycle version 5.61.0 to assess the effect of each cooling system on cycle output and efficiency. Table 9 displays the results of the analysis, and the report concludes that the base design has the lowest capital cost and far better thermal performance than the alternative cooling technologies. The authors recommend

the wet cooling design because the advantages in capital cost, performance, and revenue outweigh the concern over the significant amount of makeup water required.

Table 9 - Estimated Water Consumption and Treatment Costs for Beacon Solar Energy Project at Annual and Summer Conditions [130]

	OPTION 2: Pre-treatment	OPTION 4: Air Cooled Condenser	OPTION 5: Hybrid Wet/Dry Cooling
Annual/Summer Makeup (gpm)	3353/4054	178 / 192	157 / 2502
Annual/Summer Blowdown (gpm)	197 / 240	0 / 0	0 / 144
Annual/Summer Flow to Evap Ponds (gpm)	462 / 563	82 / 92	36 / 349
Annual Makeup (AFY)	1599	79	625
Annual Makeup Savings (AFY) compared to Opt. 2	0 (compared to Option 2)	1520	974
O&M Costs ($1000) per year (excluding labor)	$1,420	$132	$815
Capital Costs ($1000)	$21,158	$2,500	$11,116

As mentioned in Section 2.4, Turchi et al. [109] also calculate the operational water use associated with trough CSP. They describe an assessment of the performance, cost, and water use associated with 13 different cases covering three different geographic locations and wet, dry, and hybrid cooling technologies (see Figure 21). The results for the average water consumption per unit electricity generation are: 3.5 m^3/MWh (wet) and 0.3 m^3/MWh (dry). The authors note that the water consumption for the wet-cooled trough design is greater than that of other wet-cooled Rankine cycle plants (2.2 m^3/MWh for coal and 3.2 m^3/MWh for nuclear - assuming closed-loop cooling towers with onsite evaporation ponds) because the trough plant has lower cycle efficiency and more frequent startup and part-load operation. In addition, the authors

compare CSP water use with other land-intensive activities (see Figure 22), and conclude that "in a relative sense, "growing megawatts" uses much less water than growing other commodities".

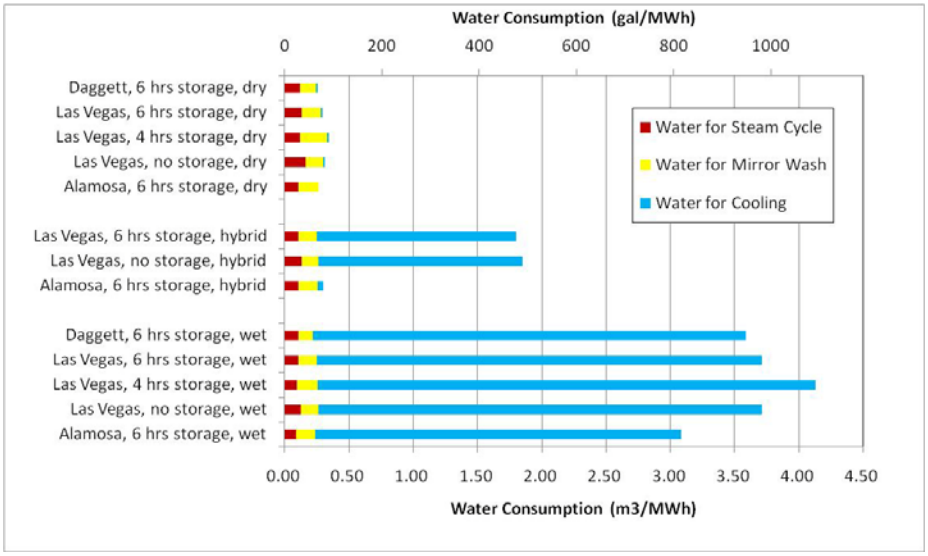

Figure 21 - Estimated water consumption for the 13 cases [109]

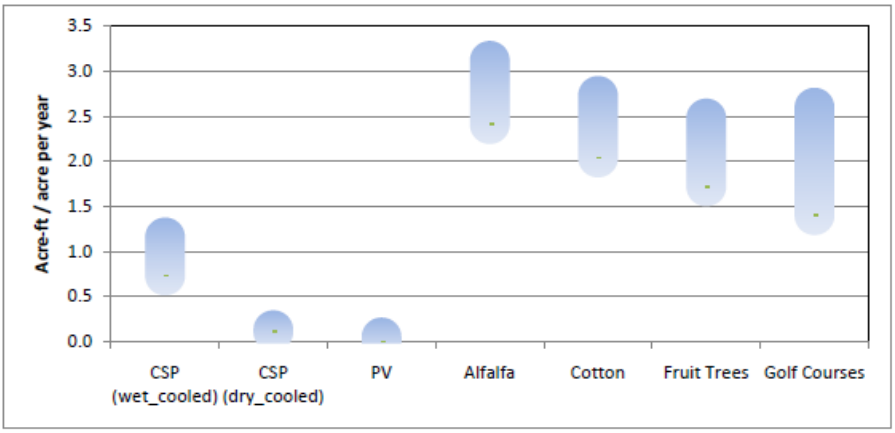

Figure 22 - Water consumption by different land-intensive activities in the Southwest [109]

Wet-cooled CSP includes parabolic trough and power tower. Power towers are at the low end of the range because they have higher thermal efficiency than trough. Dry-cooled CSP includes troughs, towers, and dish/engine systems. PV plants use water for panel washing only.

2.6 Multi-Criteria Decision Analysis

Multi-criteria decision analysis (MCDA) is a tool that allows decision-makers to incorporate a diverse set of criteria in the evaluation of a set of alternative choices. Although it has become a more popular decision-making tool in recent decades, relatively few studies have applied it to energy issues, and even fewer have applied it to CSP. This section describes three studies that investigate the historical use of MCDA in environmental and energy decision-making in general and two studies that apply MCDA to CSP specifically.

Kiker et al. [131] present a literature review of MCDA techniques and propose a generalized framework for applying these techniques to environmental projects to make environmental decision-making more structured and tractable. They note that almost all decision analysis methods involve creating a decision matrix, synthesizing the information in the matrix, and ranking alternatives accordingly. Each method approaches these last two steps in different ways and incorporates some type of algorithm to select an optimal solution. Some MCDA methods rank options; some provide a partial ranking; some select a single optimal choice; and some differentiate between acceptable and unacceptable choices. The authors describe in detail three main MCDA methods: multi-attribute utility/value theory (MAUT/MAVT), the analytical hierarchy process (AHP), and outranking, and summarize environmental management studies that have used each of these techniques in the past.

MAUT and AHP are similar in that they communicate comparative merits of alternatives based on a numerical score derived from a single scale. The numerical scores are derived by assessing the performance of alternatives with respect to an individual criterion and aggregating into an

overall score. The overall scores can be summed, averaged, or weighted to indicate preference for some criteria over others. MAUT attempts to transform a set of "messy" attributes into a simple expression that decision-makers can synthesize in order to maximize the utility (or value) of a decision. This method assumes the decision-maker is rational, has perfect knowledge, makes consistent judgments, and always maintains the same preferences.

AHP is similar to MAUT but uses a quantitative comparison method based on pair-wise comparisons of decision criteria instead of using utility and weighting functions. The results are compiled in matrix form, and each individual criterion is paired against all others. The decision-maker applies a numerical scale to all pair-wise comparisons of criteria and alternatives. This method relaxes the rationality assumption of MAUT to reflect the idea that people are better at making relative judgments than absolute judgments.

Outranking does not assume that there is one optimum solution to a problem, but rather acknowledges that one choice may have a degree of dominance over another. These models compare two alternatives at a time in terms of each criterion, and evaluate to what degree a preference for one choice can be established without using a prescribed scale. The focus of the outranking method is on the strength of evidence that favors one alternative over another, and it is most often selected when criteria are not easily aggregated, measurement scales vary over wide ranges, and units are too different to be comparable.

Based on this review of MCDA techniques and a review of previous studies that apply these techniques to environmental problems, Kiker et al. create a framework for applying MCDA to

environmental decision-making. The key recommendations are: 1) involve a diverse group of people to represent the "decision-maker" (i.e. policy-makers, financiers, scientists, engineers, the general public, etc); 2) design an adaptable structure to approach the problem and ensure that local concerns can be incorporated; 3) generate alternatives, evaluation criteria, and value judgments; 4) apply MCDA methods to rank alternatives; 5) iterate through the process as much as necessary to generate the required outputs.

Greening and Bernow [132] state that MCDA methods are the ideal tools for environmental and energy policy development. They review and classify several different MCDA methods and provide recommendations for the implementation of these methods in currently evolving integrated assessment (IA) frameworks. They note that the key strength of MCDA methods compared to neoclassical economical approaches is the ability to identify tradeoffs, co-benefits, and compromise solutions to complex policy and planning problems. They also list similar characteristics for all MCDA methods: a finite number of alternatives, a quantity of attributes that depends on the nature of the problem, a set of units specific to each attribute, a system of characterizing the importance of each attribute, and a matrix format that combines attributes and alternatives. A table is presented that classifies different MCDA methods based on the level of information required and the relevant feature of that information. The table identifies "mathematical programming models", which use various weights for decision variables, as the primary method for energy and environmental policy evaluation. These models generally include cardinal ranking of alternatives and require "information on value judgments regarding the importance of an overall objective and the development of weights proportional to the relative value unit changes in the value function".

The authors explain that in the beginning stages of any MCDA process, the methods used to elicit value judgments can strongly influence the results of the analysis. They describe AHP in similar terms as the above study and note that it is the most widely applied MCDA method in the analysis of energy and environmental issues. Several examples of studies that have applied AHP to these issues are presented in the article, including studies of national energy policy development and analysis in the UK, U.S. and other regions, electricity expansion and planning, and the evaluation of impacts from new technologies. Greening and Bernow also describe MAUT and identify applications of this method to the selection of sites for nuclear repositories, integrated resource planning, the selection of power generation facility sites, the development of national energy policy, and water use planning.

In addition, the authors describe a set of mathematical programming methods that generate many possible non-dominated alternatives and represent the decision variables in a single-objective or multiple-objective function(s) as the distance from an established goal for each objective. A key advantage of these methods is they can represent attributes by their physical quantities rather than by monetized estimates of costs and benefits. Mathematical programming methods incorporate weights that sum to one and are proportional to the relative value of unit changes in the true attribute value function. In this way, the objective function can be additive and linear, and ideally identify the Pareto efficient alternative (i.e., no single attribute can be improved without degrading at least one of the other attributes). Greening and Bernow present a set of studies that have incorporated mathematical programming MCDA methods, including studies that analyze national energy policies, electrical generation expansion, regional energy system

planning, risk assessments, facility siting decisions for energy supply technologies, and analyses of tradeoffs between market and non-market valued attributes like environmental amenities.

Greening and Bernow suggest that future MCDA methods be incorporated with IA to combine geophysical/ecological and socioeconomic models to evaluate emissions reduction or adaptation strategies. These methods should address: the ultimate choice between policy options, communications necessary to involve decision-makers, and possible future investigations. The authors suggest a transparent, flexible and iterative environmental and energy policy decision support framework with the following components: 1) credible environmental change process models; 2) a model of the qualitative and quantitative impacts on social, cultural, economic, environmental and energy systems; 3) an option screening model that presents tradeoffs between a small subset of key attributes; 4) a decision-support model that incorporates several MCDA methods and accurately depicts desired environmental and energy goals, decision-maker preferences, and techno-economic detail.

Diakoulaki and Karangelis [133] use MCDA and cost-benefit analysis to examine four mutually exclusive scenarios for the expansion of the electricity system in Greece, with a strong focus on the role of renewable energy sources in this mix. They calculate the technical, economic, and environmental performance of the four scenarios for the year 2010. Diakoulaki and Karangelis use the Preference Ranking Organization Method of Enrichment Evaluation (PROMETHEE) method for MCDA, which uses a pair-wise comparison of alternatives in each single criterion in order to determine the potential preference of one alternative other another. The decision-maker

defines indifference and/or preference thresholds for each criterion. Diakoulaki and Karangelis use the methodological framework and external cost estimates for energy technologies in Greece outlined in the ExternE project of the EC for the cost-benefit analysis and calculate the sum of cost and benefit components on an annual basis. The scenarios represent a wide range of parameters and were created by official authorities involved in designing energy policies for Greece. The authors consider the following attributes in their analysis: LCOE, baseload electricity generation capability, dispatchability (ability to respond to peak load), security of "fuel" supply, CO_2, SO_2, and NO_x emissions. The following independent weighting options are examined separately: 1) equal weights for all criteria; 2) 50% importance to economic criteria; 3) 50% to technical criteria; and 4) 50% to environmental criteria. In the cost-benefit analysis, they calculate the total social cost as the sum of: private production cost, cost of electricity deficit, cost of peak power deficit, cost of CO_2 emission allowances, and external cost of SO_2 and NO_x emissions. The authors conclude that the scenario with the highest penetration of renewable energy sources is the best compromise for the attributes studied.

Cavallaro [134] also uses the PROMETHEE method and outlines the following procedure for this method: 1) identify alternatives; 2) define a set of criteria; 3) categorize preferences as outright, weak, indifferent, or incomparable; 4) create a payoff matrix (based on a cardinal or ordinal scale), which tabulates for each criterion-alternative pair, the quantitative and qualitative measures of the effect produced by that alternative with respect to that criterion; and 5) determine the multi-criteria reference index by expressing the degree of preference as a number from 0 (no preference) to 1 (outright preference), defining a preference function, and defining a vector of importance weights for each criterion. Weights can be set directly by the decision-

maker or a formal elicitation of weights can be conducted by an analyst, which can follow a variety of methods. Cavallaro uses the Simos Approach, which involves the following steps: 1) write the name of each criterion on a card and give it to the decision-maker in random order; 2) ask the decision-maker to order the cards by increasing importance; and 3) calculate the importance weight from the rank order.

Cavallaro uses data from the ECOSTAR study and applies this MCDA method to the selection of a CSP technology for power generation while considering a number of technical, economic and environmental criteria. He considers twelve alternative CSP technologies: 1) trough with oil HTF (50 MW); 2) trough with DSG (47 MW); 3) Fresnel lens (similar to trough but lower operational temperature and flat mirrors) with DSG (50 MW); 4) power tower with molten salt as HTF (50 MW); 5) power tower with molten salt HTF (17 MW); 6) power tower with DSG (11 MW); 7) power tower with DSG (5 x 11 MW); 8) power tower with atmospheric air as HTF (10 MW); 9) power tower with atmospheric air as HTF (5 x 10 MW); 10) ISCC power tower with pressurized air (14 MW); 11) ISCC power tower with pressurized air (4 x 14 MW); and 12) dish-engine system. He does not consider any trough options with TES. The analysis incorporates the following criteria: investment costs, O&M costs, LCOE, technological maturity (measured qualitatively on a 3-point scale), environmental impacts (area-specific: noise disturbance, odors, and risk to ecosystems - measured qualitatively on a 3-point scale, operating temperature, and solar capacity factor. He does not consider quantitative environmental impacts such as pollutant emissions, wildlife mortality, or water use. The two hybrid technologies received the highest score in the MCDA, prompting Cavallaro to conclude that “pure thermal solar power is not yet close to being competitive”, yet he is not explicit about what he means by “competitive”.

Cavallaro conducted a second study [57] in which he investigates the feasibility of using a molten salt HTF in a trough CSP plant through the fuzzy multi-criteria Technique Order Performance by Similarity to Ideal Solution (TOPSIS) method. In this method, "fuzzy" refers to the use of a "fuzzy-set", which allows for uncertain approximate reasoning and allows decision making with estimated values where information is incomplete or uncertain. The TOPSIS method selects as the optimal solution the alternative with the shortest distance from the positive-ideal solution (maximize benefit) and the longest distance from the negative-ideal solution (minimize cost). Cavallaro uses the following specific TOPSIS algorithm: 1) generate alternatives; 2) identify evaluation criteria; 3) choose ratings for alternatives with respect to chosen criteria; 4) ascertain the weight of the criteria; 5) construct a fuzzy decision matrix; 6) normalize the fuzzy decision matrix; 7) apply weights to decision matrix; 8) determine the positive-ideal and negative-ideal solutions; 9) calculate the distances between each alternative and the positive-ideal and negative-ideal solutions; and 10) calculate a closeness coefficient to determine the ranking order of all alternatives.

His results rank the following alternative HTF/TES configurations in a trough CSP plant in order from most preferred to least preferred: 1) direct 2-tank molten salt TES at 500^{o}C (highest rank); 2) direct thermocline molten salt TES at 500^{o}C; 3) Therminol VP-1 with no TES; 4) direct thermocline molten salt TES at 450^{o}C; 5) direct 2-tank molten salt TES at 450^{o}C; 6) direct 2-tank Therminol VP-1 TES; 7) direct thermocline Therminol VP-1 TES (lowest rank). The following criteria were incorporated in the analysis quantitative data mainly from Kearney et al. [135]: investment costs, O&M costs, LCOE, LCOE reduction potential, electricity production, state of

knowledge/degree of reliability (qualitative), environmental risk and safety (qualitative), land use, and freezing point (qualitative).

2.7 Conclusions from Literature Review

The extensive literature review presented in this chapter highlights the necessity for further research in CSP and TES. Although parabolic trough CSP plants are being developed at an increasingly rapid pace, there are very few published academic studies that examine the social implications of this development in the United States. The following limitations can be seen in the research area of performance and economic modeling as it applies to CSP and TES:

1) The majority of published work is directly or indirectly linked to NREL's Excelergy and SAM models.
2) In published studies, there little consideration for the link between varying TES capacities/configurations and selecting the optimal solar field area.
3) Many studies are based on European solar insolation values and markets.
4) Many studies do not document assumptions precisely enough to provide a transparent analysis
5) Many cost calculations either include subsidies or are unclear about whether they include subsidies

In the area of environmental life cycle assessment, the limitations are even more severe. There are a few studies that calculate the life cycle greenhouse gas emissions for trough CSP plants, but not one of them has transparent documentation of assumptions; is specific to U.S. CSP development; accounts for varying storage capacities/configurations; considers the current

industry standard in TES (indirect molten salt TES); and also considers varying solar field sizes. In addition, there has been little investigation into life cycle water use and land use associated with trough CSP.

There are only two published studies that attempt to combine technical, economic, and environmental concerns into a decision framework that policy makers can use. However, they have limitations in terms of the data they use, the technologies they incorporate, and the environmental criteria they model. Renewable portfolio standards/goals and federal renewable energy incentives have become the main driving force behind CSP development in the U.S. So far, these incentives have not encouraged TES as a key component of the U.S. CSP industry. If the nation is serious about moving toward a low-carbon future in which solar energy may need to take on a baseload role, it is critical that policy-makers understand the social implications of developing CSP with TES so they can decide whether to target TES in future policy decisions. The study conducted here is unique in that it combines a complex hourly physical engineering-economic model with an environmental life cycle assessment of pollutant emissions and resource use (based on the physical parameters in the physical model) in a MCDA framework to provide recommendations to policy-makers as to whether TES should be incorporated with near-term trough installations from a societal standpoint.

Chapter 3: PT Plant Performance Model

This chapter describes the performance model I developed in Matlab to simulate the hourly and annual electricity generation of three different parabolic trough plant configurations: 1) with no thermal energy storage and no backup system; 2) with 1-12 hours of molten-salt thermal energy storage (TES); and 3) with a natural gas-fired heat transfer fluid heater (NG) that matches the hourly and annual electricity generation of each TES capacity (1-12 hours). As mentioned in the previous chapter, these configurations were selected to enable a comparison of primarily solar plants with different backup technologies. Technologies such as ISCC, in which solar energy contributes a small percentage to overall electricity generation, are not included in this study in order to limit the focus to primarily solar-based technologies. The following sections describe in detail the inputs and calculations used in the performance model to set the design parameters for each plant configuration. They also describe the inputs and calculations used in the hourly simulation, which estimates the annual electricity generation as the sum of the hourly electricity generation over the course of a year.

Figure 23 shows that the results from the performance model described in this chapter are used in the economic model, which is described in Chapter 4, to calculate the levelized cost of electricity (LCOE), which is used to select the final solar field size for the plant with no storage/backup and for all of the cases with TES. It is necessary to use an iterative process based on a particular objective function to select the final solar field area because the aperture area of the collectors greatly influences the cost and electricity generation of the power plant. The unsubsidized, pre-tax LCOE has been selected as the objective function for solar field area selection for the plants

with TES because it is a measure of the cost of plant construction and operation over the economic lifetime of the plant compared to electricity generation. Chapter 4 provides more information about the LCOE calculation, and Chapter 6 provides more information about how the selection of a different objective function affects the selected solar field area. The engineering-economic model diagram for the parabolic trough plants with natural gas backup would look very similar to Figure 23 except that the hourly electricity generation from the plant with TES is a key input to the NG backup performance model, and the final solar field size is selected to minimize the difference between the annual electricity generation from the plant with TES and the plant with NG backup. The difference in annual electricity generation was selected as the objective function for solar field area selection for the plants with NG backup in order to simulate two plants that are the same size and with the same hourly and annual electricity generation for comparative purposes. The performance model results presented at the end of this chapter are based on the solar field sizes selected through these two different processes.

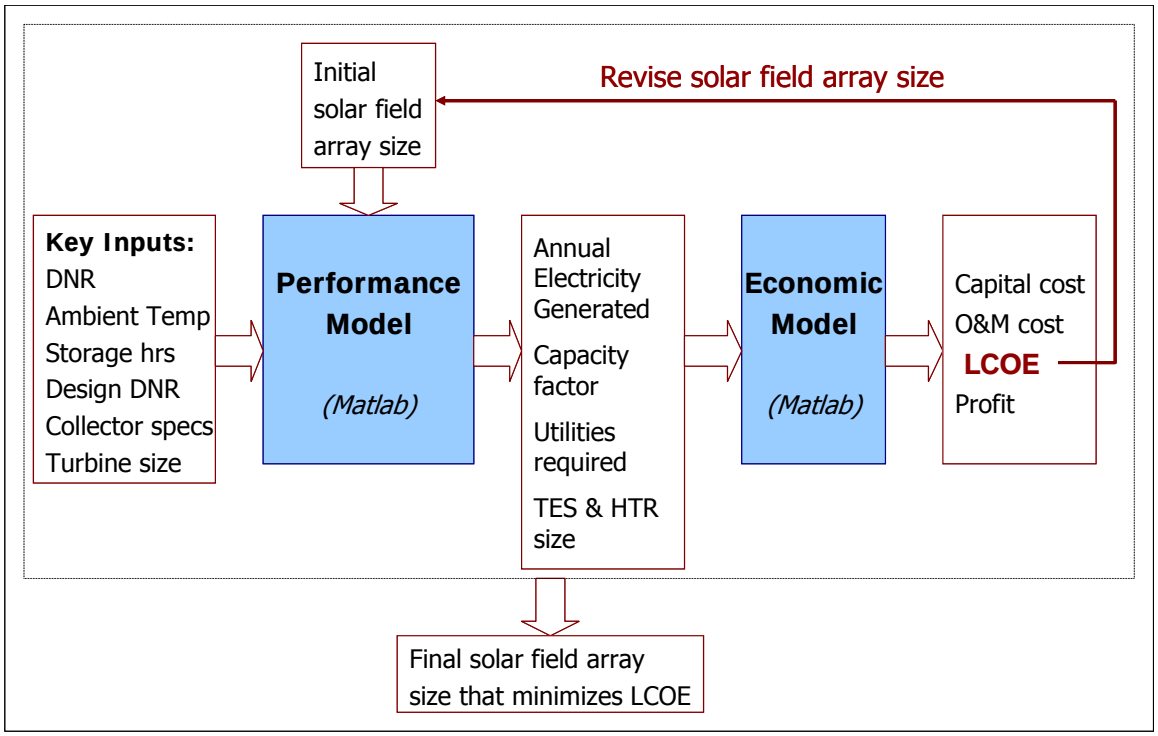

Figure 23 - Engineering-Economic Model Diagram for Plant with TES and no storage/backup[12]

Figure 24 presents a plant schematic of the no storage/backup configuration. A gross turbine capacity of 110 megawatts (MW) was selected. The turbine size, along with the design state of the steam entering the turbine and the design state of the HTF leaving the solar field determine the design parameters for the main components of the steam cycle: steam generator, solar reheater, deaerator, low-pressure preheater, and condenser. These design parameters determine the design mass flow rates of the steam and the heat transfer fluid, which, in conjunction with the design direct normal radiation, determine the base solar field area. The size of the HTF heater is determined by the changes in temperature and mass flow rates that result from the hourly simulation. Typical meteorological year (TMY3) direct normal radiation (DNR) and ambient temperature data for Daggett, California [136] were used as inputs to the hourly simulation,

[12] DNR = direct normal radiation; TES = thermal energy storage; HTR = natural gas-fired heater; O&M = operation and maintenance; LCOE = levelized cost of electricity

which consists of a series of component-based mass and energy balances to simulate the hourly and annual performance of the system. This location was selected to represent the general area of the country where most developers are considering new CSP projects. Chapter 6 explores the effect of weather data for other locations and the effect of parameters input values that differ from the base case presented in this chapter on key model results.

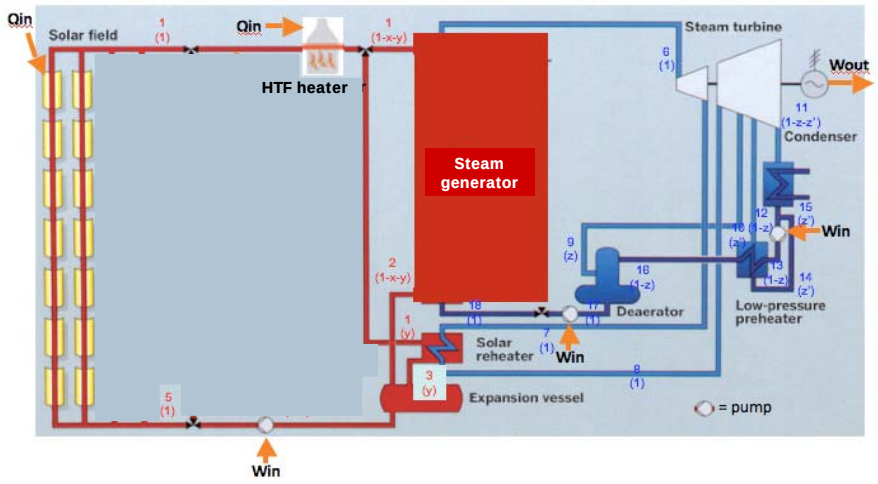

Figure 24 – Schematic of Parabolic Trough Plant with No Storage/Backup (adapted from [10])

Hourly DNR enters the solar field and is concentrated on the heat transfer fluid (HTF) in the receiver tubes (red). The HTF is pumped to the power cycle where energy is transferred to steam (blue) via the steam generator and reheater. The heat from the steam drives the turbines to generate power (W_{out}) and the cooled HTF returns to the solar field. The HTF heater (Q_{in} on the red line) is used to maintain the HTF temperature above freezing when altering the HTF mass flow rate fails to prevent freezing. Five pumps are used in the system, and the work required to operate them is shown as W_{in}. Red numbers refer to HTF thermodynamic states, blue numbers refer to steam states, and numbers and letters in parentheses represent mass flow fractions.

Figure 25 presents a schematic of the parabolic trough plant configuration with thermal energy storage. This diagram is similar to Figure 24 except for the presence of the two-tank molten salt thermal energy storage system shown in green, the salt heater, and a larger solar field area. The size of the storage tanks and heat exchanger are determined by the storage capacity specified at the beginning of the model simulation. The size of the salt heater is determined by the temperature and mass flow rate calculations in the hourly simulation. The solar field area is

larger in Figure 25 than Figure 24 so the solar field can capture and store more energy throughout the day than is needed to run the power cycle.

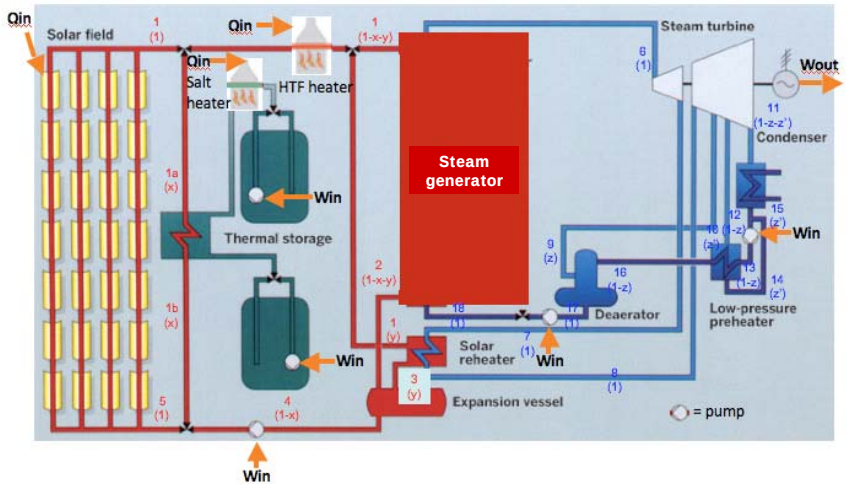

Figure 25 - Schematic of Parabolic Trough Plant with Thermal Energy Storage (adapted from [10])

When the TES system is charging, some HTF flows to the heat exchanger to transfer energy to molten salt. Hot salt is stored in one tank and cold salt in the other. When the ambient temperature threatens to freeze the salt, the salt heater is activated to maintain the temperature above freezing. The heat energy input to the two heaters from natural gas combustion is represented as Q_{in}.

Figure 26 presents a schematic of the third parabolic trough plant configuration modeled in this study: natural gas backup. This picture is very similar to Figure 24 except that the solar field area is larger to capture enough energy to match the hourly and annual electricity generation of the plant with TES. It is also necessary to increase the HTF heater size as the NG plant attempts to match the electricity generation of TES plants with larger and larger storage capacities.

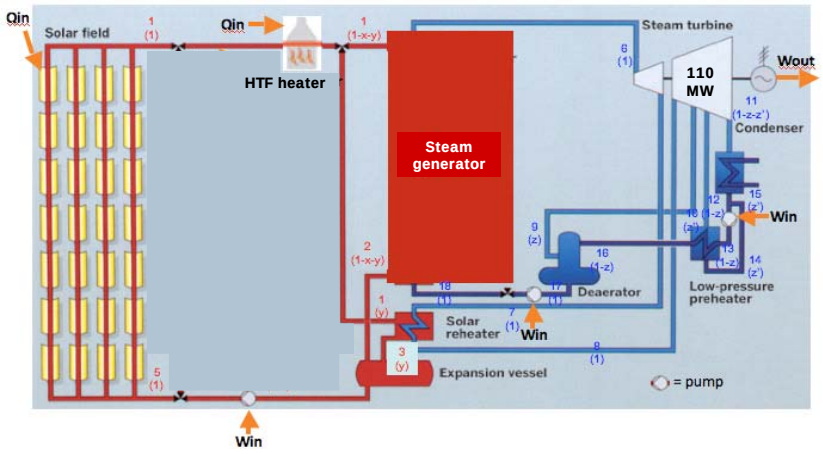

Figure 26 - Schematic of Parabolic Trough Plant with Natural Gas Backup (adapted from [10])

Sections 3.1 through 3.3 describe the specific input values and calculations used to calculate the design parameters for the solar field, power cycle, and HTF system in all three plant configurations. Section 3.4 describes the specific input values and calculations used to calculate the design parameters for the storage system in the plant configuration with TES. Section 3.5 describes the hourly simulation that was created to represent plant operation under DNR and ambient weather conditions that deviate from the design point for each plant configuration. Each hourly simulation runs for 8,760 cycles to simulate plant operation for a full year. Section 3.6 describes the final calculation of performance model outputs, and Section 3.7 presents performance model results.

3.1 Solar Field Design Parameters

Section 3.5 describes the hourly simulation, which involves several distinct plant operation modes for each different plant configuration (see Table 14). One of these operation modes, Day_SOLAR, is used to specify design point conditions for the solar field, HTF system, and

power cycle for all three plant configurations. Figure 27 displays a schematic of this specific operation mode, including the main components and material flows modeled. The TES system and HTF heater are not shown in this diagram because they remain idle while only the energy from the solar field is used to provide heat input to the power cycle.

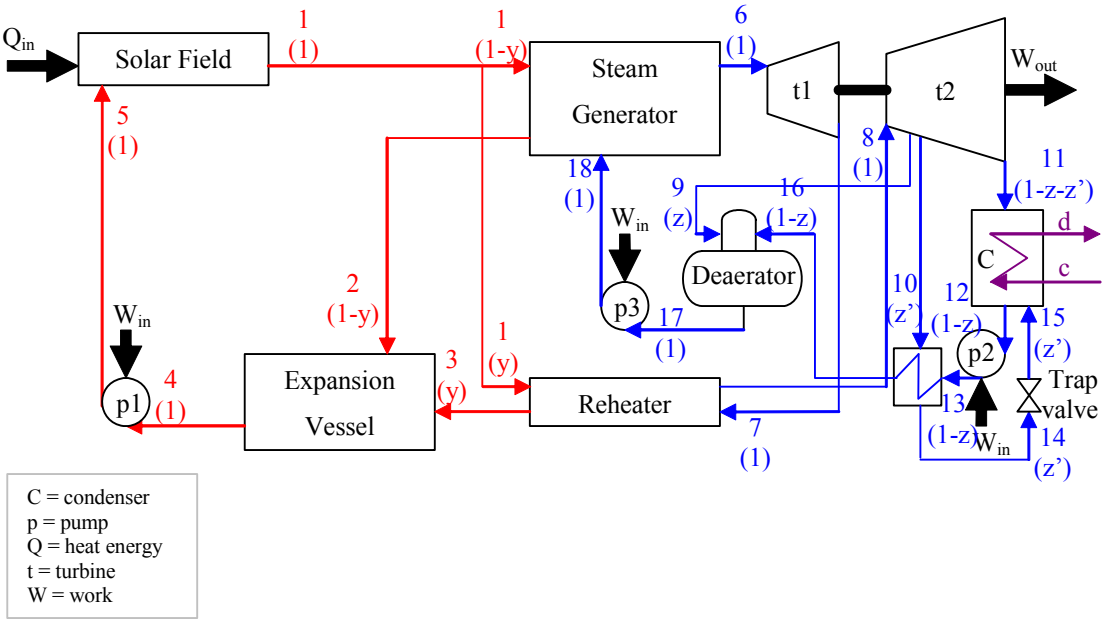

Figure 27 - Plant Schematic for Day_SOLAR mode.

The design parameters associated with the solar collector assemblies (SCA) were identified first, in order to calculate a base solar field area and design solar field thermal output. These calculations required an estimate of the total length of absorber and header piping in the solar field. Figure 28 shows the general solar field layout used in the piping calculations, where "hot" header piping refers to the pipe that carries the hot HTF from each SCA loop to the power block, and "cold" header piping refers to the pipe that carries the cooled HTF from the power block heat exchanger to each SCA loop.

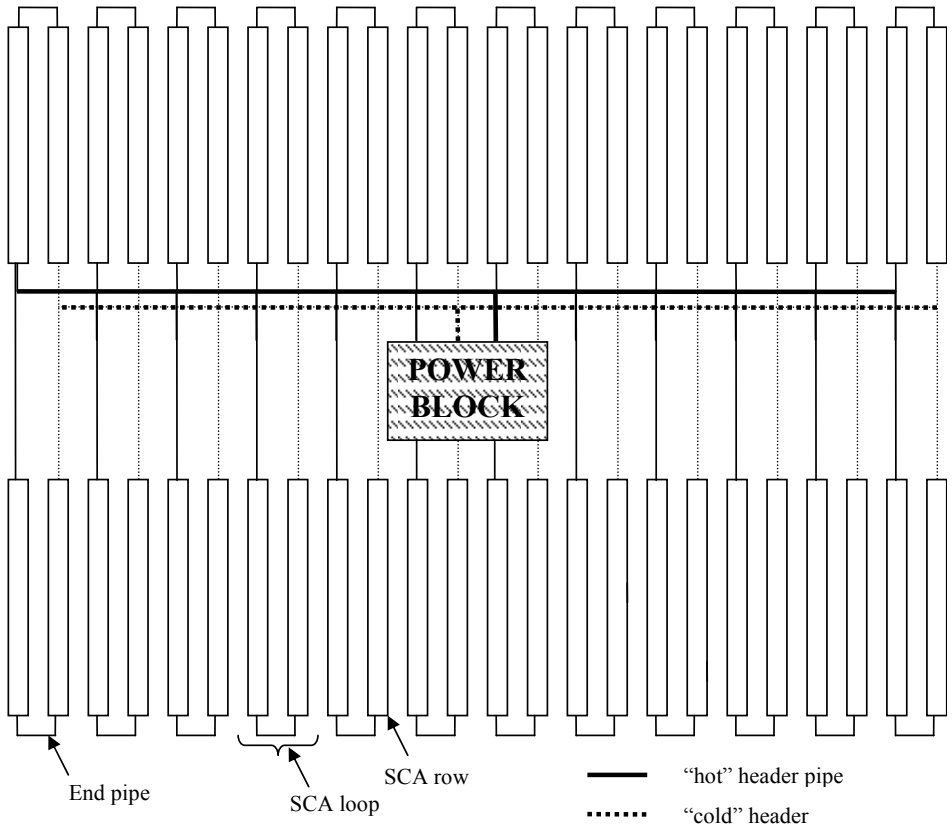

Figure 28 - Solar Field Layout for Piping Calculations

Table 10 presents the design parameters used to calculate the base solar field area, piping length, and design solar field thermal output in Equations 1 through 21. The location selected for this analysis was Daggett, California. A solar multiple was used to vary the total solar field area to a value larger than the base solar field area (A_b) during two different solar field area selection processes described at the beginning of this chapter. In the design configuration shown here, the solar multiple has a value of one for simplicity.

Table 10 - Solar Field Design Parameters for Daggett, CA

(Bold-faced items were calculated using the equations displayed below)

Symbol	Description	Design Value	Units
DNR	Direct normal radiation [137]	950	W/m^2
F_R	Mirror reflectivity factor - the fraction of DNR that is reflected from the mirror toward the receiver tube [138]	93	%
F_I	Intercept factor - the fraction of DNR reflected by the mirror that reaches the glass cover of the receiver tube [138]	95	%
F_T	Transmissivity factor - the fraction of DNR incident on the glass receiver tube that passes through the tube to the steel pipe [139]	96.5	%
F_A	Absorptivity factor - the fraction of DNR incident on the outer wall of the steel absorber pipe that is absorbed by pipe [139]	96	%
η_{opt}	**Collector peak optical efficiency**	**82**	**%**
a	Coefficient for SCA thermal loss function [138]	2.895474	
b	Coefficient for SCA thermal loss function [138]	-0.0164	
c	Coefficient for SCA thermal loss function [138]	0.000065	
T_5	Temperature of HTF state 5 [103]	293	^oC
T_1	Temperature of HTF state 1 [103]	393	^oC
T_{amb}	Ambient temperature	25	^oC
K_{TL}	**SCA thermal loss coefficient**	**4.25**	**W/m^2K**
W_{out}	Turbine gross power output	110	MW
d_o	Outer diameter of the steel absorber pipe [138]	0.07	m
l_{sca}	Length of one Eurotrough SCA [140]	148.5	m
θ	Sun incidence angle on the aperture plane	0	^{o}
A_{IAM}	Coefficient for IAM calculation [137]	1	
B_{IAM}	Coefficient for IAM calculation [137]	0.0506	
C_{IAM}	Coefficient for IAM calculation [137]	-0.1763	
F_{IAM}	Incidence angle modifier - quantifies the effect of the incidence angle on the collector optical efficiency and useful aperture area of the SCA [141]	1	
F_S	Mirror soiling factor - represents the progressive soiling of mirrors and glass tubes after washing [138]	97	%
η_{RC}	Initial Rankine cycle efficiency (used to calculate base solar field area) [141]	37.5	%
A_b	**Base solar field area - the collector aperture area necessary to capture sufficient thermal energy to run the power block at the design parameters**	**388,979**	**m^2**
SM	Solar multiple - coefficient used to calculate total solar field area	1	
A	**Total solar field area**	**388,979**	**m^2**
N_{sca}	**Number of SCAs in solar field**	**476**	
w_{sca}	SCA width [140]	5.77	m
$A_{scacalc}$	**Calculated SCA aperture area**	**856.8**	**m^2**
A_{sca}	Useful SCA mirror aperture area [23]	817.5	m^2
A_{gap}	**Area of gaps between mirrors and modules in SCA**	**39.3**	**m^2**
L_{gap}	**Length of absorber pipe for mirror and module gaps**	**3,245**	**m**
L_{sca}	**Total length of SCA absorber pipe**	**70,659**	**m**

n_{scarow}	Number of SCAs in a row	4	
$l_{betweensca}$	Distance between each SCA in a row [137]	1	m
N_{rows}	**Number of rows in solar field**	**119**	
$L_{betweensca}$	**Total length of absorber piping used to connect SCAs within a row**	**357**	**m**
N_{loops}	**Number of SCA loops in solar field**	**59**	
$l_{betweenrow}$	Distance between each row [137]	15	m
$L_{endpipe}$	**Total length of absorber pipe used to connect SCA loops**	**892**	**m**
$L_{absorber}$	**Total length of absorber pipe in solar field**	**75,152**	**m**
$L_{coldheader}$	**Length of "cold" header piping**	**1,215**	**m**
$L_{hotheader}$	**Length of "hot" header piping**	**1,173**	**m**
L_{header}	**Total length of header piping in solar field**	**2,388**	**m**
L_{pipe}	**Total solar field pipe length**	**77,540**	**m**
Q_{sf}	**Design solar field thermal output**	**270**	**MW**

$$\eta_{opt} = F_R * F_I * F_T * F_A \text{ [138]} \quad (1)$$

$$K_{TL} = a + b * ((T_5+T_1)/2 - T_{amb}) + c * ((T_5+T_1)/2 - T_{amb})^2 \text{ [138]} \quad (2)$$

$$\theta = ACOS[SQRT(1 - (COS(S_{alt}) - 1 * COS(S_{alt}) * (1 - COS(S_{az} - 1)))^2)]; \quad (3)$$

where S_{alt} = solar altitude and S_{az} = Solar Azimuth [141]

$$F_{IAM} = A_{IAM} + (B_{IAM} \div COS(\theta)) * \theta + (C_{IAM} \div COS(\theta)) * \theta^2 \text{ [137]} \quad (4)$$

$$A_b = (W_{out}/\eta_{RC} + K_{TL} * \pi * d_o * l_{sca} * ((T_5+T_1)/2 - T_{amb})) / (DNR * \cos(\theta) * F_{IAM} * \eta_{opt} * F_S) \text{ [138]} \quad (5)$$

$$A = A_b * SM \quad (6)$$

$$N_{sca} = A \div A_{sca} \quad (7)$$

$$A_{scacalc} = l_{sca} * w_{sca} \quad (8)$$

$$A_{gap} = A_{scacalc} - A_{sca} \quad (9)$$

$$L_{gap} = N_{sca} * (A_{gap} \div w_{sca}) \quad (10)$$

$$L_{sca} = N_{sca} * l_{sca} \quad (11)$$

$$N_{rows} = N_{sca} \div n_{scarow} \quad (12)$$

$$L_{betweensca} = (n_{scarow}-1) * l_{betweensca} * N_{rows} \quad (13)$$

$$N_{loops} = N_{rows} \div 2 \quad (14)$$

$$L_{endpipe} = l_{betweenrow} * N_{loops} \quad (15)$$

$$L_{absorber} = L_{gap} + L_{sca} + L_{betweensca} + L_{endpipe} \quad (16)$$

$$L_{coldheader} = (N_{loops} - 1) * (w_{sca} + l_{betweenrow}) \quad (17)$$

$$L_{hotheader} = L_{coldheader} - 2 * (w_{sca} + l_{betweenrow}) \quad (18)$$

$$L_{header} = L_{coldheader} + L_{hotheader} \quad (19)$$

$$L_{pipe} = L_{absorber} + L_{header} \quad (20)$$

$$Q_{sf} = (A * DNR * \cos(\theta) * \eta_{opt} * F_{IAM} * F_S - K_{TL} * \pi * d_o * L_{pipe} * ((T_5+T_1)/2 - T_{amb}))/1000000 \text{ [138]} \quad (21)$$

3.2 Power Cycle Design Parameters

After the solar field area, piping length, and design solar field thermal output were calculated, the Rankine power cycle design conditions were identified. Table 11 lists the key design parameters used in Equations 22-29 to calculate the thermodynamic states and mass flows in the Rankine power cycle. All of these parameters were either taken directly from or calculated from Kelly and Kearney [103], which has the most transparent and comprehensive technical description of a trough plant with storage currently available in the literature. State 6 was set using the specified temperature and pressure as inputs to Cantera, which is an open source program that can be used to set thermodynamic states using a pair of thermodynamic properties [142]. Equations 22 through 30 were developed by applying mass and energy balances based on the thermodynamic principles to the main Rankine cycle components. Equations 22 and 24 were used to calculate the enthalpy at states 7, 9, 10, and 11, and Equations 23 and 24 were used to calculate the enthalpy of states 13 and 18. The enthalpies of states 8, 16, and d were calculated using Equation 25, and states 12 and 14 were set in Cantera by assuming a vapor fraction of zero and an isobaric closed feedwater heater and condenser. The trap valve was assumed to be isenthalpic to find state 15, and Equation 29 was used to find the power output for the low and high pressure turbines, as well as the required power input for the three pumps. Equation 30 calculated the design net Rankine cycle power output. Figure 29 displays the T-s diagram for the design Rankine cycle that resulted from these calculations.

Table 11 - Rankine Cycle Design Conditions (adapted from [103])

(Bold-faced items were calculated using the equations displayed below)

Symbol	Description	Design Value	Units
p_6	Steam pressure at state 6	100.01	bar
p_7	Steam pressure at state 7	19	bar
p_8	Steam pressure at state 8	17	bar
p_9	Steam pressure at state 9	7	bar
p_{10}	Steam pressure at state 10	2	bar
T_{10}	Steam temperature at state 10	373	^oC
p_{11}	Steam pressure at state 11	0.08	bar
p_{18}	Steam pressure at state 18	102	bar
T_c	Cooling water temperature at state c	25	^oC
p_c	Cooling water pressure at states c and d	1.01	bar
T_d	**Cooling water temperature at state d**	**37**	**^oC**
η_{t1}	Isentropic efficiency of high-pressure turbine	85.2	%
η_{t2}	Isentropic efficiency of low-pressure turbine	85	%
η_p	Isentropic efficiency of pumps	80	%
η_{sg}	Steam generator effectiveness of heat exchange	97	%
η_{rh}	Reheater effectiveness of heat exchange	97	%
η_c	Condenser effectiveness of heat exchange	73	%
η_{fwh}	Closed feedwater heater effectiveness of heat exchange	80	%
m_{steam}	**Mass flow rate of steam in Rankine cycle**	**107**	**kg/s**
z	**Mass flow fraction of steam exiting LP turbine at state 9**	**0.05**	
z'	**Mass flow fraction of steam exiting LP turbine at state 10**	**0.17**	
W_{t1}	**Power output from HP turbine**	**31**	**MW**
W_{t2}	**Power output from LP turbine**	**79**	**MW**
W_{p2}	**Power required for pump 2**	**0.09**	**MW**
W_{p3}	**Power required for pump 3**	**1.4**	**MW**
W_{netR}	**Net Power from Rankine Cycle**	**108.5**	**MW**

$w_t = \eta_t * (h_i - h_{es})$, (22)

where w = power per unit mass, h = enthalpy, i = inlet, e = exit, and s = isentropic

$w_p = (h_i - h_{es})/ \eta_p$ (23)

$h_e = h_i - w$ (24)

Heat exchanger: $h_e = h_i + \eta * (h_{es} - h_i)$ (25)

where η = effectiveness of heat transfer (used for steam generator, reheater, condenser and fwh

$z = (h_{17} - h_{16}) \div (h_9 - h_{16})$ (26)

$z' = (z \bullet (h_{16} - h_{14}) + h_{14} - h_{16}) \div (h_{14} - h_{12})$ (27)

$m_{steam} = W_e \div (h_6 + h_8 - h_7 - z \bullet h_9 - z' \bullet h_{12} - (1 - z - z') \bullet h_{11})$ (28)

$W = w * m_{steam}$ (29)

$W_{netR} = W_{t1} + W_{t2} - (W_{p2} + W_{p3})$ (30)

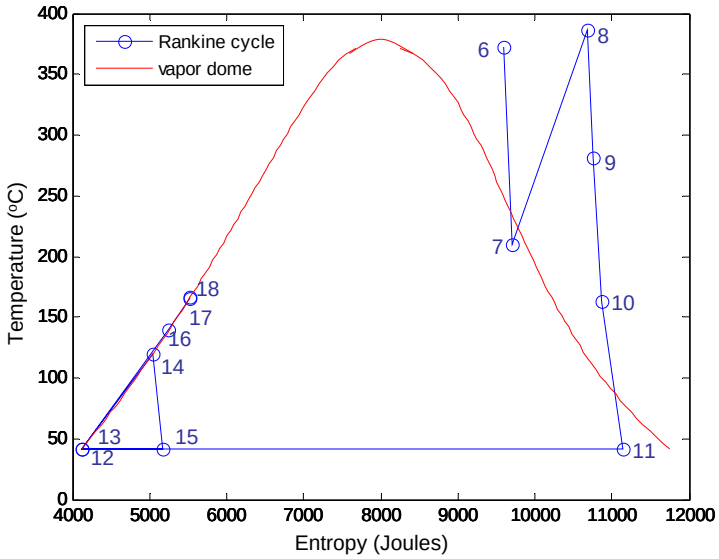

Figure 29 – T-s Diagram for Rankine Cycle at Design Point

Blue numbers refer to unique thermodynamic water/steam states indicated in Figure 27

3.3 HTF System Design Parameters

Once the Rankine cycle design states were set, the design states for the Therminol VP-1 cycle needed to be defined (see Table 12). Similar to the Rankine cycle, the specified parameters for the HTF cycle were derived from Kelly and Kearney [103]. Again, this study has the most transparent and comprehensive technical description of a trough plant with storage currently available in the literature. Equations 31-41 were developed by applying mass and energy balances based on thermodynamic principles to main components in the cycle (except where noted). A mathematical program was created to calculate the enthalpy and temperature of states 2, 4, 5, the HTF mass flow rate, and the power input to pump 1. The challenge was that each state depended on the state before it, and although state 5 was specified in the beginning of the program, a new state 5 would be calculated by the end of the program. Therefore, the program

was set up to calculate the difference between the initial and resulting temperature values for this state (ΔT_5). This ΔT_5 value was then minimized using the Matlab optimization function "fmincon" to find the initial T_5 value that resulted in the smallest ΔT_5 at the end of the program. The key constraint in this optimization was that m_{HTF} had to be between 0.00001 kg/s and 1.2 times the design value.

Table 12 - Heat Transfer Fluid (HTF) Cycle Design Conditions

(Bold-faced items were calculated using the equations displayed below)

Symbol	Description	Design Value	Units
Q_{HTFmin}	**The minimum heat input needed to run the Rankine cycle at design conditions**	**245**	**MW**
T_2	**HTF temperature at state 2**	**300**	**°C**
T_3	HTF temperature at state 3	225	°C
T_4	**HTF temperature at state 4**	**292**	**°C**
p_4	**HTF pressure at state 4**	**1.1**	**bar**
T_5	**HTF temperature at state 5**	**292**	**°C**
p_5	HTF pressure at state 5	6.2	bar
m_{HTF}	**Mass flow rate of HTF in solar field**	**1,206**	**kg/s**
y	**Mass flow fraction of HTF entering the reheater**	**0.11**	
W_{p1}	**Power required for pump 1**	**0.94**	**MW**
W_{net}	**Net power output**	**107.6**	**MW**

$$Q_{HTFmin} = (m_{steam} * (h_{18} - h_6)) \quad (31)$$
$$m_{HTF} = Q_{HTFmin} / (h_1 - h_5) \quad (32)$$
$$h_{HTF} = 1.377 * T^2 + 1.498e3 * T - 1.834e4 \text{ [141]} \quad (33)$$
$$y = -(m_{steam} * (h_7 - h_8)) \div (m_{HTF} * (h_1 - h_3)) \quad (34)$$
$$h_2 = h_1 + (m_{steam} * (h_{18} - h_6)) / ((1-y) * m_{HTF}) \quad (35)$$
$$h_4 = (1-y) * h_2 + y * h_3 \quad (36)$$
$$\text{Density: } \rho_{htf} = -7.762e\text{-}4 * T^2 - 6.367e\text{-}1 * T + 1.074e3 \text{ [141]} \quad (37)$$
$$w_{p1} = \rho_4^{-1} * (p_4 - p_5) / \eta) \quad (38)$$
$$h_5 = h_4 - w_{p1} \quad (39)$$
$$T_{htf} = 7.4333e\text{-}17 * h^3 - 2.4625e\text{-}10 * h^2 + 6.3282e\text{-}4 * h + 1.2403e1 \text{ [141]} \quad (40)$$
$$W_{net} = W_{netR} - W_{p1} \quad (41)$$

First, an initial Therminol VP-1 mass flow rate (m_{HTF}) value was calculated using Equations 31 and 32, and initial enthalpy values (h_1 and h_5) were calculated using the design inputs and

equation 33. Next, the mass fraction of HTF to the reheater was calculated using Equation 34, and the enthalpy of state 2 was defined using the steam generator energy balance, shown as Equation 35. State 3 was defined based on thermodynamic property values obtained from Kelly and Kearney [103], and the enthalpy of state 4 was calculated through the expansion vessel energy balance depicted in equation 36. Equations 37 and 38 were used to calculate the intensive power input to pump 1, and Equation 39 defined the enthalpy of state 5 at the end of the cycle. After the enthalpy of each state was defined, the temperature of each state was found through Equation 40. Once the minimization of ΔT_5 was complete, the total power of pump 1 could be calculated using equation 29 (substituting m_{HTF} for m_{steam}), and finally the design net power output of the system (before factoring in parasitic losses from auxiliary equipment) was calculated using Equation 41.

3.4 Thermal Energy Storage System Design Parameters

Once the system design point was established for the "solar only" operation mode, the molten salt thermal energy storage system could be designed. Figure 30 and Figure 31 display the system designs associated with the "TES charge" (Day_TESC) and "discharge" (Day_TESD) cycles, respectively (see Table 14 in section 3.5 for a description of these operation modes); variables "a" and "b" represent the molten salt thermodynamic states flowing between the hot and cold storage tanks and the oil-to-salt heat exchanger.

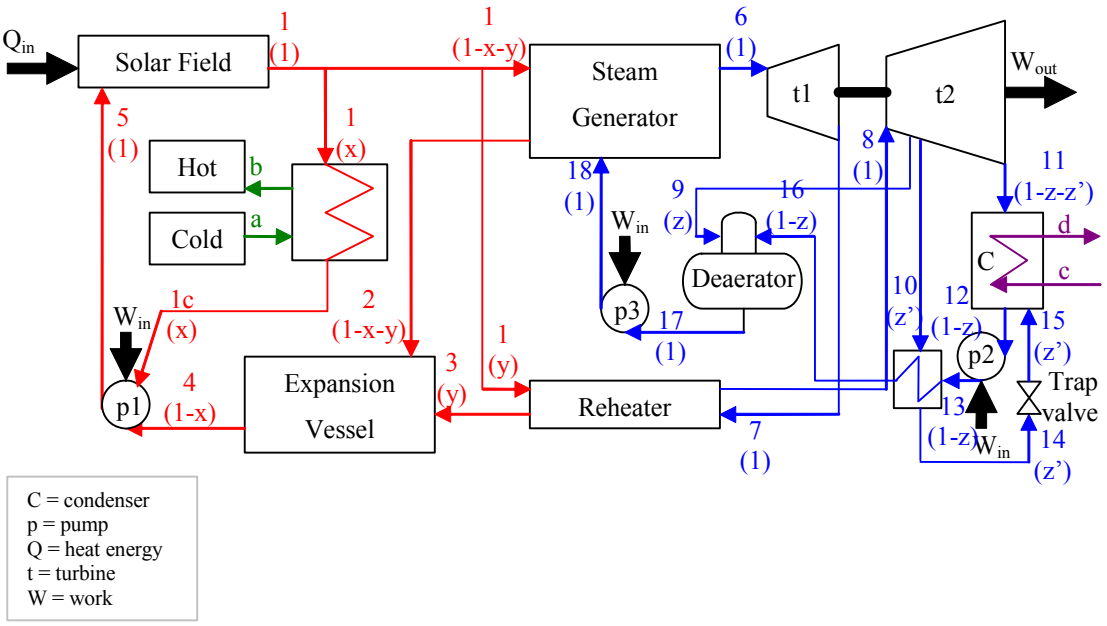

Figure 30 - Schematic of Day_TESC Mode.

Green lines and variables "a" and "b" refer to molten salt flows and states, respectively

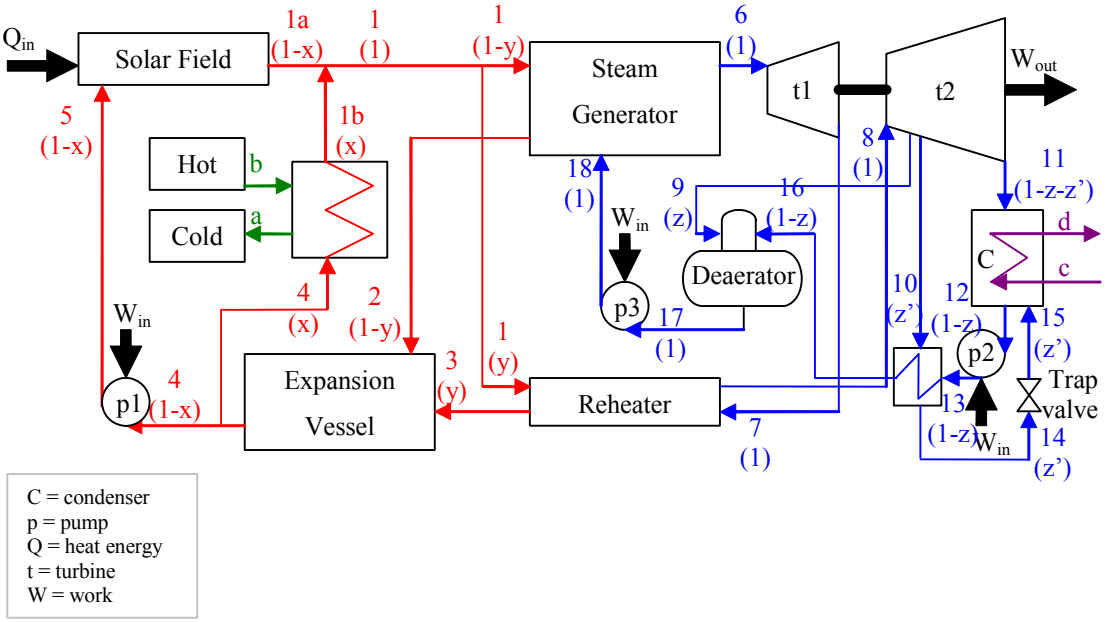

Figure 31 -Schematic of Day_TESD Mode.

Green lines and variables "a" and "b" refer to molten salt flows and states, respectively

Table 13 shows the key parameters associated with the TES system design states. The design temperatures and heat exchanger effectiveness values were obtained from Kelly and Kearney [103], and Equation 42 calculated the enthalpies for these states. Equations 43-54 were developed by applying mass and energy balances based on thermodynamic principles to main components in the TES system. The enthalpies were used to calculate the heat exchanger effectiveness values in Equations 43 and 44. The minimum HTF mass flow rate was calculated as ten percent of the design point based on personal communication with experts in the industry, and the design mass flow fraction from TES (x_d) was calculated using equation 46. Equations 47 and 48 define the storage capacity as the amount of energy needed to operate the turbine at full capacity for the number of storage hours specified. The storage capacity was calculated to reflect the maximum amount of heat that would be needed from the system during any single hour, using the design m_{HTF} multiplied by an increase factor ($F_{mHTFmax}$). There is a tradeoff in the selection of $F_{mHTFmax}$ in that a greater value will increase plant operational hours by increasing the size of the storage system, but a larger storage system will also increase the capital cost of the plant. In order to prevent unreasonable sizing of the storage system, a nominal value of 1.5 was selected after observing that m_{HTF} rarely exceeded 1.5 times the design value during several hourly simulations. Equations 51 and 52 illustrate how the total amount of salt for the storage system was calculated and how the maximum allowable amount of salt in one tank was calculated for the hourly simulation. Equations 53 and 54 re-calculate the net system power output to include the pump power required for the TES system.

Table 13 - Thermal Energy Storage System Design Parameters

(Bold-faced items were calculated using the equations displayed below)

Symbol	Description	Design Value	Units
T_a	Temperature of salt at state a [103]	291	°C
T_b	Temperature of salt at state b [103]	381	°C
$T_{saltmin}$	Minimum salt temperature in order to keep it well above the freezing point (220°C)	250	°C
T_{1b}	**Temperature of HTF at state 1b during discharge cycle**	**371**	**°C**
T_{1c}	Temperature of HTF at state 1c during charge cycle [103]	301	°C
η_{hxh}	**TES heat exchanger effectiveness of heating**	**88**	**%**
η_{hxc}	**TES heat exchanger effectiveness of cooling**	**91**	**%**
m_{HTFmin}	**Minimum HTF mass flow rate to prevent freezing in pipes**	**121**	**kg/s**
x_d	**HTF mass flow fraction during discharge cycle**	**0.9**	
$F_{mHTFmax}$	Factor used to increase m_{HTF} for Q_{TES} calculation	1.5	
$Q_{TEShourly}$	**Maximum amount of heat energy released from the TES system during a discharge hour**	**313**	**MWht**
t_{TES}	Hours of storage - amount of time the turbine can operate solely on heat from TES system (*example for data that follow*)	6	hrs
$Q_{TEStotal}$	**TES storage capacity**	**1,876**	**MWht**
m_{salt}	**Mass flow rate of salt**	**2,315**	**kg/s**
F_{salt}	Extra salt factor - to account for amount of salt that always needs to remain in tank [103]	1.14	
$M_{saltmin}$	**Minimum amount of salt that must remain in each tank at all times**	**3,989,664**	**kg**
$M_{salttotal}$	**Total mass of salt needed for system**	**56,995,200**	**kg**
$M_{salthotmax}$	**Maximum amount of salt allowed in hot (or cold) TES tank**	**53,005,536**	**kg**
F_{pTES}	Factor used to calculate TES pump power [141]	150	J/kg

**Sample values (displayed in red) were calculated for 6 hr TES with SM = 2.23*

$h_{salt} = 8.6e\text{-}2 \bullet T^2 + 1.443e3 \bullet T$ [141] (42)

$\eta_{hxh} = (h_b - h_a)/(h_{bs} - h_a)$, *where h_{bs} refers to the isentropic enthalpy* (43)

$\eta_{hxc} = (h_{1c} - h_1)/(h_{1cs} - h_1)$, *where h_{cs} refers to the isentropic enthalpy* (44)

$h_{1b} = \eta_{hxh} * (h_{1bs} - h_4) + h_4$, *where h_{1bs} refers to the isentropic enthalpy* (45)

$x_d = 1 - (m_{HTFmin}/ m_{HTF})$ (46)

$Q_{TEShourly} = (x_d * m_{HTF} * F_{mHTFmax} * (h_4 - h_{1b}))/1000000$ (47)

$Q_{TEStotal} = Q_{TEShourly} * t_{TES}$ (48)

$m_{salt} = (Q_{TEShourly} * 1000000)/ (h_b - h_a)$ (49)

$M_{salttotal} = m_{salt} * 3600 * t_{TES} * F_{salt}$ (50)

$M_{saltmin} = M_{salttotal} * ((F_{salt} - 1)/2)$ (51)

$M_{salthotmax} = M_{salttotal} - M_{saltmin}$ (52)

$W_{pTES} = F_{pTES} * m_{salt}$ (53)

$W_{net} = W_{netR} - W_{p1} - W_{pTES}$ (54)

3.5 Hourly Simulation

Once the system design conditions were specified, the hourly simulation was developed as a series of conditional statements relating to eight unique operational modes, which are presented in Table 14. The table also presents the criteria used to select each mode in the unique hourly simulation algorithm for each plant configuration. In order for the mode to be activated, both criteria need to be satisfied. The first calculations at the beginning of each hour of the simulation are the SCA thermal loss coefficient (K_{TL}) and the solar field thermal energy (Q_{sf}) using equations 2 and 21, respectively. These calculations require hourly inputs for DNR, T_{amb}, F_{IAM}, θ, and T_5 and T_1 from the previous hour. The first hour of the simulation for each plant configuration is on January 1st at 1:00 am. The selected mode is Night_SD, and T_5 and T_1 are both set at 100^{o}C for this first hour. Operation modes Day_TESC, Day_TESD, Night_TESD, and Night_TESFP are only used by the plants with thermal energy storage, and HYBRID is only used by the plants with natural gas backup. Modes Day_SOLAR, Night_SD, and Night_FFP are used by all plant configurations.

Table 14 - Plant Operation Modes for Hourly Simulation

Mode ID	Description	Criteria
Day_TESC	"TES Charge": Only the solar field delivers thermal energy to the power cycle; excess solar energy "charges" the TES system	$Q_{SF} > Q_{HTFmin}$ $M_{salthot} < M_{salthotmax}$
Day_SOLAR	"Solar Only": Only the solar field delivers thermal energy to the power cycle; the TES system is idle	$0 < Q_{SF} \leq Q_{HTFmin}$ $M_{salthot} \leq M_{saltmin}$
Day_TESD	"TES Discharge": The solar field and the TES system deliver thermal energy to the power cycle	$0 < Q_{SF} < Q_{HTFmin}$ $M_{salthot} > M_{saltmin}$
Night_TESD	"TES Discharge": Only the TES system delivers thermal energy to the power cycle; HTF circulates through the solar field at a minimum mass flow rate to stay warm	$Q_{SF} \leq 0$ $M_{salthot} > M_{saltmin}$
HYBRID	The solar field and the natural gas-fired heater heat the oil to the temperature required to generate the same amount of electricity as PT-TES	$W_{PT\text{-}TES} > W_{PT\text{-}NG}$

Night_SD	"Shutdown": The power cycle is idle; HTF circulates through the solar field at a minimum mass flow rate to stay warm	$Q_{SF} \leq 0$ $M_{salthot} \leq M_{saltmin}$
Night_TESFP	"TES Freeze Protection": The power cycle is idle; HTF circulates through the solar field at a minimum mass flow rate, and the TES system protects the HTF from freezing	$Q_{SF} \leq 0$ $M_{salthot} > M_{saltmin}$ $T_{HTF} \leq 50^oC$
Night_FFP	"Fossil Freeze Protection": The power cycle is idle; HTF circulates through the solar field at a minimum mass flow rate, and the natural gas-fired heater protects the HTF from freezing	$Q_{SF} \leq 0$ $M_{salthot} \leq$ min $T_{HTF} \leq 50^oC$

3.5.1 Overview of Hourly Simulation Algorithms

Figure 32 presents a flow diagram of the algorithm used in the hourly simulation of a parabolic trough plant with no storage and no natural gas backup (except for HTF freeze protection). The key inputs are the design parameters described in sections 3.1-3.4, the hourly direct normal radiation (DNR) and hourly ambient temperature from the TMY3 weather file for Daggett, CA, and the hourly HTF temperature at the inlet of the solar field calculated in the previous hour. Equation 21 calculates the thermal output from the solar field (Q_{sf}), and if this value is greater than zero, then operation mode DAY_SOLAR calculates the hourly electricity generation. If this value is less than zero, or if DAY_SOLAR fails, then either Night_SD or NIGHT_FFP calculates the parasitic energy needed to keep the power cycle idle and the HTF circulating through the solar field at a minimum mass flow rate. The latter mode is selected if the HTF temperature is less than 50^oC. Any operation mode that involves power cycle operation will fail if it does not meet all of the following constraints:

1) $50^oC \leq T_2 \leq 300^oC$

2) $0 \leq y \leq 0.5$

3) $m_{HTFmin} < m_{HTF} < m_{HTFmax}$

4) $50 \leq T_{HTF} \leq 393^{o}C$ [35]

5) $M_{salt} + M_{salthot,\ at\ t-1} < M_{saltmax}$ (TES modes only)

6) $0 \leq x \leq 0.9$

The maximum mass flow rate for constraint three is set at two times the design mass flow rate for the nominal results, and the effect of this parameter on model results is examined in Chapter 6.

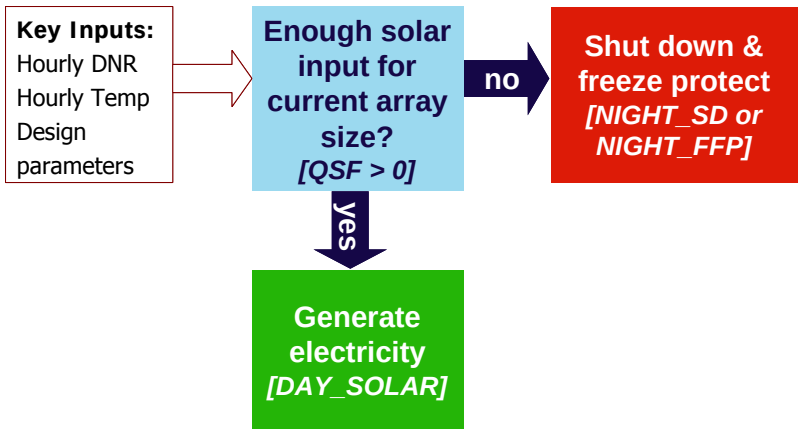

Figure 32 - Hourly Simulation Algorithm for Plant with No Storage/Backup

Figure 33 displays a flow diagram of the algorithm used in the hourly simulation of a parabolic trough plant with thermal energy storage. The key inputs are the same as the plant with no storage, except for $M_{salthot}$, the mass of the salt in the hot storage tank, which determines whether there is enough energy remaining in storage to generate electricity with Day_TESD or Night_TESD or provide freeze protection with Night_TESFP. The initial question is the same as for the plant with no storage/backup as well, but if there is enough solar input for the current array size, then this algorithm determines if there is more than needed to run the power cycle at full capacity. If so, then operation mode Day_TESC is activated to calculate hourly electricity

generation and the new $M_{salthot}$ value based on adding the excess solar thermal energy to the TES system. If there is not more energy than is needed to run the power cycle, then Day_SOLAR calculates the hourly electricity generation. If there is not enough energy to run the power cycle at full capacity and there is energy remaining in storage, then either Day_TESD or Night_TESD calculates the hourly electricity generation based on supplementing thermal energy input to the power cycle from the TES system.

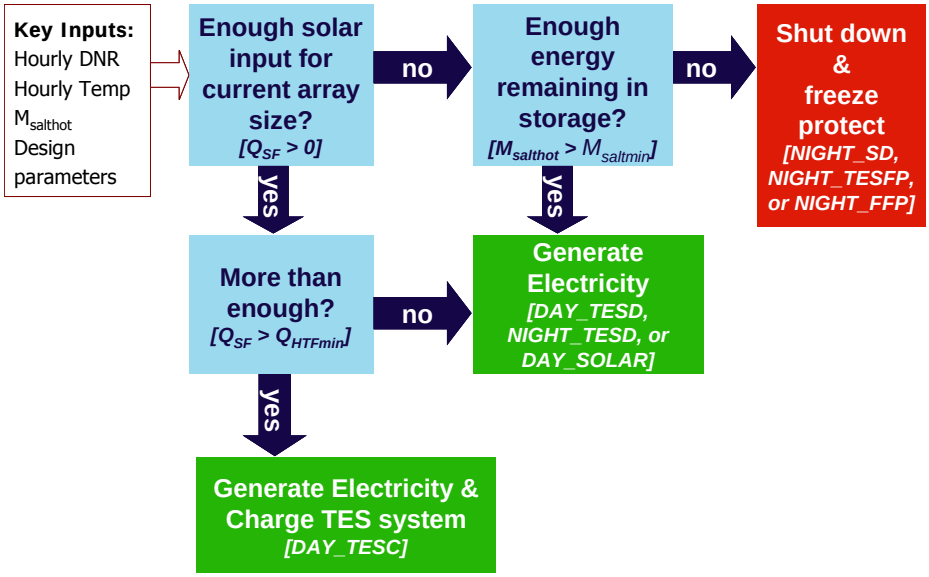

Figure 33 - Hourly Simulation Algorithm for Plant with TES

Figure 34 presented a flow diagram of the hourly simulation algorithm for the parabolic trough plant with natural gas backup. It differs from the algorithm presented in Figure 32 in that when there is not enough solar input for the current array size and the plant with TES generated electricity, the plant with NG backup is forced to generate the same amount of electricity as the plant with TES using the HYBRID operation mode.

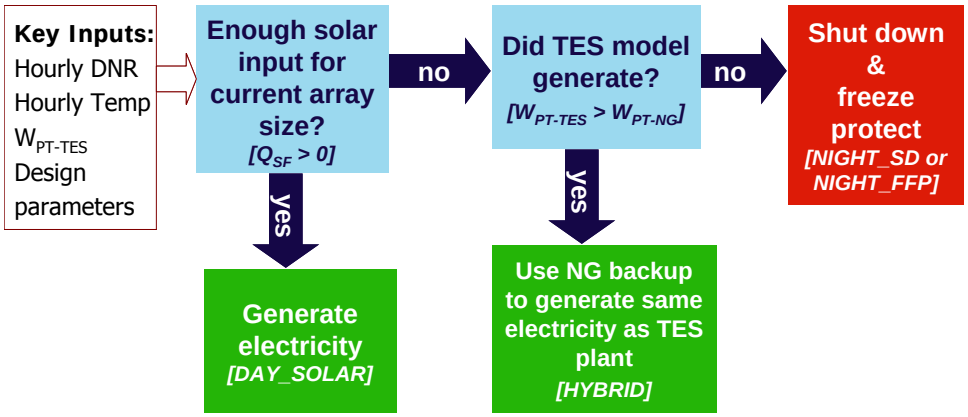

Figure 34 - Hourly Simulation Algorithm for Plant with NG Backup

This section has described a general overview of the conditional algorithms used to select each operation mode presented in Table 14 during the hourly simulation for each of the three main plant configurations modeled in this study. The next section provides a more detailed description of how each operation mode calculates its key outputs.

3.5.2 Detailed Description of Operation Modes

The first operation mode presented in Table 14, **Day_TESC** (see Figure 30), operates when $Q_{sf} > Q_{HTFmin}$ and M_{salt} in the hot tank is less than $M_{saltmax}$. This mode initially sets HTF state 1 at the design point in order to calculate m_{HTF} using equation 32 and h_5 from the previous hour, and then it calculates the mass flow fraction x as $(Q_{sf}/Q_{HTFmin}-1)$. Day_TESC sets the rest of the HTF and salt states using energy balance equations presented in sections 3.1-3.4, under the constraints presented in section 3.5.1. These constraints are satisfied through modifications to mass flow rates, but if these modifications fail to meet the constraints, the simulation chooses Day_SOLAR to operate for that hour instead of Day_TESC. Originally, all modes used Cantera and the energy balance equations and parameters presented in section 3.2 to set the Rankine cycle states.

However, the repeated use of Cantera caused the total run time of the 8,760 simulations to exceed 15 minutes. Given that 50-100 iterations of the entire program would be required for each of the 25 plant configurations modeled in this study in order to select the solar field area that minimizes the LCOE, this run time was too long. Matlab identified the Cantera operations as the key portion of the code that was slowing the program, so water/steam states 9-18 were set at the design point, and a parametric evaluation was conducted to approximate the relationship between T_1 and both the net Rankine cycle power and the enthalpies of states 6, 7, and 8. The parametric evaluation varied T_1 from 204 - 395^{o}C and calculated the Rankine cycle water/steam states and net power output for each 0.1^{o}C increase in that range. The full results of this evaluation are presented in Appendix A, and Equations 53-57 resulted from fitting curves to the results. These equations were used in all of the hourly operation modes in place of the more accurate Cantera-thermodynamic calculations, reducing the run time to about 30 seconds instead of 15 minutes. Day_TESC also calculates the enthalpy of state h_{1c}, the power required for pump 1, and the enthalpy of state 5 using Equations 37, 40, 44, 58, and 59.

$$h_6 = 1.4698E+04 \bullet T_1 - 1.8493E+07 \quad (53)$$

$$T_6 = 0.8845 \bullet T_1 + 26.779 \quad (54)$$

$$h_7 = -11.51 \bullet T_1^2 + 11320 \bullet T_1 - 1.5931e7 \quad (55)$$

$$h_8 = 2.6102E+03 \bullet T_1 - 1.3763E+07 \quad (56)$$

$$W_{netR} = 321830 \bullet T_1 - 18500000 \quad (57)$$

$$W_{p1} = m_{HTF} * [[x * \rho_{1c}^{-1} * (\rho_{1c} - p_5)] \div \eta_p + [(1-x) * \rho_4^{-1} * (p_4-p_5)] \div \eta_p] \quad (58)$$

$$h_5 = x * h_{1c}+(1-x) * h_4 - w_{p1} \quad (59)$$

The second mode presented in Table 14, **Day_SOLAR** (see Figure 27), operates when Day_TESC fails and/or the selection criteria presented in the table are satisfied. Day_SOLAR operates under Day_TESC constraints 1-4, which are satisfied through modifications to mass flow rates. If these modifications fail to meet the constraints, the hourly simulation attempts to

run Day_TESD instead of Day_SOLAR. Day_SOLAR initially sets HTF state 1 at the design point in order to calculate m_{HTF} using Equation 32 and h_5 from the previous hour. If this calculation results in m_{HTF} less than m_{HTFmin}, Day_SOLAR adjusts m_{HTF} to m_{HTFmin} and uses Equation 32 to re-calculate the enthalpy of state 1. The Rankine cycle states are initially calculated with Equations 53 through 57, and y and h_2 are calculated with Equations 34 and 35, respectively. If these calculations result $T_2 < 50^oC$, then Day_SOLAR sets T_2 equal to this lower bound and re-calculates y with Equation 65 and h3 with Equation 67. If the constraints still aren't satisfied, Day_SOLAR runs through a series of iterations to adjust mass flow and/or enthalpy values with the equations listed this chapter. For example, if y is greater than the upper constraint, Day_SOLAR sets y to 0.5 and re-calculates m_{HTF} with equation 64 and h_1 with equation 32.

$$m_{HTF} = [m_{steam} * (h_7-h_8)] \div [y * (h_1-h_3)] \quad (64)$$
$$y = 1 + [(m_{steam} * (h_{18} - h_6)) \div ((h_1 - h_2) * m_{HTF})] \quad (65)$$
$$m_{HTF} = -[m_{steam} * (h_{18} - h_6)] \div [(1-y) * (h_1 - h_2)] \quad (66)$$
$$h_3 = h_1 + [m_{steam} * (h_7 - h_8)] \div [y * m_{HTF}] \quad (67)$$

If any of the values violate the constraints at this point, Day_SOLAR fails. If all of the constraints are satisfied, then Day_SOLAR calculates h_4, h_5, W_{p1}, and W_{net} with Equations 36, 39, 38, and 41, respectively. This complex set of conditional commands is intended to partially represent the flexibility of the power plant to adapt to less-than-ideal conditions. However, these commands are far from perfect. In reality, a plant operator would have access to real-time power plant operational information and be able to adjust fluid mass flow rates and solar collector angles to maximize power output continuously. Moreover, a plant operator would be able to adjust the steam mass flow rates and steam cycle states. For simplicity, these parameters have

been set to the design values in order to attempt to balance the flexibility of a real power plant with the need for simplicity required of an engineering model.

If Day_SOLAR fails, the hourly simulation selects **Day_TESD** for the TES plant configuration (see Figure 31) when the Table 14 selection criteria are satisfied. This mode initially sets m_{HTF} equal to m_{HTFmin} in order to maximize the temperature of the HTF at the outlet of the solar field (T_{1a}). Then, Day_TESD calculates the enthalpy of state 1a with Equation 32 and h_5 from the previous hour. If T_{1a} exceeds the design point, Day_TESD sets T_{1a} at the design point and calculates an initial m_{HTF} value with equation 32. Next, Equation 68 calculates x; Equation 45 calculates h_{1b}, using h_4 from the previous hour as an input; Equation 69 calculates h_1; and m_{HTF} is re-set to equal $m_{HTFdesign}$. The rest of the fluid states and mass flow rates are calculated pursuant to the same constraints and mass flow rate modifications as Day_SOLAR, with the following additional constraint: $M_{salthot} > M_{saltmin}$. In order to ensure this constraint is satisfied, Day_TESD used Equations 70 and 71 to calculate the amount of salt needed to obtain h_{1b}, and checks whether the constraint is satisfied by comparing the result of Equation 72 with the design value $M_{saltmin}$. If the constraint is satisfied, Day_TESD calculates the remaining salt in the cold tank with Equation 73. If the constraint is not satisfied, then the amount of salt in the hot tank ($M_{salthot}$) is set equal to $M_{saltmin}$, and Equations 74-77 and 69 calculate M_{salt}, m_{salt}, m_{HTF}, h_{1a}, and h_1.

$$x = 1 - (m_{HTF}/m_{HTFdesign}) \quad (68)$$

$$h_1 = (1-x) * h_{1a} + x * h_{1b}; \quad (69)$$

$$m_{salt} = (m_{HTF} * x * |h_{1b}-h_{4o}|) \div |h_a - h_b|; \text{ where } h_{4o} = h_4 \text{ from the previous hour} \quad (70)$$

$$M_{salt} = m_{salt} * 3600 \quad (71)$$

$$M_{salthot} = M_{salthot,\ t-1} - M_{salt}; \text{ where } M_{salthot,\ t-1} = M_{salthot} \text{ from the previous hour} \quad (72)$$

$$M_{saltcold} = M_{saltcold,\ t-1} + M_{salt} \quad (73)$$

$$M_{salt} = M_{salthot,\ t-1} - M_{saltmin} \quad (74)$$

$$m_{salt} = M_{salt} \div 3600 \quad (75)$$

$$m_{HTF} = [m_{salt} * |h_b - h_a|] \div [x * |h_{4o} - h_{1b}|] \quad (76)$$

$$h_{1a} = h_{5o} + (Q_{SF} * 1000000) \div (m_{HTF} * (1 - x)); \text{ where } h_{5o} = h_5 \text{ from the previous hour} \quad (77)$$

$x = 1 - (m_{HTFmin}/m_{HTF})$ (78)

$h_{1b} = h_{4o} + [m_{salt} * |h_b - h_a|] \div [m_{HTF} * x]$ (79)

$Q_{saltFP} = m_{salt} * (h_a - h_{amin}) * 3600$; where h_{amin} = the minimum h_a value to satisfy the constraint (80)

Once h_1 has been re-calculated, it is necessary to determine if state 1 satisfies the constraint for the steam cycle input as described above ($320^oC \leq T_1 \leq 393^oC$). If the constraint is satisfied, Equations 53 through 57 calculate the steam cycle parameters, and the remaining HTF states are calculated in a similar manner as Day_SOLAR. If T_1 is less than the lower bound of the constraint, the mode fails, but if it is greater than the upper bound of the constraint, then Day_TESD adjusts x with Equation 78, and Equations 70-73 re-calculate m_{salt}, M_{salt}, $M_{salthot}$, and $M_{saltcold}$. The enthalpy of states 1b and 1 are re-calculated with Equations 79 and 69, respectively. If the T_1 and $M_{salthot}$ constraints still are not satisfied at this point, the mode fails. As long as all constraints are satisfied, Day_TESD then calculates the Rankine cycle parameters and the remaining HTF cycle parameters with the equations listed previously. Finally, if T_a is less than 250^oC, equation 80 calculates the freeze protection (FP) energy required from the salt heater to raise the temperature to this minimum value.

If the first four operational modes listed in Table 14 fail for the plant with TES, the hourly simulation selects **Night_TESD**, which operates in a similar fashion as Day_TESD except that it is specifically designed to run when $Q_{sf} \leq 0$. The schematic for the two modes is identical, and the main difference between the mathematical models is in the way m_{HTF} is calculated. The primary objective in Day_TESD is to maintain T_{1a} at or near the design value, and m_{HTF} is calculated to reach this objective. The objective in Night_TESD is to keep T_{1a} as high as possible, but it is not likely that it will approach the design value since it is unlikely that $Q_{sf} > 0$. The hourly simulation selects Night_TESD in two situations: 1) the selection criteria in Table 14

have been met; or 2) the first three modes in the hierarchy failed, and the simulation is moving down the list. In the second situation, it is possible that Q_{sf} is actually greater than zero but so small that none of the other modes worked. Therefore, Night_TESD initially sets m_{HTF} to m_{HTFmin} and calculates h_{1a} with Equation 32 and h_5 from the previous hour. If this results in $T_{1a} < T_{5o}$, then the solar field is losing too much heat to raise the temperature of the HTF, and Night_TESD re-calculates m_{HTF} with Equation 32 after setting $T_{1a} = T_{5o} - 2$ (T_{1a} needs to be slightly less than T_{5o} to avoid dividing by zero). If this results in $m_{HTF} > m_{HTFdesign}$, then Night_TESD caps m_{HTF} at 2 times $m_{HTFdesign}$ and re-calculates. The reasoning behind this calculation is that it would not be economical to make m_{HTF} too large because then the pump 1 power would be excessive, and shutdown mode would probably be preferable. Chapter 6 will explore the sensitivity of results to changes in this parameter. The rest of the calculations in Night_TESD are virtually identical to Day_TESD.

The **HYBRID** operation mode, used only by the plant configuration with natural gas backup, uses a natural gas-fired heater to maintain the HTF temperature at a certain level in order to generate the same amount of electricity in a given hour as a comparable plant with TES. HYBRID operates under one of two conditions: 1) $Q_{SF} > 0$, and Day_SOLAR failed to generate the same W_{net} as the corresponding PT-TES simulation; or 2) $Q_{SF} < 0$, but $W_{net} > 0$ for the corresponding TES simulation. In other words, HYBRID is activated when the comparable TES simulation resulted in more net electricity for that hour than the NG backup configuration can accomplish using Day_SOLAR. Figure 35 presents a schematic for the HYBRID operation mode.

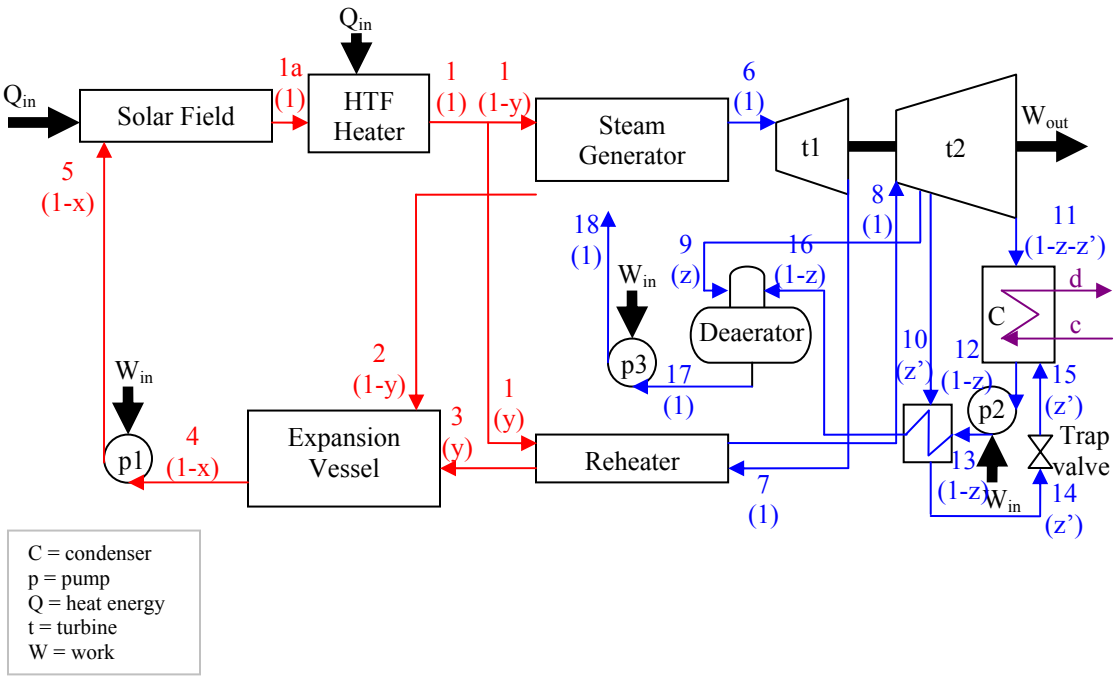

Figure 35 - PT-NG Plant Schematic for HYBRID Operation Mode

HYBRID has the same constraints as Day_SOLAR and begins with similar calculations for m_{HTF} and h_{1a} as Day_TESD. Then, HYBRID sets h_1 equal to h_1 from the comparable PT-TES simulation, and calculates the Rankine cycle parameters with Equations 53-59, and y and h_2 with Equations 34 and 35, respectively. After that, HYBRID conducts a similar series of checks and balances as Day_TESD to ensure that the y and T_{HTF} constraints are satisfied, and then it calculates the remaining HTF cycle parameters in the same way as Day_TESD and Day_SOLAR. The energy required for the natural gas-fired heater to raise the HTF temperature from T_{1a} to T_1 is calculated with equation 81, substituting state 1 and 1a enthalpies in place of state 4a and 4b enthalpies.

The first five modes in Table 14 enable the power cycle to operate and the plant to generate electricity. If all of these four modes fail, then the plant must shut down. **Night_SD** is the simplest of the shutdown modes (see Figure 36), in which the power cycle is idle and shaded in grey, and the HTF circulates the solar field at m_{HTFmin} to maintain the HTF temperature at $T_{4design}$, in order to reduce start-up time and energy in the morning hours. During this mode, the m_{HTF} entering and exiting the expansion vessel is modified to keep as much HTF in the vessel as necessary to maintain temperatures at the design value of T_4.

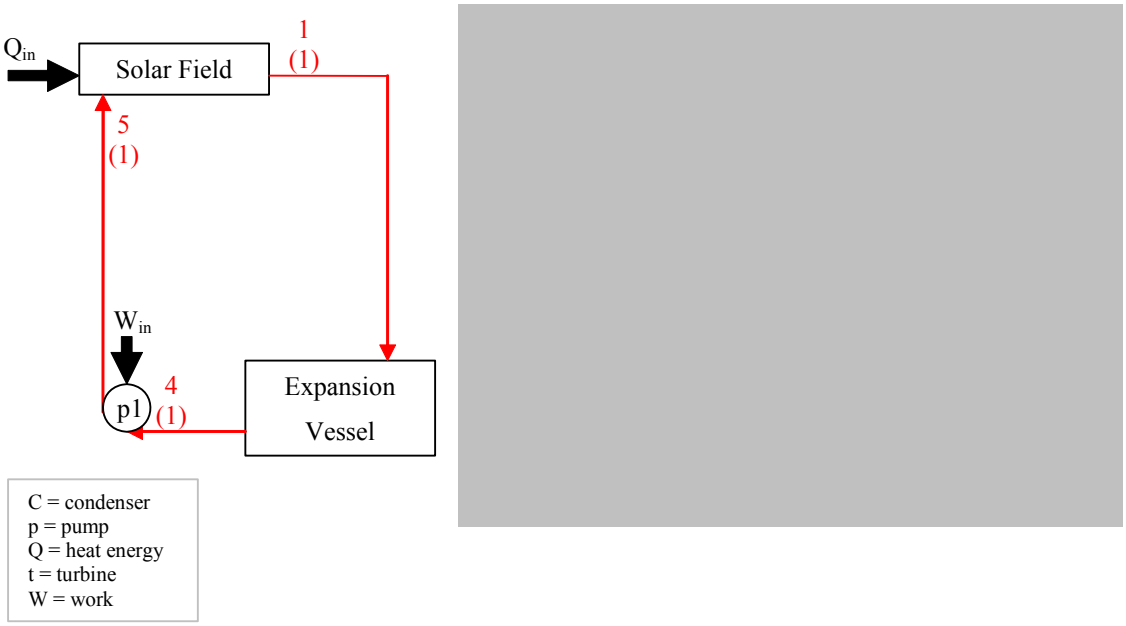

Figure 36 - Night_SD Plant Schematic

When Night_SD fails to maintain HTF temperatures above the design value of T_4, either **Night_FFP** or **Night_TESFP** is employed to prevent HTF freezing. Night_FFP looks and operates like Night_SD except the objective is to keep HTF temperatures above the minimum value of 50°C, and a natural gas-fired HTF heater, placed between the expansion vessel and

pump 1, is used when the expansion vessel energy balance fails to meet this objective. Equation 81 shows how Night_FFP calculates the required heat from the natural gas-fired heater.

$$Q_{htr} = m_{HTF} * (h_{4a}-h_{4b}) * 3600 \quad (81)$$

The hourly simulation selects Night_FFP only as a last resort when both Night_SD and Night_TESFP have failed. Night_TESFP performs the same function as Night_FFP except the TES system, rather than a natural gas-fired heater, is used to provide freeze protection when there is enough energy in the TES system (see Figure 37). Night_TESFP uses similar calculations to Day_TESD and Night_TESD to calculate the parameters associated with the TES system.

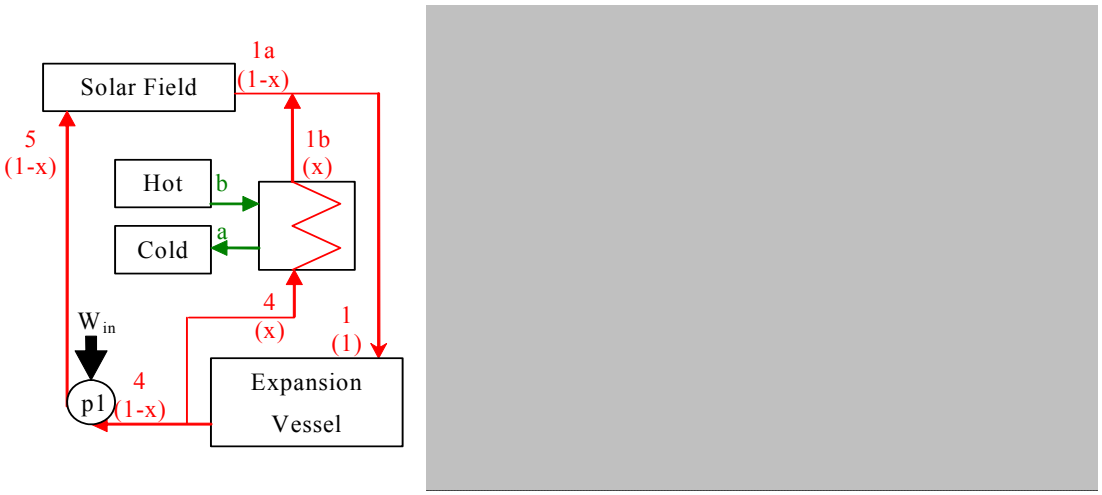

Figure 37 - Night_TESFP Plant Schematic

3.6 Final Calculation of Key Performance Model Outputs

After the hourly simulation code iterates through all 8,760 hours, the annual net electricity generation and plant capacity factor can be calculated. The electrical losses due to the HTF, TES and Rankine cycle pumps have been accounted for in the hourly W_{net} calculation described above. There are, however, other parasitic electrical losses (electronic motors, drives, computers, etc), which have not been thermodynamically modeled, that must be accounted for in the calculation of net electrical output (see Table 15). The equations used to calculate the total parasitic losses from the system (Equations 82 through 91) are the same equations used in the empirical trough Solar Advisor Model (SAM) [141].

Table 15 - Parasitic Energy Losses and Net Electricity Output (adapted from [141])

(Bold-faced items were calculated using the equations displayed below)

Symbol	Description	Design Value*	Units
E_{GROSSD}	Design turbine gross electric output	110	MWh
F_{PB}	Fixed power block loss factor	0.0055	MWh/ MWh
$E_{PARFIXED}$	**Fixed parasitic energy losses for power plant - calculated for each hour of simulation**	**0.605**	**MWh**
F_{BOP}	Balance of plant loss factor	0.02467	MWh/ MWh
$E_{PARBOPD}$	**Design parasitic losses from balance of plant operations**	**2.7**	**MWh**
A_{BOP}	Balance of plant coefficient	0.517	
B_{BOP}	Balance of plant coefficient	0.483	
F_{PBLOAD}	**Hourly power block load factor - ratio of actual to design electric output**	**1**	**MWh/ MWh**
E_{PARBOP}	**Hourly parasitic losses from balance of plant operations - calculated during any hour that the power block operates**	**2.7**	**MWh**
F_{CT}	Cooling tower loss factor	0.017045	MWh/ MWh
E_{PARCTD}	**Design parasitic losses from cooling tower operations**	**1.9**	**MWh**
A_{CT}	Cooling tower coefficient	0.794	
B_{CT}	Cooling tower coefficient	0.242	
C_{CT}	Cooling tower coefficient	-0.036	
E_{PARCT}	**Hourly parasitic losses from cooling tower operations - calculated during any hour that the power block operates**	**1.5**	**MWh**

F_{HTR}	Natural gas-fired heater loss factor	0.02273	MWh/ MWh
$E_{PARHTRD}$	**Design parasitic losses from natural gas-fired HTF heater**	**2.5**	**MWh**
Q_{HTR}	**Hourly thermal energy required from heater for HTF freeze protection; calculated in plant operation modes**	**0**	**MWh**
$F_{HTRLOAD}$	**Heater load factor - the ratio of heat energy supplied by the HTF heater to the design thermal input of the Rankine cycle**	**0**	
A_{HTR}	Heater coefficient	0.517	
B_{HTR}	Heater coefficient	0.483	
E_{PARHTR}	**Hourly parasitic losses from natural gas-fired HTF heater - calculated during any hour that the heater operates**	**0**	**MWh**
E_{SCA}	SCA tracking energy for Eurotrough collector	125	Wh/ sca
E_{PARSCA}	**Hourly parasitic loss from SCA tracking - calculated during any hour the solar field is tracking the sun**	**0.13**	**MWh**
E_{NET}	**Hourly net electricity generation**	**102**	**MWh**
E_{SOLD}	**Hourly electricity sold**	**102**	**MWh**
E_{BOUGHT}	**Hourly electricity purchased**	**0**	**MWh**
$E_{ANNUAL1}$	**Annual net electricity generation - the sum of hourly electricity generation**	**380**	**GWh**
$E_{ANNUAL2}$	**Annual net electricity generation - the sum of hourly electricity sold**	**460**	**GWh**
CF_1	**Plant capacity factor, based on $E_{ANNUAL1}$**	**39**	**%**
CF_2	**Plant capacity factor, based on $E_{ANNUAL2}$**	**48**	**%**

[*] *Values in red are reported from hour 129 (mode DAY_TESC) of a full simulation of a plant with 6hr TES and SM of 2.23 for illustrative purposes.*

$$E_{PARFIXED} = F_{PB} * E_{GROSSD} \quad (82)$$

$$E_{PARBOPD} = F_{BOP} * E_{GROSSD} \quad (83)$$

$$F_{PBLOAD} = W_{net}/ E_{GROSSD} \quad (84)$$

$$E_{PARBOP} = E_{PARBOPD} * (A_{BOP} * F_{PBLOAD} + B_{BOP}) \quad (85)$$

$$E_{PARCTD} = F_{CT} * E_{GROSSD} \quad (86)$$

$$E_{PARCT} = E_{PARCTD} * (F_{PBLOAD} * A_{CT}^2 + F_{PBLOAD} * B_{CT} + C_{CT}) \quad (87)$$

$$E_{PARHTRD} = F_{HTR} * E_{GROSSD} \quad (88)$$

$$F_{HTRLOAD} = Q_{HTR}/Q_{HTFmin} \quad (89)$$

$$E_{PARHTR} = E_{PARHTRD} * (A_{HTR} * F_{HTRLOAD} + B_{HTR}) \quad (90)$$

$$E_{PARSCA} = (E_{SCA} * N_{sca})/1000000 \quad (91)$$

$$E_{NET} = W_{net} - (E_{PARFIXED} + E_{PARBOP} + E_{PARCT} + E_{PARHTR} + E_{PARSCA}) \quad (92)$$

$$E_{SOLD} = E_{NET}, \text{ when } E_{NET} > 0 \quad (93)$$

$$E_{BOUGHT} = |E_{NET}|, \text{ when } E_{NET} < 0 \quad (94)$$

$$E_{ANNUAL1} = \sum E_{NET} \quad (95)$$

$$E_{ANNUAL2} = \sum E_{SOLD} \quad (96)$$

$$CF_1 = E_{ANNUAL1} \div (E_{GROSSD} * 8760) \quad (97)$$

$$CF_2 = E_{ANNUAL2} \div (E_{GROSSD} * 8760) \quad (98)$$

The parasitic loss equations are relatively straightforward, and Table 15 presents (in red) illustrative results from the 129th hour of a complete simulation of a PT plant with 6 hours of TES and a SM of 2.05. The annual electricity generation and capacity factor calculations are more complex. Traditional thermodynamic modeling of power systems suggests that Equation 95 should calculate the annual electricity generation because the net energy is the sum of the energy inputs and outputs in the system. In reality, there is a distinction between energy consumption during night and day hours. If the power cycle is operating, it is reasonable to assume that the electricity generated by the system can be used to power the pumps and auxiliary equipment. However, when the power cycle is not operating, the power plant is purchasing electricity from the grid to run the pumps and auxiliary equipment for HTF freeze protection. From a thermodynamic standpoint, this distinction may not be important because the end sum is the same whether you add energy inputs and outputs together in one sum or separate electricity sold and bought on an hourly basis and add them together at the end. But from a business standpoint, the distinction is very important. It is unclear whether the annual electricity generation values that are reported in the literature for currently operating PT plants subtract nighttime pump and auxiliary loads, but it is reasonable to assume that they do not because the important value for the developer, utility, and public is how much energy was generated and *sold*. Furthermore, it is much more accurate for economic modeling to separate sold energy and purchased energy because the power plant is, in reality, purchasing electricity from a utility during nighttime hours. Since this study addresses both thermodynamic and economic aspects of the power plant, the results of both calculations will be reported in this chapter, but subsequent chapters will only use $E_{ANNUAL2}$ and CF_2.

The total annual water consumption is an important calculated physical parameter that will be used in the economic model and the environmental life cycle assessment. The performance model described in preceding sections includes a wet cooling system, and the primary water consumption in these power plants is through evaporation, blowdown and drift in the cooling system [44]. The model described above uses Equation 99 to calculate the mass of coolant used in the Rankine Cycle for each hour of the simulation. The sum of these hourly coolant calculations yields an annual mass, which can be converted to an annual coolant volume using the density of the coolant at the design outlet temperature. For the nominal results, it is assumed that about 4% of the coolant water that cycles through the system will be lost to evaporation, blowdown and drift [143]. Equation 100 calculates the total annual water consumption under the assumption that 95% of the total water consumption from the plant is due to the cooling system [95].

$$M_{coolant} = -3600 * [(m_{steam} * ((1 - z - z') * h_{11} + z' * h_{15} - (1 - z) * h_{12})) \div (h_c - h_d)] \quad (99)$$

$$M_{water} = [0.04 * \sum M_{coolant}] \div 0.95 \quad (100)$$

$$F_{DC} = -0.00003 * T_{amb}^3 + 0.002 * T_{amb}^2 - 0.045 * T_{amb} + 1.318 \text{ [44]} \quad (101)$$

The performance model also includes a dry cooling option, which uses fans to air-cool the steam exiting the turbines (see Figure 38). The following changes were applied to the wet-cooled performance model to simulate the dry-cooled systems:

1) Multiply hourly cooling tower parasitic energy losses by a factor of 1.05 [44]
2) During operational hours only, multiply the hourly net electricity output from the wet-cooled system by F_{DC} (see equation 101)
3) Multiply water consumption per MWh by 0.07

These changes are explained in more detail in Appendix B.

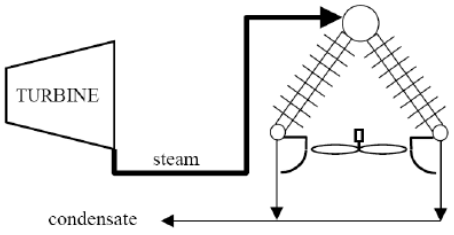

Figure 38 - Schematic of Dry Cooling System [44]

3.7 Nominal Performance Results

The performance results for the nominal (base case) input parameters outlined in the previous sections are presented in the following figures. The results were run for each of the plant configurations described at the beginning of this chapter: 1) no storage/backup (0 hours); 2) with TES (1-12 hours); and 3) with NG backup (equivalent to 1-12 hours of TES). An hour of storage refers to the capacity required to operate the steam cycle at full capacity for an hour. Figure 39 shows the relationship between hours of storage, storage salt quantity and storage system thermal capacity in megawatt-hours thermal (MWht). The relationships are linear as described in Equations 48 and 50; although this relationship does not incorporate salt that may be required to stay in the pipes.

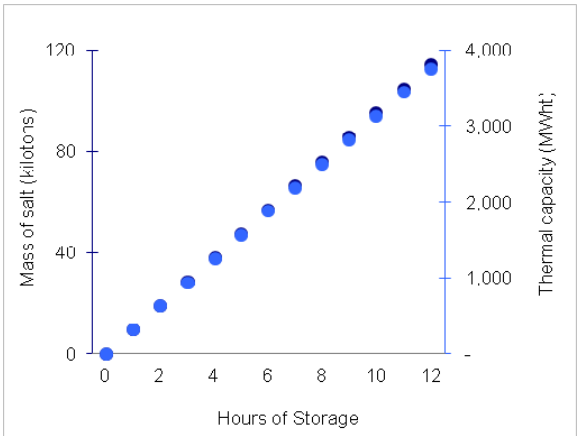

Figure 39 - Relationship between hours of storage, storage salt quantity, and system thermal capacity

As explained previously, the selection of the solar field area has a large influence on model results. The solar field area for the plant with no storage/backup and the plants with TES was selected as the area that gives the minimum levelized cost of electricity (LCOE), and the solar field area for the plants with NG backup was selected to match the annual electricity output from the respective TES simulation. Although Chapter 4 describes the LCOE calculation, it is necessary to present the solar field area results here in order to put the performance results in the proper context. For each equivalent storage capacity presented in Figure 39, the LCOE was calculated for a range of solar multiples from 0.8 to 4.5. Figure 40 shows the results of these simulations for five of the 13 storage capacities modeled. In all cases, the LCOE decreases with increasing solar field area as the increase in electricity generation from the larger aperture area (at the same turbine capacity) outweighs the increase in costs associated with building, operating, and maintaining a larger solar field area. For each case shown in the figure, there is a point where the LCOE reaches a minimum, and then it increases as each incremental increase in electricity generation is insufficient to outweigh the incremental increase in plant costs.

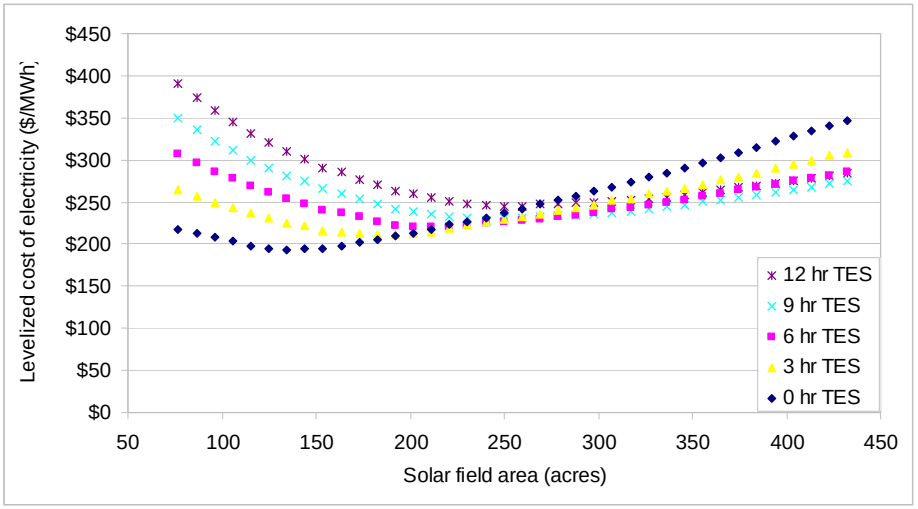

Figure 40 - Initial selection of solar field area for TES cases

From this set of results, a narrower range was selected as the set of solar field areas that results in LCOEs within 5% of the minimum LCOE from the first set of simulations. Figure 41 displays the results of this second level of simulations for two of the 13 storage capacities modeled. The minimum LCOE for the no storage/backup case is calculated to be approximately $193/MWh with a solar field area of 137 acres, and the minimum LCOE for the 3 hr TES case is $211/MWh with a solar field area of 188 acres. The smaller resolution used in this set of simulations (one acre instead of ten acres) results in a set of results that appears less smooth than the results from the initial range. This is because the hourly simulation is a complex set of conditional statements that activate specific operational modes depending on calculations in the previous hour. With a smaller resolution to the solar field area steps (one acre instead of ten acres), the differences in annual electricity generation, which stem from differences in hourly electricity generation, become more apparent.

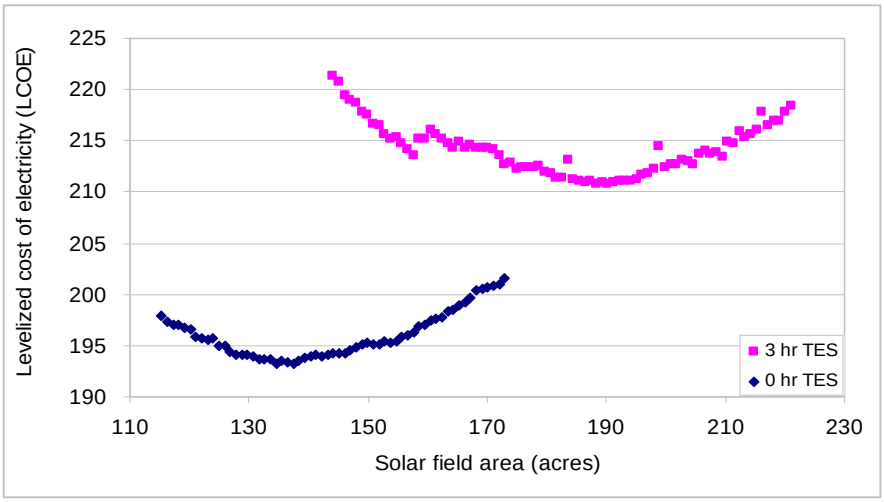

Figure 41 - Second tier selection of solar field area for TES cases

Once the nominal solar field areas were selected for each storage capacity, the hourly electricity generation values from each plant with TES were used as inputs to run simulations for the NG backup configuration at each equivalent TES capacity in order to select the NG backup solar field area that resulted in the smallest difference in annual electricity generation between the TES and NG cases ($E_{annualTES} - E_{annualNG}$). Figure 42 shows the results of these simulations for five of the 13 NG cases modeled. It is important to note that the algorithm for the NG configuration attempts to match the hourly and annual electricity generation of the respective TES case in order to model two different power plant configurations that use solar energy with a backup system, rather than a power plant that uses natural gas with a small amount of solar energy. This constraint causes the NG configuration to be unable to match the TES annual electricity generation with smaller solar field areas. With larger solar field areas, the NG configuration meets its solar quota and is able to generate more electricity with the natural gas backup system than the respective TES plant is able to generate with the storage system.

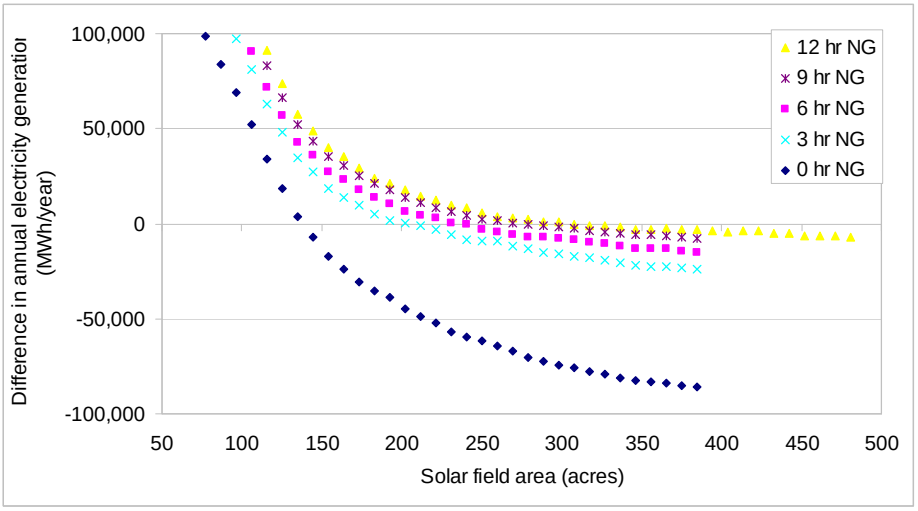

Figure 42 - Initial selection of solar field area for NG backup cases

From this set of results, a narrower range was selected as +/- 10 acres from the minimum absolute value of the difference in annual electricity generation for each NG case. Figure 43 displays the results of this second level of simulations for two of the 13 NG cases modeled. The 0 hr NG results are much more sensitive to changes in solar field area because this system is identical to the 0 hr TES case, and it does not use the natural gas backup system in the same way as the NG cases that attempt to match the other storage capacities. Both 0 hr cases only use the natural gas-fired heater for HTF freeze protection during plant shutdown; whereas, the other NG cases use the heater to match TES input during operational hours. Therefore, the NG 1-12 hr results are less sensitive to changes in solar field area than the 0 hr NG case because they have more flexibility in meeting the annual electricity generation of the respective TES case.

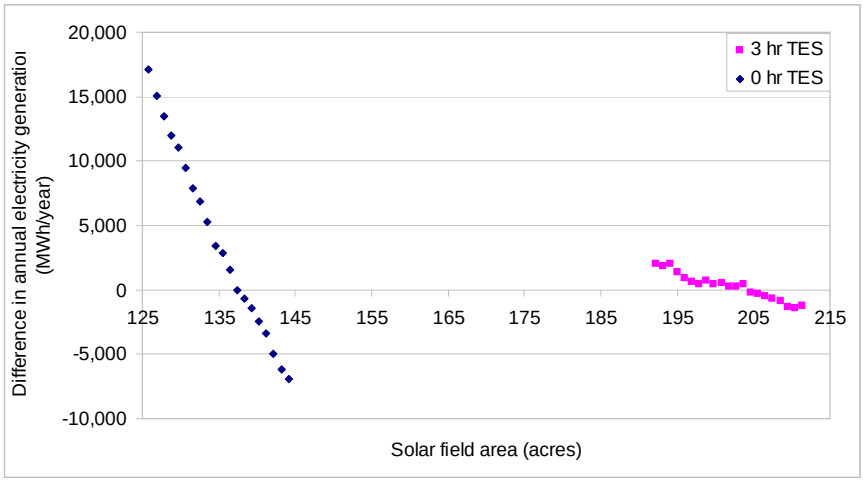

Figure 43 - Second tier selection of solar field area for NG backup cases

These two methods of solar field area selection resulted in the nominal solar field areas presented in Figure 44. The plant with no storage/backup (represented by the two markers at 0 hr equivalent storage) has a solar field area of 137 acres, and the solar field area increases with TES capacity and NG backup capacity to a maximum value at 12 hours of 261 acres and 302 acres, respectively. Each consecutive increase in TES capacity (shown in orange) results in a solar field area 0.4% - 20% higher than the previous storage capacity, and 2-3 hr TES show the largest increase. These increases occur in order to capture more solar energy for the larger storage capacities. The solar field areas for the NG cases follow a similar pattern as the TES cases relative to each smaller NG backup capacity. The NG plants required solar field areas 3-15% larger than the respective TES case in order to meet the same hourly solar electricity generation requirements during sunny hours.

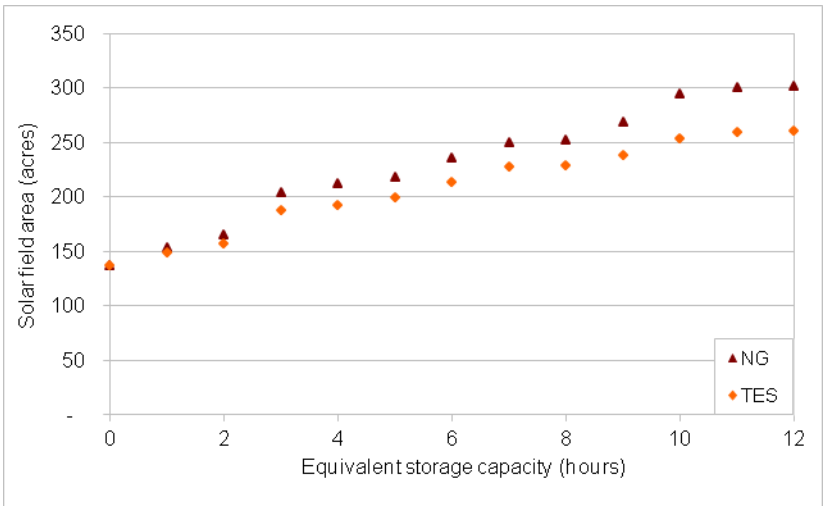

Figure 44 - Nominal solar field area results

Figure 45 displays the net annual electricity generated and the annual electricity bought and sold for all plant configurations and nominal solar field areas modeled. The plant with no storage/backup sells about 300 GWh of electricity to the grid annually, and this value increases by 2-12% with each incremental increase in TES and NG. For each plant configuration modeled here, there are hours during the year when the power cycle does not operate because there is not enough solar input (cloudy periods and nighttime) and there is not enough energy in the storage system (during the winter for larger storage capacities). During these hours, it is necessary to purchase electricity from the grid for parasitic energy loads from pumps, electronics, and other miscellaneous sources. The plant with no storage/backup purchases 82 GWh of electricity annually for parasitic nighttime loads, and this amount decreases by 0.1-0.7% with each incremental increase in TES/NG backup.

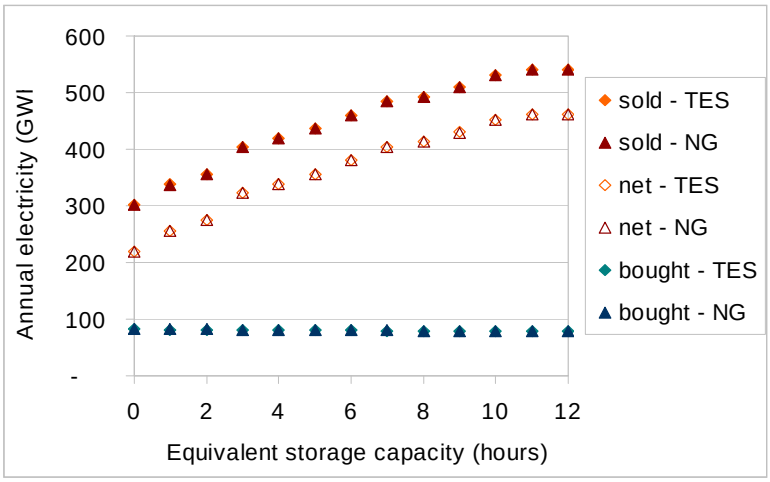

Figure 45 - Annual electricity generated and purchased

The net electricity generation is the difference between the electricity sold to the grid throughout the year and the electricity purchased from the grid throughout the year. The plant with no storage/backup generates about 220 GWh of net electricity annually, and this value increases by 2-17% with each incremental increase in TES/NG backup. As section 3.6 explained, the annual electricity purchased from the grid mainly represents the electricity required for nighttime heat transfer fluid freeze protection and is incorporated into the cost model as part of the annual operation and maintenance costs. Therefore, the annual electricity sold is the metric used in the LCOE calculation and for the solar field area selection. The NG annual electricity generation deviates by between zero and 0.08% from the respective TES scenarios, which confirms that appropriate solar field areas were selected for the NG cases, as described above.

Figure 46 shows the annual capacity factor for each equivalent storage capacity modeled, calculated by both methods described in section 3.6. The net capacity factor was calculated as the ratio of the net electricity generation and the product of the gross turbine capacity and number of hours in a year. The plant with no storage/backup has a net capacity factor of 23%,

and this value increases to a maximum of 48% with 12 hours of TES/NG backup. By contrast, the "sold" capacity factor was calculated as the ratio of the electricity sold to the grid and the product of the gross turbine capacity and number of hours in a year. The plant with no storage/backup has a "sold" capacity factor of 31%, and this value increases to a maximum of 56% with 12 hours of TES/NG backup. Each capacity factor value based on net electricity is 8-9 percentage points lower than the respective capacity factor based on sold electricity because the net value calculation essentially subtracts the bought electricity from the sold electricity. The capacity factor based on sold electricity is probably more important to grid operators and utilities as it represents the overall percentage of the year that the power plant will be operating at full capacity.

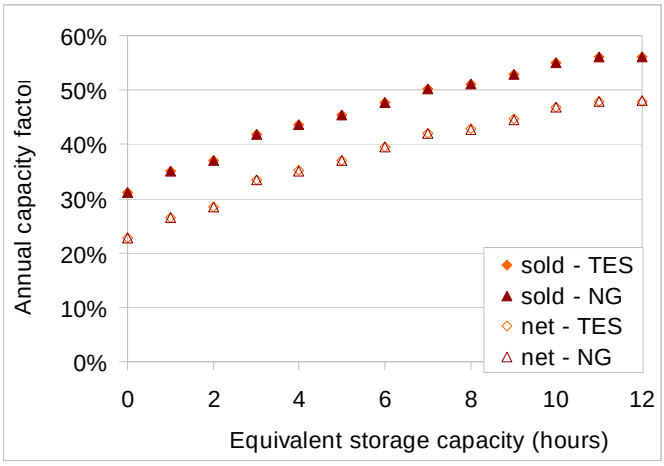

Figure 46 - Average annual plant capacity factor

Figure 47 shows the percentage of annual electricity that was generated using the natural gas-fired heater for the NG cases. The amount increases from 7% with 1 hr NG backup to 31% with 12 hrs NG backup as the power plant is required to generate more and more electricity during non-solar hours to match the electricity generation of the equivalent plant with TES. The majority of electricity generation still comes from the solar input to the power plant, but there is

a question of whether the NG plants at higher capacities would qualify as renewable energy technologies under federal and state incentive guidelines.

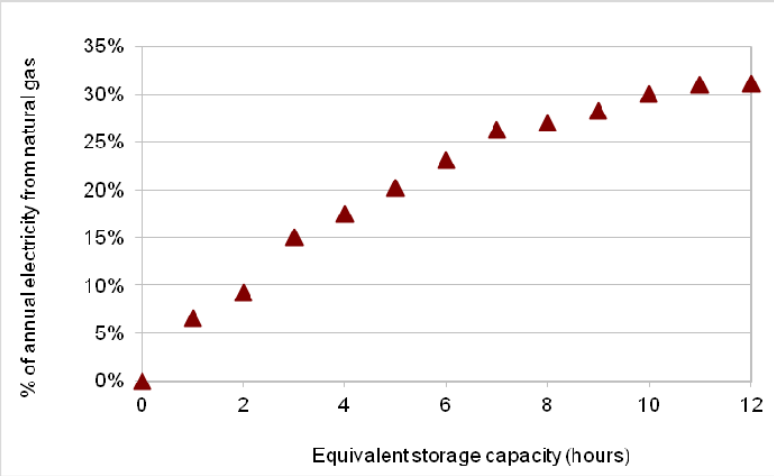

Figure 47 - Percentage of annual electricity sales generated using natural gas

Figure 48 shows the amount of natural gas used annually by all three plant configurations for all equivalent storage capacities modeled. The natural gas use for TES plants and the plant with no storage/backup is solely for HTF freeze protection and varies from about 40,000 MMBtu/yr with no storage/backup to 200,000-320,000 MMBtu with TES. With increasing storage capacity, the natural gas use for the NG plants exceeds the natural gas use for the TES plants by up to a maximum of nine times the TES quantity at the 11 and 12 hour capacities.

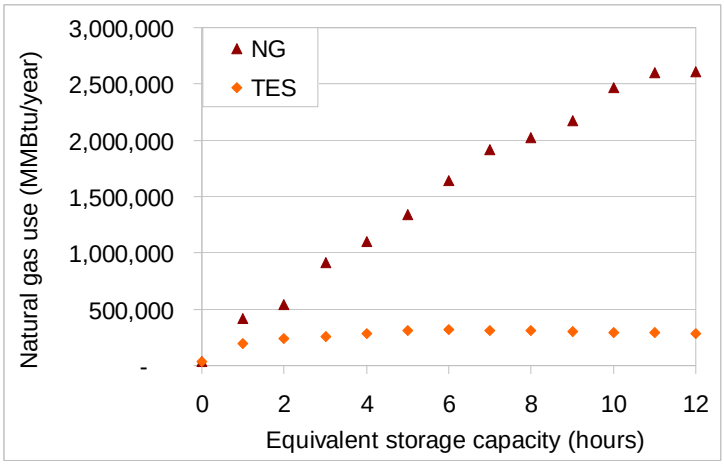

Figure 48 - Annual natural gas use

It is difficult to compare these performance model results with reported values for existing parabolic trough plants for several reasons, including:

1. The results from this model are for a specific location and set of weather data (Daggett, CA) and may not be comparable to other locations.
2. It is unclear whether reported annual electricity generation values and capacity factors reflect sold or net electricity.
3. This model simulates a specific situation in which the storage system charges whenever there is excess direct normal radiation and discharges whenever there is insufficient radiation. In reality, plant operators may dispatch storage in order to meet certain capacity requirements or to gain the highest electricity pricing during the day.
4. The solar field area for the nominal TES cases was selected to minimize the LCOE. The solar field area for existing plants may have been selected for a different goal such as to maximize profit or annual electricity generation or to capitalize on peak pricing periods.

With these caveats in mind, the performance model results presented in this chapter compare reasonably well with the reported values from existing plants. Based on the weather data input

for Daggett, California, the nominal results case can be most closely compared with the SEGS plants shown in Table 6. The reported annual capacity factors for those plants range from 29% for the older plants to 36% for the newer plants. These values correspond to model results for 0-2 or 0-5 hrs of storage depending on whether the reported capacity factor is based on sold or net power. Although the SEGS plants do not have storage, they have a natural gas-fired boiler that can contribute up to 25% of thermal input to the power cycle. However, historically some of the plants have used this backup system only to compensate for cloudy periods or to meet summer evening peak demand periods. When natural gas prices have been high, plant operators have scaled back on the natural gas use [144]. Due to these operational considerations and due to the fact that SEGS use a boiler to add steam to the power cycle rather than a heater to heat the oil in the solar field, it may not be accurate to compare the SEGS plants to the model outputs for the 7 hr PT-NG model (which has 25% electricity from the natural gas heater). Since the reported SEGS average annual generation values include periods of time during which the full capacity of the natural gas backup system has not been used, the SEGS plants may be more equivalent to a plant with less than 7 hours of storage. In this case, the performance model results are within a reasonable range of the performance of an actual plant.

Using the TMY3 weather file for Las Vegas, Nevada as an input to the performance model instead of the weather file for Daggett, CA enables a rough comparison with the reported values for Nevada Solar One, which is a 64 MW trough plant with no TES and 2% natural gas backup. When the nominal performance model inputs are used for plant with no storage/NG backup at a solar field area equal to the reported area for Nevada Solar One (88 acres), the resulting model

capacity factor based on electricity sales is 22%. This is very close to the reported capacity factor of 23% from Table 6.

Chapter 4: PT Plant Economic Model

The economic model calculates the total plant capital cost, expected annual operation and maintenance (O&M) costs, levelized cost of electricity (LCOE), expected annual profit, and carbon price necessary for the technology to be competitive with conventional fossil fuel-generated electricity. Reliable and up-to-date cost data for concentrated solar power (CSP) and thermal energy storage (TES) are difficult to obtain due to the increasingly competitive and ever-changing CSP market. However, the National Renewable Energy Laboratory (NREL) recently contracted WorleyParsons to develop an updated cost estimate for the Solar Advisor Model (SAM) in 2009 [43]. That study is the most transparent and comprehensive source of parabolic trough and TES cost data currently available. NREL developed the updated cost model for SAM after integrating the results of the WorleyParsons study with information gathered from various discussions with industry representatives. The cost model described in this chapter is an adaptation of the updated SAM cost model, based on a 100 MW PT plant with six hours of indirect molten salt TES and a solar field aperture area of 854,000 m^2. All cost components were obtained from the SAM Parabolic Trough Cost Model 5-12-2010 spreadsheet [39]. The following sections explain the overall structure of the cost model used in this study and the specific aspects that deviate from the SAM cost model.

4.1 Total Plant Capital Cost

The total plant capital cost is the sum of the direct and indirect capital costs. Table 16 presents the key parameters used in Equations 102-158 to calculate the total plant capital cost and levelized annual capital cost (LAC) for six scenarios in the three plant configurations modeled in

this study (no storage/backup, TES and NG backup): 1) pre-tax unsubsidized with wet cooling; 2) post-tax unsubsidized with wet cooling; 3) post-tax subsidized with wet cooling; 4) pre-tax unsubsidized with dry cooling; 5) post-tax unsubsidized with dry cooling; 6) post-tax subsidized with dry cooling. The NG configuration and no storage/backup configuration use the same calculations as the TES configuration, except with the exclusion of any TES inputs. Equations 102-132 calculate the main plant component costs, which are used in Equations 133 and 134 to calculate the direct plant capital costs for the wet- and dry-cooled configurations, respectively. These equations and parameters are taken directly from the SAM Parabolic Trough Cost Model 5-12-2010 spreadsheet, with the following adaptations: 1) Equations 119-122 increase the capital cost of the dry cooling system pursuant to the analysis described in Appendix B; and 2) Equations 129 and 132 calculate the cost of a salt heater for the TES system and a heat transfer fluid heater, respectively. Appendix C describes the origin of heater cost equations in more detail. The indirect capital costs are calculated by the same method and same parameters as the SAM spreadsheet. Table 16 shows in red the total capital cost results for a PT-TES plant with 6 hours of TES with wet and dry cooling. Equation 144 shows how the total plant capital cost is reduced with the federal investment tax credit (ITC), which is currently applied as a cash grant option. For simplicity, Equations 135, 136 and 141 through 158 represent only the wet-cooled case, but similar equations are used in the model for the dry-cooled configuration.

Table 16 - Levelized Annual Capital Cost Parameters

(Bold-faced items were calculated using the equations displayed below)

Parameter	Description	Unit	Nominal Value
Direct Capital Cost			
A_{ref}	Reference solar field area	m^2	854,000
$C_{SI,prep}$	**Site improvement cost – site preparation**	**$M**	**$1.8**
$C_{SI,C\&G}$	**Site improvement cost – clearing and grubbing**	**$M**	**$0.4**
$C_{SI,GDRRD}$	**Site improvement cost – grading, drainage, remediation, retention, detention**	**$M**	**$9.9**
$C_{SI,RPF}$	**Site improvement cost – roads, parking, fencing**	**$M**	**$10**
$C_{SI,WSI}$	**Site improvement cost – water supply infrastructure**	**$M**	**$1.4**
C_{SI}	**Total cost of site improvements**	**$M**	**$24**
$C_{HTF,FPS}$	**Heat transfer fluid system cost – freeze protection system**	**$M**	**$0.5**
$C_{HTF,U}$	**Heat transfer fluid system cost – ullage system**	**$M**	**$0.9**
$C_{HTF,p}$	**Heat transfer fluid system cost – pumps**	**$M**	**$5.1**
$C_{HTF,ENBS}$	**Heat transfer fluid system cost – expansion, nitrogen blanketing system**	**$M**	**$6.6**
$C_{HTF,SFPIVF}$	**Heat transfer fluid system cost – solar field piping, insulation, valves, fittings**	**$M**	**$43**
$C_{HTF,\ PBPIVF}$	**Heat transfer fluid system cost – power block piping, insulation, valves, fittings**	**$M**	**$1.0**
$C_{HTF,FSS}$	**Heat transfer fluid system cost – foundations and support structures**	**$M**	**$1.9**
$C_{HTF,f}$	**Heat transfer fluid system cost – fluid**	**$M**	**$19**
C_{HTF}	**Total cost of heat transfer fluid system**	**$M**	**$78**
$C_{SCA,unit}$	Unit cost of solar collector assemblies and installation	$/$m^2$	$295
C_{SCA}	**Total cost of solar collector assemblies and installation**	**$M**	**$256**
C_{SF}	**Total cost of solar field**	**$M**	**$358**
C_{PBunit}	Unit cost of power block	$/kW	$941
C_{PB}	**Total cost of power block**	**$M**	**$104**
F_{CCT}	Fraction of power block cost that is directly related to cooling system		9%
C_{CT}	**Unit cost of wet cooling system**	**$/kW**	**$85**
F_{CDC}	Capital cost increase factor for dry cooling system		2
C_{DC}	**Unit cost of dry cooling system**	**$/kW**	**$170**
$C_{PBDCunit}$	**Unit cost of power block with dry cooling**	**$/kW**	**$1,026**
C_{PBDC}	**Total cost of power block with dry cooling**	**$M**	**$113**
Q_{TESref}	Reference TES thermal capacity	kWht	1,750
$C_{saltunit}$	Unit cost of Solar Salt	$/kg	$1
C_{salt}	**Total cost of Solar Salt**	**$M**	**$57**
$C_{TES,PHX}$	**Thermal energy storage system cost - pumps and heat exchangers**	**$M**	**$31**
$C_{TES,T}$	**Thermal energy storage system cost - tanks**	**$M**	**$45**

$C_{TES,PIVF}$	**Thermal energy storage system cost - piping, insulation, valves & fittings**	**$M**	**$1.5**
$C_{TES,FSS}$	**Thermal energy storage system cost - foundations and support structures**	**$M**	**$0.5**
$C_{TES,IC}$	**Thermal energy storage system cost - instrumentation and controls**	**$M**	**$6**
$HD_{salthtr}$	**Heat duty of salt heater, calculated as the maximum $\|Q_{saltFP}\|$**	**MMBtu/hr**	**1,611**
C_{TEShtr}	**Total cost of natural gas-fired heater for salt freeze protection**	**$M**	**$22**
C_{TES}	**Total cost of TES system**	**$M**	**$165**
$C_{TESunit}$	**Unit cost of TES system**	**$/kWh**	**$88**
HD_{htfhtr}	**Heat duty of HTF heater, calculated as the maximum $\|Q_{htr}\|$**	**MMBtu/hr**	**110**
C_{HTFhtr}	**Total cost of natural-gas fired HTF heater**	**$M**	**$1.8**
C_c	Contingency for unforeseen costs that may arise in the future; percentage of total direct capital cost	**% of C_{direct}**	10%
C_{direct}	**Total direct capital cost of power plant**	**$M**	**$691**
$C_{directDC}$	**Total direct capital cost of power plant with dry cooling**	**$M**	**$701**
Indirect Capital Cost			
$C_{directREF}$	Reference direct capital cost	$M	$659
R_{EPMC}	Cost of engineering, procurement, management and construction - includes plant design, construction management, commissioning/start-up, owner's costs, and interest during construction	% of C_{direct}	15%
C_{EPMC}	**Total cost of engineering, procurement, management and construction**	**$M**	**$108**
R_{PLM}	Project, land and miscellaneous costs - includes permitting, licensing, legal, and land costs	% of C_{direct}	4%
C_{PLM}	**Total project, land and miscellaneous costs**	**$M**	**$18**
F_{land}	Ratio of total land to solar field area		4.1
F_{landDC}	Ratio of total land to solar field area for plant with dry cooling		3.9
A_{total}	**Total land area required for power plant**	**km^2**	**3.6**
$A_{totalDC}$	**Total land area required for power plant with dry cooling**	**km^2**	**3.4**
$C_{land,unit}$	**Unit cost of land**	**$/acre**	**$10,000**
C_{land}	**Total cost of land**	**$M**	**$8.8**
C_{landDC}	**Total cost of land for plant with dry cooling**	**$M**	**$8.4**
R_{taxS}	Sales tax rate, applied to 84% of direct capital costs	%	8.75%
C_{tax}	**Total cost of sales tax**	**$M**	**$51**
$C_{indirect}$	**Total indirect capital cost of plant**	**$M**	**$186**
$C_{indirectDC}$	**Total indirect capital cost of plant with dry cooling**	**$M**	**$188**
Total Capital Cost			
C_{cap}	**Total plant capital cost**	**$M**	**$878**
C_{capDC}	**Total plant capital cost with dry cooling**	**$M**	**$889**

ITC	Federal investment tax credit, currently applied as a grant	% of C_{cap}	30%
C_{capITC}	**Total plant capital cost with ITC**	**$M**	**$614**
$C_{capDCITC}$	**Total plant capital cost with dry cooling and ITC**	**$M**	**$623**
Financial Parameters			
F_{debt}	Debt fraction	%	40%
k_L	Loan rate	%	8%
$F_{equityP}$	Equity fraction (preferred)	%	8%
k_{eP}	Cost of equity (preferred)	%	5.34%
$F_{equityC}$	Equity fraction (common)	%	52%
k_{eC}	Cost of equity (common)	%	8.74%
t_b	Book life	years	30
i	**Discount rate**	**%**	**8.17%**
CRF	**Capital recovery factor**	**%**	**9.03%**
LAC	**Levelized annual capital cost, pre-tax, unsubsidized**	**$M**	**$79**
P_{loan}	**Uniform annual loan payment**	**$M**	**$31**
$loan_o$	**Initial loan balance at time zero**	**$M**	**$351**
$I_{loan,j}$	**Loan interest for year j**	**$M**	**varies**
R_{taxC}	Corporate tax rate (federal + California)	%	43.84%
NPV_{int}	**Net present value of the loan interest as applicable for federal tax deductions**	**$M**	**$115**
F_{asset}	Percentage of direct capital cost considered as the depreciable asset	%	84%
V_{asset}	**Value of the depreciable asset**	**$M**	**$580**
F_{dep}	Depreciation factor, varies by year pursuant to federal depreciation schedule	%	varies
NPV_{dep}	**Net present value of general depreciation as applicable for federal tax deductions**	**$M**	**$73**
LAC_{tax}	**Levelized annual capital cost, after-tax, unsubsidized**	**$M**	**$62**
NPV_{depA}	**Net present value of accelerated (5-yr) depreciation as applicable for federal tax deductions**	**$M**	**$101**
LAC_{ITC}	**Levelized annual capital cost, after-tax, with federal investment tax credit applied as a cash grant**	**$M**	**$39**

**Sample values, displayed in red, are presented for 6 hours TES with a SM of 2.23*

$$C_{SI,prep} = 1799000 * [A \div A_{ref}]^{0.9} \quad (102)$$

$$C_{SI,C\&G} = 376000 * [A \div A_{ref}]^{0.9} \quad (103)$$

$$C_{SI,GDRRD} = 9742000 * [A \div A_{ref}]^{0.9} \quad (104)$$

$$C_{SI,RPF} = 10176000 * [A \div A_{ref}]^{0.9} \quad (105)$$

$$C_{SI,WSI} = 1402000 * [A \div A_{ref}]^{0.9} \quad (106)$$

$$C_{SI} = C_{SI,prep} + C_{SI,C\&G} + C_{SI,GDRRD} + C_{SI,RPF} + C_{SI,WSI} \quad (107)$$

$$C_{SF} = A * C_{SFunit} \quad (108)$$

$$C_{HTF,FPS} = 469000 * [A \div A_{ref}]^{0.9} \quad (109)$$

$$C_{HTF,U} = 926000 * [A \div A_{ref}]^{0.9} \quad (110)$$

$$C_{HTF,p} = 5066000 * [A \div A_{ref}]^{0.9} \quad (111)$$

$$C_{HTF,ENBS} = 6537000 * [A \div A_{ref}]^{0.9} \quad (112)$$

$$C_{HTF,SFPIVF} = 42200000 * [A \div A_{ref}] \quad (113)$$

$$C_{HTF,\ PBPIVF} = 1000000 * [A \div A_{ref}]^{0.9} \quad (114)$$

$$C_{HTF,FSS} = 1842000 * [A \div A_{ref}]^{0.9} \quad (115)$$

$$C_{HTF,f} = 19174000 * [A \div A_{ref}] \quad (116)$$

$$C_{HTF} = C_{HTF,FPS} + C_{HTF,U} + C_{HTF,p} + C_{HTF,ENBS} + C_{HTF,SFPIVF} + C_{HTF,\ PBPIVF} + C_{HTF,FSS} + C_{HTF,f} \quad (117)$$

$$C_{PB} = C_{PBunit} * W_{out} * 1000 \quad (118)$$

$$C_{CT} = C_{PBunit} * F_{CCT} \quad (119)$$

$$C_{DC} = C_{CT} * F_{CDC} \quad (120)$$

$$C_{PBDCunit} = C_{PBunit} * (1- F_{CCT}) + C_{DC} \quad (121)$$

$$C_{PBDC} = C_{PBDCunit} * W_{out} * 1000 \quad (122)$$

$$C_{salt} = M_{salttotal} * C_{saltunit} \quad (123)$$

$$C_{TES,PHX} = 29766000 * [Q_{TEStotal} \div Q_{TESref}]^{0.8} \quad (124)$$

$$C_{TES,T} = 42882000 * [Q_{TEStotal} \div Q_{TESref}]^{0.8} \quad (125)$$

$$C_{TES,PIVF} = 1418000 * [Q_{TEStotal} \div Q_{TESref}]^{0.8} \quad (126)$$

$$C_{TES,FSS} = 520000 * [Q_{TEStotal} \div Q_{TESref}]^{0.8} \quad (127)$$

$$C_{TES,IC} = 5677000 * [Q_{TEStotal} \div Q_{TESref}]^{0.8} \quad (128)$$

$$C_{TEShtr} = 13402* HD_{salthtr} + 367158 \quad (129)$$

$$C_{TES} = C_{salt} + C_{TES,PHX} + C_{TES,T} + C_{TES,PIVF} + C_{TES,FSS} + C_{TES,IC} + C_{TEShtr} \quad (130)$$

$$C_{TESunit} = C_{TES} \div (Q_{TEStotal} * 1000) \quad (131)$$

$$C_{HTFhtr} = 13402 * HD_{htfhtr} + 367158 \quad (132)$$

$$C_{direct} = (C_{SF} + C_{PB} + C_{TES} + C_{HTFhtr}) * (1 + C_c) \quad (133)$$

$$C_{directDC} = (C_{SF} + C_{PBDC} + C_{TES} + C_{HTFhtr}) * (1 + C_c) \quad (134)$$

$$C_{EPMC} = R_{EPMC} * C_{direct} * [C_{direct} \div C_{directREF}]^{0.9} \quad (135)$$

$$C_{PLM} = R_{PLM} * C_{direct} * [C_{direct} \div C_{directREF}]^{0.9} \quad (136)$$

$$A_{total} = F_{land} *A \quad (137)$$

$$A_{totalDC} = F_{landDC} *A \quad (138)$$

$$C_{land} = C_{land,unit} * A_{total} \quad (139)$$

$$C_{landDC} = C_{land,unit} * A_{totalDC} \quad (140)$$

$$C_{tax} = R_{taxS} * 0.84 * C_{direct} \quad (141)$$

$$C_{indirect} = C_{EPMC} + C_{PLM} + C_{land} + C_{tax} \quad (142)$$

$$C_{cap} = C_{direct} + C_{indirect} \quad (143)$$

$$C_{capITC} = (1 - ITC) * C_{cap} \quad (144)$$

$$i = F_{debt} * k_L + F_{equityP} * k_{eP} + F_{equityC} * k_{eC} \quad (145)$$

$$CRF = i \div (1 - (1+i)^{-tb}) \quad (146)$$

$$LAC = C_{cap} * CRF \quad (147)$$

$$P_{loan} = C_{cap} * F_{debt} * [k_L \div (1 - (1 + k_L)^{-tb})] \quad (148)$$

$$loan_o = C_{cap} * F_{debt} \quad (149)$$

$$I_{loan,j} = loan_{(j-1)} * k_L \quad (150)$$

$$loan_j = loan_{(j-1)} + I_{loan,j} - P_{loan} \quad (151)$$

$$NPV_{int} = \Sigma\ [(loan_{(j-1)} * k_L * R_{taxC}) \div (1 + i)^j], \text{ for } j = 1 \text{ to } t_{loan} \quad (152)$$

$$V_{asset} = C_{direct} * F_{asset} \quad (153)$$

$$V_{dep,j} = V_{asset,j} * F_{dep,j}, \text{ for } j = 1 \text{ to end of depreciation schedule} \quad (154)$$

$$V_{asset,j} = V_{asset,(j-1)} - V_{dep,(j-1)} \quad (155)$$

$$NPV_{dep} = \Sigma\ [(V_{dep,j} * R_{taxC}) \div (1 + i)^j], \text{ for } j = 1 \text{ to end of depreciation schedule} \quad (156)$$

$$LAC_{tax} = [C_{cap} - (NPV_{dep} + NPV_{int})] * CRF \quad (157)$$

$$LAC_{ITC} = [C_{capITC} - (NPV_{depA} + NPV_{intITC})] * CRF \quad (158)$$

The financial parameters were selected to be consistent with the SAM default utility independent power producer (IPP) financial parameters [137] and the Electric Power Research Institute (EPRI) Technical Assessment Guide (TAG) recommendations for renewable power generation financing [145]. Equation 147 shows the simplest LAC calculation, the pre-tax unsubsidized scenario, which amortizes the capital cost of the plant over the plant lifetime through the use of a capital recovery factor. The post-tax unsubsidized LAC calculation uses Equations 148-157 and incorporates tax deductions from loan interest and depreciation, using a 30-year general depreciation schedule [146]. Equation 158 is essentially the same as Equation 157 except that it applies the ITC to the debt and equity portions of the capital investment and uses the accelerated 5-year depreciation schedule [146].

4.2 Operation and Maintenance Costs

Table 17 and Equations 159-179 display the parameters and calculations used in the O&M model, which were obtained from the SAM spreadsheet and adjusted for use in this study in the following ways: 1) Equation 167 calculates the cost of service contracts for water treatment for the dry cooling case based on decreases observed in Kelly [102] and discussed in Appendix B; 2) Equation 169 calculates the annual natural gas use using values from the performance model; 3) Equation 171 calculates the annual volume of water for the wet-cooled configuration by dividing

M_{water} from Chapter 3 by the density of water at the design state d and then adjusting this calculation from m^3 to gallons; 4) Equation 172 reduces the value of V_{H2Oa} for the dry-cooled configuration to 7% of the value of the wet-cooled parameter pursuant to the information presented in Appendix B; 5) Equation 175 calculates the annual auxiliary electricity purchase primarily as the sum of the nighttime electricity for pumps and other equipment to maintain the power plant in shutdown mode; 6) the nominal unit cost of natural gas (C_{NGunit}) presented in Table 17 is the national average natural gas price between 1997 and 2008 [147]; 7) the unit cost of auxiliary electricity ($C_{auxunit}$) is the mean commercial price of electricity in California between 1998 and 2008 [148]. The natural gas and auxiliary electricity unit costs were obtained from the U.S. Energy Information Administration and inflation-adjusted to $2009 using the CPI calculator [41]. The sensitivity of model results to both of these parameters is explored in Chapter 6. The O&M cost assumptions are nearly identical for all three plant configurations modeled, except that the costs for the no storage/backup and NG configurations exclude any reference to TES parameters. The red values in Table 17 are illustrative results from the 6 hr TES case with a SM of 2.23.

Table 17 - Operation and Maintenance Cost Parameters

(Bold-faced items were calculated using the equations displayed below)

Parameter	Description	Unit	Nominal Value
Fixed labor costs			
C_{ADMIN}	Cost of administration personnel: plant manager, administrative aide, financial manager, purchasing, human resources, plant engineer, performance engineer, information technology, and clerks	$M	$0.9
$C_{OPS,PEOT}$	**Cost of operations personnel: plant equipment operators and technicians**	**$M**	**$0.5**
$C_{OPS,other}$	Cost of operations personnel: operations managers, senior operators, control room operators	$M	$0.5
C_{OPS}	**Total cost of operations personnel**	**$M**	**$1**
$C_{PBTESm,TC}$	**Cost of power block and TES maintenance personnel: technicians, electricians, and clerks**	**$M**	**$0.5**

$C_{PBTESm,other}$	Cost of power block and TES maintenance personnel: supervisors, foremen		$0.1
C_{PBTESm}	**Total cost of power block and TES maintenance personnel**	**$M**	**$0.6**
$C_{SFm,TC}$	**Cost of solar field maintenance personnel: technicians and clerks**	**$M**	**$0.7**
$C_{SFm,other}$	Cost of solar field maintenance personnel: supervisors and foremen	$M	$0.1
C_{SFm}	**Total cost of solar field maintenance personnel**	**$M**	**$0.8**
$C_{OMlabor}$	**Total cost of labor for operations and maintenance**	**$M**	**$3.4**
Fixed other costs			
$C_{SC,G}$	**Cost of service contracts: groundskeeping**	**$M**	**$0.1**
$C_{SC,MW}$	**Cost of service contracts: mirror washing**	**$M**	**$0.4**
$C_{SC,WT}$	Cost of service contracts: water treatment	$M	$0.15
$C_{SC,WTDC}$	Cost of service contracts: water treatment for dry cooling	$M	$0.09
$C_{SC,other}$	Cost of service contracts: control systems, office equipment	$M	$0.2
C_{SC}	**Total cost of service contracts**	**$M**	**$0.8**
C_{SCDC}	**Total cost of service contracts with dry cooling**	**$M**	**$0.7**
Variable costs			
C_{NGunit}	Unit cost of natural gas	$/MMBtu	$5.92
η_{htr}	Efficiency of natural gas-fired heater	%	80%
η_{HTFhx}	Efficiency of heat exchanger in natural gas-fired heater	%	90%
Q_{NGa}	**Quantity of natural gas needed to supply annual heat input to salt and HTF heaters**	**MMBtu**	**311,660**
C_{NGa}	**Total annual cost of natural gas for heaters and power cycle**	**$M**	**$1.8**
V_{H2Oa}	**Volume of water required annually to operate power plant**	**million gallons per year**	**689**
V_{H2OaDC}	**Volume of water required annually to operate power plant with dry cooling**	**million gallons per year**	**$46**
$C_{H2Ounit}$	Unit cost of water	$/gallon	$0.0014
C_{H2Oa}	**Annual water cost**	**$M**	**$1.0**
C_{H2OaDC}	**Annual water cost with dry cooling**	**$M**	**$0.06**
$C_{auxunit}$	Unit cost of auxiliary electricity	$/MWh	$135
F_{aux}	Factor to represent the quantity of auxiliary electricity required for each MWh of electricity generated by the power plant	MWh/MWh	0.0103
Q_{aux}	**Amount of auxiliary electricity purchased by power plant each year**	**MWh/year**	**80,172**
C_{aux}	**Annual cost of auxiliary electricity purchase**	**$M**	**$11**
$C_{utilities}$	**Total annual cost of utilities**	**$M**	**$14**
C_{OMmisc}	**Annual cost of miscellaneous materials and maintenance for site improvements, solar field, HTF, TES, natural gas heaters, and the power cycle**	**$M**	**$4**
C_{OM}	**Total annual cost of plant operation and maintenance**	**$M**	**$22**

**Sample values, displayed in red, are presented for 6 hours TES with a SM of 2.23*

$$C_{OPS,PEOT} = 536786 * [A \div A_{ref}] \quad (159)$$

$$C_{OPS} = C_{OPS,PEOT} + C_{OPS,other} \quad (160)$$

$$C_{PBTESm,TC} = 476472 * [A \div A_{ref}]^{0.7} \quad (161)$$

$$C_{PBTESm} = C_{PBTESm,TC} + C_{PBTESm,other} \quad (162)$$

$$C_{SFm,TC} = 675505 * [A \div A_{ref}] \quad (163)$$

$$C_{SFm} = C_{SFm,TC} + C_{SFm,other} \quad (164)$$

$$C_{OMlabor} = C_{ADMIN} + C_{OPS} + C_{PBTESm} + C_{SFm} \quad (165)$$

$$C_{SC} = C_{SC,G} + C_{SC,MW} + C_{SC,WT} + C_{SC,other} \quad (166)$$

$$C_{SC,WTDC} = 0.600169516 * C_{SC} \quad (167)$$

$$C_{SCDC} = C_{SC,G} + C_{SC,MW} + C_{SC,WTDC} + C_{SC,other} \quad (168)$$

$$Q_{NGa} = [(\Sigma|Q_{htr}| + \Sigma|Q_{saltFP}|) \div (1000000 * \eta_{htr} * \eta_{HTFhx})] * 0.00094781712 \quad (169)$$

$$C_{NGa} = Q_{NGa} * C_{NGunit} \quad (170)$$

$$V_{H2Oa} = (M_{water} \div 993.3408) * 264.172052358 \quad (171)$$

$$V_{H2OaDC} = V_{H2Oa} * (1\text{-}0.93) \quad (172)$$

$$C_{H2Oa} = V_{H2Oa} * C_{H2Ounit} \quad (173)$$

$$C_{H2OaDC} = V_{H2OaDC} * C_{H2Ounit} \quad (174)$$

$$Q_{aux} = \sum [F_{aux} * E_{SOLD}] + \sum E_{BOUGHT} \quad (175)$$

$$C_{aux} = Q_{aux} * C_{auxunit} \quad (176)$$

$$C_{utilities} = C_{NGa} + C_{H2Oa} + C_{aux} \quad (177)$$

$$C_{OMmisc} = 0.003* C_{SF} * [A \div A_{ref}] + 0.003 * C_{TES} * [Q_{TEStotal} \div Q_{TESref}]^{0.7} + 0.01 * C_{HTFhtr} + 0.02 * C_{PB} \quad (178)$$

$$C_{OM} = C_{OMlabor} + C_{SC} + C_{utilities} + C_{OMmisc} \quad (179)$$

4.3 Levelized Cost of Electricity (LCOE)

Table 18 and Equations 180-185 show the six levelized LCOE calculations performed for each plant configuration. The solar field area for the TES and no storage/backup cases shown in Chapters 3-5 was selected by minimizing the pre-tax, unsubsidized LCOE, but Chapter 6 explores how some illustrative results differ when each of the other five LCOE alternatives is selected as the objective function for this optimization.

Table 18 - Levelized Cost of Electricity (LCOE) Alternatives

(Nominal values were calculated for 6 hr TES with SM = 2.23)

Parameter	Description	Nominal Value ($/MWh)
LCOE	Pre-tax, unsubsidized	$220
$LCOE_{DC}$	Pre-tax, unsubsidized	$232
$LCOE_{tax}$	Post-tax, unsubsidized	$183
$LCOE_{taxDC}$	Post-tax, unsubsidized	$293
$LCOE_{ITC}$	Post-tax, subsidized	$133
$LCOE_{ITCDC}$	Post-tax, subsidized	$139

$$LCOE = (LAC + C_{OM}) \div E_{ANNUAL2} \quad (180)$$

$$LCOE_{DC} = (LAC_{DC} + C_{OMDC}) \div E_{ANNUAL2DC} \quad (181)$$

$$LCOE_{tax} = (LAC_{tax} + C_{OM}) \div E_{ANNUAL2} \quad (182)$$

$$LCOE_{taxDC} = (LAC_{taxDC} + C_{OMDC}) \div E_{ANNUAL2DC} \quad (183)$$

$$LCOE_{ITC} = (LAC_{ITC} + C_{OM}) \div E_{ANNUAL2} \quad (184)$$

$$LCOE_{ITCDC} = (LAC_{ITCDC} + C_{OMDC}) \div E_{ANNUAL2DC} \quad (185)$$

4.4 Expected Annual Profit

Table 19 and Equations 186-193 describe the calculations for two different annual revenue alternatives and six different annual profit alternatives. In a deregulated electricity market, the price the generator will receive for electricity will be determined via two main mechanisms: the spot market or a power purchase agreement (PPA). While this statement certainly oversimplifies the complexities of the U.S. electricity market, it is a useful context for examining the different profit scenarios a PT generator may face. In this analysis, the spot market scenario is represented by the hourly average real-time price of electricity from the California Independent System Operator (CAISO) from 2008 [149]. In this scenario, Equation 186 calculates the annual revenue for the power plant based on the hourly average real-time price from CAISO, and Equations 188, 190, and 192 calculate the expected pre-tax unsubsidized, post-tax unsubsidized, and post-tax subsidized annual profits, respectively. The PPA scenario is represented by a fixed price, which is applied to any electricity sold by the plant. This scenario represents the current situation for all operating parabolic trough plants and plants under construction/development [3]. Equation 187 calculates the annual revenue, and Equations 189, 191, and 193 calculate the expected annual profits for this scenario using a nominal fixed price of $200/MWh. Illustrative revenue and profit results of for the 6 hr TES configuration with a SM of 2.23 are displayed in red in Table 19. The model repeats these calculations for the dry-cooled configurations.

Table 19 - Expected Annual Revenue and Profit Alternatives

(Bold-faced items were calculated using the equations displayed below)

Parameter	Description	Unit	Nominal Value
p	Price of electricity (hourly)	$/MWh	varies
p_{PPA}	Power purchase agreement (PPA) price of electricity	$/MWh	$200
R	**Annual revenue based on competitive hourly electricity pricing**	**$M**	**$36**
R_{PPA}	**Annual revenue based on a fixed price of electricity set through a PPA**	**$M**	**$92**
P	**Pre-tax, unsubsidized expected annual profit based on competitive hourly electricity pricing**	**$M**	**-$66**
P_{PPA}	**Pre-tax, unsubsidized expected annual profit based on a fixed price of electricity set through a PPA**	**$M**	**-$9**
P_{tax}	**Post-tax, unsubsidized expected annual profit based on competitive hourly electricity pricing**	**$M**	**-$49**
P_{PPAtax}	**Post-tax, unsubsidized expected annual profit based on a fixed price of electricity set through a PPA**	**$M**	**$8**
P_{ITC}	**Post-tax, subsidized expected annual profit based on competitive hourly electricity pricing**	**$M**	**-$26**
P_{PPAITC}	**Post-tax, subsidized expected annual profit based on a fixed price of electricity set through a PPA**	**$M**	**$31**

**Nominal values were calculated for 6 hr TES with SM = 2.23*

$$R = \sum [p * E_{SOLD}] \quad (186)$$

$$R_{PPA} = p_{PPA} * E_{ANNUAL2} \quad (187)$$

$$P = R - LCOE * E_{ANNUAL2} \quad (188)$$

$$P_{PPA} = R_{PPA} - LCOE * E_{ANNUAL2} \quad (189)$$

$$P_{tax} = R - LCOE_{tax} * E_{ANNUAL2} \quad (190)$$

$$P_{PPAtax} = R_{PPA} - LCOE_{tax} * E_{ANNUAL2} \quad (191)$$

$$P_{ITC} = R - LCOE_{ITC} * E_{ANNUAL2} \quad (192)$$

$$P_{PPAITC} = R_{PPA} - LCOE_{ITC} * E_{ANNUAL2} \quad (193)$$

4.5 Case Study Economic Results

This section presents the results of the economic model for the three plant configurations examined (no storage/backup, TES, and NG) for the base case input values presented in the previous sections. Chapter 6 includes a sensitivity analysis that quantifies the sensitivity of model results to changes in key input parameters due to uncertainty and variability. Figure 49

presents the total plant capital cost (in 2009 $billion) for four scenarios for each plant configuration: 1) unsubsidized plants with a wet cooling system; 2) unsubsidized plants scenario with a dry cooling system; 3) subsidized plants with an investment tax credit (ITC) and a wet cooling system; and 4) subsidized plants with the ITC and a dry cooling system. The plant with no storage/backup has an unsubsidized plant capital cost of $0.4 billion ($4,000/kW). The unsubsidized capital costs for the TES plants with range from $0.5 to $1.2 billion (approximately $5,000-$12,000/kW), while the unsubsidized NG costs range from $0.6 to $0.9 billion (approximately $6,000-$9,000/kW). Each incremental increase in TES increases the total plant capital cost by 3-20% compared to the previous TES capacity. The largest incremental increase is observed from two to three hours of TES, and the smallest is observed from 11 to 12 hrs of TES. Each incremental increase in NG backup increases the total plant capital cost by 0-16% compared to the previous NG capacity. The plants with 5 hrs, 8 hrs, and 12 hrs of NG backup show the smallest increase in total plant capital cost from the previous hour at close to 0%.

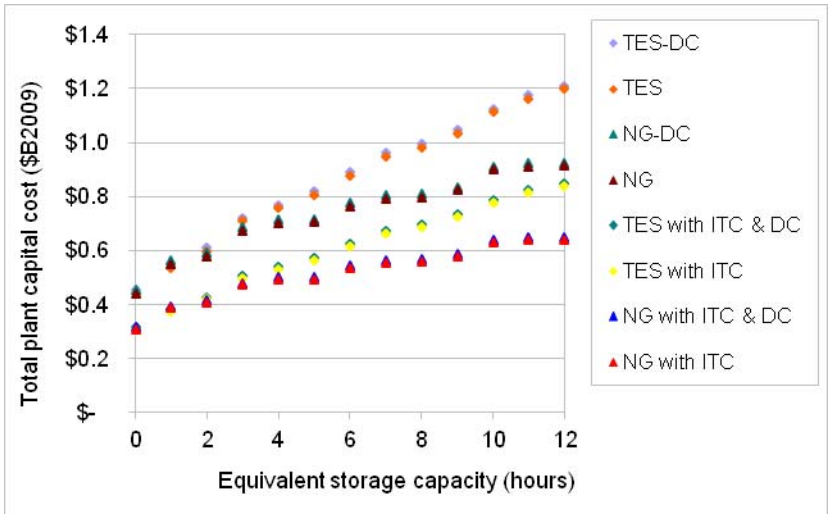

Figure 49 - Subsidized and unsubsidized total plant cost

(DC = dry cooling; ITC = investment tax credit)

With the ITC subsidy and accelerated depreciation, the plant with no storage/backup has a total plant capital cost of $0.3 billion. The TES total plant capital costs range from $0.4 to $0.8 billion (approximately $3,000-$8,000/kW), while the NG costs range from $0.4 to $0.6 billion (approximately $3,000-$6,000/kW). In the subsidized scenarios, the ITC takes 30% off the direct capital costs of the plant. As reported in Table 6 in Chapter 2, the most recently operating PT plant in the United States, Nevada Solar One with 0 hr TES, had a capital cost of $4,108/kWe, nearly identical to the 0 hr TES unsubsidized model result. The reported value likely includes the ITC with standard depreciation [150]. The subsidized cost from the model ($3,087/kW) is about 25% lower than the reported cost for Nevada Solar One. However, the model is based on a 100 MW plant, and Nevada Solar One is 64 MW. The model value for 0 hr TES also does not incorporate the extra cost of a larger natural gas heater needed for the 2% backup capacity Nevada Solar One has. Without knowing more detail about the calculations and assumptions behind the reported value for Nevada Solar One, it is impossible to know why there is a difference from the model result.

In each model scenario, the 0 hr configuration has the lowest capital cost. There is not much difference between the TES and NG cases until 3 hrs of equivalent storage capacity. From 3-12 hours, the TES costs are consistently 6-31% higher than the NG costs because of the higher cost of the storage system relative to the natural gas-fired heater. The total plant costs for each of the scenarios with dry cooling (DC) are approximately 1-2% higher than the wet-cooled counterparts.

Figure 50 shows the relative contributions of the major system components to the total plant capital costs. For all plant configurations, the solar field is most expensive component, contributing 52% of the capital cost of the 0 hr configuration. This drops to 36% of the cost of the 12 hr TES plant, as the cost of the storage system increases from 9% at 1 hr TES to 24% at 12 hr. Comparatively, the natural gas-fired heater contributes less than 1% of the total plant cost for all TES capacities and 0.4% - 9% of the cost of the NG configurations. The contribution of the power cycle cost to the total decreases linearly with increasing storage capacity since it is a fixed cost that becomes overshadowed by the increasing costs of the storage system and solar field (for the TES cases only). The relative contributions from indirect capital costs (which include engineering, procurement, construction, land, sales tax, and miscellaneous as described in Table 17) and contingency costs increase linearly for all equivalent storage capacities since they are percentages of the direct capital costs.

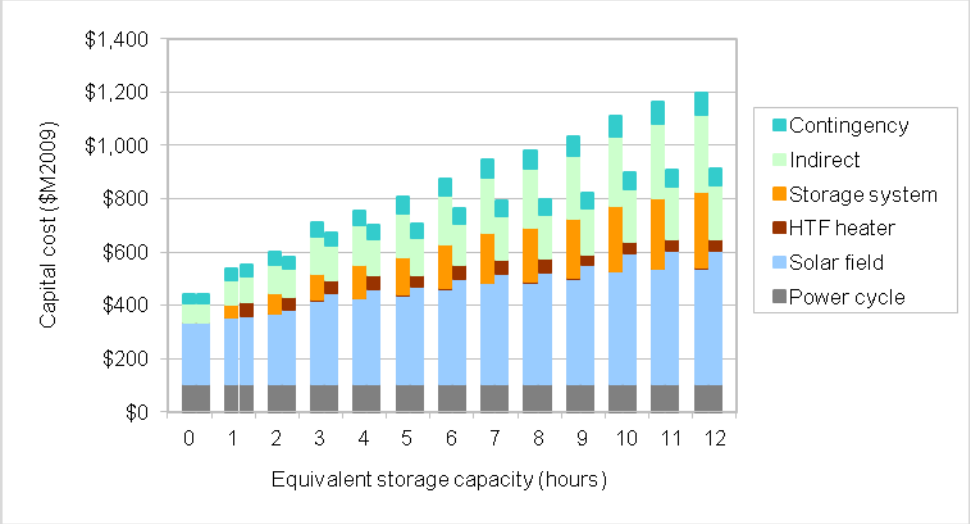

Figure 50 - Comparison of main component costs to the total capital cost

(TES on the left and NG on the right)

As explained in section 4.1, three different levelized annual capital costs (LAC) were calculated for each plant configuration in order to represent: 1) the pre-tax, unsubsidized (nominal) cost; 2) the post-tax unsubsidized cost; and 3) the post-tax subsidized cost. These results, which have the same relative patterns as the total plant capital cost results, are displayed in Figure 51 for both the wet- and dry-cooled plant types. The dry-cooled costs are 1-3% higher than the wet-cooled counterparts. The post-tax costs are lower overall than the corresponding pre-tax costs due to the savings associated with depreciation and loan interest.

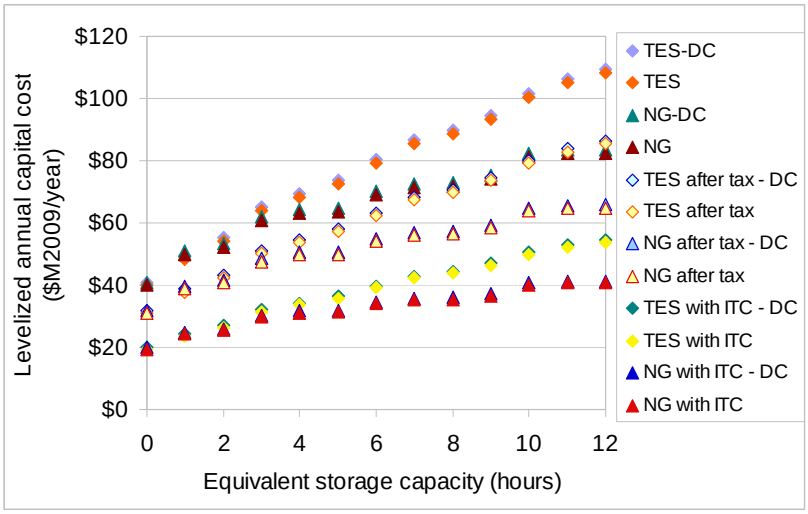

Figure 51 - Levelized annual capital cost

The annual operation and maintenance (O&M) costs for each plant configuration are displayed in Figure 52. The plant with no storage/backup has the lowest annual O&M costs at $18M/yr. O&M costs increase with increasing TES to $20M/yr with 1 hr TES and up to $24M/yr with 12 hrs TES. Each incremental increase is 1-7% compared to the next smallest TES capacity. The O&M costs for the NG plants range from $21M/yr with 1 hr NG to $38M/yr with 12 hr NG, representing incremental increases of 3-17%. These NG O&M costs are 10-58% higher than the

respective TES costs due to the relatively large annual natural gas purchase. The dry-cooled plant configurations save about $1 million/year in O&M costs compared to their wet-cooled counterparts because of the reduced annual water purchase.

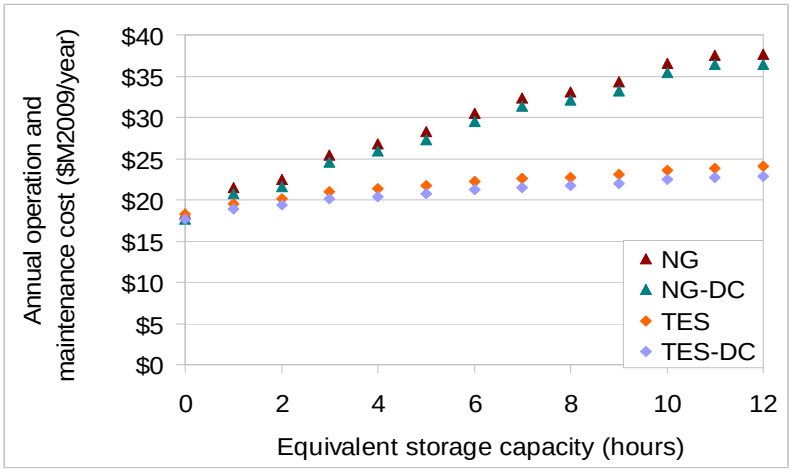

Figure 52 - Annual operation and maintenance costs

Figure 53 shows the relative contribution of labor, service contracts, and utilities to the total annual O&M costs. Labor costs increase slightly with higher equivalent storage capacities and larger solar field areas to maintain. Electricity and natural gas purchases represent the largest portions of the annual O&M costs. At 0 hr TES, electricity purchases represent 63% of the total annual O&M costs, decreasing to 47% of the 12hr TES O&M costs and to 30% of the comparable NG costs. Natural gas purchases are approximately 1% of the total O&M costs for the 0 hr TES case and increase to 9% of the 6 hr TES configuration as more natural gas is required for storage salt freeze protection. Natural gas purchases for the NG cases range from 12% at the 1 hr equivalent to 41% at the 12 hr equivalent.

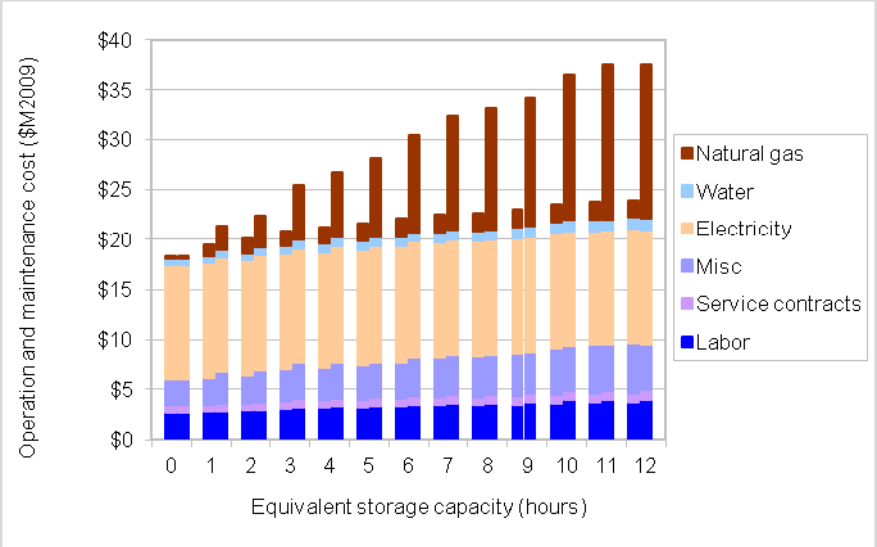

Figure 53 - Breakdown of annual operation and maintenance costs by component

(TES on the left and NG on the right)

As Equation 180 showed, the ratio of the sum of the levelized annual capital cost (LAC) and the annual O&M costs to annual electricity sold gives the levelized costs of electricity (LCOE) presented in Figure 54. For each set of results presented, the plant with no storage/backup has the lowest LCOE. LCOE increases 4% with 1 hr TES compared to the no storage/backup case, and each incremental increase in TES beyond 1 hr TES adds 1-2% to the LCOE to the point where the plant with 12 hr TES has a LCOE 26% higher than the plant with no storage/backup and 21% higher than the LCOE of the lowest TES capacity. NG backup also increases the LCOE compared to the no storage/backup case by 9% with 1 hr NG backup and up to 15% with 12 hr NG backup. For smaller storage capacities (1-4 hrs of equivalent storage), the unsubsidized LCOE for the NG plant is 1-5% higher than the respective TES plant. For larger storage capacities (5-12 hrs), the NG LCOE is 2-9% lower than the respective TES plant.

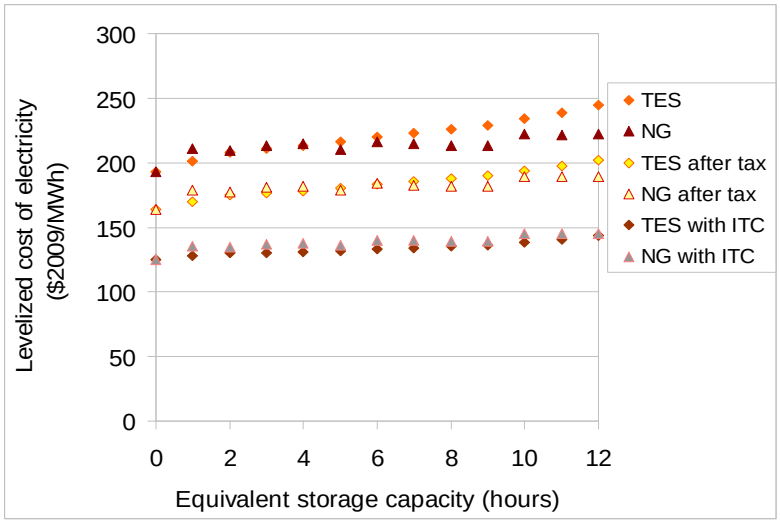

Figure 54 - Levelized cost of electricity

The combination of ITC and accelerated depreciation causes the LCOE of the NG configurations to be 1-6% higher than the respective TES cases since the ITC reduces the capital cost of the TES plants but does not change the NG O&M costs. For simplicity, the dry-cooled results are not presented in Figure 54, but they are $11-13/MWh (5-7%) higher than their respective unsubsidized counterparts; $9-11/MWh (4-7%) higher than their respective unsubsidized post-tax counterparts; and $6-7/MWh (4-7%) higher than their subsidized counterparts.

Figure 55 compares the expected annual revenue calculated with a $200/MWh power purchase agreement (PPA) to the expected annual revenue calculated with the real-time price of electricity from the California Independent System Operator (CAISO) – see Equations 186 and 187. The revenue increases with increasing equivalent storage capacity/backup as annual electricity generation increases, and the PPA generates about 3 times more revenue than the hourly pricing.

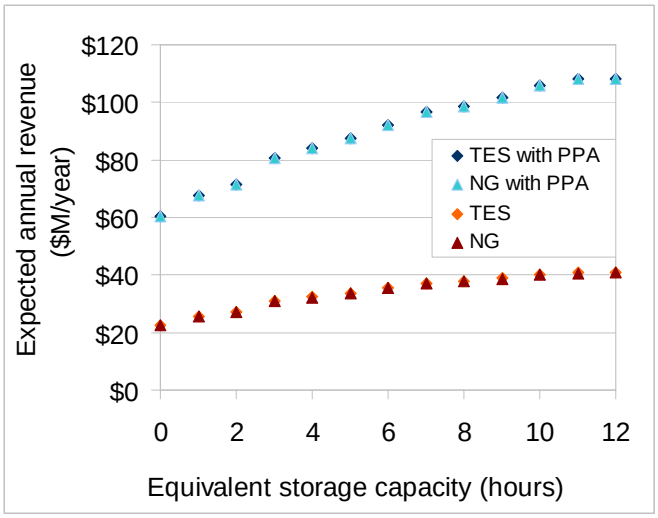

Figure 55 - Expected annual revenue for two pricing options

Figure 56 presents the expected annual profit for the various incentive and pricing scenarios modeled. All of the unsubsidized scenarios result in negative annual profits (i.e., losses), with similar patterns across different plant configurations as the LCOE results. The assumed 30% ITC is not sufficient to guarantee an annual profit with hourly electricity pricing. However, the PPA alone is enough to bring the unsubsidized pre-tax annual profit of the plant with no storage/backup into the positive region with a value of $2 million per year. Nearly all of the unsubsidized post-tax scenarios with the PPA result in a profit. These range from $1M with 11 hr TES to $10M with 1 hr TES and from $6M with 12 hr NG to $9M with 5 hr NG. The case with no storage/backup (0 hr) has the highest unsubsidized post-tax PPA profit, with $11M/year.

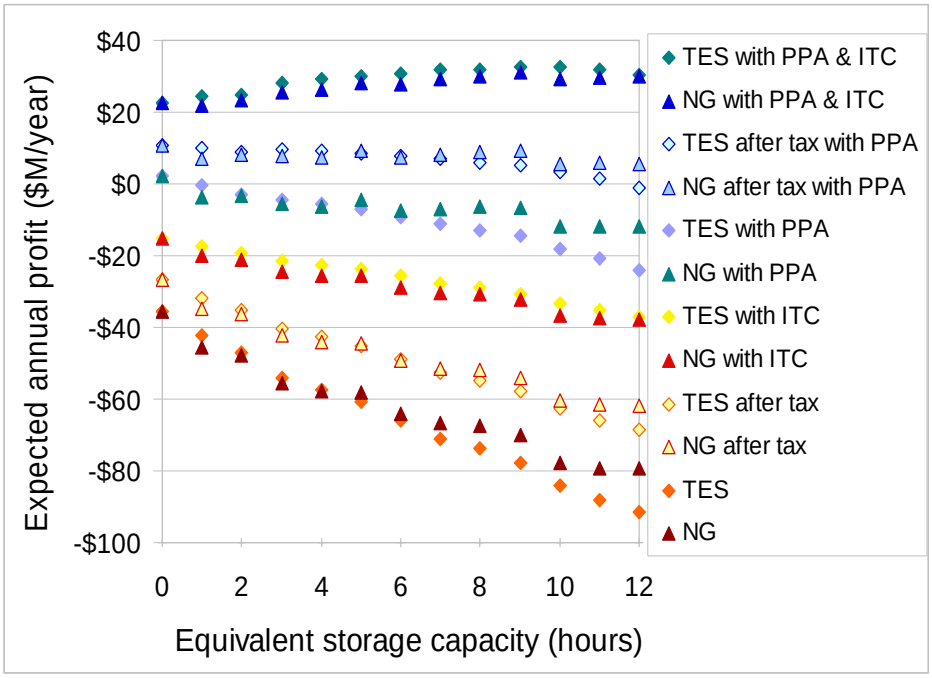

Figure 56 - Expected annual profit

The combination of the ITC and PPA results in the highest annual profit for each plant configuration. In all other incentive/pricing combinations, the 0 hr case has the highest profit (lowest loss) compared with other capacities. With the ITC/PPA combination, the 0 hr case has nearly the lowest annual profit at $23M. Annual profit with TES increases from $24M with 1 hr to a maximum of $33M with 10 hr (an increase of 8% and 43%, respectively, over 0 hr). The profit for the NG backup cases ranges from $22M with 1 hr (decrease of 3% compared to 0 hr) to a maximum of $31M with 9 hr (an increase of 35% over 0 hr). Furthermore, all NG profit results are 2-11% lower than the comparable PT-TES cases when the ITC/PPA combination is modeled. These results indicate that the current federal ITC combined with a reliable PPA may provide an incentive for TES over natural gas backup.

Chapter 5: Environmental Life Cycle Assessment (LCA)

Life cycle analysis (LCA) is a method of assessing the environmental and/or economic impacts of a product or process from the "cradle to the grave". Two main approaches to LCA include process and economic input-output (EIO-LCA). A process-based LCA attempts to quantify the effects of each process flow associated with the production and disposal of a product or process. Limitations to this method include data availability, time, and cost as the analysis attempts to include more indirect process flows (further upstream or downstream from direct production). EIO-LCA is a relatively quick analysis that uses aggregated sectors of the entire U.S. economy to quantify the direct and indirect effects from each economic sector of a specific dollar amount output in one sector. The main limitation of this method is that the entire economy is aggregated into 428 sectors, which may not accurately reflect the specific industries involved in the production of a product. The analysis used in this study is a hybrid LCA, which incorporates process-based data where available and supplements with EIO data where necessary.

5.1 Life Cycle Inventory (LCI)

This hybrid environmental LCA compares the greenhouse gas emissions, energy, water and land use associated with the production of one megawatt-hour (MWh) of electricity from a parabolic trough plant operating with and without storage ((PT-TES and PT-NG, respectively). Figure 57 displays the system boundary used in this assessment. The boundary includes the supply of raw materials and manufacture of key system components (including the solar field, TES system, heat transfer fluid (HTF) system, power block and balance of plant (BOP) in order to construct

the power plant. The operation and maintenance stage of the LCA includes electricity to operate pumps and other auxiliary equipment, water for mirror washing and the power cycle cooling system, makeup HTF, natural gas for the HTF and storage fluid heaters, and diesel fuel for maintenance trucks. Makeup HTF is necessary because over time some of the HTF will vaporize, spill, or degrade due to the high operating temperatures. The final stage considered in this LCA is dismantling the power plant and disposing of key system components.

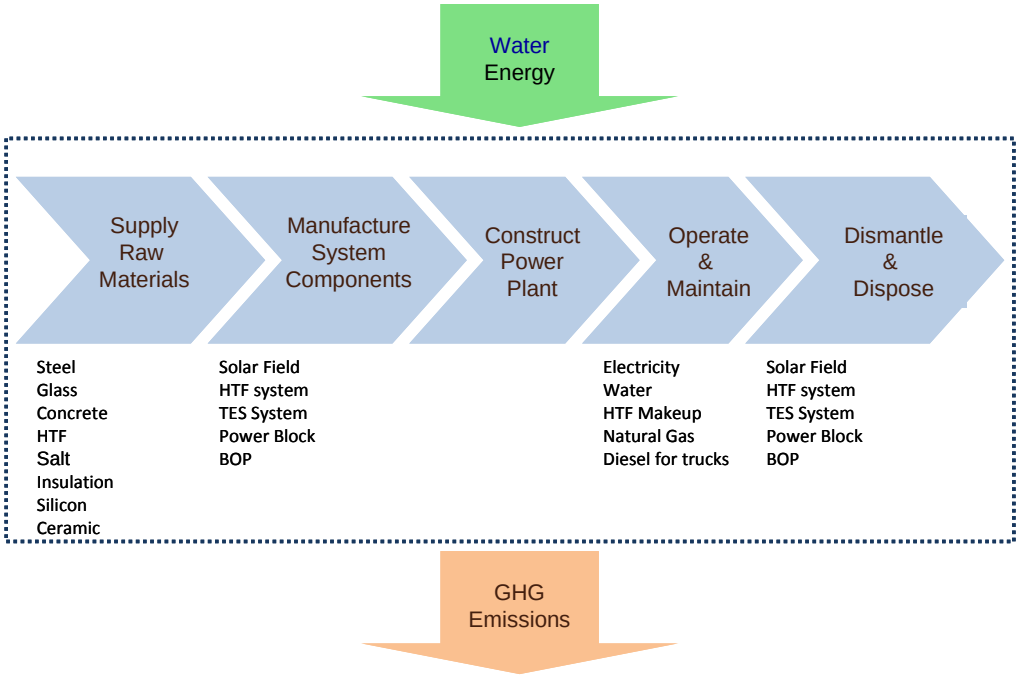

Figure 57 - Environmental Life Cycle Assessment Boundary

The first step in the LCA was to conduct a life cycle inventory (LCI), which is an accounting of the material requirements and monetary values that will be used to estimate the environmental impacts in the process-based and EIO impact assessments, respectively. For the purposes of this report, the LCI has been divided into two stages: 1) power plant construction and 2) power plant operation and maintenance. The first stage includes the supply of raw materials and manufacture

of system components required to construct the power plant (as depicted in Figure 57). A LCI was not conducted for the "dismantle and disposal" stage due to time and data constraints, but literature values for the environmental impacts associated with this stage are included in impact assessment. The following sub-sections describe the LCI estimates for each of these stages.

5.1.1 Power Plant Construction LCI

Table 20 presents the material requirements and monetary values for the main components of the case study power plant with six hours of thermal energy storage and a solar multiple of 2.23. The solar collector assembly (SCA) material estimates are based on data obtained from Lupfert et al. [24], Solel [151], and Kreith et al. [138], and the following assumptions: 1) 10% of the SCAs in the solar field are "strong", designed for high wind loads; 2) steel comprises 40% and borosilicate glass comprises 60% of the receiver tube mass; 3) 99% of the mirror mass is due to the reflective glass, and the rest is split evenly between the ceramic fasteners and silicone adhesive; and 4) each SCA element requires twenty-one 80-lb bags of concrete for the foundation (based on an estimate of one and a half 2ft x 2ft x 2ft posts per element and online concrete calculators [152],[153]. These data were used to calculate the material requirements for one collector, and these requirements were multiplied by the number of collectors needed for the optimized solar field (12,610 collectors for 1,061 SCAs in the case study plant presented in Table 20).

Table 20 - Material Requirements and Monetary Values for Power Plant Construction Life Cycle Inventory* *(nominal values for 6hr TES, SM = 2.23)*

Component	Material	Unit	Total Life Cycle Quantity	Total per MWh
Solar Collector Assembly				
Eurotrough 150m Concentrator structure	Galvanized steel	kg	14,000,000	1.0
Flabeg mirrors	Low-iron float glass	kg	9,300,000	0.67
Fasteners	Ceramic	kg	47,000	0.0034
Adhesives	Silicone	kg	47,000	0.0034
Solel UVAC4 receiver tube	Stainless steel	kg	410,000	0.030
Solel UVAC4 receiver tube	Borosilicate glass	kg	620,000	0.045
SCA Foundations	Concrete	m^3	4,500	0.00033
Heat Transfer Fluid (HTF) System				
Header piping	Carbon steel	kg	2,300,000	0.17
Header piping	Insulation	kg	3,000,000	0.22
HTF	Therminol VP-1	kg	2,800,000	0.20
Thermal Energy Storage (TES) System				
Tanks	Carbon steel	kg	2,300,000	0.17
Tanks	Insulation	kg	1,500,000	0.11
Foundation	Concrete	m^3	6,900	5.0E-04
Storage Fluid	Solar Salt	kg	57,000,000	4.1
Heat Exchangers	EIO-LCA	$	22,000,000	1.6
Pumps	EIO-LCA	$	9,400,000	0.68
Power Cycle and Other				
Turbine & Generator	EIO-LCA	$	62,000,000	4.5
Natural Gas-Fired Heaters for salt and HTF	EIO-LCA	$	24,000,000	1.7
Balance of Plant	EIO-LCA	$	41,000,000	3.0
Site Work and Infrastructure	EIO-LCA	$	150,000,000	11

**See Appendix E for a complete list of the specific Simapro databases and processes used to obtain the environmental impact factors*

Carbon steel and mineral wool insulation were selected as the materials for the HTF header piping because they are the materials used by Kelly and Kearney [96], and Simapro has databases for these materials. The amount of these materials and the initial amount of HTF were calculated based on the layout presented in Figure 28 in Chapter 3 and a series of equations that estimate the cross-sectional area of piping segments of varying sizes (see Equations 194-212). The "hot" header piping carries hot HTF from the solar field to the power block heat exchangers, and the "cold" header piping carries cold HTF from the power block heat exchangers to the solar

field. The header piping closest to the power block must have a larger diameter than the header piping at the far end of the solar field because as the HTF travels through the header piping, it branches off into the absorber tubes on either side of the header piping (see Figure 28 in Chapter 3). Therefore, the amount of steel and insulation needed for each segment of header piping varies with the distance of the pipe from the solar field.

$N_{seg} = N_{loops} \div 4$; where N_{seg} = number of header pipe segments in one half of solar field (194)

$l_{seg} = w_{sca} + l_{betweenrow}$; where l_{seg} = length of segment (195)

$d_{isegH(1)} = N_{seg} * 2 * d_i$; where $d_{isegH(1)}$ = inner diameter of segment 1 of hot header & d_i = inner diameter of absorber tube (196)

$d_{isegH(i)} = d_{isegH(i-1)} - 2 * d_i$; where $d_{isegH(i)}$ = inner diameter of segment (i) of hot header for i = 1 to N_{seg} (197)

$d_{thsegH(i)} = R_{thH} * d_{isegH(i)}$; where R_{thH} = average ratio of hot header wall thickness to inner diameter (=0.0108 [96]) (198)

$d_{osegH(i)} = d_{isegH(i)} + d_{thsegH(i)}$; where $d_{osegH(i)}$ = outer diameter of segment (i) of hot header (199)

$A_{steelsegH(i)} = \pi * (d_{osegH(i)} \div 2)^2 - \pi * (d_{isegH(i)} \div 2)^2$; where $A_{steelsegH(i)}$ = cross-sectional area of steel in segment (i) of hot header (200)

$v_{steelsegH(i)} = A_{steelsegH(i)} * l_{seg}$; where $v_{steelsegH(i)}$ = volume of steel in hot header segment (i) (201)

$V_{steelH} = 2 * \Sigma(v_{steelsegH})$; where V_{steelH} = total volume of steel in hot header (202)

$M_{steelH} = \rho_{steel} * V_{steelH}$; where M_{steelH} = mass of steel in hot header & ρ_{steel} = density of steel (=7.86 tonnes/m^3) (203)

$M_{steelheader} = M_{steelH} + M_{steelC}$; where $M_{steelheader}$ = total mass of steel in header piping & M_{steelC} = mass of steel in cold header (204)

$d_{thinsH(i)} = R_{thinsH} * d_{thsegH(i)}$; where $d_{thinsH(i)}$ = thickness of insulation in hot header segment & R_{thinsH} = average ratio of hot header insulation to pipe thickness (=22) (205)

$A_{inssegH(i)} = \pi * ((d_{osegH(i)} + 2 * d_{thinsH(i)}) \div 2)^2 - \pi * (d_{osegH(i)} \div 2)^2$; where $A_{inssegH(i)}$ = cross-sectional area of insulation in segment (i) of hot header (206)

$v_{inssegH(i)} = A_{inssegH(i)} * l_{seg}$; where $v_{inssegH(i)}$ = volume of insulation in hot header segment (i) (207)

$V_{insH} = 2 * \Sigma(v_{inssegH})$; where V_{insH} = total volume of insulation in hot header (208)

$M_{insH} = \rho_{ins} * V_{insH}$; where M_{insH} = mass of insulation in hot header & ρ_{ins} = density of insulation (=240.28 kg/m^3) (209)

$M_{insheader} = M_{insH} + M_{insC}$; where $M_{insheader}$ = total mass of insulation in header piping & M_{insC} = mass of insulation in cold header (210)

$V_{HTF} = 0.5 * (L_{absorber} * \pi * (d_i/2)^2 + \Sigma(l_{seg} * \pi * (d_{isegH(i)} \div 2)^2) + \Sigma(l_{seg} * \pi * (d_{isegC(i)} \div 2)^2))$; where V_{HTF} = total volume of HTF (211)

$M_{HTF} = V_{HTF} * \rho_{HTFmax}$; where ρ_{HTFmax} = maximum density of HTF (at T_{min}) & M_{HTF} = total mass of HTF (212)

Equation 194 calculates the number of header pipe segments in one half of the solar field, and Equation 195 calculates the length of each segment as the sum of the SCA width and the distance between each row of SCAs. Equation 196 calculates the inner diameter of the first hot header

segment as twice the product of the absorber tube inner diameter and the number of header segments in order to have enough space for all segments to receive HTF from absorber tubes on both sides of the header piping. Equation 197 reduces the inner diameter of each subsequent segment by twice the inner diameter of the absorber since one less SCA loop will be emptying into each subsequent segment. Equation 198 calculates the thickness of the steel wall in each hot header segment using the average ratio of wall thickness to inner pipe diameter obtained from the NREL piping model [96] as a linear scaling factor. Equation 199 calculates the outer diameter of the header pipe as the sum of the inner diameter and steel thickness. Equation 200 calculates the cross-sectional area of the hot header segment as the difference between the total cross-sectional area and the inner cross-sectional area, and Equation 201 calculates the volume of steel needed in each hot header segment. Equation 202 calculates the total volume of steel for the hot header as twice the sum of the steel in the segments (since the original calculations were based on one half of the solar field), and Equation 203 calculates the total mass of the steel for the hot header. The model repeats Equations 196 through 203 for the cold header, and Equation 204 calculates the total steel for all headers.

A similar method is used in Equations 205-210 to calculate the total mass of insulation for the header piping, and Equations 211 and 212 calculate the initial total mass of HTF needed for the power plant under the assumption that there needs to be enough HTF to at least fill half the space in the total absorber space and a quarter of the space in the header piping. This assumption results in similar HTF volumes per unit aperture area as those reported in Cohen et al. [95] and SAM [137]. This is considered an initial mass because HTF will be lost over time to vaporization and degradation and will need to be replaced annually.

The TES system incorporates two tanks (one for hot fluid and one for cold fluid), and each tank requires insulation and a foundation. The quantities of carbon steel, thermal insulation, and concrete were obtained from regression analyses on the total costs and unit costs associated with varying TES capacities reported in Kelly and Kearney [103]. The data used and equations resulting from these regressions are presented in Appendix D. Due to time constraints and lack of data, the EIO-LCA method was used to estimate the resource requirements and greenhouse gas emissions associated with the manufacture of the TES heat exchangers and pumps, and Table 20 displays the cost inputs to the EIO-LCA model for these components, which were derived from the cost model results described in Chapter 4. Chapter 3 describes how the performance model calculates the total mass of the storage fluid ($M_{salttotal}$) used in the TES system. Table 20 also presents the values from the cost model for the power cycle, heaters and site work and infrastructure (including the total direct site work costs and the total indirect engineering, procurement, management and construction (EPCM) and project, land and miscellaneous (PLM) costs discussed in Chapter 4). For the purposes of the EIO-LCA inventory, 60% of the total power cycle cost from the economic model was attributed to the turbines and generators, and 40% was allocated to the balance of plant (cooling towers, pumps, heat exchangers) because that is the approximate distribution in the SAM spreadsheet [39].

5.1.2 Operation and Maintenance LCI

In general, the operation and maintenance (O&M) LCI estimates the utilities included in the annual O&M cost model described in Chapter 4: auxiliary electricity, water for the power cycle cooling system and mirror washing, and natural gas for the HTF and storage fluid heaters. In

addition, the O&M LCI estimates diesel fuel for the solar field maintenance trucks and the amount of HTF required annually to make up for HTF lost through vaporization, spills and degradation. Table 21 presents the material requirements and monetary values for the O&M LCI for the case study plant with 6 hours of TES and a solar multiple of 2.23. The total annual natural gas and water amounts and cost of auxiliary electricity from the economic model were multiplied by the plant lifetime of 30 years to obtain the values presented in the table. The total lifetime diesel fuel mass was calculated based on the following assumptions: 1) on average, one truck will drive the entire length of the collectors (approximately 160,000 m for the case study plant) once a day to check for maintenance issues and/or wash mirrors; 2) the truck's gas mileage is 15 miles per gallon on average; and 3) the density of diesel fuel is 0.85 kg/L [154]. The total lifetime O&M HTF mass calculation is based on the assumption that approximately 0.5% of the initial HTF mass will be lost to vaporization, spills and degradation each year, and new HTF will be purchased each year to replace the loss.

Table 21 - Material Requirements and Monetary Values for Operation and Maintenance Life Cycle Inventory

Item	Purpose	Unit	Total Life Cycle Quantity	Total per MWh
Electricity	Parasitic loads and nighttime HTF pumping	$	340,000,000	25
Water	Mirror washing and power cycle cooling	thousand gallons	21,000,000	1.5
Natural Gas	HTF and storage fluid heaters	MMBtu	9,600,000	0.69
Diesel fuel	Maintenance trucks	kg	250,000	0.018
Heat transfer fluid (HTF)	Makeup for vaporization, spillage and degradation	kg	420,000	0.031

5.2 Environmental Impact Assessment

The water use, greenhouse gas emissions, and energy requirements associated with the life cycle stages described above were estimated using the Simapro 7.1 databases where physical measurements were available and the EIO-LCA U.S. 2002 (428) Benchmark Model - Producer Price [155] where economic data were available. In Simapro, the IPCC GWP 100a method estimated the greenhouse gas emissions (GHG) and the Cumulative Energy Demand (CED) V1.06 method estimated the energy requirements. Water use was calculated as the sum of the following substances in the "Raw" compartment of the database inventory if available: "Water, well, in ground", "Water, river", and "Water, lake". If none of these substances were available, then water use was obtained from the substance "Water, unspecified natural origin" in the "Raw" compartment. The EIO-LCA model reports GHG emissions, total energy, and water use based on a specified amount of economic activity. Table 22 presents the environmental factors obtained from these sources and the units upon which they are based. Appendix E includes a full list of the specific databases used within Simapro and EIO-LCA and the specific processes included for each item.

Table 22 - LCA Environmental Impact Factors

Item	Use	Unit	CED (MWh/ unit)	GHG (kg CO_{2eq}/ unit)	Water use (gallons/ unit)
Construction					
Site work & infrastructure	General construction	$	2.3E-03	0.61	5.6
Galvanized steel	Solar Collector Assembly (SCA)	kg	9.1E-03	2.9	0.1
Low-iron float glass solar mirrors	SCA	kg	0.041	8.8	7.7
Ceramic	SCA	kg	0.012	2.6	3.7
Silicone	SCA	kg	0.018	2.9	1.6
Stainless steel	SCA	kg	0.028	6.1	24
Borosilicate glass	SCA	kg	0.015	3.2	2.1
Concrete	SCA, TES foundations	m^3	0.41	267	152
Therminol VP-1	Initial and makeup HTF	kg	0.031	3.0	1.2
Carbon steel	TES tanks and HTF header piping	kg	6.3E-03	1.1	0.33
Insulation	TES tanks and HTF header piping	kg	5.1E-03	1.5	2.8
Solar salt	TES system	kg	1.80E-05	0.0038	0.0094
Salt pumps	TES system	$	2.4E-03	0.56	8.5
Heaters and heat exchangers	HTF and salt heaters and TES heat exchanger	$	3.1E-03	0.79	9.9
Turbines and Generators	Power Block	$	1.6E-03	0.40	4.7
Other manufacturing	Balance of plant	$	2.5E-03	0.63	7.9
Operation and Maintenance					
Diesel*	Maintenance vehicles	kg	0.07	4.7	0.70
Natural Gas*	HTF and salt heaters	MMBtu	1.2	89	0.0054
Electricity	Auxiliary loads	$	7.5E-03	2.3	61
Dismantle and Disposal [127]					
Solar Field	For plant with wet cooling	m^2* MWh	5.4E-10	8.7E-07	4.5E-07
Solar Field-DC	For plant with dry cooling	m^2* MWh	5.1E-10	8.4E-07	4.2E-07
HTF System	For plant with wet cooling	m^2* MWh	1.5E-10	5.2E-07	2.5E-07
HTF System-DC	For plant with dry cooling	m^2* MWh	1.4E-10	5.1E-07	2.4E-07
TES System	For plant with wet cooling	MWh_{th}* MWh	1.2E-06	3.4E-04	6.4E-04
TES System-DC	For plant with dry cooling	MWh_{th}*MWh	1.2E-06	3.3E-04	6.2E-04
Power Block	For plant with wet cooling	MW*MWh	7.3E-07	1.3E-03	6.1E-04
Power Block-DC	For plant with dry cooling	MW*MWh	7.6E-07	7.8E-04	6.1E-04

* *The diesel and natural gas GHG emission factors include combustion as follows:* $GHG_{combustion} = CO_{2combustion} + CO_{2eqCH4release}$. *For diesel:* $CO_{2combustion}$ *= (5.83 MMBtu/barrel * 7.46 barrels per metric ton * 73.15 kg* CO_2 *emissions per MMBtu)/1000*

*(sources of data: [156],[157],[158], respectively; and $CO_{2eqCH4release}$ = (0.0051 g CH_4 emissions per mile [158] * annual miles driven * GWP)/(annual mass of diesel * 1000). The annual miles driven are calculated as the product of the length of the solar field piping and 365 days. The GWP refers to the global warming potential of methane, which is 25[159]. For natural gas: $CO_{2combustion}$ = 53.06 kg CO_2 per MMBtu [158]; and $CO_{2eqCH4release}$ = GWP * 0.001 kg per MMBtu [158]*

Therminol VP-1 is a synthetic fluid and a eutectic mixture of 73.5% diphenyl oxide (also known as diphenyl ether and phenyl ether [160]) and 26.5% biphenyl [35]. Unfortunately, Simapro does not have a database for Therminol VP-1, diphenyl ether, phenyl ether, or biphenyl. Therefore, proxies were selected to represent the manufacture of the two components of Therminol VP-1, and Table 22 presents the weighted sum of the impact factors for these proxies. Since diphenyl ether is a side product in the production of phenol [161], the Ecoinvent database 'Phenol, at plant/RER S' was selected to represent the life cycle environmental impacts of diphenyl ether production. Biphenyl (also called diphenyl, phenylbenzene, 1,1'-biphenyl, or limonene) can be produced from coal tar, crude oil, and natural gas by distillation [162]. Since the specific production source for Therminol VP-1 in CSP generation is unknown, Table 22 presents the average of the results from representative Simapro databases for coal tar, crude oil, and natural gas. Coal tar is a by-product of the carbonization of coal to make coke [163]; therefore, the ETH-ESU 96 database 'Coal Cokes S' was used to represent impacts from coal tar production. This database represents coke produced from coal and the byproducts: coal-tar, ammonia, light oils, and "coal-gas". The average ratio of tars to coke from Rubchevskii et al (0.055825 [164]) was used to allocate impacts to coal tar production alone. The energy content of coke was assumed to be 29.6 MJ/kg [165] in order to convert the Simapro results from impacts per MJ to impacts per kg.

The portion of biphenyl production environmental impacts attributed to natural gas production was calculated as the sum of the impacts from the same Simapro databases as those used for the

operation and maintenance natural gas: 'Natural gas, at extraction site NREL/US'; 'Natural gas, processed, at plant NREL /US'; and 'Natural gas, at consumer/RNA with US electricity' (U.S. LCI Database and Ecoinvent). A density of 0.8 kg/m^3 [166] was used to convert the values in Simapro to impacts per kg. The portion of biphenyl production environmental impacts attributed to crude oil production was calculated as the sum of the impacts from: 'Crude oil, production GB, at long distance transport/kg/RER' and the average of data from 'Crude oil production onshore S' and 'Crude oil, at production onshore/RME S' (Ecoinvent).

The storage salt thermodynamic properties in the performance model and the unit cost in the economic model are based on "solar salt" (see Table 3), which is binary nitrate salt consisting of a eutectic mixture of 60% sodium nitrate ($NaNO_3$) and 40% potassium nitrate (KNO_3) [37]. It is possible to mine these compounds or produce them synthetically, and since approximately 60% of the solar salt market share is from mining [127], this LCA assumes the compounds are mined. Unfortunately, Simapro does not have a database for mined solar salt, sodium nitrate or potassium nitrate. Therefore, proxies were selected to represent the solar salt mining and production process in order to obtain the environmental impact factors presented in Table 22. Figure 58 represents the mining process of the company SQM, the self-proclaimed leading producer of mined nitrate salts in the world. Solar salt is mainly produced from mined caliche ore, which is extracted from shallow surfaces using explosives and then crushed and leached [167]. Since this is a form of surface mining with explosives [168], a mined proxy that uses a similar method was selected for use in Simapro; the database for vermiculite was the closest match. Vermiculite is a natural mineral found in Russia, South Africa, China, and Brazil and is often used for insulation [169]. The Ecoinvent database 'vermiculite, at mine/kg/ZA with US

electricity' includes "excavation by digger, blasting, transportation within mine", but it does not include crushing. The Ecoinvent database 'Limestone, crushed, for mill/CH S' was used to represent the environmental impacts of crushing and processing the caliche to form solar salt because this database includes the processes: "primary crushing, washing, and transportation by conveyor belt" [170]. The salt environmental impact factors presented in Table 22 are the sum of the impact factors from these two databases.

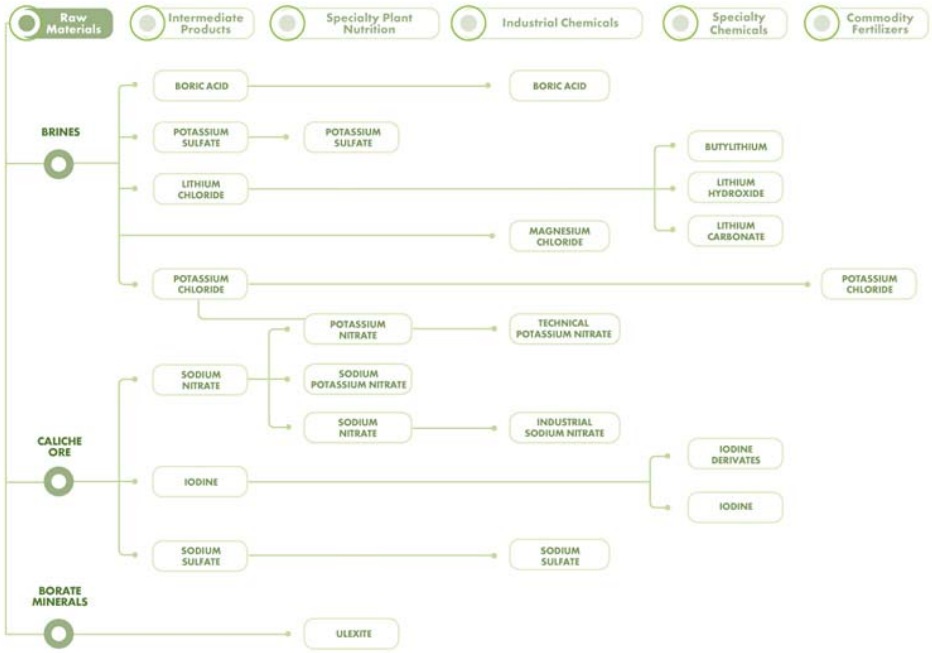

Figure 58 - Mining Processes Used in the Production of Solar Salt [171]

The land use assessment is based on the life cycle land use of only the operational stage of the power plant due to time constraints and uncertainty concerning proper allocation of upstream land use. In reality, the land use from the operational stage is probably more important to policy-makers than the upstream land use since CSP plants tend to occupy vast stretches of desert land that may encroach on threatened or endangered desert species. Therefore, for the purposes of this study, the "life cycle land use" (A_{LC}) refers to the values calculated in Equations 181 and 182, in contrast with the solar field area and total power plant area, which are not scaled by

lifetime electricity generation. The coefficients in Equations 213 and 214 were obtained from the ratio of solar field aperture area to total power plant area used in the Worley Parsons CSP studies for the updated SAM version [43],[45].

$$A_{LC} = [4.1 * A] \div [E_{ANNUAL2} * t_b] \quad (213)$$

$$A_{LCDC} = [3.9 * A] \div [E_{ANNUAL2DC} * t_b]; \text{ for plant with dry cooling} \quad (214)$$

The environmental impacts from dismantling and disposing of the main plant components at the end of the plant lifetime were obtained from Burkhardt et al. [127] and divided by the reference total solar field area, gross turbine capacity, and storage capacity (in megawatt-hours thermal (MW_{hth})) reported in the study, resulting in units of impact factor per (reference unit times MWh). These values were scaled linearly for use in this study by multiplying the appropriate value by the ratio of the nominal unit to the reference literature unit. For example, Burkhardt et al. report the value for the GHG emissions from the dismantle and disposal stage of a parabolic trough plant with a 1,990 MWht TES system to be 0.68 $kgCO_{2eq}$/MWh. For the purposes of this study, this value was multiplied by the ratio of the nominal storage capacity to the reference capacity of 1,990 MWht to estimate the TES system dismantle and disposal GHG emissions for various storage capacities.

5.4 Nominal Results from Environmental Analysis

As described above, the environmental analysis includes five sets of calculations: 1) Cumulative Energy Demand (CED); 2) life cycle greenhouse gas (GHG) emissions; 3) life cycle water; 4) life cycle land use (on-site only); and 5) carbon price for PT to be competitive with a new coal-

fired power plant. The nominal results for each of these analyses are presented in the following sub-sections.

5.4.1 Cumulative Energy Demand

Figure 59 presents the nominal results for the cumulative energy demand calculation for storage and no storage with and without dry cooling. The CED increases from a value of 0.5 MWh per MWh with no storage/backup to a maximum value of 6.5 MWh per MWh with 12 hrs NG (13 fold increase). The CED for each dry-cooled case is 5-9% higher than the respective wet-cooled case for all plant configurations because the dry-cooled systems generate less electricity over the plant lifetime than the wet-cooled systems since the power cycle is less efficient. The CED for the NG cases increases steadily from 1.8 times the TES case at 1 hr to 6.7 times at 12 hr. This is due primarily to the increase in annual natural gas consumption with increasing equivalent storage capacity. On the other hand, the CED for the plants with storage increases from 1.1 MWh/MWh at 1 hr storage (twice the no storage/backup value) to 1.2 MWh/MWh at 2 hr TES and then decreases steadily to 0.9 MWh/MWh with 12 hr TES. The different trend for the TES plants can be explained by the fact that annual natural gas use for HTF freeze protection does not vary significantly across TES capacities, so with larger storage capacities, the larger amount of annual electricity generation balances out any small increase in natural gas consumption to result in a net decrease per MWh electricity generated after 2 hr TES.

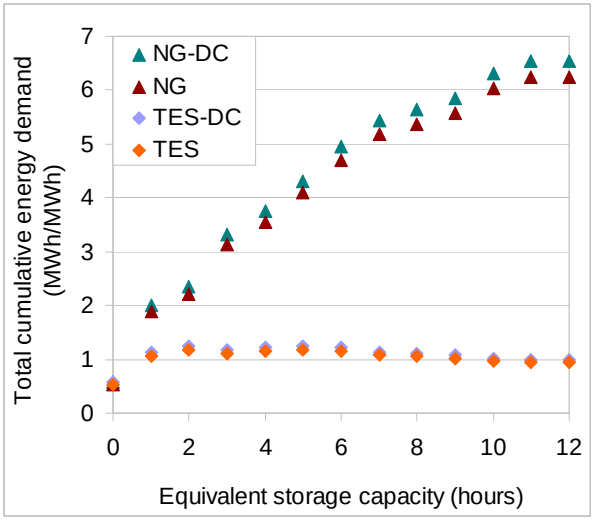

Figure 59 - Total cumulative energy demand

Intuitively, a CED value of 6.5 MWh/MWh seems high because it implies that six times as much energy output is required as primary energy input to get generate one MWh of electricity. Upon closer inspection, it was revealed that using the Simapro database to calculate the upstream impacts from natural gas extraction, processing, and transportation and also self-calculating the combustion impacts may have led to double-counting the natural gas environmental impacts. The following Ecoinvent databases were used originally to calculate the upstream impacts of natural gas extraction, processing and transportation from refinery to distribution site, respectively: "Natural gas, at extraction site NREL /US (U.S. LCI Database with Ecoinvent Supplement)"; "Natural gas, processed, at plant NREL /US (U.S. LCI Database with Ecoinvent Supplement)"; and "Natural gas, at consumer/RNA with US electricity U (Ecoinvent)". In the inventory for the first two databases, there is an input of 1.03 and 1.08 m^3 raw natural gas per m^3 natural gas output, respectively. The energy content associated with these amounts of natural gas is roughly equal to the CED output reported in the Ecoinvent databases, and since no other energy input is listed in the inventory, it can be tentatively concluded that the primary energy

content of the fuel is counted in the CED reported by the database. Therefore, only the combustion stage will be considered for the remaining results concerning CED and greenhouse gas emissions from natural gas. Figure 60 displays the revised lifecycle CED results when the upstream natural gas production impacts are eliminated. Now, the results range from 0.4 to 1.8 MWh/MWh, a much more reasonable range given that any considerable amount of natural gas will increase the CED to greater than one due to the fact that the heater will not be able to harness 100% of the primary energy content in the fuel.

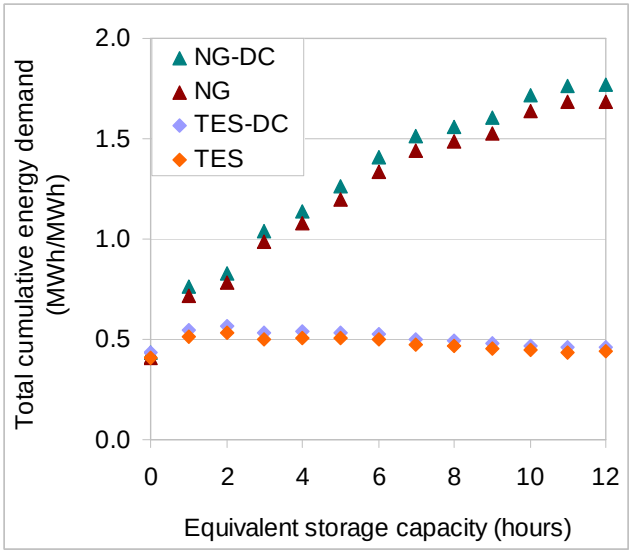

Figure 60 - Total cumulative energy demand (revised to exclude natural gas extraction/processing)

Figure 61 shows the contribution of each stage of the life cycle assessment to the total CED for each equivalent storage capacity for the wet-cooled designs only. The operation stage contributes the most to the total due the annual natural gas consumption, and this trend is even more prominent in the NG backup cases. CED from dismantle and disposal is negligible compared to the other two stages.

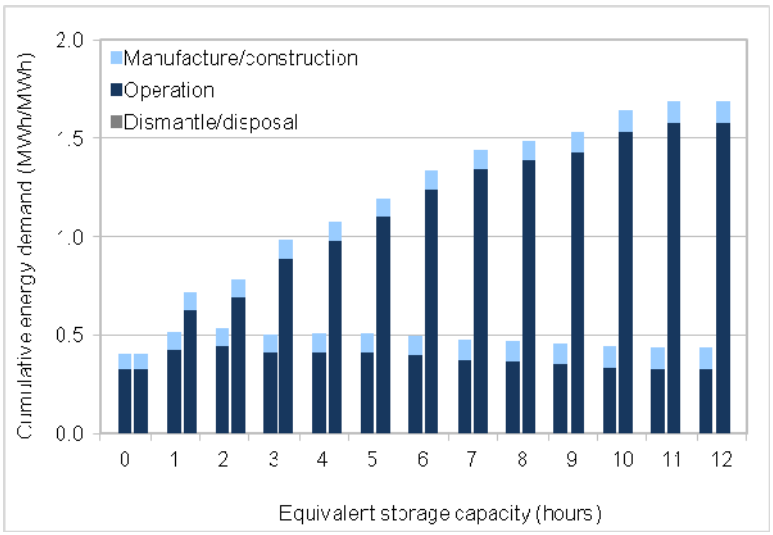

Figure 61 – Relative contribution of life cycle stage to total CED

(TES on the left and NG backup on the right)

Figure 62 shows the relative contribution of the manufacture and construction of each main plant component to the total manufacture/construction portion of the CED. The solar field is the single largest contributor to the manufacture/construction CED, decreasing from 48% of the total with no storage/backup to 34% with 12 hr storage. This decrease occurs as the share from the TES system increases from 0% with no storage/backup to 14% with 11 hr TES, and the contribution from the HTF system (including from the natural gas-fired heater) increases from 5% with no storage/backup to 14% with 12 hr TES. The contribution from the power block and balance of plant decreases with increasing TES capacity as the total contribution from these two stays constant but the net annual electricity generation from each plant increases. The site work and infrastructure contribution increases with increasing total plant capital cost. The NG cases follow similar trends with respect to power block, balance of plant, site work and infrastructure, but the solar field contribution first decreases to 40% with 1 hr NG; increases to 43% with 9 hr NG; and decreases again to 42% with 12 hr NG. Meanwhile, the HTF contribution increases

steadily to 25% at 12 hr NG as a larger natural gas-fired heater is needed to match the larger storage capacity.

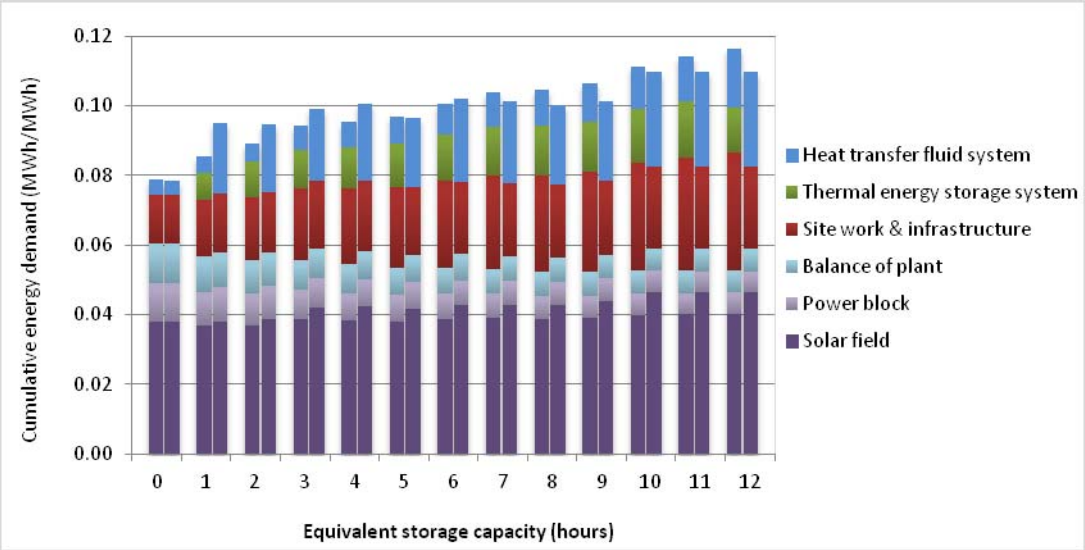

Figure 62 - Relative contribution of key plant components to manufacture/construction total CED

(TES on the left and NG backup on the right)

Figure 63 is similar to Figure 62 except it shows in more detail how the CED of individual materials contributes to the total manufacture/construction CED. The manufacture of the mirrors makes up the largest single material contribution to the total at 25-35% depending on th equivalent storage capacity. The CED impacts from the ceramic fasteners, silicon adhesives, boroglass receiver envelopes, stainless steel receiver tubes, concrete foundations, carbon steel and insulation for the storage tanks and header piping, TES heat exchanger and pumps, and nitrate salt each make up between close to 0% and 6% of the total manufacture/constuction CED. The natural gas-fired heater contributes between 1% of the total with no storage/backup to a maximum of 16% with 1 hr NG. The contribution from the power bloack and balance of plant each decrease from about 15% with no storage/backup to 6% with 12 hr NG. The contribution

from site work and infrastructure is significant at 18%-29% of the total manufacture/construction stage. Since the CED values for this component were obtained from the EIO-LCA method, it may be worthwhile in the future to calculate the direct effects from the process-based method in the future for comparison.

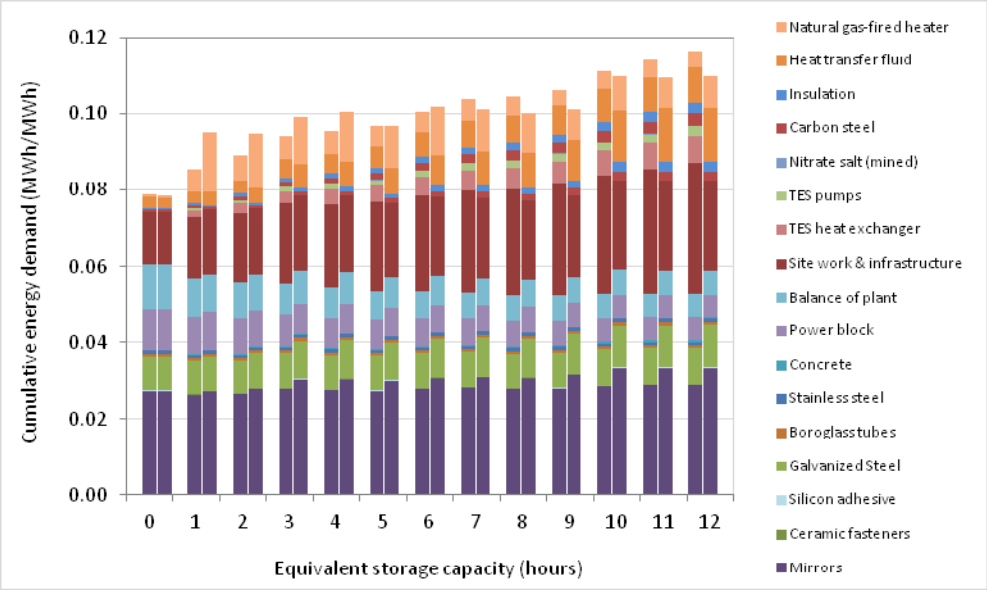

Figure 63 - Relative contribution of key materials/components to manufacture/construction total CED

(TES on the left and NG backup on the right)

Figure 64 displays the relative contribution of each key component of the operation stage to the total operational stage CED. With no storage/backup, the indirect CED from electricity for auxiliary loads, especially nighttime HTF pumping, makes up 88% of the operational total, while natural gas for on-site HTF freeze protection is 12%, and diesel fuel for solar field maintenance trucks and makeup HTF are close to 0% each. Electricity remains the largest single contributor to operational stage CED for all of the successive TES capacities, decreasing to 50% of the total with 12 hr TES, while natural gas increases to 49% of the total at this capacity. For the NG plant

configuration, natural gas quickly overtakes electricity as the single largest contributor to the operational stage CED, increasing from 58% of the total at 1 hr NG to 90% at 12 hr NG. Similar to the TES cases, HTF makeup and diesel fuel remain close to 0% of the total operational stage CED for the NG cases.

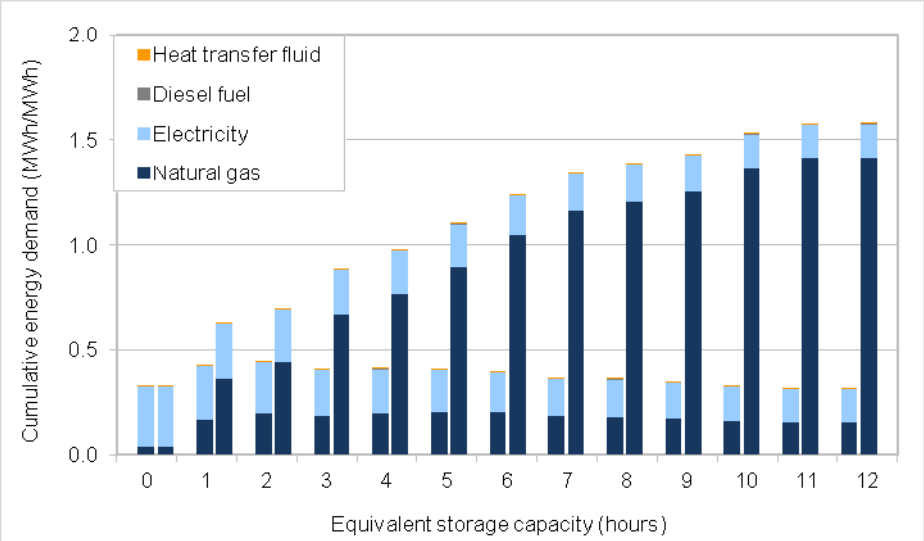

Figure 64 - Relative contribution of key components to operational stage CED total

(TES on the left and NG backup on the right)

5.4.2 Life Cycle Greenhouse Gas Emissions

Figure 65 displays the total life cycle greenhouse gas (GHG) emissions for each plant configuration with wet cooling and dry cooling. These results exclude the upstream emissions from natural gas extraction and processing in order to avoid the potential double-count described in relation to CED previously. Life cycle GHG emissions increase from 120 $kgCO_{2eq}$/MWh with no storage/backup to a maximum of 130 $kgCO_{2eq}$/MWh with 2 hr TES (16% increase) and decrease again to a minimum of 110 $kgCO_{2eq}$/MWh with 12 hr TES (6% decrease from no

storage/backup). With NG backup, the GHG emissions increase steadily from 170 $kgCO_{2eq}$/MWh, with 1 hr NG (47% increase from no storage/backup and 27% increase from 1 hr TES) to a maximum of 330 $kgCO_{2eq}$/MWh with 12 hr TES equivalent (about 3 times the no storage/backup and 12 hr TES values). Figure 65 displays the same basic trends as Figure 60 since GHG emissions are directly related to fossil fuel use, and the bulk of CED is comprised of primary energy from fossil fuels. The GHG results for the plants with TES and no storage/backup are within the range of 17-185 $kgCO_{2eq}$/MWh reported in the literature and summarizes in section 2.5.

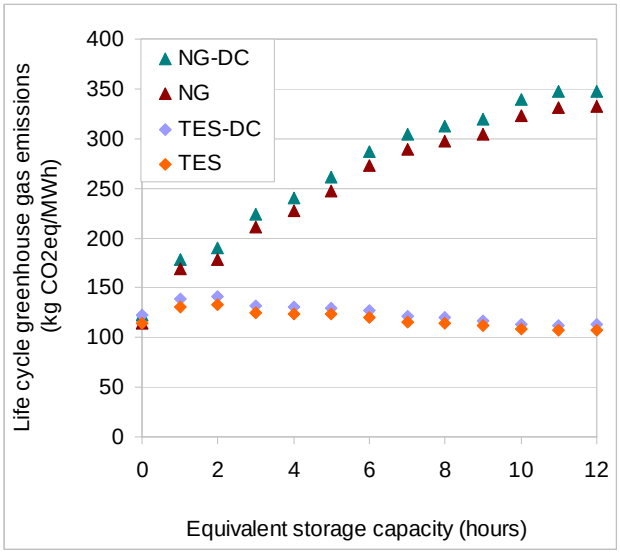

Figure 65 - Life cycle greenhouse gas emissions

No literature values were found to compare the parabolic trough cases with NG backup. However, Table 23 lists the mid-point life cycle GHG emission values reported by Jaramillo et al. [172] for several leading fossil fuel electricity generation technologies. At a range of 170-330 $kgCO_{2eq}$/MWh, the parabolic trough cases with NG backup have greater life cycle GHG emissions than the literature value for NGCC with CCS, and similar GHG emissions to IGCC with CCS and PC with CCS. NGCC life cycle emissions without CCS are only 20-40% higher

than parabolic trough with 7-12 hours of NG backup. There is a lot of uncertainty associated with comparing LCA results from two different studies due to the myriad assumptions, boundaries, and data sources that can be used. Therefore, this is a rough comparison to put the NG cases in context with other electricity generation technologies.

Table 23 - Life Cycle GHG Emissions for Fossil Fuel-Fired Electricity Generation [172]

Electricity generation technology	Life cycle GHG emissions (kg CO_{2eq}/MWh)
Pulverized coal (PC)	1,000
Integrated gasification combined cycle (IGCC)	900
Natural gas combined cycle (NGCC)	400
PC with carbon capture and sequestration (CCS)	180
IGCC with CCS	140
NGCC with CCS	90

Figure 66 displays the relative contribution of each life cycle stage to the total GHG emissions for the wet-cooled cases presented in Figure 65. The results for the dry-cooled cases were similar but slightly higher in each stage. The trends shown in this figure are similar to those displayed in Figure 61 due to the link between primary fossil energy use and GHG emissions. Again, the operational stage is the largest contributor to life cycle GHG emissions for all three plant configurations at all storage/backup capacities.

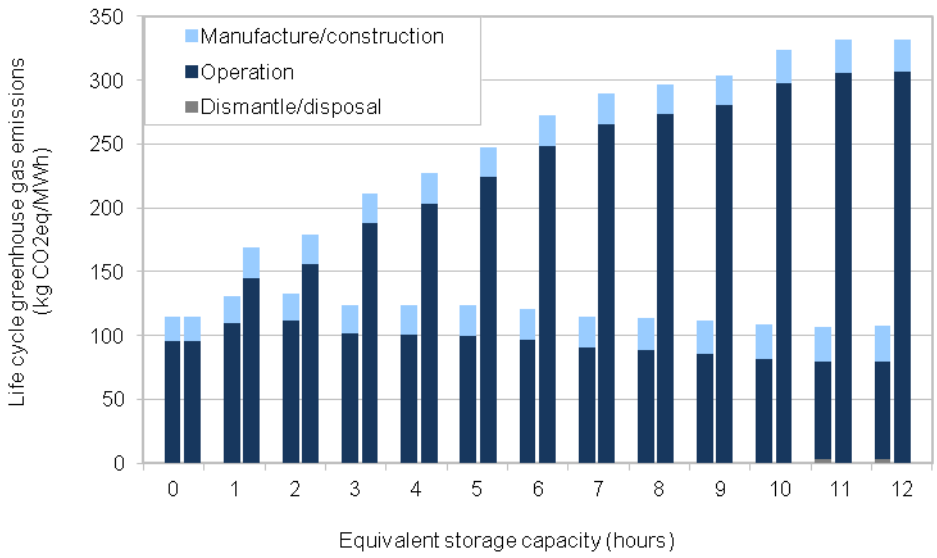

Figure 66- Relative contribution of life cycle stage to total GHG emissions

(TES on the left and NG backup on the right)

Figure 67 displays the relative contribution of the key plant components (including the heat transfer fluid system, thermal energy storage system, site work and infrastructure, balance of plant, power block, and solar field) to the life cycle GHG emissions from the manufacture/construction stage. These results include similar trends as seen in Figure 62 due to the relationship between primary fossil fuel energy use and GHG emissions.

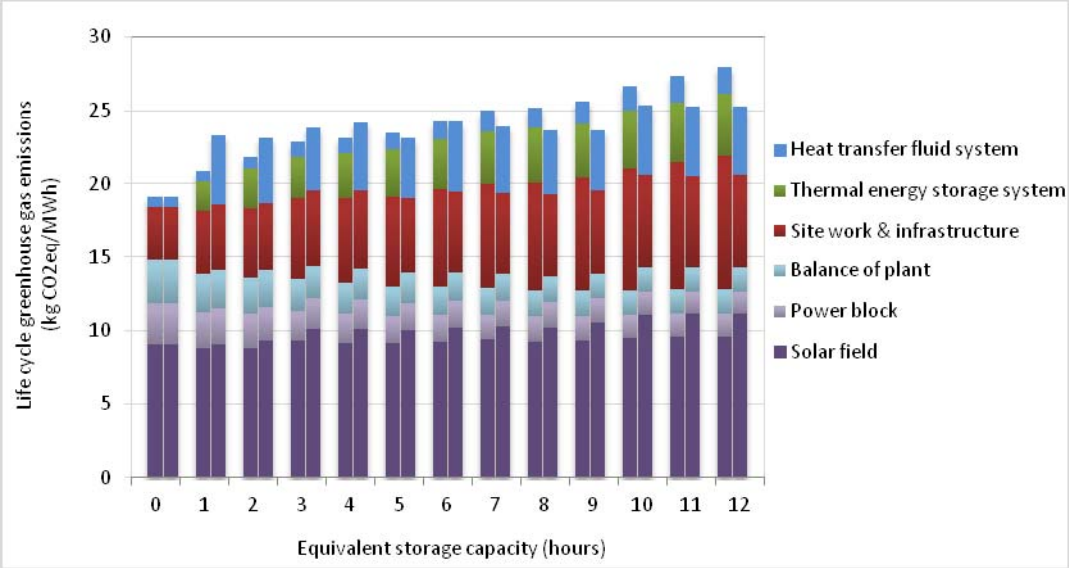

Figure 67 - Relative contribution of key plant components to manufacture/construct total GHG emissions

(TES on the left and NG backup on the right)

Figure 68 displays the relative contribution of the key materials in each of the components from Figure 67 to the life cycle GHG emissions from the manufacture/construction stage. These results include similar trends as seen in Figure 63 due to the relationship between primary fossil fuel energy use and GHG emissions.

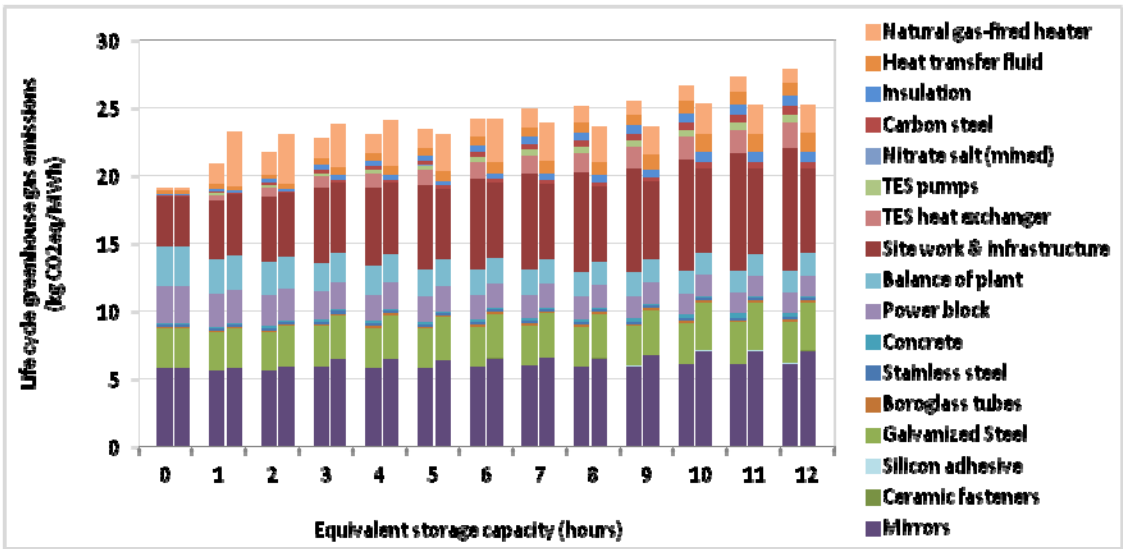

Figure 68 - Relative contribution of key materials/components to manufacture/construction total GHG emissions (*TES on the left and NG backup on the right)*

Figure 69 displays the relative contribution of the following components to the life cycle GHG emissions from the operational stage of the wet-cooled designs: makeup heat transfer fluid, diesel fuel for maintenance trucks, electricity for auxiliary loads, and natural gas for HTF freeze protection and backup. These results include similar trends as seen in Figure 64 due to the relationship between primary fossil fuel energy use and GHG emissions. Indirect GHG emissions from auxiliary electricity make up the largest portion of operational stage GHG emissions for the no storage/backup plant configuration and all of the TES cases, and GHG emissions from on-site natural gas use comprise the largest percentage of operational stage emissions for the NG cases.

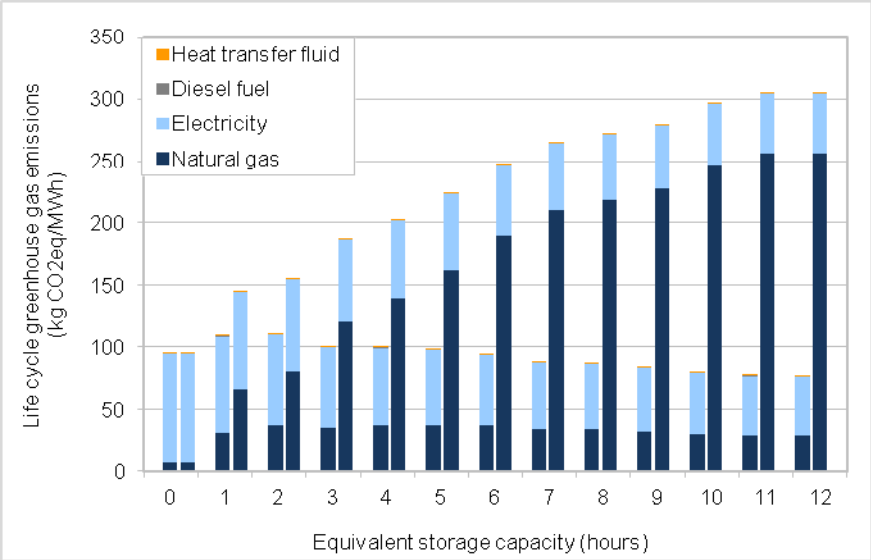

Figure 69 - Relative contribution of key components to operational GHG emissions total

(TES on the left and NG backup on the right)

5.4.3 Life Cycle Water Use

Figure 70 presents the results of the life cycle water use calculations, which range from a maximum of about 3,900 gallons per MWh with wet cooling and no storage/backup to a minimum of approximately 1,600 gallons/MWh with 12 hours of NG backup and dry cooling. In contrast to the CED and GHG emissions results, which were distinguished by backup system, the water use results differ markedly when comparing cooling types and are relatively similar when comparing backup systems. All of the wet-cooled life cycle water use results are between 1.4 and 1.8 times the life cycle water use results of the respective dry-cooled cases; whereas, the TES/NG results vary +/- 1% from each other for the wet-cooled cases and up to 3% for the dry-cooled cases. When wet cooling is used, the life cycle water use for the NG cases is slightly

larger than for the TES cases until 7 hrs of equivalent storage capacity, when the TES cases begin to have slightly larger life cycle water values than the NG cases. When dry cooling is used, the same trend is observed, but the switch happens at 5 hr equivalent TES capacity instead of 7 hr.

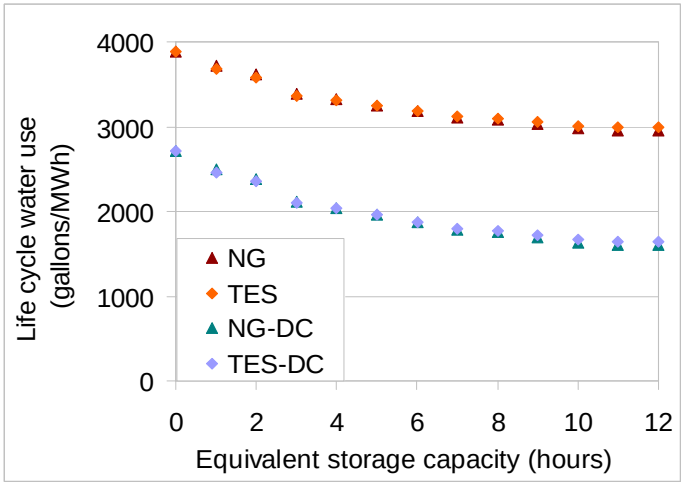

Figure 70 - Life cycle water use

Figure 71 displays the relative contribution of each stage to the life cycle water use of the wet-cooled cases, and the operational stage is the largest single contributor for all cases. The manufacture/construction stage comprises 3-6% of the total for cases with TES and 3-5% for cases with NG backup. The dismantle/disposal stage contributes less than 1% to the total for all cases.

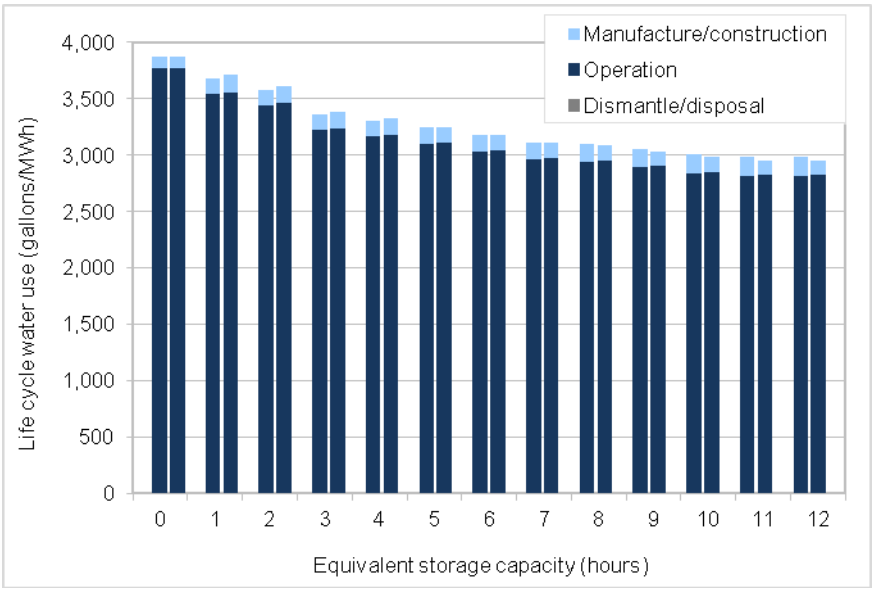

Figure 71 – Relative contribution of each life cycle stage to total water use in plants with wet cooling

(TES on the left and NG backup on the right)

Figure 72 shows the same basic trends for the dry-cooled cases; although the relative percentage contribution from manufacture/construction is slightly increased compared to the wet-cooled cases simply because of the lower operational stage values.

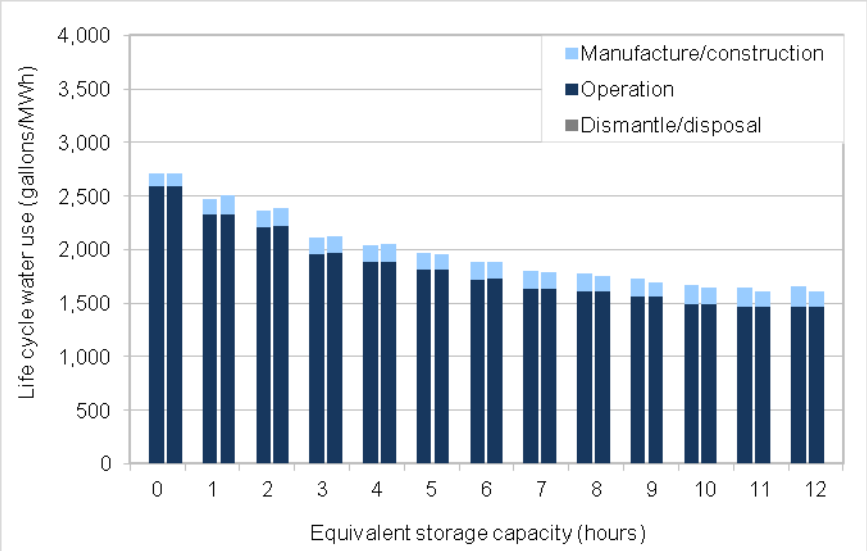

Figure 72 – Relative contribution of each life cycle stage to total water use in plants with dry cooling

(TES on the left and NG backup on the right)

Figure 73 presents the relative contrubution to the manufacture/construction stage of the life cycle water use for the wet-cooled cases from the following key plant components: HTF system, TES system, site work and infrastructure, balance of plant, power block, and solar field. The manufacture/construction stage trends and values were similar for the dry-cooled cases but slightly higher due to the decreased efficiency of the power cycle and slightly lower annual electricity generation. The single largest contributor to the manufacture/construction life cycle water use is site work and infrastructure with 33% of the total at no storage/backup and increasing to 47% of the total with 12 hr TES. With the NG backup cases, this contribution is less dramatic as it decreases to 26% with 1 hr NG backup and then gradually rises to 43% with 12 hr NG backup. Similar to the CED and GHG emissions results, site work and infrastructure results for life cycle water use were derived from EIO-LCA, specifically from the US 2002 (428) Producer Price model for "Construction, Other non-residential". Given the significant contribution of this category to manufacture/construction life cycle water use, it may be

worthwhile in the future to investigate site work and infrastructure from a process-based life cycle approach for comparison. The solar field and HTF system (which includes the natural gas-fired heater) contribute up to 5% each to the total manufacture/construction stage life cycle water use for all cases that use TES. The contribution from the solar field is minimal for the NG cases as well, but the HTF system contributes a maximum of 32% with 1 hr NG to a minimum of 22% with 12 hr NG. The TES system is a significant contributor to the TES results with 18% at 1 hr TES increasing to 26% with 12 hr TES. The power cycle and balance of plant contributions decrease steadily across equivalent storage capacities as the annual electricity generation relative to the power block capacity increases.

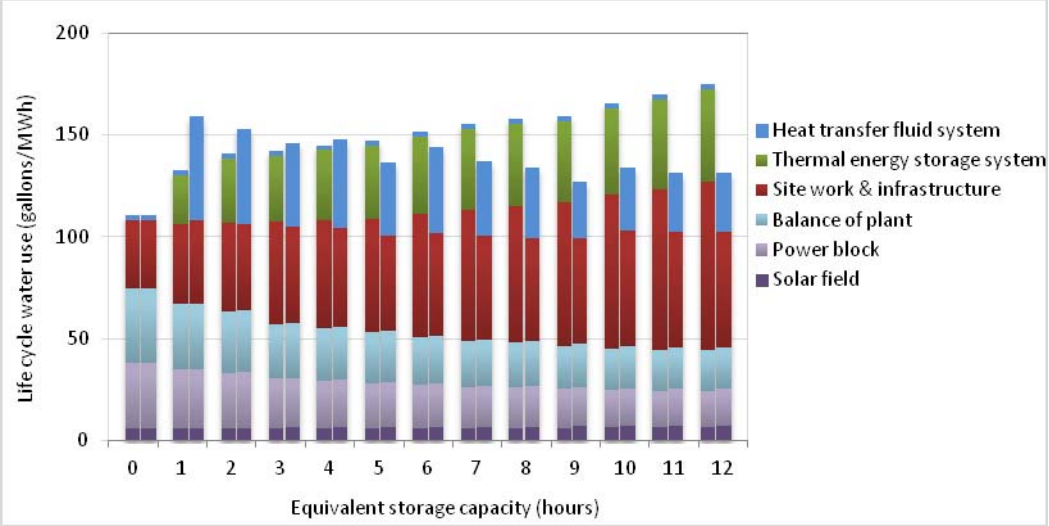

Figure 73 – Relative contribution of key plant components to manufacture/construction stage total water use
(TES on the left and NG backup on the right)

Figure 74 presents the same results as Figure 73 organized by contribution from material rather than main system component. This figure shows site work and infrastructure still to be the largest single contributor, followed closely by the natural gas-fired heater for the NG cases and

then power block/ balance of plant for all of the cases. The TES heat exchanger is the next biggest contributor for the TES cases.

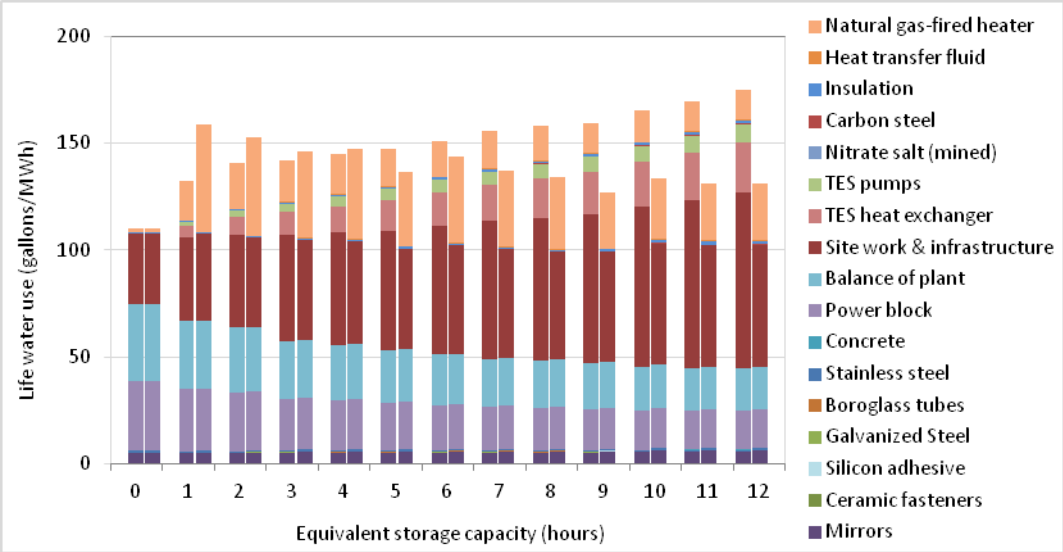

Figure 74 – Relative contribution of key materials/components to manufacture/construct total water use
(TES on the left and NG backup on the right)

Figure 75 shows the relative contribution of makeup HTF, diesel fuel, natural gas, electricity, and steam cycle makeup/mirror washing to the operational stage total life cycle water use for the wet-cooled cases. Only indirect electricity and on-site steam cycle/mirror washing make meaningful contributions to this stage, with electricity comprising 62% of the total with no storage/backup and decreasing to 46% with 12 hr TES/NG backup. Only about 5% of the water use for steam cycle makeup/mirror washing is actually for mirror washing; therefore, roughly 38% of the operational stage life cycle water use is from on-site steam cycle makeup with no storage/backup, increasing to up to 54% of the total with 12 hr TES/NG backup. The electricity values were calculated from EIO-LCA and adapted to the average California electricity mix. It may be more accurate to determine the exact electricity mix in the region of a specific PT power

plant location and calculate the real water use per MWh of electricity supplied by each generator. The water use for steam cycle makeup and mirror washing was calculated by the thermodynamic model.

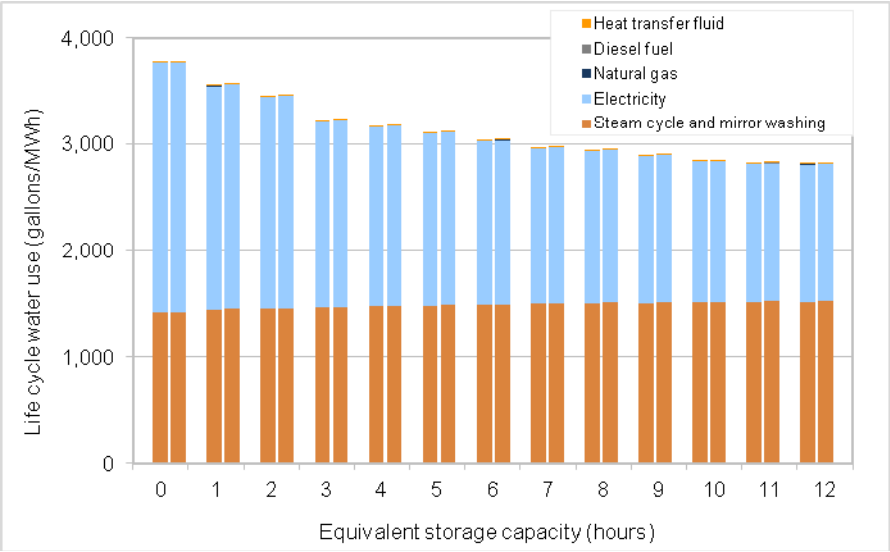

Figure 75 – Relative contribution of key components to operation stage water use (wet cooling)

(TES on the left and NG backup on the right)

Figure 76 shows the relative contribution of makeup HTF, diesel fuel, natural gas, electricity, and steam cycle makeup/mirror washing to the operational stage total life cycle water use for the dry-cooled cases. Dry cooling reduces the steam cycle contribution to a minimum of 4% with no storage/backup up to a maximum of 7% with 12 hr TES/NG backup. The electricity contribution increases to 92-96% of the total operational water use, and the rest of the contributions remain negligible.

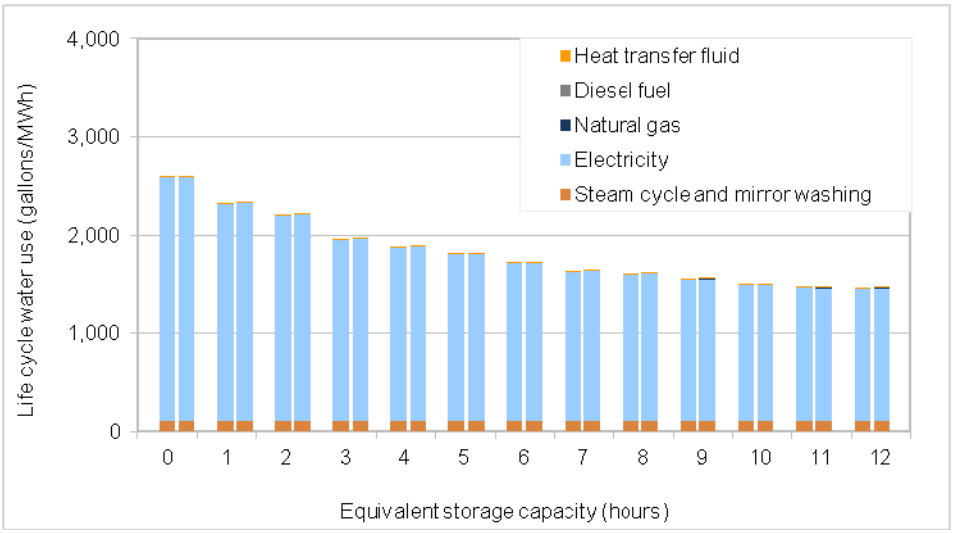

Figure 76 – Relative contribution of key components to operation stage water use (dry cooling)

(TES on the left and NG backup on the right)

5.4.4 Life Cycle Land Use

Figure 77 displays the life cycle land use results (which only incorporate the land use associated with the actual footprint of the power plant as described previously). Life cycle land use decreases from 2.7 ft^2/MWh with no storage to 2.6 ft^2/MWh with 1 hr TES (4% decrease) and increases to a maximum of 2.9 ft^2/MWh with 12 hr TES (12% increase from minimum at 1 hr TES). The NG cases follow a similar trend, with a minimum of 2.7 ft^2/MWh with 1 hr backup and a maximum of 3.3 ft^2/MWh with 12 hr backup (22% increase from minimum at 1 hr NG). The life cycle land use for the NG cases is higher overall than for the TES cases because the plants with NG backup require a slightly larger solar field area to match the TES annual and hourly electricity generation. The dry-cooled cases vary less than 1% from the respective wet-cooled cases.

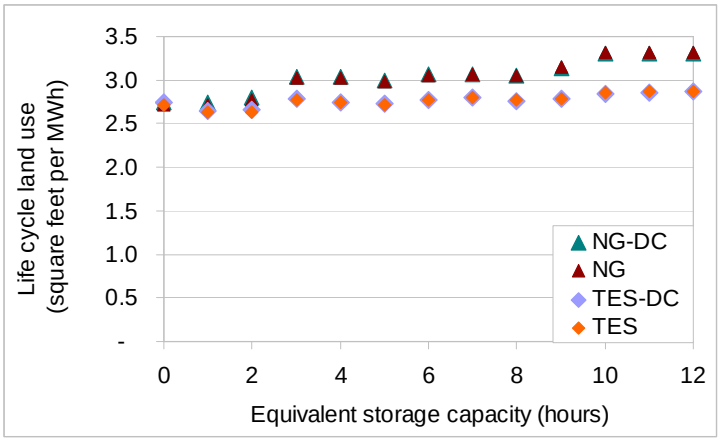

Figure 77 - Life cycle land use

5.4.6 Summary of Nominal Environmental Results

To summarize the results of the environmental analysis, adding TES can slightly reduce life cycle GHG emissions and land use compared to no storage/backup. However, the relative differences between the two plant configurations are so small that given the model uncertainty examined in Chapter 6, it is probably more accurate to say that TES and no TES/backup have similar GHG and land use values. CED and on-site water use is similar for TES and no TES/backup as well. TES and NG backup lower life cycle water use compared to no TES/backup. The NG backup cases have significantly higher CED and life cycle GHG emissions than the TES and no TES/backup configurations. The TES and NG cases have similar life cycle water use values, which decrease steadily with increasing storage capacity/NG backup. The dry-cooled cases have similar CED, life cycle GHG emissions, and land use to the wet-cooled cases and dramatically lower life cycle and on-site water use than the wet-cooled cases.

Chapter 6: Sensitivity Analysis

The model developed in this study is a representation of a complex power plant, and the accuracy of the model in representing a real power plant is dependent on the uncertainty and variability in key parameters. In order to understand how robust the model is for comparing systems with different storage/backup configurations, a series of analyses were conducted to examine the sensitivity of key results to main input parameters. Table 24 presents a range of values for each parameter tested in the sensitivity analyses. It also displays the nominal values used in the Chapter 3-5 analyses, and the reference table or section in the report that describes the parameter in more detail.

Table 24 - Input Parameter Values for Sensitivity Analysis

Symbol	Input Parameter	Unit of Measurement	Lower Bound	Nominal Value	Upper Bound	Reference in Report
DNR_{hourly}	Hourly direct normal radiation	Wh/m^2	varies	Daggett, CA	varies	Chapter 3
$T_{ambhourly}$	Hourly ambient temperature	^oC	varies	Daggett, CA	varies	Chapter 3
m_{HTF}	Design mass flow rate	kg/s	600	1,206	2,000	Table 13
$m_{HTFmaxfactor}$	Maximum HTF mass flow rate factor	None	0.4	2	3	Section 3.5
$m_{HTFminfactor}$	Minimum HTF mass flow rate factor	None	0.07	0.1	0.2	Table 14
T_{HTFmin}	Minimum HTF temperature	^oC	50	50	290	Section 3.5
$F_{allcost}$	Factor to adjust all cost inputs	None	0.7	1	1.3	Chapter 6
$C_{auxunit}$	Unit cost of auxiliary power	$/MWh	$122	$135	$159	Table 18
C_{NGunit}	Unit cost of natural gas	$/MMBtu	$3.69	$5.92	$9.02	Table 18
$C_{H2Ounit}$	Unit cost of water	$/gallon	$0.0010	$0.0014	$0.0018	Table 18
t_b	Book life	years	20	30	40	Table 17
F_{debt}	Debt fraction	None	0	0.4	0.8	Table 17
$F_{equityP}$	Preferred equity fraction	None	0.00	0.08	0.16	Table 17
$F_{equityC}$	Common equity fraction	None	0.12	0.52	0.92	Table 17
k_L	Loan rate/ cost of debt	None	0.06	0.08	0.10	Table 17
k_{eP}	Cost of preferred equity	None	0.04	0.0534	0.07	Table 17
k_{eC}	Cost of common equity	None	0.06	0.0874	0.11	Table 17

The hourly direct normal radiation (DNR) and ambient temperature input values that were used to generate the nominal results presented in Chapters 3-5 are from the Typical Meteorological Year (TMY3) data file for Daggett, CA. Three data files for other locations in the southwest United States were used as inputs for the sensitivity analysis. Since these are hourly values, the relative lower and upper bound changes for each hour of the simulation, which is why these values are presented as "N/A" in Table 24. The next four inputs listed in the table concern the mass flow rate and the minimum temperature of the heat transfer fluid (HTF). As described in Chapter 3, the design mass flow rate was calculated though a series of iterations through thermodynamic mass and energy balance equations designed to represent a power plant cycle that has the same HTF state 5 enthalpy output as input. However, during real power plant operation, the state 5 output does not have to be the same as the input; in fact, it will likely be different, and it can be desirable for it to be different if that means more electricity generation for the plant. Therefore, the design mass flow rate, along with the minimum and maximum factors used to define the constraints described in section 3.5, was varied across a wide range. The minimum operating temperature of the HTF is defined by the Therminol VP-1 manufacturer; yet the power plant operator need not let the HTF reach the specified minimum. If the HTF temperature is maintained above a higher threshold, less DNR will be required to raise the temperature of the inlet HTF to the outlet design value. However, a higher minimum HTF temperature requires more freeze protection in the form of natural gas. The effect of this tradeoff on model results is examined by varying the minimum value up to 290^{o}C.

Most of the input parameters for the economic model are based on the Solar Advisor Model, which is based on the WorleyParsons cost estimation study for a parabolic trough power plant

with 6.3 hours of storage. In that study, WorleyParsons acknowledge that they report costs with +/-30% uncertainty. This uncertainty is incorporated in the sensitivity analysis by varying all cost inputs across this range using $F_{allcost}$. The unit utility costs are subject to uncertainty with respect to market price, especially natural gas and electricity. Water prices may also see increases in the desert in the future as water scarcity issues become more prevalent. The natural gas and electricity unit price sensitivity bounds were selected as the lower and upper bounds from the Energy Information Administration data for the United States and California, respectively, between 1998 and 2008. The water cost bounds were selected to represent a +/-30% range.

The financial parameters are subject to a large amount of uncertainty concerning market volatility, perceived project risk by potential lenders, and the financial assets of the project developer. The equity fractions are dependent on the debt fraction, so the range reported in the table for common equity fraction represents the relative remaining fraction after debt is varied and preferred equity is held at the nominal value.

6.1 Effect of Weather Data on Key Results

Weather data may be the single most important source of uncertainty and variability in solar power plant modeling because DNR greatly influences electricity generation and solar field sizing, and thermal losses are highly dependent on ambient temperature. In general, it is best to site CSP projects in areas with at least 6 kWh/m^2/day of DNR, and Daggett, CA is reported to be in the range of 7.5-8 kWh/m^2/day [173]. TMY3 data for three other geographic regions in the southwest United States with average DNR values in the range of 7-8 kWh/m^2/day were selected

to represent alternative hourly weather profiles, and model results were obtained for each weather dataset for the 6 hr TES case. For each dataset, the solar field area was selected to minimize the levelized cost of electricity (LCOE) in order to be consistent with the nominal model results. Table 25 presents illustrative performance, economic, and environmental results of this analysis. As a reminder, the solar multiple is a coefficient used to make the total solar field area larger than the base solar field area for the purpose of the two different solar field area selection procedures (minimize LCOE for the TES and no storage/backup cases; and minimize the difference in annual electricity generation between TES and NG for the NG cases).

Table 25 - Illustrative Results with Different Weather Input Data

Results	Daggett, CA	Edwards AFB, CA	Imperial county, CA	Flagstaff, AZ
Solar multiple	2.23	2.30	2.29	2.15
Solar field area (acres)	214	221	220	207
Capacity factor	48%	45%	49%	41%
Unsubsidized, pre-tax levelized cost of electricity ($/MWh)	$220	$241	$218	$250
Annual profit ($M)	-$66	-$71	-$66	-$69
Life cycle greenhouse gas emissions (kg CO2eq/MWh)	120	138	130	148
Operational water use (gallons/MWh)	1,497	1,502	1,493	1,493
Distance from Daggett, CA (miles)	0	100	200	350

** Results are for 6 hr TES with SM optimized for lowest LCOE; relatively optimum values are displayed in red*

The alternative weather files generate solar field areas 4% lower and up to 3% larger; capacity factors 13% lower and up to 3% higher; levelized cost of electricity (LCOE) values 1% lower and up to 14% higher; annual profit values 7% lower and up to 1% higher; and greenhouse gas (GHG) emission values up to 24% higher compared to the nominal case of Daggett, CA. The operational water use varies by less than 1%. The Flagstaff weather file results in the smallest

solar field area and capacity factor and largest LCOE and GHG emissions. The Imperial County weather file results in the largest annual capacity factor and lowest LCOE.

The cumulative probability distribution functions (CDFs) for DNR and dry bulb temperature offer some insight into these trends. Figure 78 shows that Imperial County has higher DNR values than the other three locations for the majority of the daytime hours, and Figure 79 shows that it has the highest overall ambient temperatures (less thermal losses in the solar field). These circumstances combine to explain the high capacity factor and low LCOE relative to the other three locations. However, Imperial County has a slightly lower annual profit than Daggett, CA, which has higher maximum DNR values. This may mean that the Daggett case is able to generate more electricity during higher electricity price hours. Although Flagstaff has the highest maximum DNR values, it has lower DNR values for most of the daytime hours, and Figure 79 shows that Flagstaff has the lowest ambient temperatures of the four case studies, which leads to higher thermal losses. The increase in GHG emissions with the Imperial County data compared to Daggett is likely due to hourly variations in the natural gas requirement for freeze protection.

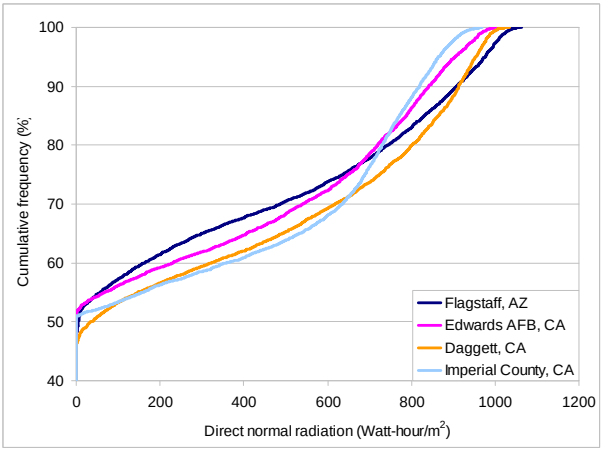

Figure 78 - Cumulative probability distribution function (CDF) of direct normal radiation (DNR)

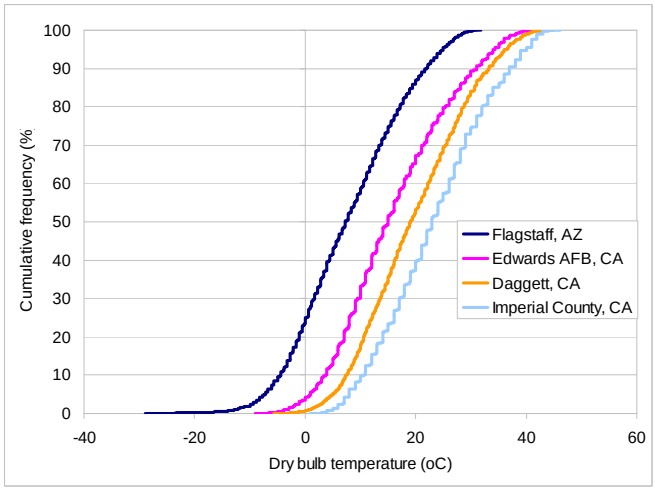

Figure 79 - Cumulative probability distribution function (CDF) of dry bulb temperature

This analysis indicates that the model results are sensitive to weather data variations, and future analyses should incorporate a range of weather input data for each hour to better represent the uncertainty associated with predicting future weather patterns and variability associated with hourly weather changes.

6.2 Sensitivity of LCOE to Performance Model Inputs

Figure 80 shows how changes in the performance input values from Table 24 affect the unsubsidized, pre-tax levelized cost of electricity calculation for the 6 hr TES case with a solar multiple of 2.23. In general, decreases in input values relative to the nominal values results in a lower LCOE, and increases show the opposite trend. The minimum HTF temperature has little effect on the LCOE, and even the maximum HTF mass flow rate factor requires a nearly 30% increase in order to achieve a 10% increase in LCOE. Although the variations in LCOE are small relative to the variations in the input parameter values, the fact that LCOE decreases

unilaterally with decreases in mass flow rate parameters indicates that mass flow rate should be varied along with the solar multiple in the LCOE optimization.

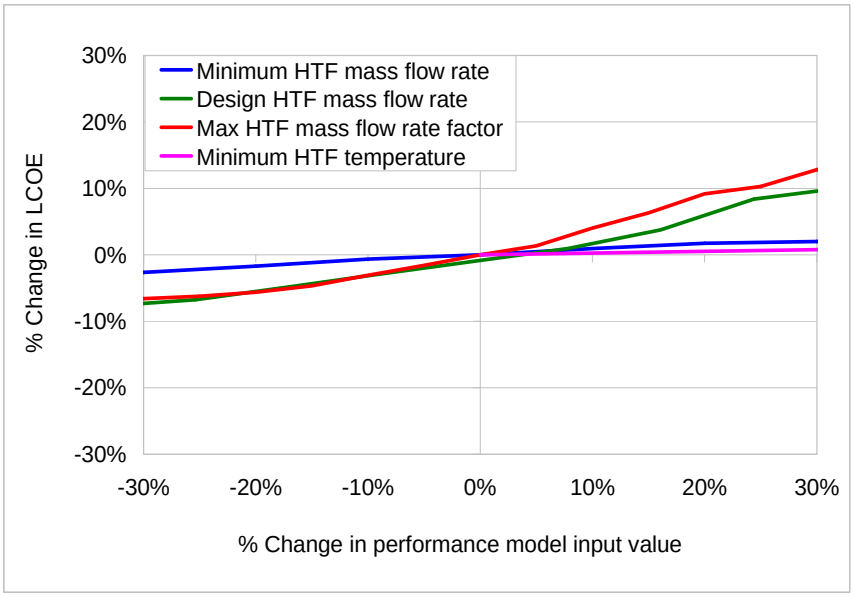

Figure 80 - Effect of changes in performance inputs on LCOE for 6hr TES, SM = 2.23

Figure 81 shows the effect of changes in performance inputs on unsubsidized, pre-tax LCOE for 6 hr NG with a solar multiple of 2.46. In this case, the maximum mass flow rate factor has less of an effect on the LCOE relative to the 6 hr TES case because the operational modes that use storage are more often limited by the max factor than the other modes. Consistent with the TES case, a smaller mass flow rate lowers the LCOE. A larger minimum HTF temperature lowers the LCOE as well. This is most likely because the cost of the natural gas has more of an influence on NG LCOE than on TES LCOE, and the quantity of natural gas is affected by the minimum HTF temperature.

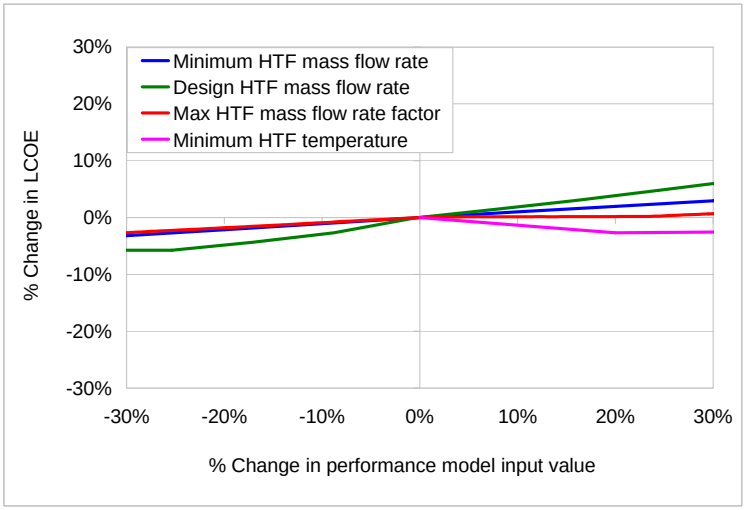

Figure 81 - Effect of changes in performance inputs on LCOE for 6 hr NG, SM = 2.46

Figure 82 shows the effect of performance input variation on unsubsidized, pre-tax LCOE for the case with no storage/backup (only enough NG backup for freeze protection), with a solar multiple of 1.43. In this case, the design HTF mass flow rate has been selected properly to minimize LCOE, but a lower minimum mass flow rate could lower the LCOE. Still, the results are not very sensitive to changes in these parameters as a nearly 20% decrease in minimum mass flow rate causes about a 5% decrease in LCOE. The maximum mass flow rate factor has very little influence on the results.

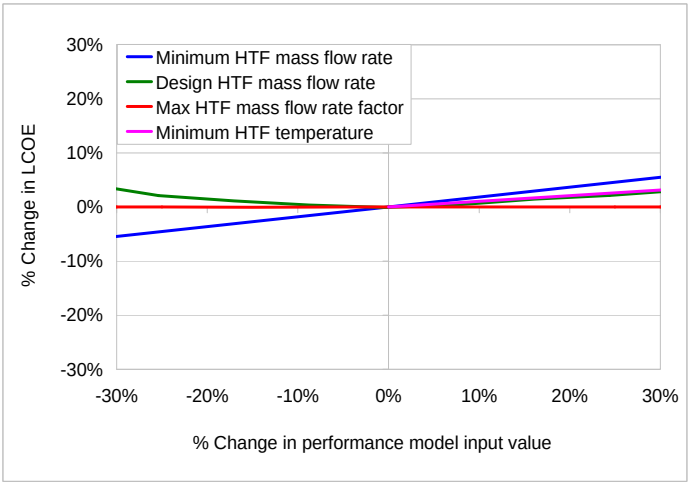

Figure 82 - Effect of changes in performance model inputs on LCOE for 0 hr TES, SM = 1.43

Since these performance parameters are not independent of each other in the model calculations, the two parameters that showed the most influence to model results in the preceding figures were varied simultaneously. Figure 83 shows the results of this analysis for the 6 hr TES case with a SM of 2.23. The combination of a design mass flow rate of 600 kg/s (50% less than the original design) and a maximum mass flow rate factor of 1.6 (20% lower than the original) results in a LCOE of $194/MWh, 12% lower than the nominal result presented in Chapter 4.

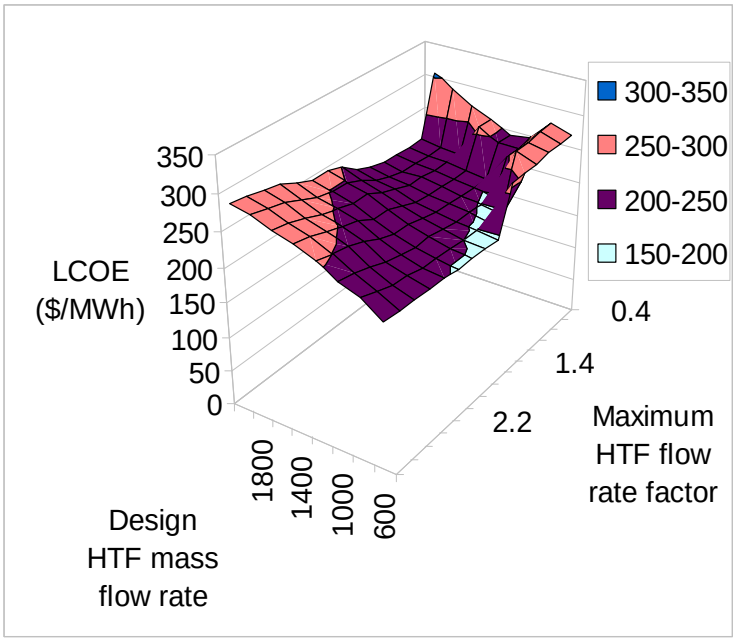

Figure 83 - Effect on unsubsidized, pre-tax LCOE of varying two HTF mass flow rate parameters at the same time for 6 hr TES, SM = 2.23

Figure 84 shows the same analysis with the no storage/backup case. In this case, the original parameter values were nearly on target, as the original maximum mass flow rate factor of 2, along with a design mass flow rate of 1,200 kg/s (0.5% less than the nominal value) results in a LCOE of $193.00/MWh, less than 1% lower than the nominal result ($193.17).

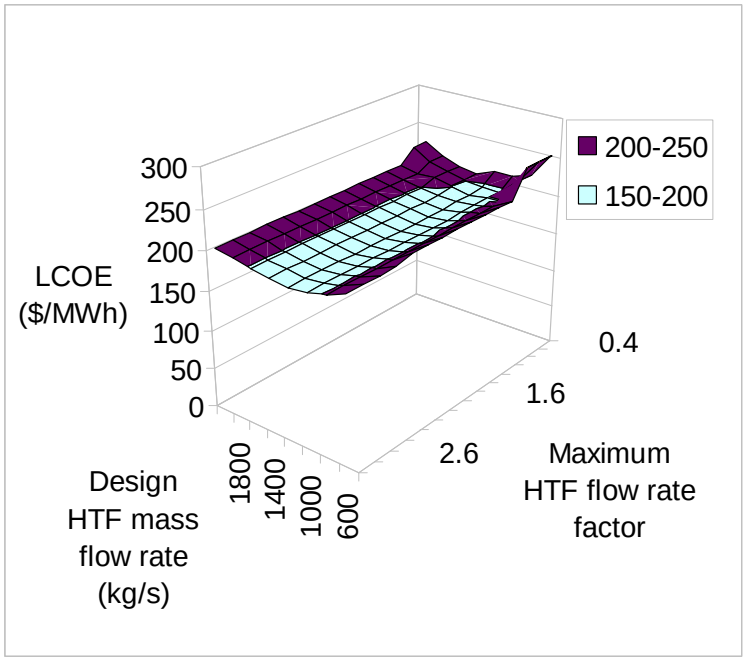

Figure 84 - Effect on unsubsidized, pre-tax LCOE of varying two HTF mass flow rate parameters at the same time for no storage/backup, SM = 1.43

Figure 85 shows the results of this analysis for the 6 hr NG case. In this case, the combination of a design mass flow rate of 800 kg/s (34% less than the original design) and a maximum mass flow rate factor of 1.8 (10% lower than the original) results in a LCOE of $202/MWh, 6% lower than the nominal result.

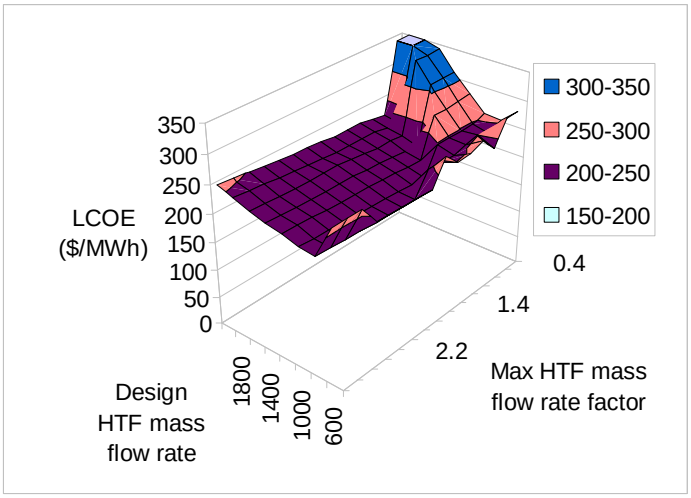

Figure 85 - Effect on unsubsidized, pre-tax LCOE of varying two HTF mass flow rate parameters at the same time for 6 hr NG, SM = 2.46

In the nominal set of results, the 6 hr NG LCOE was $4/MWh (2%) less than the respective TES LCOE. These results show the NG value to be $8/MWh (4%) higher than the TES value. However, in the original case, the NG solar field area was selected to minimize the difference in annual electricity generation between the two plants. If the TES parameters change, then the NG area needs to be re-sized to match the annual electricity generation again. Figure 86 shows the results of this process.

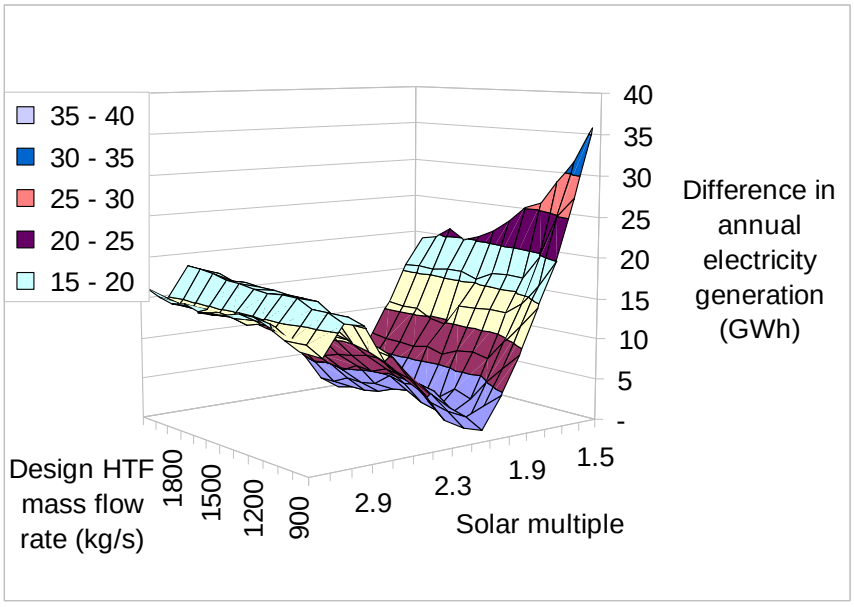

Figure 86 – Selecting a new solar multiple for 6 hr NG based on performance model sensitivity results *(max HTF flow rate factor = 1.6)*

The combination of a solar multiple of 2 instead of 2.46, and a design mass flow rate of 2,000 kg/s results in the smallest difference in electricity generation between the 6 hr NG case and the 6 hr TES case with a 1.6 max HTF flow rate factor and 600 kg/s design mass flow rate. This combination for NG results in a LCOE of $210/MWh, 3% lower than the 6 hr NG nominal result but 8% higher than the new 6 hr TES result.

The results of the sensitivity analysis on performance model input values indicates that it is critical to vary the HTF design mass flow rate parameters along with the solar multiple in order to achieve the lowest LCOE for each storage capacity configuration. Moreover, this process not only changes the results of the individual plant configuration, but also changes the relative NG results. In other words, varying the mass flow rate parameters simultaneously resulted in a lower LCOE for 6 hr TES than for 6 hr NG where previously (in Chapter 4) NG had the lower value. The maximum variation in LCOE from the performance model sensitivity analysis was 12% with 6 hr TES.

6.3 Sensitivity of LCOE to Economic Model Inputs

Figure 87 shows the effect of variations in economic input values on unsubsidized, pre-tax LCOE for the nominal 6 hr TES case. Not surprisingly, the results are most sensitive to varying all of the costs inputs at the same time. A 20% decrease/increase in all costs simultaneously results in a 30% decrease/increase in LCOE. Out of the individual variations, the LCOE result is most sensitive to book value (i.e. plant lifetime). Decreasing the book value has a larger effect on the LCOE than increasing it; a 30% decrease in book value results in a 10% increase in LCOE, but a 30% increase in book value results in only a 5% decrease in LCOE. Based on the experience with the Solar Electric Generating Stations (SEGS), it is unlikely that a book value of less than the nominal value of 30 years would reflect the true project lifetime in any case. It is more likely that a larger book life may be more appropriate.

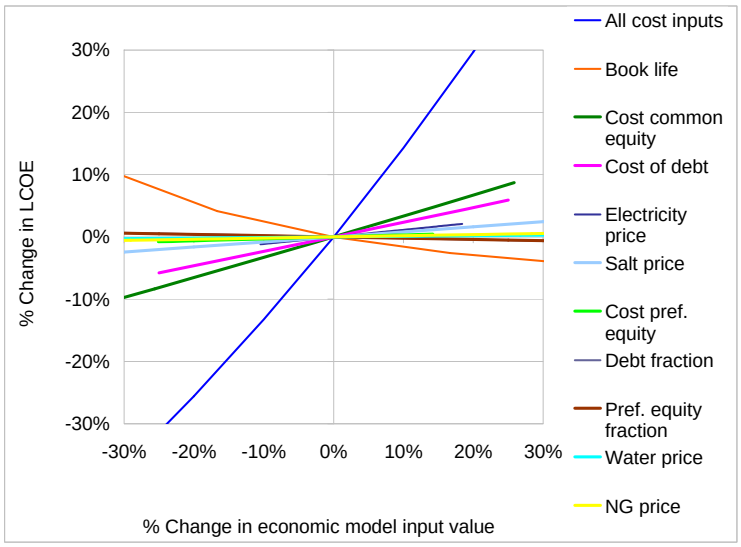

Figure 87 - Effect of changes in economic model inputs on LCOE for 6 hr TES, SM = 2.23

The next largest influence on unsubsidized, pre-tax LCOE is the cost of common equity because in the nominal case, the equity portion was 60%. This is followed closely by the cost of debt. The cost of preferred equity does not influence the results much at all because it is such a small portion of the financing. In terms of utility costs, the electricity cost has the largest influence on LCOE and then water price and natural gas price, but the salt price has more influence than either water or natural gas. Except for the case of varying all costs simultaneously, none of these input values change the LCOE more than 10% on their own when varied up to 30%.

The no storage/backup results look almost identical to Figure 87, with the following exceptions: 1) the water price has slightly more influence on results than the natural gas price; and 2) each variable has slightly less of an effect on LCOE compared to the same variable in the 6 hr TES case, except for the electricity price, which has about twice the effect on the no storage/backup case as on the 6 hr TES case. Similarly, the 6 hr NG case showed nearly identical results as well, with the following exceptions: 1) the natural gas price takes the place of the salt price as the 6th

most important economic factor since it has about five times the effect on LCOE for 6 hr NG as for 6 hr TES; and 2) the electricity price is slightly more influential for NG than for TES.

6.4 Sensitivity of LCA results to Changes in Inputs

Chapter 5 showed that the majority of life cycle greenhouse gas emissions for all plant configurations modeled in this analysis can be attributed to the operation stage, and specifically, to electricity and natural gas use. In addition, many of the life cycle emissions from the manufacture/construction stage resulted from the economic input-output (EIO) LCA method. Since the electricity and natural gas use are calculated by the performance model, and the EIO-LCA values depend on economic inputs, the effect of the same parameters discussed in the previous sections of this chapter were analyzed on life cycle greenhouse gas emissions. Figure 88 displays the results of this analysis, in which the maximum HTF mass flow rate factor has an interesting effect on life cycle GHG emissions. When the factor is decreased by 30%, it causes less than a 5% decrease in GHG emissions. However, when it increased beyond about 8%, the effect becomes more significant, and less than a 13% increase in the factor causes a 30% increase in LCOE. This effect is due to a sharp increase in natural gas use for storage salt freeze protection beyond a certain threshold. When the max factor is allowed to keep increasing, it allows the storage system modes to calculate a larger mass flow rate for the storage salt. Since the calculation of the heat required for freeze protection depends directly on the salt mass flow rate, if this increase happens during periods of low ambient temperature, the natural gas input for salt freeze protection will increase. For the same reason, the design mass flow rate has a similar effect on life cycle GHG emissions.

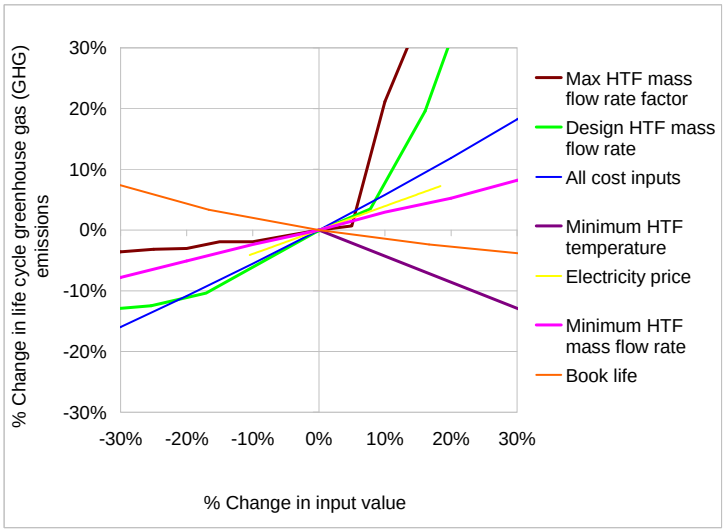

Figure 88 - Effect of changes in key input values on life cycle greenhouse gas emissions for 6hr TES, SM = 2.23

Varying all of the cost inputs at the same time has the next largest effect on GHG emissions because of the large effect of EIO-LCA values on manufacture/construct emissions, and because a large portion of the operational stage GHG emissions comes from the cost of electricity input to the EIO-LCA. The minimum HTF temperature is important to GHG emissions because it dictates the amount of natural gas that is used. If the minimum is increased, it will require limitations on the power cycle to maintain a higher HTF outlet temperature from the heat exchangers, but if a higher temperature is maintained overall, there will be less of a need for natural gas freeze protection at night. Finally, the book like has an effect on the GHG results because it determines how much electricity will be generated over the life cycle of the plant being modeled.

Figure 89 shows the effects on life cycle GHG emissions for 6 hr NG. Overall, variations in all of the inputs have less of an effect on the life cycle GHG emissions of the NG backup configuration because the emissions are largely dictated by the natural gas combustion for the

HTF heater, which is not affected much by these variables. The maximum HTF mass flow rate factor affects the NG backup GHG results much less compared to TES because the NG configuration does not use salt freeze protection, and the operational modes that are limited by the maximum HTF mass flow factor do not use freeze protection for the HTF. Therefore, the factor does not affect natural gas combustion to the same degree with NG as it does with TES. The cost inputs have less of an effect on GHG emissions because in contrast to the TES configuration, the dominant contributor to NG backup GHG emissions is natural gas combustion, not electricity, and the natural gas emissions factor does not depend on economic values.

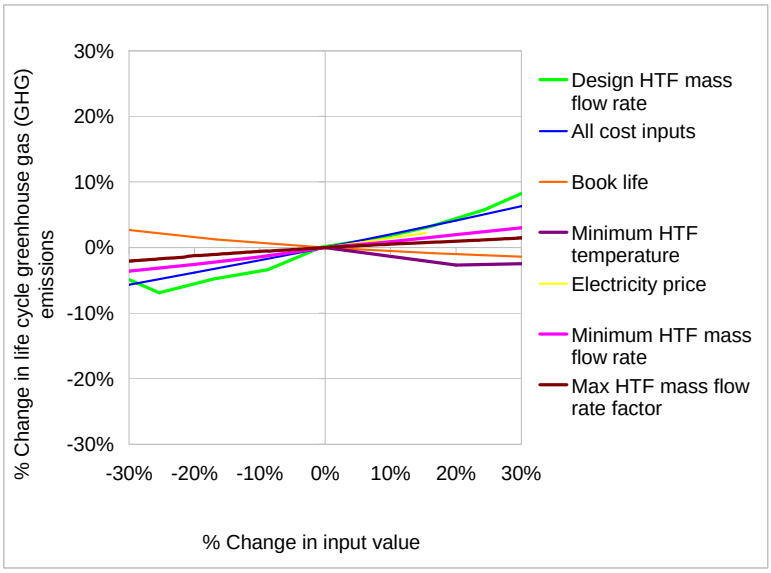

Figure 89 - Effect of changes in key input values on life cycle greenhouse gas emissions for 6 hr NG, SM = 2.46

Figure 90 shows the effect of changes in input values on operational water use for the 6 hr TES configuration. Overall, the changes have little effect on operational water use, with a maximum effect of increasing by about 5% with a 20% decrease in the maximum HTF mass flow rate factor. The minimum HTF mass flow rate has almost no effect on operational water use because it is mainly only a concern during shutdown modes, which do not use water.

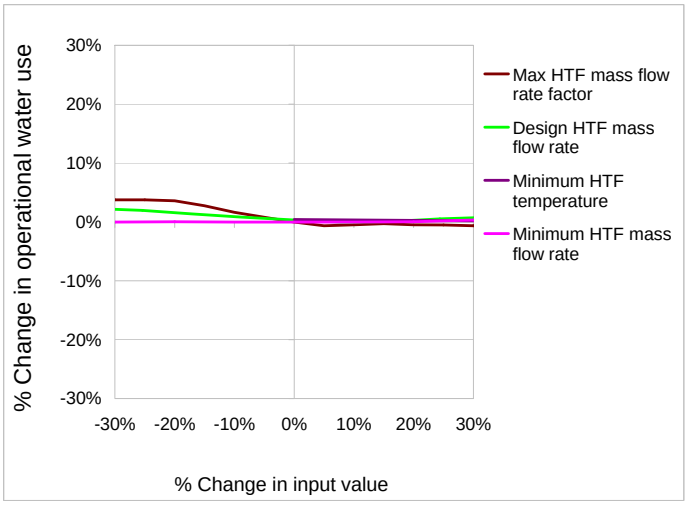

Figure 90 - Effect of changes in key input values on operational water use for 6 hr TES, SM = 2.23

6.5 Effect of Different Objective Functions on Solar Field Area Selection

As shown in Chapters 3 and 4, the solar field area has a significant effect on plant performance and cost. For this reason, it has been important in this analysis to select the solar field area that minimizes cost for each storage configuration. However, specifying a different objective function for this process may change the solar field area and, hence, all other model results. Table 26 shows how the solar multiple and solar field area change when a different objective function is specified for the 6 hr TES case across a solar multiple range of 0.8 to 4.5. The highest solar multiple in the range gives the highest capacity factor. The nominal objective function (unsubsidized, pre-tax LCOE) requires the same solar multiple as the same LCOE with dry cooling and both post-tax LCOEs. The subsidized LCOEs (with ITC and accelerated depreciation) require a slightly larger solar field area to reach the minimum and even slightly larger for the dry cooling subsidized LCOE. All of the profit values that use hourly electricity pricing are maximized with the smallest solar multiple, but the values that use the power purchase agreement require solar multiples of 2.08, 2.33, and 2.71 for the unsubsidized pre-tax,

post-tax, and subsidized post-tax annual profits, respectively. These results highlight how important it is to select the proper solar multiple (and design HTF mass flow rate) for each unique objective function.

Table 26 - Solar Field Area Selection Pursuant to Different Objective Functions

Objective function	Solar multiple/ solar field area (acres) that optimizes the objective function:						
	0.8/ 77	2.08/ 200	2.23/ 214	2.33/ 224	2.35/ 226	2.71/ 260	4.5/ 432
Capacity factor							X
Unsubsidized pre-tax LCOE (nominal)			X				
Unsubsidized pre-tax LCOE with dry cooling			X				
Unsubsidized post-tax LCOE			X				
Unsubsidized post-tax LCOE with dry cooling			X				
Subsidized post-tax LCOE				X			
Subsidized post-tax LCOE with dry cooling					X		
Unsubsidized pre-tax annual profit	X						
Unsubsidized pre-tax annual profit with dry cooling	X						
Unsubsidized post-tax annual profit	X						
Unsubsidized post-tax annual profit with dry cooling	X						
Subsidized post-tax annual profit	X						
Subsidized post-tax annual profit with dry cooling	X						
Unsubsidized pre-tax annual profit with PPA		X					
Unsubsidized pre-tax annual profit with PPA and dry cooling		X					
Unsubsidized post-tax annual profit with PPA				X			
Unsubsidized post-tax annual profit with PPA and dry cooling				X			
Subsidized post-tax annual profit with PPA						X	
Subsidized post-tax annual profit with PPA and dry cooling						X	

6.6 Insights from Sensitivity Analysis

The preceding investigations show that decreasing the value of the following parameters will decrease the LCOE for the nominal 6 hr TES configuration: design HTF mass flow rate, maximum HTF mass flow rate, minimum HTF mass flow rate, all cost inputs, loan rate, and cost

of equity. Increasing the following parameter values will decrease LCOE as well: book life, debt fraction and preferred equity fraction. Similar trends were observed in the comparable NG configuration with the addition that increasing the minimum HTF temperature will decrease LCOE. The effects of performance parameters can be improved through further optimization procedures, and it is unlikely that all costs will vary simultaneously. However, approximate lower and upper bounds on the LCOE of the 6 hr TES configuration can be estimated by varying the utility costs within the bounds presented in Table 24 and the remaining parameters +/-30%. When this is done in conjunction with the new HTF mass flow rate parameters presented in this chapter, the approximate LCOE range for 6 hr TES becomes $144-243/MWh, or 35% lower to 10% higher than the nominal result from the previous chapters. In the future, a co-optimization of all HTF mass flow rate parameters and solar multiple will be performed, and a range of weather input data will be used for each hourly input in order to obtain more accurate results.

Chapter 7: Environmental-Economic Tradeoffs

The overarching research question for this study is, "should renewable energy policies be doing more to encourage thermal energy storage (TES) for concentrated solar power (CSP)?" This is a broad question that entails examining many factors that could affect the answer. The previous chapters have identified the key factors that affect this decision as mainly economic (cost and profit) and environmental (energy demand, greenhouse gas (GHG) emissions, water use, and land use) and have quantified the effect of different storage configurations on these factors. This chapter combines the data from these separate analyses into a decision-making framework in order to form an answer to the overarching research question. In this study, it is assumed that the decision-maker is a policy-maker who is trying to decide if future renewable energy policies in the region should include provisions for encouraging in new CSP plants. First, the decision will be examined in the context of basic tradeoffs between one factor and another. Then, the combined effect of key factors will be investigated through a multi-attribute utility analysis. Lastly, the decision will be examined in the context of implementing a price on greenhouse gas emissions. The next chapter will summarize these findings in the context of the sensitivity analysis that was presented in Chapter 6, and will make recommendations to policy-makers.

7.1 Simple Comparisons

The most obvious tradeoff in any decision that involves power generation in a carbon-constrained world is economic factors versus GHG emissions. Figure 91 displays the ratio of life cycle greenhouse gas emissions to levelized cost of electricity in order to compare the GHG emissions per dollar spent on each technology. The plant with no storage/backup has a ratio of

0.6 kg CO_{2eq}/$, and this ratio increases by 9% with 1 hr TES. Adding two more hours of TES decreases the ratio by 1% compared to the no storage/backup case, and 12 hrs of TES produces 26% less GHG emissions per dollar spent on the technology than no storage/backup. One hour of NG backup capacity increases the ratio by 35% compared to no storage/backup, and 12 hr NG has a ratio 150% higher than the no storage/backup configuration. Each NG case generates 23-240% more GHG emissions per dollar spent on the technology than the respective TES case, and the difference increases with increasing storage/backup capacity.

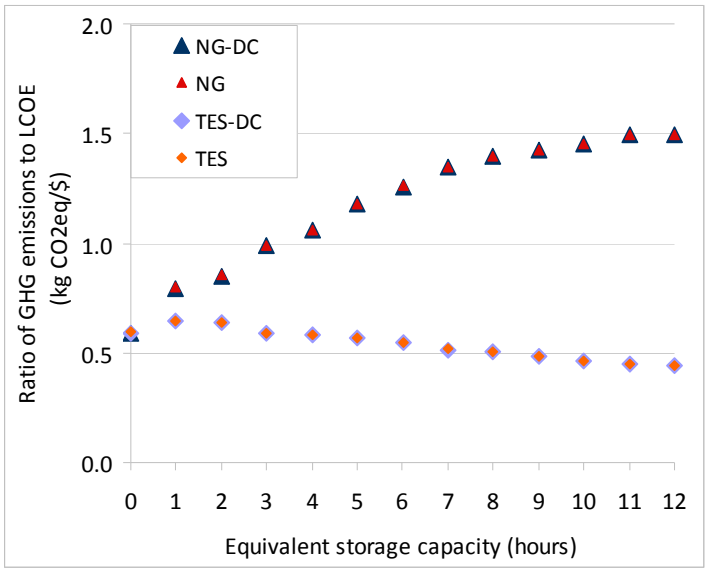

Figure 91 - A comparison of GHG emissions and levelized cost of electricity

To put the results in Figure 91 in context, Table 27 compares the ratio of GHG emissions to LCOE for five fossil fuel electricity generation technologies and five parabolic trough configurations. The GHG emissions for the fossil fuel technologies were obtained from Jaramillo et al. [172], and the LCOE values for the fossil fuel electricity generation technologies were obtained from Lazard [113]. There is a large amount of uncertainty associated with

comparing LCA and LCOE results from different studies due to the many different assumptions included in the calculations. The results for the parabolic trough configurations presented in the table were derived from the engineering-economic model and LCA described in Chapters 3-5 with the same financial assumptions as outlined in Lazard to make the economic results more comparable. However, there are still large areas of uncertainty in the comparison. For example, Lazard uses different power plant sizes for different electricity generation technologies and does not report the source of capital and O&M cost figures. Jaramillo et al. use some different databases for the LCA and different methods for some portions of the analysis than those used in this study. Therefore, the comparison in Table 27 is still a rough one overall.

Table 27 - Comparison of GHG emissions to LCOE for PT and Fossil Fuel Electricity Technologies[13]

Electricity generation technology	Life cycle GHG emissions ($kgCO_{2eq}$/MWh)	LCOE ($2008/MWh)	ratio ($kgCO_{2eq}$/$)
Pulverized coal (PC)	1,000	74	31
Integrated gasification combined cycle (IGCC)	900	104	19
Natural gas combined cycle (NGCC)	400	73	12
PC with carbon capture and sequestration (CCS)	180	135	3
IGCC with CCS	140	134	2
NGCC with CCS	90	100	2
no storage/backup	*124*	*257*	*0.5*
6 hr TES	*133*	*305*	*0.4*
12 hr TES	*122*	*342*	*0.4*
6 hr NG	*284*	*288*	*1.0*
12 hr NG	*344*	*296*	*1.2*

Nevertheless, Table 27 shows that all of the parabolic trough configurations generate less GHG emissions per dollar spent on the technology than any of the fossil fuel-generated technologies. However, the 6 hr and 12 hr NG cases have similar ratios to IGCC-CCS and NGCC-CCS. If a

[13] Parabolic trough values presented in italics were calculated using the engineering-economic model and life cycle assessment adapted to reflect the economic assumptions in Lazard [113] Lazard, "Levelized cost of energy analysis - version 2.0 ", ed, June 2008.. The GHG emissions from fossil fuel electricity generation technologies were obtained from Jaramillo et al., and the LCOE values for fossil fuel technologies are from Lazard.

policy-maker is primarily interested in the tradeoff of GHG emissions and cost of electricity, it may make sense to select TES over NG backup with a trough plant, but it may not be worthwhile to select TES over no storage/backup based on this tradeoff alone.

Another tradeoff to consider in this context is the amount of GHG emissions generated per dollar earned. This can be accomplished by dividing the total life cycle GHG emissions (per MWh) by the average profit per MWh. Figure 92 presents this ratio for each plant configuration using the subsidized post-tax expected annual profit with a $200/MWh power purchase agreement. In this scenario, the plant with no storage/backup generates the least amount of GHG emissions per dollar profit, and all of the NG configurations generate more GHG emissions per dollar than the respective TES configurations. The configuration with seven hours of TES has the lowest ratio of the plants that have a backup system. However, the ratio for 6 hr TES is only 3% greater than the ratio for 7 hr TES, and the ratio for 8 hr TES is only 1% greater than the ratio for 7 hr TES. Moreover, the ratio for 7 hr TES is only 3% lower than 1 hr TES. Given these marginal changes in the ratio and the uncertainty in model calculations described in Chapter 6, 7 hr TES should not be encouraged over 1 hr TES based on this tradeoff alone.

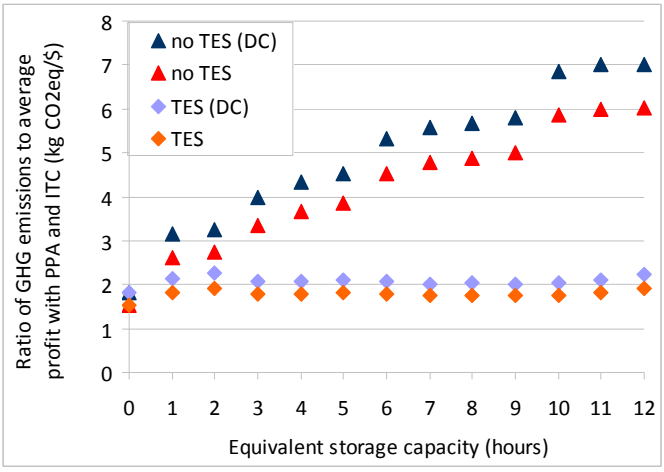

Figure 92 - Comparison of GHG emissions with profit

Figure 93 shows the ratio of on-site operational water use (steam cycle/mirror washing) to average profit (as defined above) across the range of equivalent storage capacities. Naturally, the plants with wet cooling use much more water per dollar than the plants with dry cooling. The plants with NG backup use slightly more water per dollar profit than the TES cases, and this pattern repeats for the dry-cooled cases; although it is difficult to see with the large difference between wet and dry cooling displayed on the same graph. In each cooling case, the plant with no storage/backup uses the least amount of water per dollar, and the ratio increases with storage capacity/NG backup.

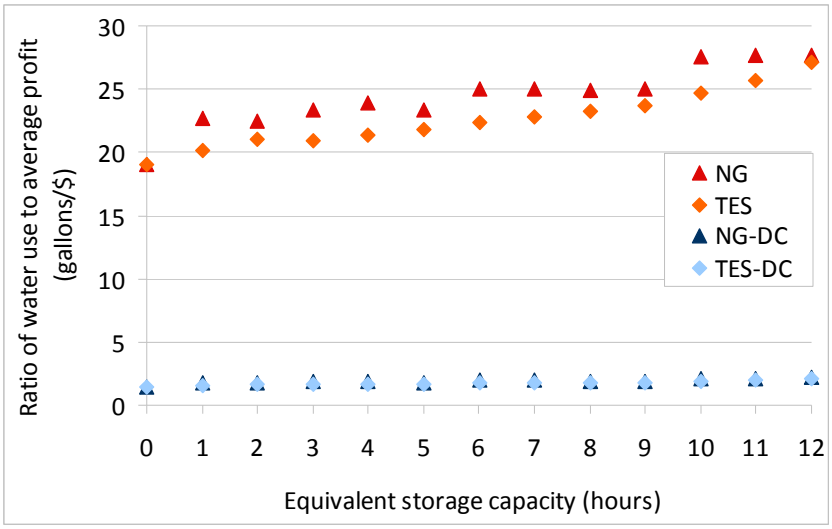

Figure 93 - Comparison of steam cycle water use and average profit

CSP plants are usually located in desert areas, which may contain endangered species populations. Therefore, it is important to minimize land use as much as possible. Figure 94 shows the ratio of total land use to average profit for each equivalent storage capacity. The plant with no storage/backup uses the least amount of land per dollar profit, and the ratio increases

with increasing storage capacity. The NG backup plants use slightly more land per dollar than the TES plants, and the dry-cooled designs use slightly more than the respective wet-cooled designs. However, for each storage capacity, the relative land use per dollar for each of the four options is similar.

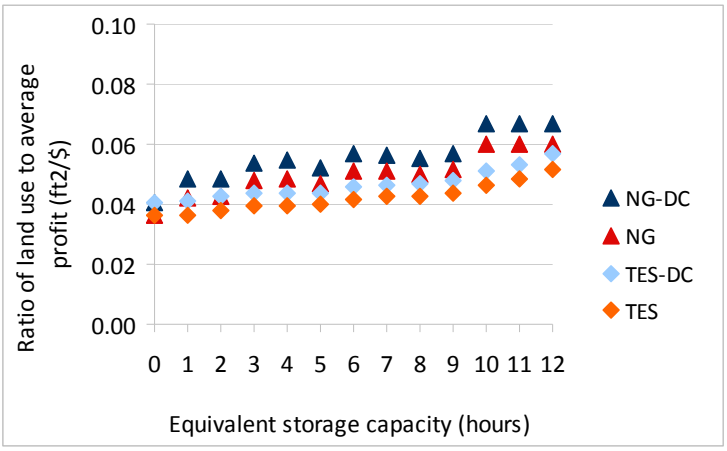

Figure 94 - Comparison of total life cycle land use to average profit

CSP does require a lot of land and as Figure 94 and Figure 77 in Chapter 5 show, in most cases more backup capacity equates to more land use. However, since the current motivation behind solar power development is GHG emissions reductions, it is useful to look at the tradeoff between GHG emissions and land use. Figure 95 shows that the plant with no storage/backup emits about 40 $kgCO_{2eq}$ per ft^2 of land. The plant with 2 hours of TES emits 20% more GHGs per unit land than the no storage/backup case, and the ratio decreases to a minimum of 37 $kgCO_{2eq}/ft^2$ with 12 hr TES (11% less than no storage/backup). The NG cases generate 25-170% more GHG emissions per square foot compared to the respective TES cases. The NG plants have higher ratios mostly because of the high GHG emissions associated with the natural gas backup system, but also because the solar field area for the NG plants with higher backup capacities is slightly larger than for the TES cases.

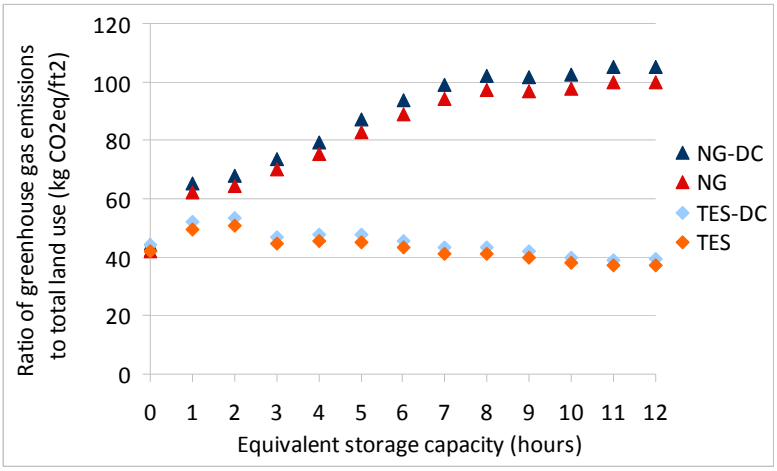

Figure 95 - Comparison of GHG emissions and total land use

These simple comparisons inform the policy-maker that encouraging storage in CSP plants is a good idea if GHG emissions and cost of electricity are the main priorities since a 12 hr TES system can reduce the GHG emissions per dollar spent by 26% compared to no storage. However, if profit or land are more important than cost, then TES should not be encouraged because the ratio of GHG emissions to these values is either higher with TES than with no TES/backup or the difference is so minimal to be rendered inconsequential given model uncertainties. If land use or water use are priorities compared with profit, no storage/backup is preferable. In all cases, TES is preferable to NG, and wet-cooling is preferable to dry cooling (except for where operational water use is considered). However, these comparisons do not provide information regarding the interaction of these tradeoffs or how to choose among the options when there is more than one priority to be considered.

7.2 Multi-Criteria Decision Analysis

As explained in section 2.6, multi-criteria decision analysis (MCDA) is a tool that allows decision-makers to incorporate a diverse set of criteria in the evaluation of a set of alternative

choices. In this study, the main evaluation criteria include annual electricity generation, levelized cost of electricity, life cycle GHG emissions, steam cycle/mirror washing water use, and total land use; and the alternative choices include all of the plant configurations modeled in this study. The MCDA conducted here involves calculating a total utility score (U) for each alternative choice using Equation 215, in which E = annual electricity generation; C = levelized cost of electricity; G = life cycle GHG emissions; W = steam cycle/mirror washing water use; L = life cycle land use; and the coefficient a-e are weights (between 0 and 1) representing the preference for each attribute. Equation 216 calculates the individual utility score for each attribute, and the preference weights can be used to examine the decision under different preferences. For example, Equation 216 calculates the utility (U_x) of the LCOE for the 6 hr TES case as ($220– $193) ÷ ($256 – $193) since the optimal value for this attribute in the range of calculated nominal values is the lowest LCOE, which is the LCOE of 0 hr TES. For all attributes other than annual electricity generation, the optimal value is the lowest value in the range of calculated values.

$$U = aU_E + bU_C + cU_G + dU_W + eU_L \quad (215)$$

$$U_x = (V_{nominal} - V_{optimal}) \div (V_{high} - V_{low}); \text{ where V = value} \quad (216)$$

Figure 96 displays the results of the MCDA when equal relative preferences (a-e each equal 0.2) are applies to the utility function. If these preferences reflect the true preferences of the policy-maker and constituents, and if the utility function is indeed reflected by Equation 215 and not more complex, then the storage configurations with dry cooling nearly dominate all other alternatives with the highest utility scores. However, the relative difference between each TES-DC utility score and the one before/after it is very small (1-3%). Moreover, the difference

between each TES-DC score and the score of the plant with no storage/backup is also small (1-5%). Given the uncertainty associated with the model, it is probably more accurate to say that no storage/backup with dry cooling and all TES capacities with dry cooling have equal preference when equal weights are applied to the utility function. Dry cooling is clearly preferred over wet cooling, and if backup is desired on its own merits, TES-DC is preferred over all other backup systems. The NG cases with wet cooling have the lowest utility scores overall.

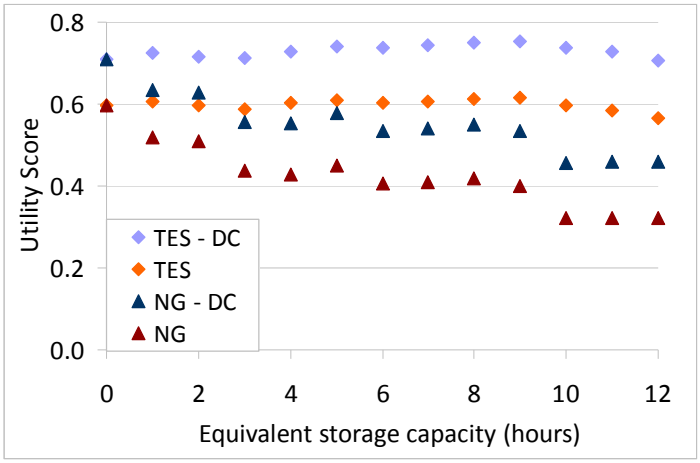

Figure 96 - MCDA results with equal preferences

In this type of analysis, the specific preferences of the decision-maker are highly influential on the results. While quantifying the specific preferences of renewable energy policy-makers in the southwestern United States is beyond the scope of this analysis, a few scenarios can be examined to give a sense of the range of variation in MCDA results based on differing preference weights. Figure 97 displays the results when a set of "environmental" weights is used. In this scenario, 90% of the preference is represented equally by the environmental attributes (GHG emissions, water and land use), and the other 10% is split between annual electricity generation and LCOE. This scenario is designed to represent a decision-maker who is most concerned with the

environmental impact of the decision, but also cares about cost and performance to a lesser degree. Not surprisingly, TES-DC is still at the top since the "equal preference" scenario included 60% combined preference for environmental attributes, but it still shows a relatively flat curve. No storage/backup is more or less equivalent to all TES-DC capacities, and the higher capacities are increasingly less desirable. NG scores are even lower relative to the TES cases than in the equal-weight scenario. NG-DC is still the least preferred option.

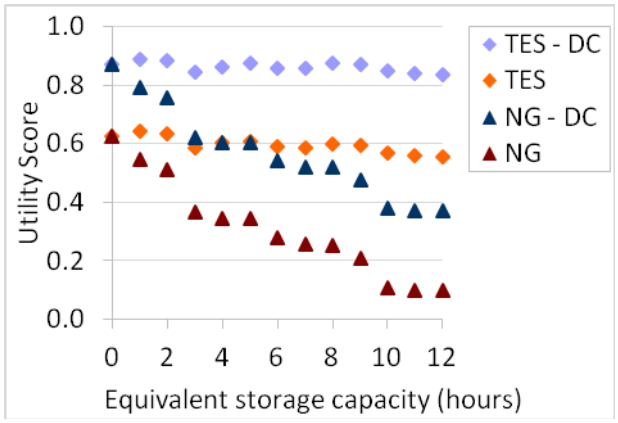

Figure 97 - MCDA results with "environmental" preferences

Figure 98 shows how the results change when "economic" preferences are applied. In this scenario, the weights are distributed as follows: a = 0.1; b = 0.8; c = 0.04; d = 0.02; e = 0.04. Eighty percent of the preference is allocated to the LCOE, and 10% to annual electricity generation. The remaining 10% is allocated to the environmental attributes with GHG emissions and land receiving slightly more of the preference than water use since the former may prove to be important financially in the future if carbon legislation is passed, and the latter affects the cost of land purchased. With water prices so low, very little economic preference is allocated to the water use attribute. In this scenario, no storage/backup has the highest utility score by far, and

utility decreases with increasing storage/backup capacity. The plant with 1 hr TES and wet cooling is preferable to 1 hr NG. At storage capacities of 2-4 hours, TES and NG are relatively equivalent, and beyond 4 hours, NG is clearly preferable to TES. A similar pattern is observed when comparing the dry-cooled options, and in certain cases NG with dry cooling is slightly preferable to TES with wet cooling.

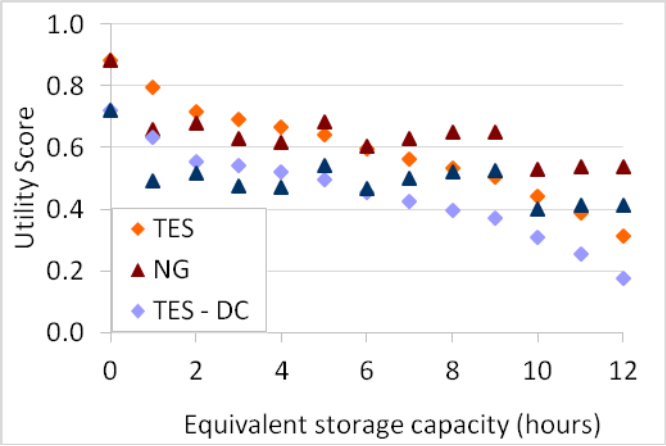

Figure 98 - MCDA results with "economic" preferences

Lastly, Figure 99 displays the MCDA results when plant performance is the priority. In this scenario, annual electricity generation receives 80% of the preference weight; 10% is allocated to LCOE; and the remaining 10% is divided among the environmental attributes in the same way as in the "economic" preference scenario. No storage/backup has the lowest utility score in this scenario, and utility increases with increasing storage capacity/backup. There is a clear hierarchy with TES with wet cooling as the most preferable option for each storage case and NG with dry cooling as the least preferable. However, the TES utility values are only 3-11% higher than the NG backup utility values for each respective storage/backup capacity. The utility of each wet-cooled case is 8-26% higher than each dry-cooled counterpart.

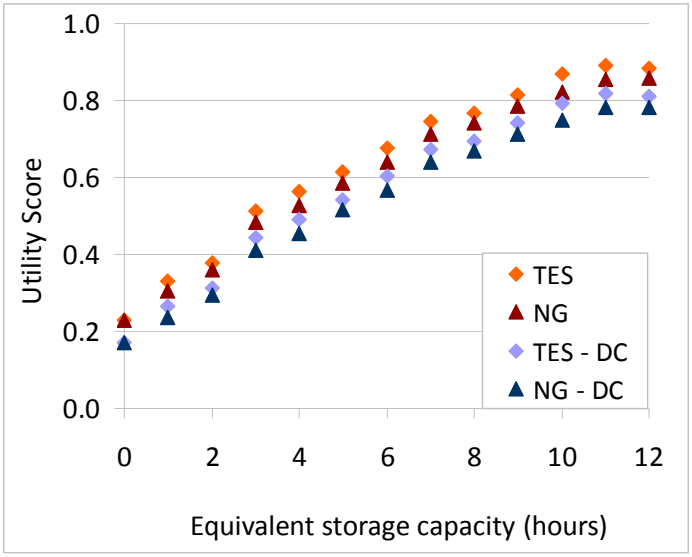

Figure 99 - MCDA results with "performance" preferences

In general, the results of the MCDA indicate that unless the decision-maker cares primarily about the performance of the power plant (how many MWh it generates annually) no storage/backup should be selected over any of the storage/backup configurations. If the decision-maker acknowledges that some backup is necessary, thermal energy storage should be encourage over natural gas backup and dry cooling should be encouraged over wet cooling unless the decision-maker has very strong economic preferences. In the case of strong economic preferences, if some type of backup system is needed, TES should be encourage at very small capacities, and NG backup should be encouraged at larger capacities.

Chapter 6 examined the sensitivity of the nominal results used in the MCDA to changes in input parameters, and concluded that if the performance model includes heat transfer fluid (HTF) mass flow rate parameters in the LCOE optimization process, a lower LCOE will be obtained for the 0 hr TES/NG, 6 hr TES, and 6 hr NG cases. In addition, this improved optimization process may

lower the LCOE of 6 hr TES relative to 0 hr TES/NG, and will cause the LCOE of 6 hr TES to be lower than 6 hr NG even when the solar field area of 6 hr NG decreases. These sensitivity analysis results suggest that re-running all of the nominal results with improved LCOE optimization could change the conclusion of the MCDA to advocate for TES over no TES.

7.3 Carbon Price

Many economists agree that an effective way to encourage widespread GHG reductions is to put a price on carbon either through a tax or a tradable permitting system. This action would in effect "fix" the market failure associated with the fact that climate change consequences (a set of externalities) are not currently valued in the cost of GHG-emitting processes. The purpose of this study is neither to argue the benefits or drawbacks of such a system, nor to propose a specific "carbon price". However, given that such a system may be implemented in the U.S. in the future, this report includes a calculation of the carbon price that would be necessary for the nominal CSP power plant configurations analyzed here to compete with a new coal-fired power plant with no CO_2 controls or capture system. Table 28 presents the parameters used in Equation 217 to estimate the carbon price. The LCOE value and operational CO_2 emissions for the coal-fired power plant were calculated using the Integrated Environmental Control Model (IECM) v6.2.4 [174], developed by researchers at Carnegie Mellon University. Appendix F includes details about the specific input values used in the IECM to calculate the LCOE of a new coal-fired power plant that could be comparable in size and financing to a new PT plant. The life cycle GHG emissions value for the coal-fired power plant were estimated by combining the upstream emissions from Jaramillo et al [172] and the operational emissions from the IECM

calculation. The nominal values for the 6 hr TES plant with a SM of 2.23 are displayed in red in Table 28.

Table 28 - Carbon Price Parameters

Parameter	Description	Unit	Nominal Value
$LCOE_c$	Coal-fired LCOE	$/MWh	$69 [174]
$LCOE_{PT}$	LCOE of parabolic trough plant	$/MWh	$220
GHG_c	Life-cycle greenhouse gas (GHG) emissions from a coal-fired power plant	tonnes CO_{2eq}/ MWh	0.97 [172],[174]
GHG_{PT}	Life-cycle GHG emissions from parabolic trough power plant	tonnes CO_{2eq} / MWh	0.12
p_{CO2}	**Carbon price required for PT plant to be competitive with coal plant**	**$/tonne CO_{2eq}**	**$180**

$$p_{CO2} = (LCOE_{PT} - LCOE_c) \div (GHG_c - GHG_{PT}) \quad (217)$$

Figure 100 displays the carbon price required for each of the nominal cases analyzed in this study to be competitive with a new coal-fired power plant. The prices range from a minimum of nearly $150/tonne CO_{2eq} with no storage/backup to a maximum of about $200/tonne CO_{2eq} with 12 hr TES and $240/tonne CO_{2eq} with 12 hr NG backup. The cases with natural gas backup require a higher carbon price than the respective cases with TES because the increase in GHG emissions associated with the additional natural gas needed to match the electricity generation from the respective TES case outweighs any increase in LCOE compared to NG backup. An even higher carbon price would be required for each configuration if the parabolic trough plants were being compared to a modern natural gas combined cycle (NGCC) power plant providing baseload electricity. Since the CO_2 emission rate from such a plant is about half that of a coal-fired plant [174], the resulting carbon prices would be roughly twice the values shown here for a comparable LCOE using NGCC.

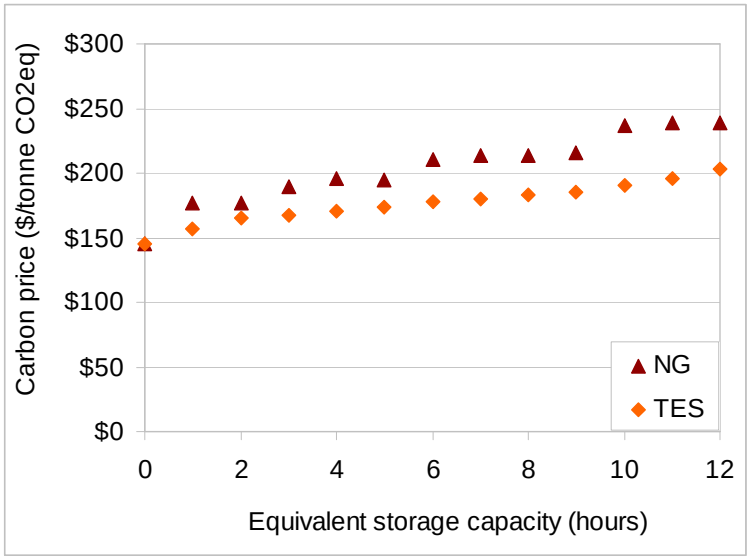

Figure 100 - Required carbon price for PT plant to be competitive with a new coal-fired power plant

The carbon price calculation does not include any incentives for the solar plant because it is assumed that if a carbon price were in effect, current incentives would be phased out over time. The carbon prices shown here are subject to the same uncertainty discussed in Chapter 6, and are likely to be lower if the solar LCOE is optimized using the HTF mass flow rate parameters in conjunction with the solar field area. Carbon prices of \$150-240/tonne CO_{2eq} are high compared to the \$20-80/tonne CO_{2eq} range suggested by the Intergovernmental Panel for Climate Change as the global price by 2030 needed to stabilize carbon at around 550 parts per million (ppm) by 2100 [15]. Furthermore, given the history of inaction by the U.S. federal government regarding setting any national carbon price at all, it is unrealistic to expect carbon prices to be set at the range reported here as necessary for parabolic trough CSP to compete with coal-fired electricity generation.

Chapter 8: Policy Recommendations and Conclusions

The overarching research question that guides this study is: should renewable energy policies be doing more to encourage thermal energy storage (TES) for concentrated solar power (CSP)? Chapter 1 outlined a series of economic and environmental questions related to this topic that were examined through the creation of an engineering-economic model of a parabolic trough CSP power plant operating with molten salt TES and a comparable model of a PT plant that uses a natural gas (NG) backup system in place of the TES system. An environmental life cycle assessment of the greenhouse gas (GHG) emissions, water and land use was also conducted, and a decision analysis examined the combined effect of the environmental and economic results on the decision to incorporate TES in a PT plant. The following conclusions address how the results of the preceding investigations can be used in conjunction with the sensitivity analysis discussed in Chapter 6 to answer the original research questions in turn. Following these conclusions, a series of policy recommendations are presented.

8.1 Economic Conclusions

The first economic question was, "can TES reduce the levelized cost of electricity (LCOE) from a CSP plant"? Chapter 4 demonstrated that when the nominal engineering-economic input parameters are used in conjunction with minimizing the LCOE by varying the solar field area, TES does not reduce the LCOE compared to no TES/backup because the incremental increase in the cost of the TES system and solar field area associated with a larger storage capacity outweighs the incremental increase in electricity generation. The LCOE of a plant with TES is

roughly equal to that of a plant with an equivalent amount of natural gas backup for TES capacities of 1-6 hours and 4-9% higher than the LCOE of plants with NG backup capacities of 7-12 hours. Incorporating taxes and current federal incentives causes the TES and NG LCOE to be nearly equal for all capacities and maintains the no storage/backup configuration as the lowest cost option. However, the sensitivity analysis in Chapter 6 demonstrated that through an optimization process that incorporates heat transfer fluid (HTF) mass flow rate design parameters, a lower LCOE can be obtained for the base cases. For the case studies examined in the sensitivity analysis, this procedure had the effect of lowering the LCOE of the 6 hr TES case to nearly equal that of the 0 hr TES case, while causing the 6 hr NG case to have a larger LCOE than the 6 hr TES case. If this process were applied to all of the original cases, it is possible that the unsubsidized LCOE of parabolic trough plants with TES could be equivalent to (or perhaps somewhat less than) that of plants with no TES/NG backup. However, the current analysis indicates that TES does not substantially reduce the LCOE of a CSP plant based on current technology and plant costs.

The second and third economic research questions were, "can TES increase the profitability of a CSP plant", and "how do different electricity pricing structures affect the profitability of TES with CSP?" Chapter 4 demonstrated that when the nominal input parameters are used in the engineering-economic model, and the unsubsidized pre-tax LCOE is considered along with historical real-time hourly electricity pricing, TES decreases the profitability of a PT plant relative to a plant with no backup system. Relative to a plant with a comparable amount of natural gas backup, TES results in nearly the same annual profit (or loss as the case is here). This trend is maintained when taxes and incentives are incorporated into the LCOE. However,

when a fixed price of $200/MWh is used in place of variable electricity pricing along with the federal investment tax credit incentive, TES does increase the profitability of the power plant up to 43% above the 0 hr TES case and 2-11% higher than the equivalent PT-NG case. If the LCOE optimization improvements suggested in Chapter 6 are implemented, it is expected that these increases would become larger as LCOE decreases. Chapter 6 also notes that these profit results are based on systems that were optimized for the lowest LCOE. Future investigations should re-run the nominal results with the improved optimization procedures and with profit as the objective function. Table 26 indicates that a smaller solar field area will increase profit at least for the 6 hr TES case when variable electricity pricing is employed, and a larger solar field area will increase profit when fixed electricity pricing and incentives are included.

The fourth economic research question was, "if TES is economically preferred over other options, how does increasing storage capacity change the results"? In the nominal cases, increasing storage capacity beyond zero increases the unsubsidized and subsidized LCOE; decreases the unsubsidized and subsidized profit with variable electricity pricing, and increases the subsidized profit with a power purchase agreement of $200/MWh up to 10 hours of storage.

The next economic research question was, "do current U.S. renewable energy incentives encourage or discourage TES from an economic standpoint?" When cost is used as the comparative criterion, the federal investment tax credit (ITC) and accelerated depreciation do very little to encourage TES over no storage/backup. These incentives decrease the difference in LCOE between a plant with TES capacities from 1 to 12 hours and one with no storage/backup, but they do not make TES cheaper than no storage/backup. When profit is the comparative

criterion, the federal incentives do encourage TES but only in conjunction with a fixed electricity price.

The last economic research question was, "are there other incentive structures that may encourage TES more effectively?" Given that the combination of the federal ITC and the fixed electricity price is the only scenario that encouraged TES in the nominal results, it is possible that a feed-in tariff (FIT), which guarantees a specific price per MWh of electricity generated, could encourage TES in a more straightforward manner. However, the FIT would have to be guaranteed at the fixed price or decrease over a predictable schedule in order for it to be considered dependable enough to encourage new investment.

8.2 Environmental Conclusions

The first environmental question posed in Chapter 1 was, "how does TES affect the life cycle greenhouse gas (GHG) emissions of a CSP plant?" Chapter 5 shows that adding storage initially increases GHG emissions from a parabolic trough CSP plant, but it can decrease life cycle GHG emissions by up to 7% when more than 3 hours of storage are added. Moreover, TES decreases life cycle GHG emissions significantly (approximately 30-210%) compared to using a natural gas-fired heater to provide the same amount of backup during the same time periods.

The next environmental question was, "how does TES affect the life cycle and operational water use of a CSP plant?" Chapter 5 showed that using TES can decrease life cycle water use from rivers, lakes and groundwater by 5-23% compared to using no storage/backup. NG and TES plants have similar life cycle water use. Using dry cooling in conjunction with TES can reduce

life cycle water use even more (30-45%) compared to the wet-cooling alternative, depending on the storage capacity. In desert areas, the on-site operational water use for steam cycle makeup and mirror washing may be more important than the life cycle water use. Increasing TES capacity/NG backup beyond zero increases this value by 2-7%.

The third environmental question was, "how does TES affect the land use associated with a CSP plant?" The "life cycle assessment" of land use presented in Chapter 5 included only the operational stage of the life cycle but examined the land use compared to the life cycle electricity generated by the power plant. This assessment showed that using TES can decrease the life cycle land use associated with a parabolic trough power plant very slightly when 1-2 hours of storage are considered along with the nominal model inputs. Beyond this amount, more storage means more land use per MWh. Plants that use natural gas backup use slightly more land than the comparable storage configuration. The sensitivity analysis in Chapter 6, however, suggests that if a multi-variable LCOE optimization that includes the HTF mass flow rate parameters is performed, the land use for the NG backup cases is likely to decrease (as was shown in the case study with the 6 hr NG configuration). Further analysis is needed to explore the potential for more storage to result in less land use across various storage/NG backup capacity options.

The last environmental research question presented in Chapter 1 was, "how does this environmental profile change with varying storage capacities?" The nominal results show that increasing storage capacity beyond 1 hour increases life cycle GHG emissions initially, and then decreases emissions beyond 2 hours of storage. Increasing storage capacity beyond 1 hour decreases life cycle water use but increases steam cycle makeup and mirror washing water use.

It also decreases life cycle land use initially but then increases land use for more than 2 hours of storage.

8.3 Policy Conclusions and Recommendations

The economic and environmental issues discussed above led to a set of policy questions that consider both aspects of TES deployment. First, is there any environmental benefit to incorporating TES with CSP compared to the economic cost? The nominal results presented in Chapter 5 show that there is a clear environmental benefit to incorporating TES with CSP in terms of decreased life cycle GHG emissions. Although TES increases the unsubsidized cost of electricity compared to no storage/backup and compared to most of the NG configurations, the analysis in Chapter 7 suggests that using TES generates less life cycle GHG emissions per dollar spent compared to no storage/backup, or compared to any of the NG configurations. In fact, 12 hours of TES can reduce GHG emissions per dollar spent by 26% compared to no storage/backup.

The next policy question was, "how might renewable energy policy be adapted to better reflect these environmental-economic tradeoffs?" The multi-criteria decision analysis in Chapter 7 examined this question from the perspective of the renewable energy policy-maker who is considering whether to include provisions in future policy that encourage TES with new CSP plants. The answer to this question is highly dependent on how important each criterion is to the policy-maker and the constituents. If the most important consideration is life cycle GHG emissions versus cost, then policy-makers may want to encourage TES over no storage/backup since TES may reduce GHG emissions relative to cost by up to 26%. TES also should be

encouraged over NG backup in this case. When there are more complex preferences with equal concern for life cycle GHG emissions, on-site water use, land use, electricity generation, and plant cost, it is not clear whether TES should be encouraged over no storage/backup. In this case, the utility (weighted preference) of no storage/backup and all TES capacities is relatively the same for all options. If other reasons for implementing backup (i.e., factors related to operation of the power grid) emerge as additional attributes, TES would be encouraged over NG backup. In all cases, the analysis shows that dry cooling should be encouraged over wet cooling.

If decisions are based primarily on economic criteria, then no storage/backup should be encouraged. If some type of backup system is needed for other reasons, the economic preferences alone do not give a strong answer to whether that backup system should be TES or NG. Alternatively, if the most important decision criterion is plant performance, then a backup system should be encouraged along with wet cooling. However, there is no strong evidence to indicate whether that backup system should be TES or NG backup.

For the CSP case studies examined here, the carbon price required for CSP to be competitive with new coal-fired power plants (whose characteristics are defined in Appendix F) ranges between $150 and $240 per ton of CO_{2eq} avoided depending on the choice of backup system. It is unlikely that any near-term federal legislation will include carbon prices high enough to provide this level of economic incentive for new CSP power plants. Therefore, other incentives would be needed to guarantee the profitability of CSP plants. As mentioned previously, the combination of current federal tax incentives together with a fixed electricity selling price provides a small incentive for thermal energy storage over no storage/backup. If policy-makers

want to continue to encourage the use and development of storage technology, it would be worthwhile to examine the economic, environmental, and social costs and benefits of feed-in tariffs since this approach could have the same effect as current federal incentives and fixed electricity pricing, but in a more straightforward and transparent way.

The conclusions and recommendations above are based on the nominal results and sensitivity analysis presented in this thesis. The following research activities are also recommended to extend the robustness of this analysis:

1) Develop a probability distribution of hourly weather inputs that represents areas in the southwest United States with >6.0 kWh/m^2/day direct normal radiation. This distribution could be used to further quantify the range of economic and environmental effects associated with the larger U.S. solar resource. It could also help quantify the realistic potential for CSP in southwestern states.
2) Perform a multi-variable optimization on each configuration examined in this study as described in Chapter 6.
3) Examine how dispatching storage at different times during the day affects the results.
4) Examine and compare how the environmental and economic implications of power plant systems on the other end of the solar-fossil hybrid spectrum (described in Chapter 2) compare to the plant configurations examined here (i.e., Integrated Solar Combined Cycle).
5) Examine how the use of unconventional natural gas (i.e., shale gas) affects the economic and (especially) environmental implications of the power plant configurations examined in this study.

References

[1] (2009-2011, March 24, 2011). *Database of State Incentives for Renewables and Efficiency: Summary Maps*. Available: http://www.dsireusa.org/summarymaps/index.cfm?ee=1&RE=1

[2] "Annual Energy Review 2009," U.S. Energy Information Administration, Office of Energy Markets and End Use 0384, 2010.

[3] B. Prior, "Concentrating Solar Power 2011: Technology, Costs and Markets," ed: Greentech Media Webinar, 2011.

[4] G. E. Cohen, "Nevada Solar One Update," in *Proceedings of the Third Concentrated Solar Power Summit US*, Hotel Nikko, San Francisco, 2008.

[5] S. E. Systems, "Solar Dish Stirling Systems Report," in *NREL CSP Technology Workshop*, 2007.

[6] (2010, February 24, 2011). *NREL: Learning - Concentrating Solar Power*. Available: http://www.nrel.gov/learning/re_csp.html

[7] A. Schwartz, "Concentrated Solar Power Could Generate 25% of the World's Electricity by 2050," *Clean Technica,* 2009.

[8] "Solar Power Plant Which Provides Energy Even at Night," *Best Solar Energy,* 2009.

[9] L. Pottinger, "Here Comes the Sun: Taking Solar Power to Grid-Scale | International Rivers," *International Rivers,* 2008.

[10] "Assessment of Parabolic Trough and Power Tower Solar Technology Cost and Performance Forecasts," Sargent & Lundy LLC Consulting Group SL 5641, 2003.

[11] S. Millennium. (2011, February 24). *The Construction of the Andasol Power Plants*. Available: http://www.solarmillennium.de/Technologie/Referenzprojekte/Andasol/Die_Andasol_Kraftwerke_entstehen_,lang2,109,155.html

[12] P. Denholm*, et al.*, "The Role of Energy Storage in Renewable Energy Generation," NREL/TP-6A2-47187, 2010.

[13] T. Woody, "Solar Energy Faces Tests On Greenness," in *New York Times*, ed. New York, February 23, 2011.

[14] T. Key, "Solar Thermal Electric Technology: 2006," Electric Power Research Institute (EPRI), San Carlos, CA 1012731, 2006.

[15] IPCC, "Climate Change 2007: Synthesis Report," 2007.

[16] (2009-2011, March 5, 2011). *Database of State Incentives for Renewables and Efficiency Solar Portal: Federal*. Available: http://www.dsireusa.org/solar/incentives/index.cfm?state=us&re=1&EE=1&spv=1&st=1

[17] (2010, March 5, 2011). *NREL: TroughNet - U.S. Parabolic Trough Power Plant Data*. Available: http://www.nrel.gov/csp/troughnet/power_plant_data.html

[18] G. J. Kolb, "Evaluation of power production from the solar electric generating systems at kramer junction," Albequerque SAND94-2909C, 1994.

[19] R. Peltier, "Nevada Solar One, Boulder City, Nevada," *Power,* pp. 40-43, 2007.

[20] EIA. (2008, March 5, 2011). *National State Electric Rankings: Table A1 - Selected Electric Industry Summary Statistics by State, 2008*. Available: http://www.eia.gov/cneaf/electricity/st_profiles/e_profiles_sum.html
[21] (August 18, 2009). *Amargosa Valley - Solar Millennium. Explosion Dangers: Solar Industrial Projects and Schools Do Not Mix!* Available: http://www.basinandrangewatch.org/AV-SolarMill-scoping-Aug2009.html
[22] NREL. (January 28, 2010). *Parabolic Trough Solar Field Technology*. Available: http://www.nrel.gov/csp/troughnet/solar_field.html#technologies
[23] H. Price*, et al.*, "Advances in Parabolic Trough Solar Power Technology," *Journal of Solar Energy Engineering,* vol. 124, p. 109, 2002.
[24] E. Lüpfert*, et al.*, "EuroTrough - Design Issues and Prototype Testing at PSA," in *ASME Solar Energy: The Power to Choose*, Washington D.C., 2001.
[25] A. Fernandez-Garcia*, et al.*, "Parabolic-trough solar collectors and their applications," *Renewable and Sustainable Energy Reviews,* vol. 14, pp. 1695-1721, 2010.
[26] Abengoa. (2010). *Abengoa Solar begins commercial operation of Solnova 1, the company's first 50-megawatt parabolic trough plant*. Available: http://www.abengoasolar.com/corp/web/en/about_us/general/news/archive/2010/solar_20100505.html
[27] Abengoa. *Abengoa solar: Solar power for a sustainable world*. Available: http://www.abengoasolar.com/corp/export/sites/solar/resources/pdf/en/presentacion.pdf
[28] Guardian. *EcoGuard Solar Boost-MP*. Available: http://www.guardian.com/guardianglass/glassproducts/EcoGuardSolarEnergyGlass/EcoGuardSolarBoostMP/index.htm
[29] H. C. W. Anderson and M. J. Fisk, *Introduction to Solar Technology*. Reading, MA: Addison-Wesley Company, 1982.
[30] Siemens. (2010). *Solar Receiver UVAC 2010*. Available: http://www.energy.siemens.com/co/en/power-generation/renewables/solar-power/concentrated-solar-power/receiver.htm#content=Technical%20Data
[31] Schott. (2011). *Get more out of it: SCHOTT Solar for large-scale application*. Available: http://www.schottsolar.com/us/references/concentrated-solar-power/
[32] A. Maccari, "Innovative Heat Transfer Concepts in Concentrating Solar Fields," in *CONCENTRATING SOLAR POWER Towards the 7th European RTD Framework Programme*, Brussels, June 27, 2006.
[33] Exxon. (January 24, 1997, March 14, 2011). *Material Safety Data Sheet: Caloria HT 43*. Available: https://www2.itap.purdue.edu/msds/docs/3863.pdf
[34] U. Herrmann and D. W. Kearney, "Survey of Thermal Energy Storage for Parabolic Trough Power Plants," *Journal of Solar Energy Engineering,* vol. 124, p. 145, 2002.
[35] Solutia. (2011, March 14, 2011). *Therminol VP-1 - Vapor Phase/Liquid Phase Heat Transfer Fluid*. Available: http://www.therminol.com/pages/products/vp-1.asp
[36] L. Moens*, et al.*, "Advanced Thermal Storage Fluids for Solar Parabolic Trough Systems," *Journal of Solar Energy Engineering,* vol. 125, pp. 112-116, 2003.
[37] D. Kearney*, et al.*, "Assessment of a Molten Salt Heat Transfer Fluid in a Parabolic Trough Solar Field," *Journal of Solar Energy Engineering,* vol. 125, p. 170, 2003.
[38] Sciencelab. (November 1, 2010, March 14, 2011). *Materials Safety Data Sheet: Silicone Fluid*. Available: http://www.sciencelab.com/msds.php?msdsId=9924925

[39] NREL, "SAM 2010 Parabolic Trough Cost Model," parabolic_trough_cost_model.xlsx, Ed., ed, 2010.
[40] L. Moens*, et al.*, "Advanced Thermal Storage Fluids for Solar Parabolic Trough Systems," *Journal of Solar Energy Engineering,* vol. 125, p. 112, 2003.
[41] BLS. (March 10, 2011). *U.S. Bureau of Labor Statistics: CPI Inflation Calculator*. Available: http://www.bls.gov/data/inflation_calculator.htm
[42] P. E. Minton, "Heat-Exchange Technology, Nonaqueous Heat-Transfer Media," *Kirk-Othmer Encyclopedia of Chemical Technology,* December 4, 2000.
[43] WorleyParsons, "CSP Parabolic Trough Plant Cost Assessment," NRELSeptember 9, 2009.
[44] "Concentrating Solar Power Commercial Application Study: Reducing Water Consumption of Concentrating Solar Power Electricity Generation," U.S. Department of Energy 2006.
[45] WorleyParsons, "Dry Cooling Option, ADDENDUM TO: CSP Parabolic Trough Plant Cost Assessment," NREL, Golden, CODecember 14, 2009.
[46] Nexant and Pilkington, "Evaluation and Performance Modeling for Integrated Solar Combined Cycle Systems and Thermal Storage Systems," NREL KAF-9-29765-09 2000.
[47] (February 18, 2011, March 8, 2011). *NREL: Concentrating Solar Power Projects - Parabolic Trough Projects*. Available: http://www.nrel.gov/csp/solarpaces/parabolic_trough.cfm
[48] P. Svoboda*, et al.*, "Comparison of DSG vs. HTF Technology for Parabolic Trough Solar Power Plants—Performance and Cost," in *Proceedings of the 1997 International Solar Energy Conference*, Washington D.C., April 27-30, 1997.
[49] E. Zarza*, et al.*, "Direct steam generation in parabolic troughs: Final results and conclusions of the DISS project," *Energy,* vol. 29, pp. 635-644, 2004.
[50] E. Zarza*, et al.*, "The DISS Project: Direct Steam Generation in Parabolic Trough Systems. Operation and Maintenance Experience and Update on Project Status," *Journal of Solar Energy Engineering,* vol. 124, p. 126, 2002.
[51] PSA. (2009). *Plataforma Solar de Almeria Bi-Annual Report 2008-2009*. Available: http://www.scribd.com/doc/45800380/Plataforma-Solar-de-Almeria-Annual-Report-2008-2009
[52] Solarlite. (2011). *Solarlite Technology*. Available: http://www.solarlite.de/en_EN/produkte/index.cfm
[53] Solarlite. (2011). *Solarlite: Kanchanaburi*. Available: http://www.solarlite.de/en_EN/projekte/index.cfm
[54] C. Gäde. (October 19, 2010). *KTSE-9100 - First solar thermal power plant with direct steam generation (DSG) in Southeast Asia*. Available: http://www.renewableenergyworld.com/rea/news/article/2010/10/ktse-9100-first-solar-thermal-power-plant-with-direct-steam-generation-dsg-in-southeast-asia
[55] M. Medrano*, et al.*, "State of the art on high-temperature thermal energy storage for power generation. Part 2 - Case studies," *Renewable and Sustainable Energy Reviews,* vol. 14, pp. 56-72, 2010.
[56] A. Fernandez*, et al.*, "Selection of materials with potential in sensible thermal energy storage," *solar energy materials and solar cells,* vol. 94, 2010.
[57] F. Cavallaro, "Fuzzy TOPSIS approach for assessing thermal-energy storage in concentrated solar power (CSP) systems," *Applied Energy,* vol. 87, pp. 496-503, 2010.

[58] R. W. Bradshaw and N. P. Siegel, "Molten Nitrate Salt Development For Thermal Energy Storage In Parabolic Trough Solar Power Systems," in *Proceedings of Energy Sustainability*, Jacksonville, Florida, August 10-14, 2008.
[59] NREL. (January 28, 2010). *Parabolic Trough Thermal Energy Storage Technology*. Available: http://www.nrel.gov/csp/troughnet/thermal_energy_storage.html#media
[60] D. Laing*, et al.*, "Solid media thermal storage for parabolic trough power plants," *Solar Energy,* vol. 80, pp. 1283-1289, October 2006.
[61] R. Tamme*, et al. Thermal Storage for Solar Power Plants*. Available: http://www.dlr.de/en/Portaldata/1/Resources/kommunikation/publikationen/109_nachrichten/dlr-nari109_en_60-63.pdf
[62] D. Laing*, et al.*, "Economic Analysis and Life Cycle Assessment of Concrete Thermal Energy Storage for Parabolic Trough Power Plants," *Journal of Solar Energy Engineering,* vol. 132, pp. 041013-1 to 041013-6, 2010.
[63] V. Morisson*, et al.*, "Thermal energy storage systems for electricity production using solar energy direct steam generation technology," *Chemical Engineering and Processing,* vol. 47, pp. 499–507, 2008.
[64] J. Birnbaum*, et al.*, "A Direct Steam Generation Solar Power Plant With Integrated Thermal Storage," *Journal of Solar Energy Engineering,* vol. 132, pp. 031014-1 to 031014-5, 2010.
[65] R. Hewett and B. Gupta, "Phase-Change Thermal Energy Storage: Final Subcontract Report," Helendale, CaliforniaNovember 1989.
[66] D. Bharathan and G. C. Glatzmaier, "Progress in thermal energy storage modeling," in *Proceedings of the ASME 2009 3rd International Conference of Energy Sustainability*, San Francisco, California, 2009.
[67] Cogentrix. (2009, March 8, 2011). *Sunray/SEGS*. Available: http://www.cogentrix.com/plants.aspx?id=15
[68] (2011, March 8, 2011). *NextEra Energy Resources: Solar Facts*.
[69] APS. (March 26, 2004, March 8, 2011). *APS to Construct Solar Trough Power Plant*. Available: http://www.solargenix.com/pdf/APS%20Press%20release.pdf
[70] ESTELA. (June 7, 2007, March 8, 2011). *ACCIONA Puts the Biggest Solar Thermal Electric Power Plant Built in the World in the Last 16 Years into Service in the USA*. Available: http://www.estelasolar.eu/fileadmin/ESTELAdocs/documents/070607_ACCIONA_NSO_EN.pdf
[71] (2011, March 8, 2011). *SolarPACES: Legislation Promoting CSP Implementation*. Available: http://www.solarpaces.org/Library/Legislation/legislation.htm
[72] (March 10, 2011). *x-rates.com: American Dollars to 1 Euro*. Available: http://www.x-rates.com/d/USD/EUR/hist2009.html
[73] D. Kearney, "Solar Electric Generating Stations (SEGS)," *IEEE Power Engineering Review,* vol. 9, pp. 4-8, 1989.
[74] APS. (June 2010, March 8, 2011). *Saguaro Solar Power Plant*. Available: http://www.aps.com/files/_files/pdf/map/Saguaro.pdf
[75] D. Bürkle. (July 1, 2009, March 10, 2011). *German Aerospace Center (DLR) - Andasol 1: The largest solar power station officially inaugurated*. Available: http://www.dlr.de/en/desktopdefault.aspx/tabid-5105/8598_read-17179/

[76] (2010, March 10, 2011). *ACCIONA Solar Power: Alvarado I*. Available: http://accionasolarpower.com/innovation/alvarado-i
[77] ESTELA. (2007-2010, March 10, 2011). *European Solar Thermal Electricity Association: Alvarado*. Available: http://www.estelasolar.eu/index.php?id=57
[78] (January 11, 2009, March 10, 2011). *Tehran Times: Iran's first solar power plant comes on stream*. Available: http://www.tehrantimes.com/index_View.asp?code=186558
[79] (2010, March 10, 2011). *Solar Cells Update: Shiraz, The First Solar power Plant in Iran*. Available: http://solarcellssale.info/solar-science/solar-power-station/shiraz-solar-power-plant-iran.html
[80] D. Babington. (July 14, 2010, March 10, 2011). *Reuters: Sicily plant offers Italy new impetus on solar front*. Available: http://in.reuters.com/article/2010/07/14/us-italy-solar-idINTRE66D2N320100714
[81] (2011, March 10, 2011). *Net Resources International: La Florida Solar Power Plant, Spain*. Available: http://www.power-technology.com/projects/lafloridasolarpowerp/
[82] M. E. Rodriguez and A. SL, "Acciona grid connects its third CSP plant in Spain," *SPAIN Energy,* pp. 10-11, January 2011.
[83] FPL. (March 10, 2011). *FPL's Martin Next Generation Solar Energy Center: World's First Hybrid Solar Energy Center*. Available: http://www.fpl.com/environment/solar/pdf/Martin.pdf
[84] FLABEG. (2010, March 10, 2011). *MIRRORS FOR PARABOLIC TROUGH*. Available: http://www.flabeg.com/index.php?id=142&L=1
[85] ACCIONA. (March 10, 2011). *Acciona Energy: Palma del Río II CSP Plant*. Available: http://www.acciona-energia.com/activity_areas/csp/instalaciones/plantasenespana/planta-termosolar-palma-del-r%C3%ADo-ii.aspx?desde=4162
[86] Abengoa. (May 24, 2010, March 10, 2011). *Abengoa Solar begins commercial operation of Solnova 3, the company's second 50-megawatt parabolic trough plant*. Available: http://www.abengoasolar.com/corp/web/en/about_us/general/news/archive/2010/solar_20100524.html
[87] Abengoa. (August 2, 2010, March 10, 2011). *Abengoa Solar Reaches Total of 193 Megawatts Operating*. Available: http://www.abengoasolar.com/corp/web/en/about_us/general/news/archive/2010/solar_20100802.html
[88] Abengoa. (March 10, 2011). *Abengoa Solar: Solutions to Global Climate ChangeParabolic Trough Plants*. Available: http://www.abengoasolar.com/corp/export/sites/solar/resources/pdf/en/Solnova_1.pdf
[89] EIB. (April 23, 2008, March 10, 2011). *European Investment Bank: Solnova 1 & 3 Concentrated Solar Power*. Available: http://www.eib.org/projects/pipeline/2007/20070384.htm
[90] J. A. Alfonso. (February 17, 2011, March 10, 2011). *Renewable Energy Magazine: La familia "Extresol" tiene un nuevo miembro*. Available: http://www.renewableenergymagazine.com/energias/renovables/index/pag/termoelectrica/colleft//colright/termoelectrica/tip/articulo/pagant/termoelectrica/pagid/14155/botid/23/
[91] (February 26, 2010, March 10, 2011). *4 Alternatives: Inaugurada Extresol-I, la primera termoeléctrica de ACS en Extremadura*. Available: http://www.4alternatives.net/conocimientos/index.php/espanol/solartermoelectrica/3215-inaugurada-extresol-i-la-primera-termoelectrica-de-acs-en-extremadura-

[92] Greentech Media. (2011). *US CSP Project Tracker*. Available: http://www.greentechmedia.com/images/wysiwyg/research-blogs/USCSPProjectTracker.pdf
[93] Y. Zong and A. Ferriere, "State of the art review of simulation tools for CSP systems," PROMES (Processes, Materials and Solar Energy) Laboratory, Odeillo, FranceNovember 2, 2007 2007.
[94] H. Price, "A Parabolic Trough Solar Power Plant Simulation Model," presented at the International Solar Energy Conference, Hawaii Island, Hawaii, March 16-18, 2003.
[95] G. E. Cohen*, et al.*, "Final report on the operation and maintenance improvement program for concentrating solar power plants," June 1999.
[96] B. Kelly and D. Kearney, "Parabolic Trough Solar System Piping Model Final Report," NREL/SR-550-40165, July 2006.
[97] NREL. (September 1, 2010). *NREL: Concentrating Solar Power Research Partnerships*. Available: http://www.nrel.gov/csp/partnerships.html
[98] H. Price and D. Kearney, "Reducing the Cost of Energy from Parabolic Trough Solar Power Plants " in *International Solar Energy Conference*, Hawaii Island, Hawaii, March 16-18, 2003.
[99] R. K. Schwer and M. Riddel, "The Potential Economic Impact of Constructing and Operating Solar Power Generation Facilities in Nevada," NREL, Las Vegas, NevadaFebruary 2004.
[100] L. Stoddard*, et al.*, "New Mexico Concentrating Solar Plant Feasibility Study," Black and VeatchFebruary 9, 2005.
[101] B. Kelly, "Nexant Parabolic Trough Solar Power Plant Systems Analysis, Task 1: Preferred Plant Size," NREL, San Francisco, California NREL/SR-550-40162, July 2006.
[102] B. Kelly, "Nexant Parabolic Trough Solar Power Plant Systems Analysis, Task 2: Comparison of Wet and Dry Rankine Cycle Heat Rejection," NREL, San Francisco, California NREL/SR-550-40163, July 2006.
[103] B. Kelly and D. Kearney, "Thermal Storage Commercial Plant Design Study for a 2-Tank Indirect Molten Salt System," National Renewable Energy Laboratory (NREL), Golden, CO SR-550-40166, 2006.
[104] L. Stoddard*, et al.*, "Economic, Energy, and Environmental Benefits of Concentrating Solar Power in California," NREL, Overland Park, Kansas NREL/SR-550-39291, April 2006.
[105] E. S. C. Cavalcanti and A. C. G. Petti, "Assessment of SEGS-Like Power Plants for the Brazilian Northeast Region," *Journal of Solar Energy Engineering,* vol. 130, pp. 014501-1 to 014501-4, February 2008.
[106] NREL. *NREL: Solar Advisor Model (SAM)*. Available: https://www.nrel.gov/analysis/sam/
[107] S. Jones*, et al.*, "TRNSYS Modeling of the SEGS VI Parabolic Trough Solar Electric Generating System," in *Proceedings of ASME International Solar Energy Conference Solar Forum 2001*, Washington D.C., 2001.
[108] M. J. Wagner*, et al.*, "A Detailed Physical Trough Model for NREL's Solar Advisor Model," presented at the SolarPACES 2010, Perpignan, France, 2010.
[109] C. S. Turchi*, et al.*, "Water Use in Parabolic Trough Power Plants: Summary Results from WorleyParsons' Analyses," NRELDecember 2010.

[110] M. J. Wagner and C. F. Kutscher, "Assessing the Impact of Heat Rejection Technology on CSP Plant Revenue," presented at the SolarPACES 2010, Perpignan, France, 2010.
[111] C. Turchi*, et al.*, "Current and Future Costs for Parabolic Trough and Power Tower Systems in the US Market," presented at the SolarPACES 2010, Perpignan, France, September 21-24, 2010.
[112] R. Sioshansi and P. Denholm, "The Value of Concentrating Solar Power and Thermal Energy Storage," *IEEE Transactions on Sustainable Energy,* vol. 1, pp. 173-183, October 2010.
[113] Lazard, "Levelized cost of energy analysis - version 2.0 ", ed, June 2008.
[114] V. Quaschning, "Technical and economical system comparison of photovoltaic and concentrated solar thermal power systems depending on annual global irradiation," *Solar Energy,* vol. 77, pp. 171-178, 2004.
[115] M. J. Montes*, et al.*, "Solar multiple optimization for a solar-only thermal power plant using oil as heat transfer fluid in the parabolic trough collectors," *Solar Energy,* vol. 83, pp. 2165-2176, 2009.
[116] A. Poullikkas, "Economic analysis of power generation from PT solar thermal plants for the Mediterranean region – a case study for the island of Cyprus," *Renewable and Sustainable Energy Reviews,* vol. 13, pp. 2474-2484, 2009.
[117] S. Izquierdo*, et al.*, "Analysis of CSP plants for the definition of energy policies:The influence on electricity cost of solar multiples, capacity factors and energy storage," *Energy Policy,* vol. 38, 2010.
[118] R. Pitz-Paal*, et al.*, "Development Steps for Parabolic Trough Solar Power Technologies With Maximum Impact on Cost Reduction," *Journal of Solar Energy Engineering,* vol. 129, p. 371, 2007.
[119] S. Izquierdo*, et al.*, "Analysis of CSP plants for the definition of energy policies: The influence on electricity cost of solar multiples, capacity factors and energy storage," *Energy Policy,* vol. 38, pp. 6215-6221, 2010.
[120] I. Purohit and P. Purohit, "Techno-economic evaluation of concentrating solar power generation in India," *Energy Policy,* vol. 38, pp. 3015-3029, 2010.
[121] B. Norton*, et al.*, "Full-Energy-Chain Analysis of Greenhouse Gas Emissions for Solar Thermal Electric Power Generation Systems," *Renewable Energy,* vol. 15, pp. 131-136, 1988.
[122] T. Tsoutsos, "Environmental impacts from the solar energy technologies," *Energy Policy,* vol. 33, pp. 289-296, 2005.
[123] C. J. KORONEOS*, et al.*, "Life Cycle Assessment of a Solar Thermal Concentrating System," presented at the Proceedings of the WSEAS Conferences Santander, Cantabria, Spain, September 23-25, 2008
[124] P. Viebahn*, et al.*, "New Energy Externalities Developments (NEEDS) for Sustainability INTEGRATED PROJECT: Final report on technical data, costs, and life cycle inventories of solar thermal power plants," 502687 2008.
[125] Y. Lechón*, et al.*, "Life Cycle Environmental Impacts of Electricity Production by Solar Thermal Power Plants in Spain," *Journal of Solar Energy Engineering,* vol. 130, pp. 021012-1 to 021012-7, May 2008.
[126] V. Piemonte*, et al.*, "Life Cycle Assessment of a High Temperature Molten Salt Concentrated Solar Power Plant," presented at the 20th European Symposium on Computer Aided Process Engineering – ESCAPE20, 2010.

[127] I. John J. Burkhardt*, et al.*, "Life Cycle Assessment of a Parabolic Trough Concentrating Solar Power Plant and the Impacts of Key Design Alternatives," *Environmental Science and Technology,* 2011.
[128] V. Fthenakis and H. C. Kim, "Land use and electricity generation: A life-cycle analysis," *Renewable and Sustainable Energy Reviews,* vol. 13, pp. 1465-1474, 2009.
[129] V. Fthenakis and H. C. Kim, "Life-cycle uses of water in U.S. electricity generation," *Renewable and Sustainable Energy Reviews,* vol. 14 pp. 2039-2048, 2010.
[130] WorleyParsons, "FPLE - Beacon Solar Energy Project Dry Cooling Evaluation," FPLS-0-LI-450-0001 Rev B, February 1, 2008.
[131] G. A. Kiker*, et al.*, "Application of Multicriteria Decision Analysis in Environmental Decision Making " *Integrated Environmental Assessment and Management* vol. 1, pp. 95–108, 2005.
[132] L. A. Greening and S. Bernow, "Design of coordinated energy and environmental policies: use of multi-criteria decision-making," *Energy Policy,* vol. 32, pp. 721–735, 2004.
[133] D. Diakoulaki and F. Karangelis, "Multi-criteria decision analysis and cost-benefit analysis of alternative scenarios for the power generation sector in Greece," *Renewable and Sustainable Energy Reviews* vol. 11, pp. 716-727, 2007.
[134] F. Cavallaro, "Multi-criteria decision aid to assess concentrated solar thermal technologies," *Renewable Energy* vol. 34, pp. 1678-1685, 2009.
[135] D. Kearney*, et al.*, "Engineering aspects of a molten salt heat transfer fluid in a trough solar field," *Energy,* vol. 29, pp. 861-70, 2004.
[136] S. Wilcox and W. Marion, "User's Manual for TMY3 Data Sets," National Renewable Energy Laboratory, Golden, Colorado NREL/TP-581-43156, 2008.
[137] NREL, "Solar Advisor Model Version 2009.10.13," ed, 2009.
[138] F. Kreith and D. Y. Goswami, Eds., *Handbook of Energy Efficiency and Renewable Energy* (The CRC Press Series in Mechanical and Aerospace Engineering. Boca Raton, Florida: CRC Press, 2007, p.^pp. Pages.
[139] Siemens. (2010). *UVAC2010 - The unrivaled benchmark in solar receiver efficiency*. Available: http://www.energy.siemens.com/hq/pool/hq/power-generation/renewables/solar-power-solutions/concentrated-solar-power/downloads/E50001-W320-A104-V2-4A00_DA_UVACreceiver_US_ohne%20Israel.pdf
[140] M. Geyer*, et al.* (2002, May 1, 2008). *EuroTrough - Parabolic Trough Collector Family Developed and Qualified for Cost Efficient Solar Power Generation*. Available: ftp://ftp.crs4.it/pub/References/trough/EuroTroughPaperZurich2002-04-01.pdf
[141] NREL, "Solar Advisor Model Reference Manual for CSP Trough Systems," ed, July 2009.
[142] D. Goodwin. (March 29, 2011). *Cantera*. Available: http://www.nsf-combustion.umd.edu/presentations/dgoodwin_speech.pdf
[143] (February, 2011). *World Nuclear Association: Cooling Power Plants*. Available: http://www.world-nuclear.org/info/cooling_power_plants_inf121.html
[144] H. Stephens, "Tour of Solar Electric Generating Station, Kramer Junction," S. Wagner, Ed., ed, 2009.
[145] Electric Power Research Institute, "TAG (R) Technical Assessment Guide: Fundamentals and Methods -- Electricity Supply," TR-100281-V3R8, 1999.

[146] United States Department of the Treasury Internal Revenue Service (IRS). (2010). *Instructions for Form 4562 - Depreciation and Amortization (Including Information on Listed Property)*. Available: http://www.irs.gov/pub/irs-pdf/i4562.pdf
[147] EIA. (November 23, 2010). *U.S. Energy Information Administration: Figure ES5. Fossil Fuel Costs for Electricity Generation*. Available: http://www.eia.doe.gov/cneaf/electricity/epa/figes5.html
[148] EIA. (January 21, 2010). *U.S. Energy Information Administration Electric Power Annual 2008 - Data Tables: Retail Electricity Price Data by Sector and State 1990 to 2008*. Available: http://www.eia.doe.gov/cneaf/electricity/epa/epa_sprdshts.html
[149] CAISO. (2010). *CAISO version 5.7.7*. Available: http://oasis.caiso.com
[150] Solar Energy Industries Association (SEIA). (2010). *The History of Solar Energy: A Look at Uses of Solar Energy from BC to ITC*. Available: http://www.seia.org/galleries/FactSheets/Factsheet_solar%20history.pdf
[151] Solel, "UVAC 2008 World's Most Advanced Solar Receiver," ed, 2008.
[152] ConcreteNetwork.com. (2011). *Concrete Calculator*. Available: http://www.concretenetwork.com/concrete/howmuch/calculator.htm
[153] CSGNetwork.com. (2011). *Standard Pre-Mix Bag Concrete Quantity And Cost Calculator*. Available: http://www.csgnetwork.com/concretecalc.html
[154] Phillips Petroleum Company. *MSDS Summary Sheet*. Available: http://www.petrocard.com/Products/MSDS-ULS.pdf
[155] Carnegie Mellon University Green Design Institute. (2010). *Economic Input-Output Life Cycle Assessment (EIO-LCA) US 2002 Industry Benchmark model - producer price*. Available: http://www.eiolca.net
[156] United States Environmental Protection Agency (EPA), "Inventory of U.S. Greenhouse Gas Emissions and Sinks 1990-2006: ANNEX 2 Methodology and Data for Estimating CO2 Emissions from Fossil Fuel Combustion," 2008.
[157] United States Energy Information Administration (EIA). (2008). *International Energy Annual 2006 - Table C.1 General Conversion Factors*. Available: http://www.eia.gov/emeu/iea/tablec1.html
[158] U. S. E. I. A. (EIA). (2011). *Voluntary Reporting of Greenhouse Gases Program Fuel Emission Coefficients*. Available: http://www.eia.gov/oiaf/1605/coefficients.html
[159] Intergovernmental Panel on Climate Change (IPCC). (2007). *IPCC Fourth Assessment Report: Climate Change 2007 Working Group I: The Physical Science Basis - 2.10.2 Direct Global Warming Potentials*. Available: http://www.ipcc.ch/publications_and_data/ar4/wg1/en/ch2s2-10-2.html
[160] Farlex. (2011). *The Free Dictionary - diphenyl oxide*. Available: http://encyclopedia2.thefreedictionary.com/diphenyl+oxide
[161] Guidechem. (2011). *Phenyl ether*. Available: http://www.guidechem.com/dictionary/101-84-8.html
[162] Taj Pharmaceuticals Limited, "Biphenyl Phenyl benzene," 2009.
[163] TruthAboutCoalTar. (2006). *About Coal Tar and Polycyclic Aromatic Hydrocarbons (PAHs): What is Crude Coal Tar and how does it differ from Refined Tar or Refined Coal Tar?* Available: http://www.truthaboutcoaltar.com/aboutcoaltar.html
[164] V. N. Rubchevskii*, et al.*, "Predicting the Yield of Coke and Coking Byproducts," *Coke and Chemistry,* vol. 4, pp. 11-16, 2009.

[165] RedOrbit. (2010). *Coal - Reference Library*. Available: http://www.redorbit.com/education/reference_library/minerals/coal/448/index.html
[166] Engineering Toolbox. *Densities and molecular weights of some common gases*. Available: http://www.engineeringtoolbox.com/gas-density-d_158.html
[167] SQM. *Caliche Ore 1*. Available: http://www.sqm.com/aspx/about/CalicheOre.aspx?varN=1
[168] Detroit Salt Company. *Surface Mining*. Available: http://www.detroitsalt.com/mining-types.htm
[169] (2011). *Vermiculite*. Available: http://en.wikipedia.org/wiki/Vermiculite
[170] Product Ecology Consultants, "Simapro 7.1," ed, 2008.
[171] SQM. *Salar Brines*. Available: http://www.sqm.com/aspx/about/SalarBrines.aspx
[172] P. Jaramillo*, et al.*, "Comparative life cycle air emissions of coal, domestic natural gas, and SNG for electricity generation," *Environmental Science & Technology,* vol. 41, pp. 6290-6296, 2007.
[173] National Renewable Energy Laboratory (NREL). (2010). *Concentrating Solar Power Resource Maps*. Available: http://www.nrel.gov/csp/maps.html
[174] CMU, "Integrated Environmental Control Model (IECM) 6.2.4 developed by Carnegie Mellon University," ed, 2010.

APPENDIX A – Rankine Cycle Simplification

The original performance model code included a series of thermodynamic calculations in a program called Cantera [1], which set all of the steam cycle states. When these calculations were incorporated into the performance model, the entire engineering-economic simulation for one storage capacity and solar field size took about 15 minutes to run. Given that at least a hundred simulations needed to be performed for each storage capacity and each equivalent configuration in the case with natural gas backup, this run-time needed to be decreased. Since a relatively small range of temperatures and enthalpies are possible with the heat transfer oil, this range was simulated with the original Cantera-based code across the whole range in $1^{o}C$ increments, and the resulting power output and key enthalpies were recorded. Then curves were fit to the data to develop simplified equations that could be used in the engineering-economic model to calculate necessary performance parameters at a fraction of the speed of the original Cantera-based model. The following figures present these data, trendlines, and equations used in the revised engineering-economic model.

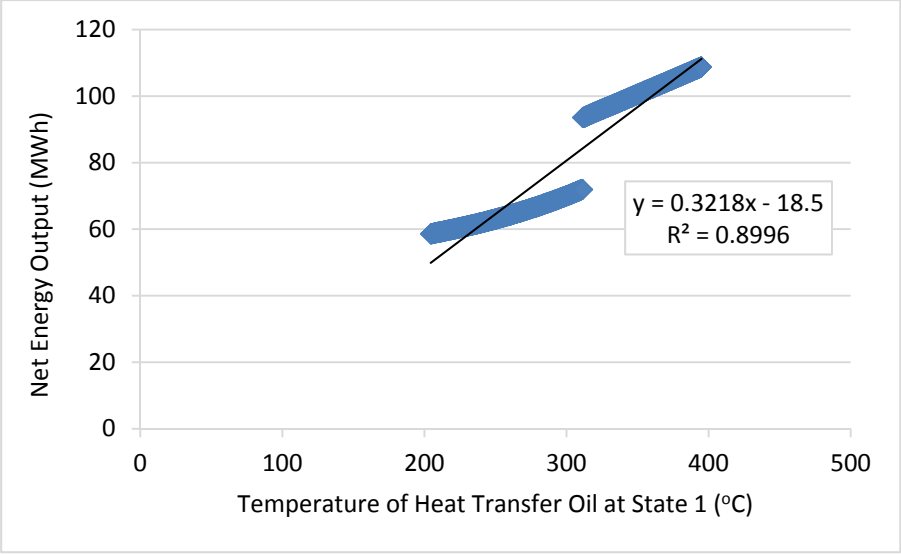

Figure 1 - Solar Field Outlet Temperature vs. Net Energy Output

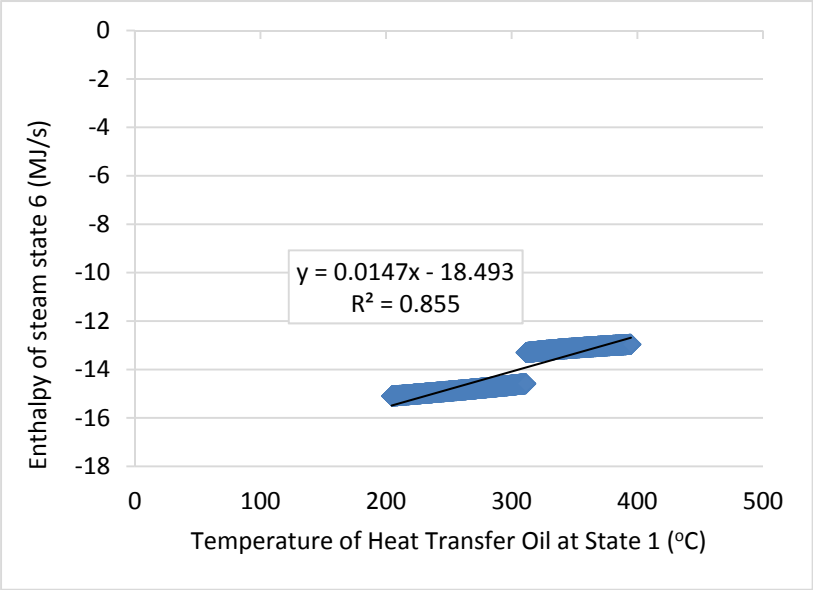

Figure 2 - Solar Field Outlet Temperature vs. Steam Enthalpy at Steam Generator Exit

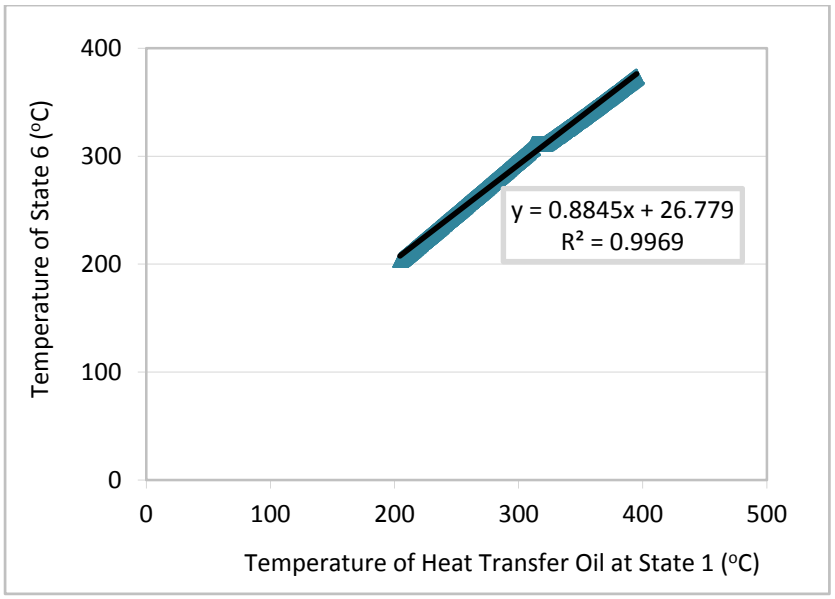

Figure 3 - Solar Field Outlet Temperature vs. Steam Temperature at Steam Generator Exit

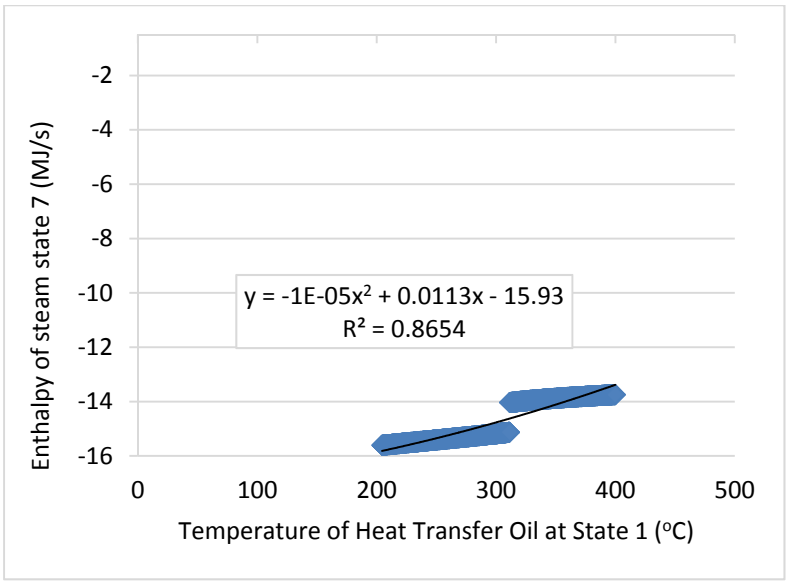

Figure 4 - Solar Field Outlet Temperature vs. Steam Temperature at Reheater Inlet

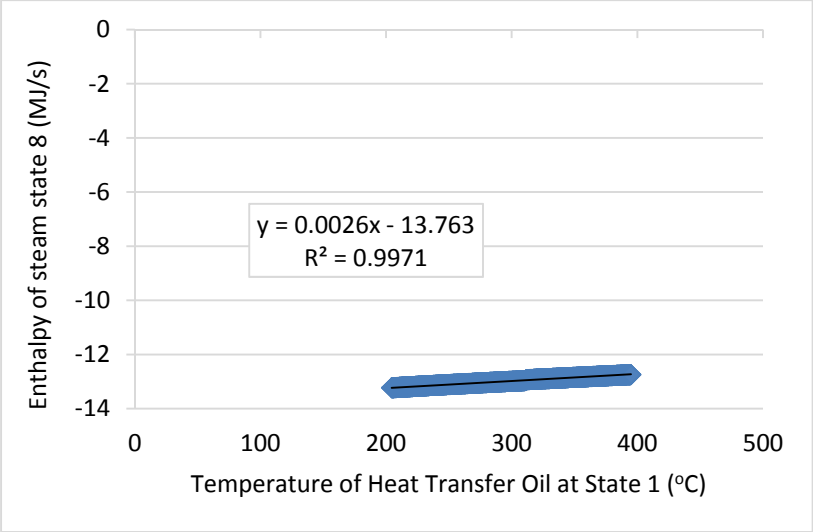

Figure 5 - Solar Field Outlet Temperature vs. Steam Temperature at Reheater Outlet

References

[1] D. Goodwin. (March 29, 2011). *Cantera*. Available: http://www.nsf-combustion.umd.edu/presentations/dgoodwin_speech.pdf

Appendix B – Model Adaptations for Dry Cooling

Due to time constraints it was not feasible to create additional thermodynamic models for the dry-cooled parabolic trough plant with thermal energy storage (PT-TES) and the PT plant with natural gas backup in place of TES (PT-NG). Instead, the results and methodology of four studies that compare wet- and dry-cooled PT systems [1],[2],[3],[4] were evaluated in order to obtain equations that could be used to adjust the wet-cooled results to simulate a dry-cooled system. This investigation yielded the conclusion that there are five key areas of adjustment to consider:

1. The Effect of Ambient Temperature on Net Output

According to Kelly [1], the ambient dry bulb temperature has a significant effect on the net power output of a PT plant with dry cooling and a very slight effect on a similar plant with wet cooling. Kelly used GateCycle and Excelergy to develop seven models of an 80 MW trough power plant with different cooling systems. Six of the models use a dry cooling system with different initial temperature differencials (ITD), and the seventh model represents a traditional wet cooling system. Kelly calculated the turbine output and fan power for each of the models for a range of dry bulb temperatures from 4 to 54^{o}C and incorporated into Excelergy equations of these two parameters as a function of dry bulb temperature. Although Kelly notes that the equation that relates dry bulb temperature to net output is a fourth order polynomial fit of the GateCycle calculations, he does not reveal the coefficients for this equation in the paper. An independent analysis of the Kelly results was conducted to re-create this equation for use in the dry cooling model for this study. Figure 1 displays a plot of the dry bulb temperature versus the

ratio of the net output from Kelly's dry-cooled model at an ITD of 39°F (the most cost-effective ITD modeled in the study) to the net output of Kelly's wet-cooled model. The fourth order polynomial fit to this plot is also displayed along with the equation and the R^2 value.

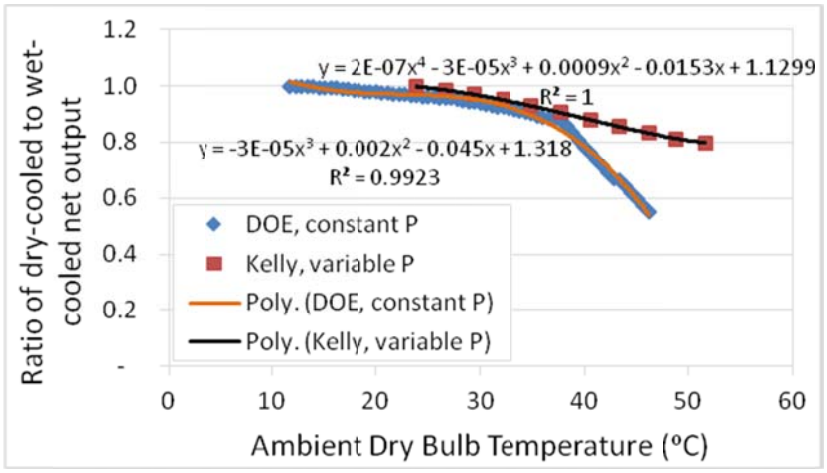

Figure 1 - Ratio of Dry- to Wet-Cooled Output as a Function of Dry Bulb Temperature

Kelly notes that these results required the air-cooled condenser pressure to increase from 0.3 to 0.5 bar in the GateCycle simulations when the dry bulb temperature increased from 42 to 54°C, but in reality system operators would maintain the condenser pressure at 0.3 bar in order to avoid "excessive aerodynamic loads on the last stage blades". Therefore, he conducted a series of additional GateCycle calculations at dry bulb temperatures greater than 42°C with the condenser pressure limited to 0.3 bar. Although Kelly's paper does not include the raw data for these "more realistic" simulations, a study by the Department of Energy (DOE) [2], which relies heavily on the Kelly study, includes a full data set of similar results. The DOE data are displayed in Figure 1 along with a polynomial curve fit, equation and R^2 value. The fourth order and third order polynomial equations were compared, and the third order results were more consistent with the raw data from the DOE study in the full temperature range, so I selected it for my dry cooling model. Since Figure 1 yielded a similar plot as that presented in the Kelly study,

and the DOE study contained a much larger dataset than the Kelly study, the DOE curve fit was chosen for use in the engineering-economic model for this study. This equation adjusts hourly net output of the plant with a dry cooling system relative to the hourly net output of the plant with a wet cooling system.

2. The Effect of Fan Power on Parasitic Energy Losses

Kelly and the DOE also provide information on the relationship between parasitic energy losses from a wet- versus dry-cooled system. Kelly reports that the dry-cooled system with the 39^{o}F ITD used 6,860 MWh of fan energy, compared with 4,124 MWh for the wet-cooled system – an increase of about 66%. The DOE study results show that the dry-cooled fan energy increased by 83% compared to the wet-cooled fan energy; however, they note that the feedwater pump energy demand was 32% lower for the dry-cooled system than the wet-cooled system (12,977 MWh compared to 19,157 MWh), resulting in a net increase in parasitic energy loss from the dry-cooling system of about 5% compared to the wet-cooling system. Since Kelly gives no information on the relative pump energies, the increase factor obtained from the DOE study was selected for use in the engineering-economic model for this study.

3. The Effect of Cooling Option on Plant Water Consumption

The DOE study and a dry-cooling study conducted by WorleyParsons for the Beacon Solar Energy Project [3] provide detailed information on water use in a PT plant with wet- versus dry-cooling. The DOE study shows that dry-cooling reduces overall water consumption by 90% (from 800 to 78 gallons/MWh); whereas the WorleyParsons study shows this value to be 95% (from 1,600 to 79 gallons/MWh). The average of these values was selected for the nominal results in the dry cooling model for this study.

4. The Effect of Cooling Option on Capital and O&M Costs

The WorleyParsons study provides a detailed breakdown of capital costs for both types of systems examined in the investigation. Table 1 lists these costs along with the ITD associated with each dry-cooled design and an increase factor, which is the ratio of the capital cost of the dry-cooled design to the reference wet-cooled design.

Table 1 - Cooling System Costs [3]

Initial Temperature Differential (^{o}F)	Capital Cost ($M)	Increase factor
Reference wet-cooled design	$33	N/A
35	$58	1.75
40	$51	1.56
45	$46	1.41

Figure 2 displays the relationship between the ITD and the increase factor using a trendline and power equation. This equation was used to calculate the increase factor for the ITD represented by the model used in this study, which is 30^{o}F. The increase factor calculated from this equation is 2.

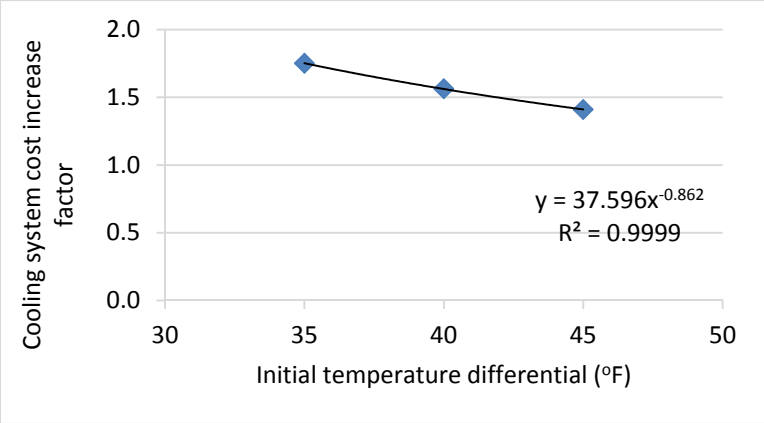

Figure 2 - Relationship between ITD and increase factor

The wet cooling system capital costs for the model used in this study were derived from power block costs in the SAM cost spreadsheet [5], which are listed in Table 2. The costs that are directly related to the cooling system are highlighted in yellow and add to $9,541,000, or about 9% of the total power block costs.

Table 2 - Power Cycle Capital Costs [5]

ITEM	TOTAL
Steam Turbine Generator Island	$34,344,000
Solar Steam Generator Equipment	$6,022,000
Blowdown System	$198,000
Cooling Systems	$5,246,000
Condensate System	$866,000
Feedwater System	$5,071,000
Auxiliary Cooling Water System	$1,177,000
Steam Piping, Insulation, Valves, & Fittings	$4,894,000
Fuel Gas Handling & Metering System	$438,000
Water Treatment System	$2,054,000
Power Distribution Systems	$16,363,000
Back-up Power Systems	$492,000
Instrumentation & Controls System	$3,386,000

Fire Protection System	$3,955,000
Foundations & Support Structures	$6,425,000
Buildings	$3,220,000
BOP Mechanical Systems	$5,275,000
BOP Electrical Systems	$5,938,000
Total	$105,364,000

Kelly indicates that the non-water operation and maintenance (O&M) costs associated with both systems is about equal, except for the process of water treatment, which is about 40% cheaper for the dry cooling system. Therefore, the service contract O&M costs were adjusted for water treatment in the engineering-economic model to reflect this ratio, and the volume of water in the utilities O&M cost section was adjusted to reflect dry cooling.

5. The Effect of Cooling Option on Land Requirements

A dry-cooled system results in a lower net plant output than a wet-cooled system, which means that the solar multiple may need to be adjusted to minimize the levelized cost of electricity (LCOE). In addition, there is a trade-off in total land change compared to a wet-cooled system where the dry-cooled system requires more land area for the air-cooled condenser but less land area for the evaporation pond. WorleyParsons [4] indicate that this tradeoff results in a net total land area increase for the dry-cooled plant compared to the wet-cooled plant. However, they incorporate an increase in solar field area in their calculations; whereas, the model used in this study is arranged to vary solar field area to minimize LCOE. Therefore, the relative increase in total land area compared with solar field area for both systems is the main concern for this study. Table 3 summarizes WorleyParsons results along with an independent calculation of a total land multiplier for each plant. The dry-cooled system actually uses less total land compared with the

solar field area than the wet system. These multipliers are used in the environmental assessment for this study.

Table 3 - Land Area Comparison Wet vs Dry Cooling (adapted from [4]

	Wet	Dry
Solar field aperture area (m^2)	987,540	1,062,750
Total land area (m^2)	4,046,873	4,143,980
Multiplier	4.1	3.9

References

[1] B. Kelly, "Nexant Parabolic Trough Solar Power Plant Systems Analysis, Task 2: Comparison of Wet and Dry Rankine Cycle Heat Rejection," NREL, San Francisco, California NREL/SR-550-40163, July 2006.

[2] "Concentrating Solar Power Commercial Application Study: Reducing Water Consumption of Concentrating Solar Power Electricity Generation," U.S. Department of Energy 2006.

[3] WorleyParsons, "FPLE - Beacon Solar Energy Project Dry Cooling Evaluation," FPLS-0-LI-450-0001 Rev B, February 1, 2008.

[4] WorleyParsons, "Dry Cooling Option, ADDENDUM TO: CSP Parabolic Trough Plant Cost Assessment," NREL, Golden, CODecember 14, 2009.

[5] NREL, "SAM 2010 Parabolic Trough Cost Model," parabolic_trough_cost_model.xlsx, Ed., ed, 2010.

APPENDIX C – Heater Costs

The costs for the natural gas-fired heaters used for heat transfer fluid (HTF) and storage salt freeze protection and for backup to match thermal energy storage capacity were obtained from a regression analysis of the data presented in Loh and Lyons [1]. Table 1 presents the original data from the report, and the cost values updated to $2009 values using the CPI inflation calculator [2]. Figure 1 displays the trendline, equation and R^2 value that resulted from the regression analysis.

Table 1 - Heater Cost Data

Heat Duty (MMBtu/hour)	Purchased Equipment Cost	Installed Cost ($1998)	Installed Cost ($2009)
2	$124,600	$96,300	$126,748
10	$263,100	$355,100	$467,375
25	$399,000	$518,600	$682,570
50	$625,400	$771,100	$1,014,905
100	$1,081,500	$1,272,800	$1,675,231
200	$1,868,900	$2,641,500	$3,476,684
300	$2,573,100	$3,534,400	$4,651,899
400	$3,228,000	$4,354,800	$5,731,692
500	$3,848,400	$5,126,000	$6,746,728

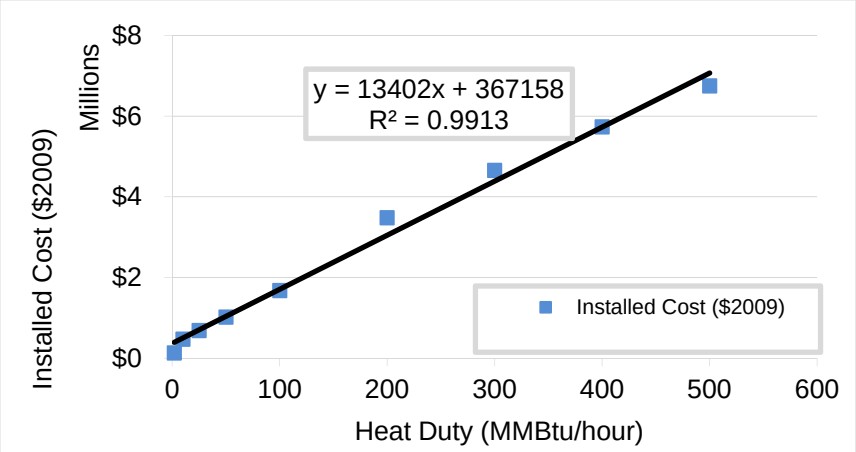

Figure 1 - Regression of heater cost data

References

[1] H. P. Loh and J. Lyons, "Process Equipment Cost Estimation," Department of Energy National Energy Technology Laboratory2002.

[2] BLS. (March 10, 2011). *U.S. Bureau of Labor Statistics: CPI Inflation Calculator*. Available: http://www.bls.gov/data/inflation_calculator.htm

APPENDIX D – TES Component Calculations for Life Cycle Inventory

The quantities of carbon steel, thermal insulation, and concrete calculated for the life cycle inventory were obtained from regression analyses on the total costs and unit costs associated with varying TES capacities reported in Kelly and Kearney [1]. Table 1 presents the data from that study and the material quantities in bold-faced type that were calculated by dividing the total cost of each component by the unit cost of the material. Figures 1-3 display the equations obtained by fitting a line to the data for the relationship between storage capacity and material quantity. These equations are used in the Life Cycle Inventory (LCI) portion of this analysis.

Table 1 - TES Material Costs and Calculated Quantities

Hours of Storage:	**2**	**4**	**6**	**9**	**12**
Storage capacity (MWht)	268	536	804	1,206	1,609
Total cost of cold tank ($1,000)	$747	$1,427	$2,097	$3,091	$4,193
Total cost of hot tank ($1,000)	$796	$1,526	$2,244	$3,311	$4,488
Tank unit cost ($/kg)	$4.40	$4.40	$4.40	$4.40	$4.40
Quantity of carbon steel for cold tank (kg)	**169,773**	**324,318**	**476,591**	**702,500**	**952,955**
Quantity of carbon steel for hot tank (kg)	**180,909**	**346,818**	**510,000**	**752,500**	**1,020,000**
Total cost of thermal insulation for old tank ($1,000)	$239	$376	$495	$659	$990
Total cost of thermal insulation for hot tank ($1,000)	$281	$442	$583	$776	$1,166
Insulation unit cost ($/m^2)	$160	$160	$160	$160	$160
Quantity of insulation for cold tank (m^2)	**1,494**	**2,350**	**3,094**	**4,119**	**6,188**
Quantity of insulation for hot tank (m^2)	**1,756**	**2,763**	**3,644**	**4,850**	**7,288**
Total cost of foundation for cold tank ($1,000)	$390	$635	$858	$1,171	$1,716
Total cost of foundation for hot tank ($1,000)	$443	$734	$1,002	$1,382	$2,004
Foundation unit cost ($/m^3)	$599	$599	$599	$599	$599
Quantity of concrete for cold tank foundation (m^3)	**651**	**1,060**	**1,432**	**1,955**	**2,865**
Quantity of concrete for hot tank foundation (m^3)	**740**	**1,225**	**1,673**	**2,307**	**3,346**

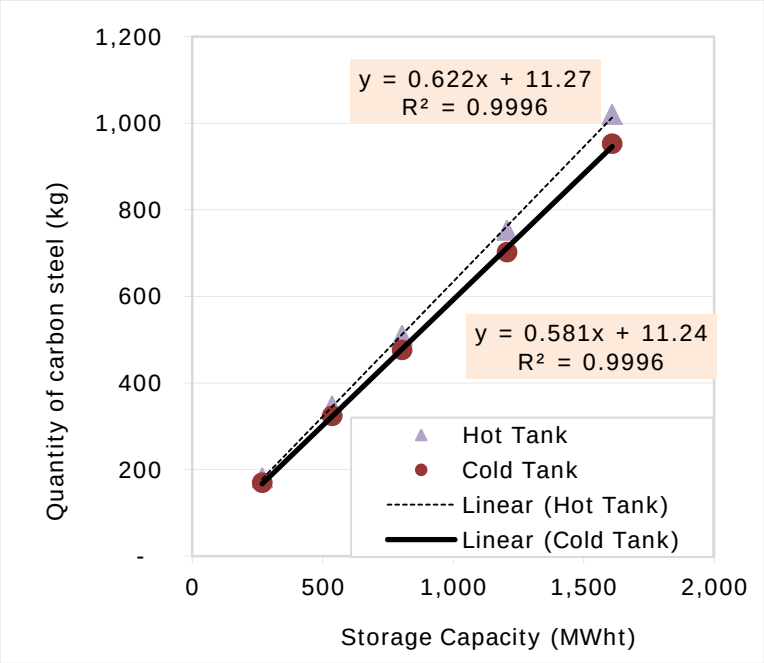

Figure 1 - Carbon Steel for Storage Tanks

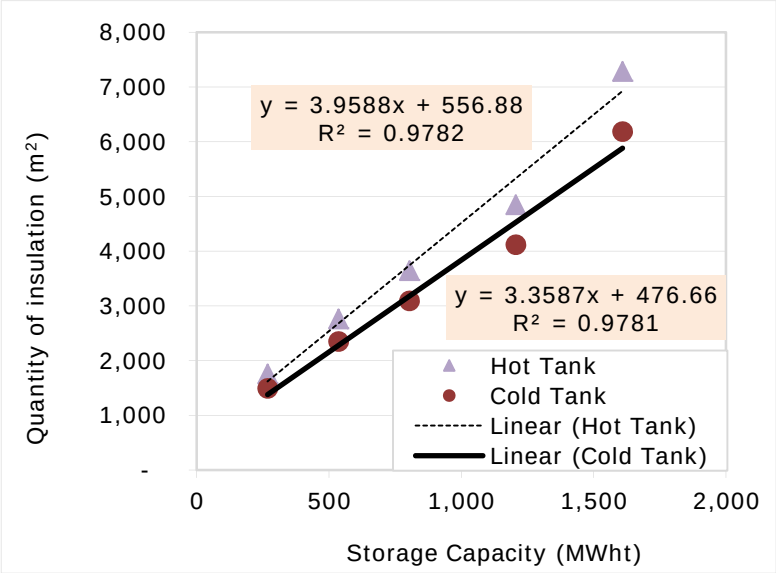

Figure 2 - Insulation for Storage Tanks

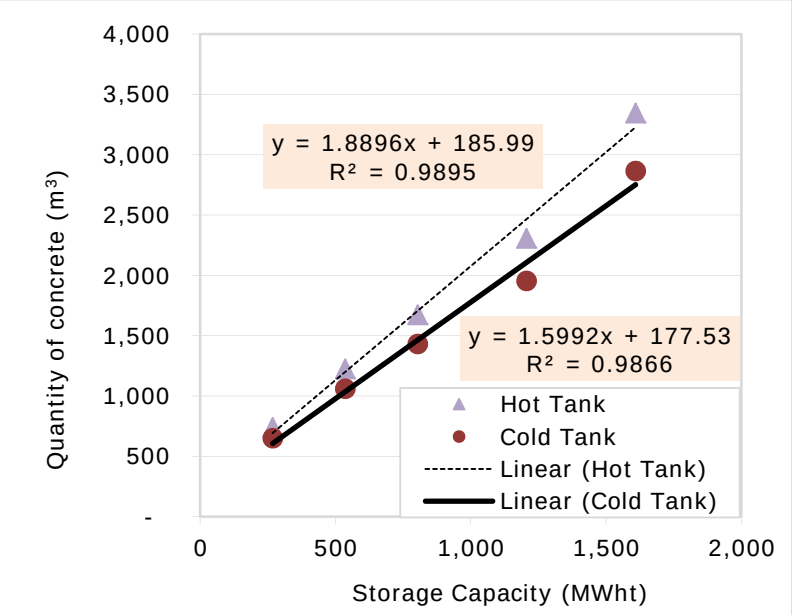

Figure 3 - Concrete for Storage Tank Foundations

References

[1] B. Kelly and D. Kearney, "Thermal Storage Commercial Plant Design Study for a 2-Tank Indirect Molten Salt System," National Renewable Energy Laboratory (NREL), Golden, CO SR-550-40166, 2006.

Appendix E – List of Databases and Processes for Environmental Impact Factors

Item	Database name	Processes included
Construction		
Site work & infrastructure	EIO-LCA US 2002 (428) Producer Price model for Construction, Other non-residential	production
Galvanized steel	Galvanized steel sheet, at plant NREL /RNA	resource extraction, refining and production
Low-iron float glass solar mirrors	Sum of data from Solar collector glass tube, with silver mirror, at plant/DE with US electricity U and Solar glass, low-iron, at regional storage/RER with US electricity U (Ecoinvent)	resource extraction, refining and production
Ceramic	Sanitary ceramics, at regional storage/CH with US electricity U (Ecoinvent)	production, transport of raw materials
Silicone	Silicone product, at plant/RER with US electricity U (Ecoinvent)	production
Stainless steel	Steel high alloy ETH S (ETH-ESU 96 System)	resource extraction, refining and production
Borosilicate glass	Sum of data from Glass tube, borosilicate, at plant/DE with US electricity U and Flat glass, uncoated, at plant/RER with US electricity U (Ecoinvent)	resource extraction, refining and production
Concrete	Concrete, normal, at plant/CH S (Ecoinvent)	production
Therminol VP-1	Allocated based on chemical composition, which includes 73.5% diphenyl oxide [Phenol, at plant/RER S (Ecoinvent)] and 26.5% biphenyl [average of: Coal Cokes S (ETH-ESU 96 System process); sum of data from Natural gas, at extraction site NREL /US (U.S. LCI Database with Ecoinvent Supplement); Natural gas, processed, at plant NREL /US (U.S. LCI Database with Ecoinvent Supplement); and Natural gas, at consumer/RNA with US electricity U (Ecoinvent); and sum of data from crude oil, production GB, at long distance transport/kg/RER and average of data from Crude oil production onshore S and Crude oil, at production onshore/RME S (Ecoinvent)]	resource extraction, refining and production
Carbon steel	average of C15I and C35I (IDEMAT 2001)	mining, concentration, processing, transportation to Rotterdam
Insulation	Mineral wool ETH S (ETH-ESU 96 System)	resource extraction, refining and production

Solar salt	Sum of data from Vermiculite, at mine/ZA S and Limestone, crushed, for mill/CH S (Ecoinvent)	resource extraction, refining and production
Salt pumps	EIO-LCA US 2002 (428) Producer Price model for Sector #333911: Pump and pumping equipment manufacturing	production
Heaters and heat exchangers	EIO-LCA US 2002 (428) Producer Price model for Sector #332410: Power boiler and heat exchanger manufacturing	production
Turbines and Generators	EIO-LCA US 2002 (428) Producer Price model for Sector #333611: Turbine and turbine generator set units manufacturing	production
Other manufacturing	EIO-LCA US 2002 (428) Producer Price model for Sector #33329A: Other industrial machinery manufacturing	production
Operation and Maintenance		
Diesel	sum of data from: average of data from Crude oil production onshore S and Crude oil, at production onshore/RME S; crude oil, production GB, at long distance transport/kg/RER; Diesel, at refinery/CH S; Diesel, at regional storage/CH S (Ecoinvent)	raw material extraction, crude oil production, diesel production, transportation to pumping station, combustion (calculated)
Natural Gas	Sum of data from Natural gas, at extraction site NREL /US (U.S. LCI Database with Ecoinvent Supplement); Natural gas, processed, at plant NREL /US (U.S. LCI Database with Ecoinvent Supplement); and Natural gas, at consumer/RNA with US electricity U (Ecoinvent)	Resource extraction, refining, production, and combustion (calculated)
Electricity	adapted the values from the EIO-LCA US 2002 (428) Producer Price model for Sector #221100: Power generation and supply to represent the average California electricity mix [1]	production
Dismantle and Disposal		
Solar Field	Divided value from Burkhardt et al. [2] by the solar field area used in their analysis	dismantle and disposal
Solar Field-DC	Divided value from Burkhardt et al. [2] by the solar field area used in their analysis	dismantle and disposal
HTF System	Divided value from Burkhardt et al. [2] by the solar field area used in their analysis	dismantle and disposal
HTF System-DC	Divided value from Burkhardt et al. [2] by the solar field area used in their analysis	dismantle and disposal
TES System	Divided value from Burkhardt et al. [2] by the solar field area used in their analysis	dismantle and disposal
TES System-DC	Divided value from Burkhardt et al. [2] by the solar field area used in their analysis	dismantle and disposal
Power Block	Divided value from Burkhardt et al. [2] by the solar field area used in their analysis	dismantle and disposal
Power Block-DC	Divided value from Burkhardt et al. [2] by the solar field area used in their analysis	dismantle and disposal

References

[1] Carnegie Mellon University Green Design Institute. (2010). *Economic Input-Output Life Cycle Assessment (EIO-LCA) US 2002 Industry Benchmark model - producer price*. Available: http://www.eiolca.net

[2] I. John J. Burkhardt, *et al.*, "Life Cycle Assessment of a Parabolic Trough Concentrating Solar Power Plant and the Impacts of Key Design Alternatives," *Environmental Science and Technology*, 2011.

APPENDIX F – IECM Inputs

This Appendix describes the inputs used in the Integrated Environmental Control Model [1] to simulate a new coal-fired power plant that is comparable with the nominal CSP plant configurations examined in this study for the purpose of calculating a carbon price. Table 1 presented the inputs used in the first graphical user interface (GUI) "Configure Plant".

Table 1 - Inputs to "Configure Overall Plant" Screen

Fuel Type	Coal
Nox Control	In-Furnace Controls, Hot-side SCR
Particulates	Fabric Filter
SO2 Control	Wet FGD
Mercury	Carbon Injection
CO2 capture	None
Cooling System	Wet Cooling Tower
Wastewater	Chemical Treatment
Flyash Disposal	No Mixing

The next GUI, "Set Parameters" includes several pages of input data. Table 2 presents the inputs to these pages that differed from the default values and the specific page in which they were entered.

Table 2 - Input parameters to "Set Parameters" pages

Parameter	Value	Units	Location
Type of dollars	constant	dollars	Overall Plant - 4. Financing
Plant of project book life	30	years	Overall Plant - 4. Financing
Real bond interest rate	8	%	Overall Plant - 4. Financing
Real preferred stock return	5.34	%	Overall Plant - 4. Financing
Real common stock return	8.74	%	Overall Plant - 4. Financing
Percent debt	40	%	Overall Plant - 4. Financing
Percent equity	8	%	Overall Plant - 4. Financing

(preferred stock)			
Percent equity (common stock)	52	%	Overall Plant - 4. Financing
Federal tax rate	0	%	Overall Plant - 4. Financing
State tax rate	0	%	Overall Plant - 4. Financing
Property tax rate	0	%	Overall Plant - 4. Financing
Investment tax credit	0	%	Overall Plant - 4. Financing
Natural Gas Cost	5.92	$/mscf	Overall Plant - 5. O&M costs
Water cost	1.4	$/kgal	Overall Plant - 5. O&M costs
Current fuel	Wyoming powder river basin	N/A	Fuel - 1. Properties
Gross electrical output	110	MW	Base Plant - 1. Performance
Unit type	Supercritical	N/A	Base Plant - 1. Performance

References

[1] CMU, "Integrated Environmental Control Model (IECM) 6.2.4 developed by Carnegie Mellon University," ed, 2010.